Diagenesis and reservoir quality of the Lower and Middle Buntsandstein (Lower Triassic), SW Germany

INAUGURAL - DISSERTATION
zur Erlangung der Doktorwürde
der Naturwissenschaftlich-Mathematischen Gesamtfakultät
der Ruprecht-Karls-Universität
Heidelberg

vorgelegt von

Dominik Soyk

Heidelberg, 2015

Diagenesis and reservoir quality of the Lower and Middle Buntsandstein (Lower Triassic), SW Germany

INAUGURAL - DISSERTATION
zur Erlangung der Doktorwürde
der Naturwissenschaftlich-Mathematischen Gesamtfakultät
der Ruprecht-Karls-Universität
Heidelberg

vorgelegt von
Dipl.-Geol. Dominik Soyk
aus Schwetzingen, Deutschland

Heidelberg, 2015
Gutachter:
Prof. Dr. Thilo Bechstädt
Prof. Dr. Harald Stollhofen

Tag der mündlichen Prüfung 08. Juni 2015

Table of Contents

Abstract

Tis research work deals with the diagenesis and reservoir quality of the Lower Triassic Buntsandstein in south-western Germany. The Buntsandstein in the study area is a continental succession with mostly fluvial and subordinately lacustrine and aeolian sediments. The most promising reservoir units are the Lower and Middle Buntsandstein, consisting mostly of stacked fluvial channel sandstones, interlayered by only thin mudstone beds. The Upper Buntsandstein is shalying upward and is thus less favourable as reservoir.

The mineralogy of the Buntsandstein indicates intense weathering. Plagioclase is completely absent, because it was already partly dissolved in the hinterland and finally replaced by kaolinite shortly after deposition. Dissolution vugs after plagioclase were apparently lost due to compaction. K-feldspar dissolution occurred after framework-supporting quartz cementation. This cement stratigraphic position is indicated by less compaction-affected vugs or "ghosts" after K-feldspar. In most cases, K-feldspar is replaced by kaolinite and minor illite. Neither plagioclase nor K-feldspar dissolution have therefore a significantly positive effect on reservoir qualities.

Regionally different quartz cementation west and east of the URG was observed: The quartz cement content on the western flank hardly reaches 10 %, while it partly exceeds 30 % on the eastern flank. Consequently porosity and permeability significantly vary: on the western flank porosities commonly exceed 15 to 20 % while they are usually below 15 to 10 % on the eastern flank. Quartz dissolution at grain contacts ("pressure solution") and particularly clay mineral transformations (smectite-illite, kaolinite-illite) were identified as probable silica sources.

A probable reason for the regional differences in quartz cementation was revealed by the fluid inclusions (FIs) trapped in the quartz cement. Homogenization temperatures (Th) in the FIs of a few hundred °C at an estimated maximum burial depth less than 1500 m proofs a hydrothermal origin of the cementing fluids. Increased Th correlate well with the above mentioned amount of regional quartz cementation: On the western flank Th are usually below 250 °C, whereas Th reach maximum values of >350 °C exclusively on the eastern flank (Odenwald).

Apart from the differing fluid temperatures the quartz cementation exhibited a significant sensitivity to clay mineral content. Particularly grain coating clay minerals (mostly illite) could restrain the precipitation of authigenic quartz on detrital grains. Clay mineral coatings are generally more abundant with decreasing grain size. Quartz cement content therefore generally also decreases with decreasing grain size, within the limits set by the strong differences in fluid temperatures.

Iron-rich and barite-filled fracture mineralizations of younger age indicate highly saturated formation waters in the subsurface of the URG, which can cause technical problems particularly during geothermal production (scalings, corrosion).

The Buntsandstein has the potential for a favourable geothermal as well as hydrocarbon reservoir (producing oil field Römerberg). However, regional diagenesis and its impact on PoroPerm properties of the matrix and rock-rigidity are essential components of reservoir properties.

Kurzfassung

Die Diagenese und Reservoirqualität des Buntsandsteins in Südwest-Deutschland wurde untersucht. Im Arbeitsgebiet handelt es sich um eine vorwiegend fluviatile und untergeordnet äolisch-lakustrine kontinentale Abfolge. Die vielversprechendsten Reservoireinheiten sind der Untere und Mittlere Buntsandstein: gestapelte fluviatile Rinnen-Sande werden von nur dünnen Feinsilt-Tonsteinlagen unterbrochen. Der Obere Buntsandstein wird zum Top hin zunehmend toniger, weshalb er als Reservoir weniger geeignet ist.

Die detritische Mineralogie des Buntsandsteins gibt einen Hinweis auf starke Verwitterung. Plagioklas ist nicht vorhanden, weil er teilweise bereits im Hinterland verwittert ist, der antransportierte verbliebene Plagioklas kurz nach der Ablagerung zu Kaolinit zersetzt wurde, eventuell vorhandene Lösungshohlräume wegen der Kompaktion verloren gingen. Die Lösung von Kalifeldspat fand dagegen erst nach der kornstützenden Quarzzementation statt. Diese Reihenfolge innerhalb der Zementstratigraphie wird belegt durch die Erhaltung von wenig durch Kompaktion beeinflussten Gesteinslösungsporen nach Kalifeldspat. Kalifeldspat wurde häufig durch Kaolinit ersetzt, weniger häufig durch Illit. Weder die Lösung von Plagioklas, noch die von Kalifeldspat verbesserte signifikant die Reservoirqualitäten.

Das Ausmaß der Quarzzementation westlich und östlich des ORG ist höchst unterschiedlich: der Gehalt an Quarzzement in Sandsteinen der westlichen Flanke erreicht kaum 10 %, während auf der östlichen Grabenflanke teilweise über 30 % Quarzzement festgestellt wurde. Entsprechend verhält sich die Verteilung von Porosität und Permeabilität: der Porenraum in Proben aus dem Westen übersteigt regelmäßig 15 bis 20 %, während er im Osten meist unter 15 bis 10 % liegt. Quarzlösung an Kornkontakten („Drucklösung“) und insbesondere Tonmineraltransformationen (Smektit-Illit, Kaolinit-Illit) sind die wahrscheinlichsten Silizium-Quellen.

Flüssigkeitseinschlüsse (FIs) in Quarzzementen zeigen den wahrscheinlichen Grund für die beobachteten Unterschiede der regionalen Quarzzementation auf. Homogenisierungstemperaturen (Th) in den Flüssigkeits-Einschlüssen von wenigen hundert Grad Celsius bei einer geschätzten maximalen Versenkung von weniger als 1500 m belegen hydrothermalen Einfluss auf die Bildung der zementierenden Lösungen. Die Th korrelieren mit dem Ausmaß der regionalen Quarzzementation: auf der Westflanke liegen die Th in der Regel unter 250 °C, während sie auf der Ostflanke im Odenwald teilweise 350 °C übersteigen.

Abgesehen von der Temperatur der Fluide reagiert die Bildung von Quarzanwachssäumen empfindlich auf die Anwesenheit von Tonmineralen. Insbesondere Häutchen (Kutane) von tangentialen Tonmineralplättchen (vorzugsweise Illit) um detritische Körner können die Ausscheidung von Quarzzement stark behindern. Illitkutane kommen häufiger in feinen als in gröberen Sandsteinen vor. Entsprechend ist der Gehalt an Quarzzement in der Feinfraktion generell geringer im Rahmen der Steuerung der Quarzzementation durch die genannten Hydrothermen.

Eisenreiche und barytische Kluftmineralisationen jüngeren Alters könnten auf stark gesättigte Formationswässer im Untergrund des ORG hinweisen, die insbesondere bei der geothermischen Produktion technische Probleme verursachen können

(Scalings, Korrosion), da derartige Wässer noch heute auftreten.
Der Buntsandstein ist eine aussichtsreiche Reservoireinheit für sowohl Geothermie als auch Kohlenwasserstoffproduktion (produzierendes Erdölfeld „Römerberg“). Die regionale Ausprägung der Diagenese und deren Auswirkungen auf Porosität-Permeabilität der Matrix und das Bruchverhalten des Gesteins sind wesentliche Bestandteile der Reservoir-Eigenschaften.

List of Abbreviations

(Neustadt) a.d.W.	(Neustadt) an der Weinstraße
Ab	Albite
Ap	Apatite
APS	Aluminium-Phosphate-Sulphate
auth	Authigenic
Brt	Barite
BSE	Back Scattered Electron
Bt	Biotite
Cc	Calcite
CEPL	Cementational Porosity Loss
Chl	Chlorite
CL	Cathodoluminescence
COPL	Compactional Porosity Loss
Dol	Dolomite
EDS	Energy Dispersive X-Ray Spectroscopy
EG	Ethylene Glycol
FI	Fluid Inclusion
Gt	Goethite
GTB	Geothermiebohrung (geothermal well)
HC	Hydrocarbon
I/S	Illite/Smectite
IC	Coating Illite
ICOMPACT	Campactional Index
IGV	Intergranular Volume
Ill	Illite
Ilm	Ilmenite
IM	Meshwork Illite
IR	Radial Illite
K-feldspar	Potassium Feldspar
Kfs	Potassium Feldspar
Kln	Kaolinite
Lith	Lithoclast
Ms	Muscovite
Pl	Plagioclase
por-fil	Pore-filling
Qtz	Quartz
repl	Replacing
Sch.	Schichten
SE	Secondary Electron
SEM	Scanning Electron Microscope
T_h	Homogenization Temperature
$T_{m\ ice}$	Ice Melting Temperature
T_t	Trapping Temperature
URG	Upper Rhine Graben
WCP	Weighted Contact Packing
XRD	X-Ray Diffractometry
XRF	X-Ray Fluorescence

1 Introduction

The early Triassic Buntsandstein in the Upper Rhine Graben (URG) is a still underexplored hydrocarbon as well as geothermal reservoir formation. The oil field Römerberg near Speyer successfully produces from a Buntsandstein reservoir since 2008. In 2013 first pumping tests from the geothermal well GTB1 Brühl, where a fracture zone in the Middle to Lower Buntsandstein was the target, were also very promising (pers. comm. B. Melchert, U. Lotz, 2014). Despite these successful exploration respectively production wells, the economic risk is still high. There are only a few publications and reports on the reservoir properties of the Buntsandstein in southwest Germany (Gaupp et al., 1998; Baaske, 1999; Stober and Jodocy, 2009; Haffen et al., 2013; Haffen et al., 2015). In contrast, numerous studies exist on the reservoir properties of the Buntsandstein in the Central European Basin, especially from North Germany and the North Sea (Füchtbauer, 1967; Cumming and Wyndham, 1975; Roos and Smits, 1983; Van Lith, 1983; Bifani, 1986; Abbots, 1991; Glennie, 1997; Feldrappe et al., 2008). However, the results from this northern segment of the basin cannot be applied to its southwestern part. The North German Buntsandstein represents a basinal facies, whereas the southwest, where the URG is located, corresponds to a basin margin (Ziegler, 1990), with mainly fluviatile and partly aeolian depositional facies. Consequently, the facies associations of the northern and southern areas are particularly different.

Geothermal Energy and Hydrocarbons in the Upper Rhine Graben
According to the Musée du Pétrole in Pechelbronn, which is located on the French, western margin of the URG, the historian Jacob Wimpfeling first mentioned the oil springs of “Baechel Brunn” in 1498. This makes the Pechelbronn oil field the earliest historically reported in Europe. After some drilling in the 19th century, exploration and production strongly increased in the early 20th century. It was in Pechelbronn, where Conrad Schlumberger recorded the first electrical resistivity well log in the world. From this time on, other oil fields in the URG were also exploited. Most familiar are probably Landau and the ‘Hessian Ried’ near Stockstadt in the northern URG. All these oil fields produced from relatively shallow Tertiary reservoirs. However, after the price increase of oil within the last decade and after oil was found in the Buntsandstein near Speyer in 2008 (originally planned as geothermal well), possible Mesozoic reservoirs were also taken into account during hydrocarbon exploration. Before, the Buntsandstein was considered a rather unfavourable reservoir rock.

The history of deep geothermal energy in the URG is much younger than the oil and gas production and not as successful as e.g. in the Molasse Basin around Munich. There are currently (March 2015) three geothermal power plants in the URG: Soultz-sous-Forêts started production in 2008, Landau and Bruchsal in 2009. Induced seismicity during production was an issue in Soultz and particularly in Landau, which resulted in concerns and protests against new geothermal power plants in the URG. In 2006, fracking of a geothermal well in the Basel area (Swiss Deep Heat Mining Project) induced earthquakes with a maximum magnitude of 3.5. This caused in 2010 the final halt of this geothermal project. The investigation of

the potential reservoir units in the URG within project AuGE (see below) might help to better understand and predict such issues.

1.1 Objectives

The German Federal Ministry for the Environment, Nature Conservation, Building and Nuclear Safety and subsequently the German Federal Ministry for Economic Affairs and Energy funded the multidisciplinary project "Outcrop Analogue Studies in Geothermal Exploration" (project 'AuGE', reference number 0325302D) in 2011. The main objective of this still ongoing study is to assess the reservoir properties to improve the understanding and predictability of potential geothermal reservoir rocks in the subsurface of the Upper Rhine Graben (URG) by a multi-method approach on outcrop analogues. For this purpose, more than 10 quarries and natural outcrops were surveyed by research groups from the GeoZentrum Nordbayern, Erlangen, and the Universities Göttingen as well as Heidelberg, each contributing to the project with a distinct discipline of Earth Sciences (facies architecture, petrophysical properties, diagenetic development, fault zone architecture, fracture analysis, 3D outcrop & fracture modelling). Industrial partners (GeoThermal Engineering GmbH, GeoEnergy GmbH, both Karlsruhe) provided additional data from the geothermal energy projects in Groß-Gerau and Brühl. Well cores from the URG subsurface were supplied by the Geological Survey of Rhineland-Palatinate; Wintershall AG and EMPG gave permission to incorporate the results in this research work.
The thesis presented here deals with the reservoir diagenesis and its implications on the fractured reservoir quality. The Triassic carbonate Muschelkalk and clastic Buntsandstein as well as the Permo-Carboniferous mixed carbonate-clastic-volcanic Rotliegend were initially selected for investigation, the latter because of the geothermal project Groß-Gerau. These stratigraphic intervals are commonly deeply buried in the URG and are thus most relevant for geothermal exploration. The diagenesis of the Muschelkalk in the subsurface of and along the URG was extensively studied by Geng (1996). The results of this thesis were reproduced at one outcrop and re-evaluated with respect to the reservoir quality of a fractured reservoir. The facies-heterogeneity of the Rotliegend in the Saar-Nahe-Basin, adjacent to the URG, is broad, but outcrops close the URG are sparse. At the same time there is large uncertainty on the facies of the Rotliegend in the subsurface of the URG because of widely lacking well cores and/or cuttings. The research on the Permo-Carboniferous was therefore postponed until a later stage, when data from Groß-Gerau become available. The reservoir diagenesis study was therefore focused on the clastic Buntsandstein (lower part of the Triassic) in close collaboration with Maria Fensterer from the GeoZentrum Nordbayern, who deals with facies architecture and petrophysics.
Deep geothermal reservoirs are always fractured reservoirs, since high production rates have to be achieved for a well to be profitable. Therefore one focus was on the fractures and the fracture cements to clarify, if the fractures in the subsurface are likely to be open or sealed. The main objective was the survey of the authigenic phases that precipitated in the matrix of the sandstones and their influence on the petrophysical and mechanical parameters of the rock. A connection between distinct diagenesis types and facies architecture was checked in collaboration with

Maria Fensterer (GeoZentrum Nordbayern). Probable mechanisms of formation were proposed for each diagenetic phase. As a synthesis, all data were compared and analysed with respect to regional patterns. The knowledge of formation mechanisms and their spatial and regional distribution can help predicting probable petrophysical and mechanical reservoir properties. These data can be used to confine thermohydraulic models before drilling and can thus reduce exploration risks and costs.

1.2 Study area

The study area is roughly outlined in Figure 1 and comprises Buntsandstein outcrops from the Palatinate Forest, the Haardt (the easternmost margin of the Palatinate Forest), the Odenwald, Kraichgau, and the northern Black Forest. Well cores were available from wells located at the western margin of the URG.
The URG is a rift basin in northern Switzerland, southwest Germany, as well as eastern France, which extends from the Basel area in the south to the Frankfurt area in the north with an average width of 30-40 km. The subsurface of the URG commonly exhibits an elevated geothermal gradient and is thus a promising province for geothermal energy production in the mentioned countries.
Outcrop and well localities are illustrated in Figure 1. Outcrop names, geographical coordinates and sample codes are attached in Appendix 9.

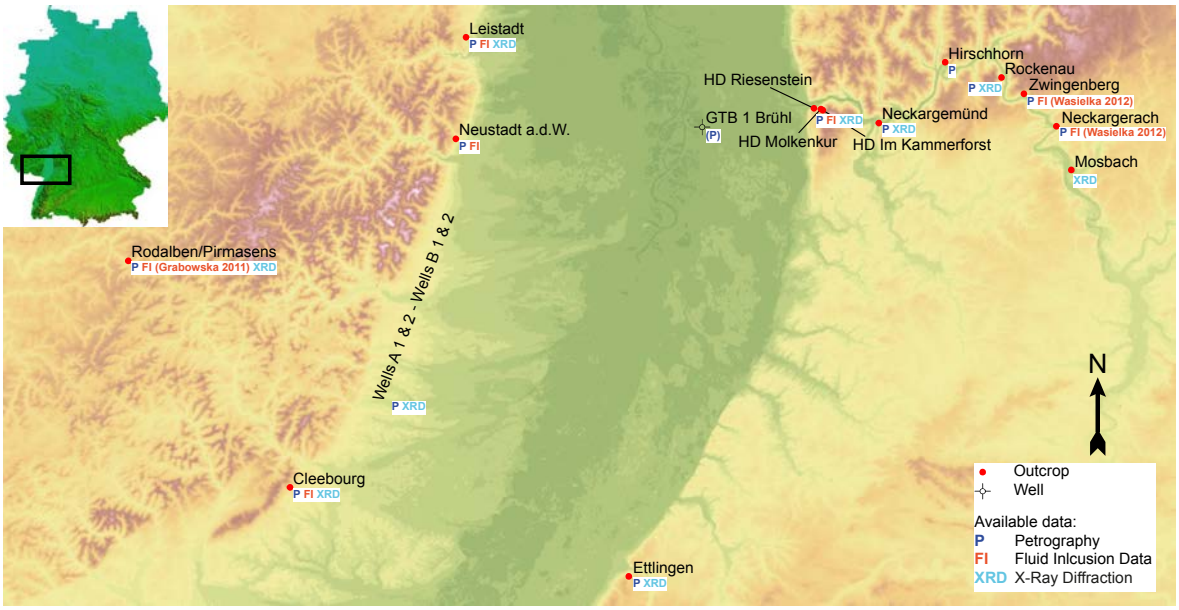

Figure 1: Buntsandstein outcrop and well localities in the study area. The outlines of the study area are marked by a black square on the map of Germany on the upper left. Well localities of wells A and B are confidential and are only roughly marked by striped areas. SRTM 90 elevation data.

1.3 Geological Setting

The study area was part of the Germanic Basin, which is also called the Central European Basin. The Germanic Basin is epicontinental and extended from Poland to England in roughly east-west direction and from the Baltic Shield in the north

to the Vindelician High and Bohemian Massif in the south-east, as well as the Armorican and London-Brabant Massifs in the west and south-west (Ziegler, 1990; Beutler and Szulc, 1999). The study area is located south-east of the Rhenish Massif near the southern basin margin (black frame in Figure 2).

During Early Buntsandstein times the basin geometry largely resembled the previous Zechstein Basin, but the basin overstepped its former margins. Clastic sediments from the basin margins in the north and south were transported towards the central Germanic Basin. A playa-lake to shallow marine environment developed in the axial part of the basin, indicated by predominantly shaly red-beds, ooid banks and locally stromatolites (Wolburg, 1961, 1968; Trusheim, 1963; Ziegler, 1990; Paul, 1999; Feist-Burkhardt et al., 2008). Fluvial, alluvial, lacustrine and minor aeolian sediments were deposited along the basin margins (Backhaus, 1974; Dachroth, 1985). In the southern part of the Germanic Basin, the transition from mostly sandy fluvial to predominantly shaly playa sediments occurred near the northern part of the Rhenish Massif (Füchtbauer, 1967). The thickness of the Lower Buntsandstein in south Germany is not much different from the thickness reached in north Germany. For the Odenwald a total of 270 m is reported (Backhaus et al., 1974). The Lower Buntsandstein in the Rhön and Fulda areas, situated further to the north, is 280 m and 340 m thick, respectively (Backhaus and Reul, 1971). In the central basin the Lower Buntsandstein can be 400 to 450 m thick (Ziegler, 1990; Feist-Burkhardt et al., 2008).

The facies architecture of the Middle Buntsandstein is initially similar to the Lower Buntsandstein. In north Germany base-level cycles of sandy fluvial flood plain and sheet flood deposits, which are overlain by shaly playa or shallow marine sediments, make up large parts of the succession (Trusheim, 1961, 1963; Wolburg, 1968). There are cycles of different order, the higher order ones represent each a formation. In contrast to the Lower Buntsandstein, during Middle Buntsandstein time the sediment supply from the hinterland increased, which coincided with an increasing humidity (Ziegler, 1990; Kürschner and Herngreen, 2010). Middle Buntsandstein sediments were particularly affected by regional tectonics, causing widely correlatable unconformities (Krämer and Kunz, 1969; Ortlam, 1974; Beutler, 1991; Aigner and Bachmann, 1992; Evans et al., 1993; Rettig, 1996; Geluk and Röhling, 1997; Nawrocki, 1997; Radies et al., 2005; Filomena and Stollhofen, 2011). These unconformities were used to propose a sequence stratigraphic framework (Aigner and Bachmann, 1992; Geluk and Röhling, 1997). Superimpiosed smaller scaled, 10 to 20 m thick cycles within the formations can be mapped over large parts of the central Germanic Basin and provide a high-resolution cyclostratigraphic framework, proven by magneto- and biostratigraphic methods as well as wireline logs. Cyclostratigraphy is assumed to be controlled by astronomical forcing of the climate, causing wet-dry cycles associated with changes of the base level, which is in this case the lake level in the basin (Szurlies, 2007, 2009).

Towards the basin margin, however, it becomes impossible to trace the above mentioned cycles and also increasingly difficult to distinguish between the different formations, because the thickness of the Middle Buntsandstein rapidly decreases from 500 to 1000 m in the north (Wolburg, 1961; Ziegler, 1990) to less than 150 m in the south (Backhaus, 1974). Sedimentation is not continuous, only part of the eroded material transported from the source areas in the south was deposited at

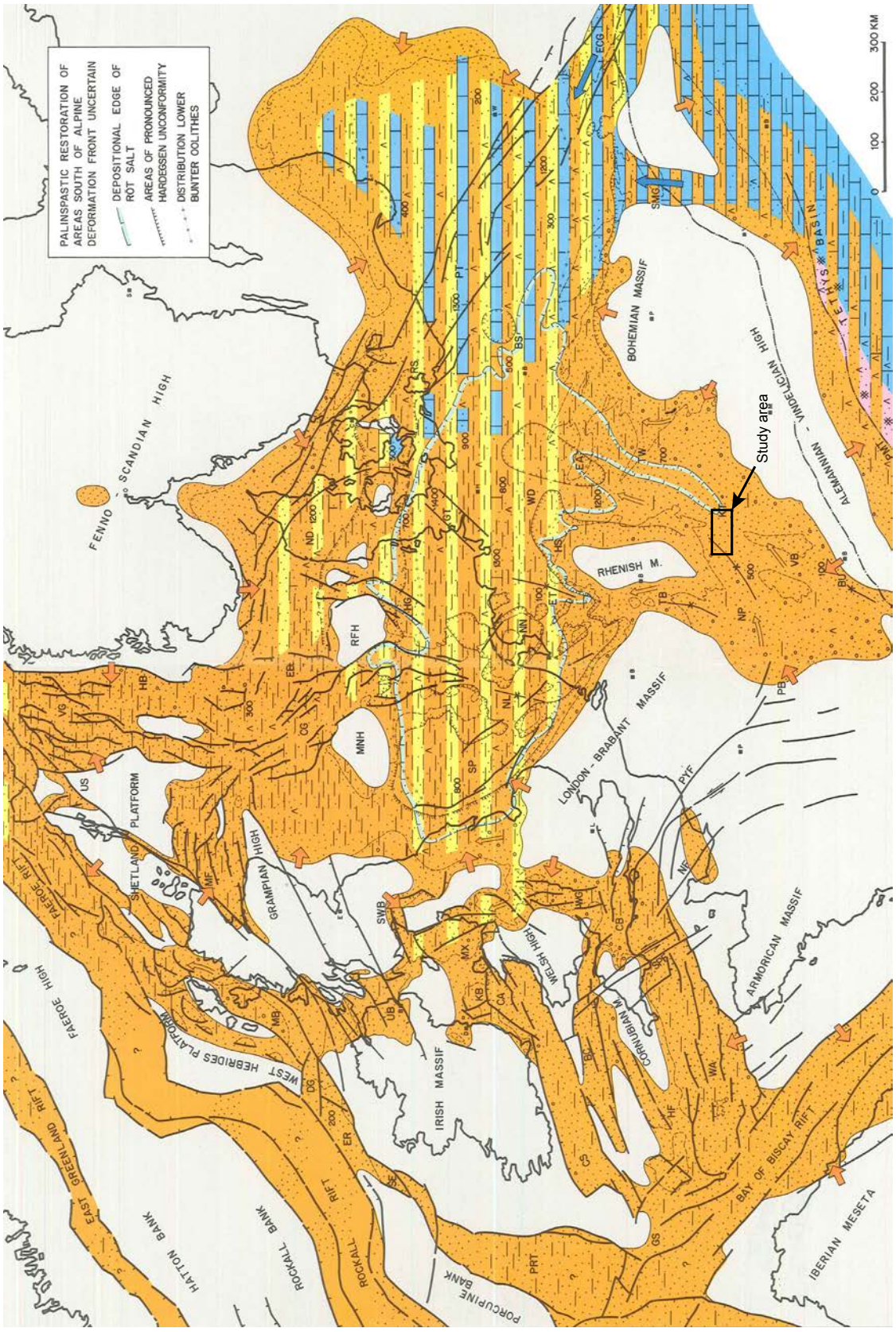

Figure 2: Buntsandstein Palaeogeography modified after Ziegler (1990). A black frame outlines the study area of this thesis.

the basin margin. Most of it bypassed and was transported to the basin centre in the north through braided streams and subordinately by wind (Backhaus, 1974; Dachroth, 1985). A part of the basin margin sediments was even reworked and the material transported further northwards.

The Upper Buntsandstein time is characterized by a marine ingression, which entered the Germanic Basin via the East Carpathian and the Silesian-Moravian Gates (Ziegler, 1990; Feist-Burkhardt et al., 2008). Marine conditions are indicated by fossiliferous limestones and sandstones as well as evaporites (halite, gypsum) (Assmann, 1933; Hinze, 1967; Gall, 1971; Backhaus, 1981; Ziegler, 1990; Cameron et al., 1992; Geluk and Röhling, 1997; Szulc, 2000; Feist-Burkhardt et al., 2008). The latter only developed in the central part of the basin. The variation of the Ca/Mg-ratio, clay mineral association and feldspar content indicates a marine-brackish depositional environment in the otherwise fossil-free sandstones and shales at the southern basin margin (Backhaus, 1981). In the Palatinate Forest the base of the Upper Buntsandstein consists of immature, coarse to medium grained sandstones, which commonly contain Middle Buntsandstein intraclasts (Dachroth, 1985; Steingötter, 2005). The sediments are fining upward to mudstones with intercalated sandstone and argillaceous limestone beds. The latter are petrographically similar to the Lower Muschelkalk, therefore the transition from the Upper Buntsandstein to the Lower Muschelkalk is determined by the last occurrence of red mudstones ("Grenzletten") in the Upper Buntsandstein (Dachroth, 1985; Steingötter, 2005). In the Odenwald the structure of the Upper Buntsandstein is generally comparable to the Palatinate Forest, although the composition of the sediments is somewhat finer grained (Backhaus, 1975). The thickness of the Upper Buntsandstein varies between 85 and 100 m in the Palatinate Forest (Steingötter, 2005) as well as between 80 and slightly above 100 m in the Odenwald (Backhaus, 1975).

Subsidence sustained during the Triassic, Jurassic and Early Cretaceous, and the Triassic Muschelkalk and Keuper as well as Jurassic limestones were deposited. Cretaceous sediments did not accumulate or are not preserved in southern Germany. Rifting in the South Atlantic and the Pyrenean Orogeny in the Late Cretaceous led to the inversion of the Germanic Basin in southern Germany (Figure 4 after Reicherter et al., 2008) and Mesozoic strata were erosionally cut.

From early Eocene times the stress field changed from an inversional to an extensional setting and the formation of the Upper Rhine Graben (URG) was initiated along preexisting Variscan, Mesozoic and Jurassic structures (Illies, 1965; 1974; Pflug, 1982; Hüttner, 1991; Ziegler, 1992; Dèzes et al., 2004; Reicherter et al., 2008). The URG is a passive rift basin and is part of the European Cenozoic rift system, which extends over a distance of 3000 km from the North Sea to the Atlantic coast of North Africa (Ziegler, 1992; Dèzes et al., 2004). The thickness of the Tertiary graben fill is highly variable. In the study area it reaches up to 3400 m at the eastern margin (Heidelberg Basin) and decreases to about 300 m at the western margin (Buness et al., 2008). Figure 3 shows a geological map of the URG and its surroundings after Eisbacher and Fielitz (2010).

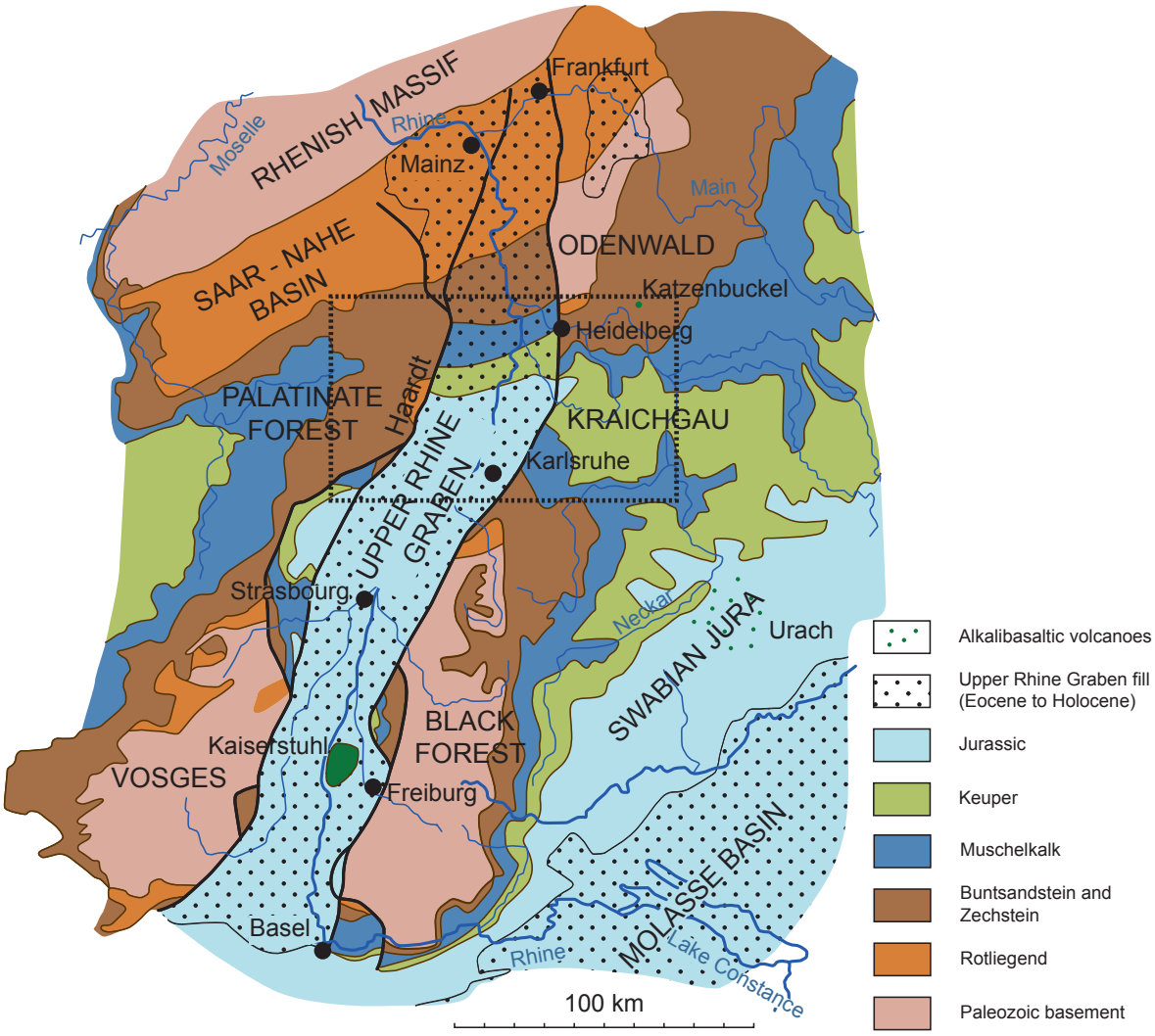

Figure 3: Geological map of the Upper Rhine Graben and its surroundings. The signatures in the URG and the Molasse basin indicate the Early Eocene erosional base before the graben/basin formation. The study area is marked by a dotted black frame. Modified after Eisbacher and Fielitz (2010).

1.4 Stratigraphy

The outcrops sampled within the project AuGE at both the eastern and western margin of the URG cover largely the same stratigraphic units (see Table 1). Lower and Middle Buntsandstein are most promising for geothermal exploitation and were thus preferably sampled. Three additional sections cover parts of the Upper Buntsandstein (Rodalben/Pirmasens, Zwingenberg, Neckargerach). The stratigraphy of the well core samples is unknown.

The subdivision of the Buntsandstein into stratigraphic units has been a controversy over the last decades. For the marginal areas in southern Germany several classifications exist (Hasemann, 1928, 1930; Backhaus, 1960, 1975; Richter-Bernburg, 1974). In this thesis the stratigraphic subdivision according to the Stratigraphic Table of Germany (Menning and German Stratigraphic Commission, 2002) was applied.

Age	Stress Field	Structures	Geodynamics
Neogene/Recent		INVERSION normal faulting strike-slip faulting (sinistral+dextral)	Alpine Collision
Palaeogene /late Eocene to Oligocene)		EXTENSION normal faulting	
Palaeogene /luntil early Eocene)		INVERSION Pyrenean collsision	continued rifting in the South Atlantic
Late Cretaceous		INVERSION strike-slip faulting (dextral) thrusting	rifting in the South Atlantic
Jurassic/ Early Cretaceous	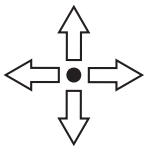	EXTENSION strike-slip faulting (NW-SE dextral) uplift?	rifting in the Central Atlantic
Triassic		normal faulting	rifting in the Central Atlantic

Figure 4: The stress field in south-west Germany from the Triassic to recent. Modified after Reicherter et al. (2008).

Three major sedimentary cycles are revealed at the southern margin of the Germanic Basin: two progradational fluvial cycles followed by retrogradation of the fluvial system (Dachroth, 1985; Aigner and Bachmann, 1992; Bourquin et al., 2006; Eisbacher and Fielitz, 2010). The first cycle started already during the Permian. The top of this cycle is marked by coarse sands or conglomerates ("Eck'sches Konglomerat)". The second progradational cycle is also marked by a conglomerate at its top ("Hauptkonglomerat"). All quarries sampled are located within this second cycle (Bausandstein, Geröllsandstein, Rehberg-Schichten). Horizontally stratified fine sandstones at the base ("Plattensandstein", "Zwischenschichten") and siltstones and mudrocks towards the top ("Rötton", "Voltziensandstein") build up the following retrogradational cycle. This part of the Upper Buntsandstein is already affected by temporary marine ingressions and passes into the shallow marine Muschelkalk carbonate succession (Backhaus, 1981, 1994).

Table 1: Stratigraphy of the Buntsandstein outcrops from the present study.

Odenwald:	
Heidelberg	Lower and Middle Buntsandstein, outcrops "Molkenkur", "Im Kammerforst" and "Riesenstein"
Neckargemünd	Lower Buntsandstein (Bausandstein)
Hirschhorn	Lower Buntsandstein (Bausandstein)
Rockenau	Lower Buntsandstein (unterer Miltenberg-Sst./Bausandstein)
Neckargerach/Zwingenberg	Lower to Upper Buntsandstein, outcrops "Wolfsschlucht" and "Margaretenschlucht"
Black Forest:	
Ettlingen	Middle Buntsandstein (Geröllsandstein), outcrop am "Schöllbronner Steig"
Alsace:	
Cleebourg	Lower Buntsandstein (Buntsandstein)
Haardt:	
Neustadt an der Weinstraße	Lower Buntsandstein (Rehberg Schichten), outcrop Hanbuch
Leistadt	Lower Buntsandstein (Rehberg Schichten), outcrop quarry Leistadt
Palatinate Forest:	
Rodalben/Pirmasens	Middle to Upper Buntsandstein (Karlstal Schichten, upper Felszone, Hauptkonglomerat, Zwischenschichten, Voltziensandstein)

2 Methods

The basis for all further analyses in this study were optical and cathodoluminescence microscopy of thin sections. Light and cathodoluminescence microscopy were applied to all samples studied. Based on these analyses, samples were chosen for further investigation by additional methods, concerning different questions (e.g. clay mineralogy, microthermometry, elemental composition of authigenic and detrital phases). If not otherwise mentioned, the analytical works were carried out in the laboratories of the Institute of Geosciences, Heidelberg University.

2.1 Sampling

More than 200 samples were acquired from both outcrops and wells. Granite was sampled at the natural outcrop Russenstein, located east of Heidelberg. Core and cuttings were available for the Buntsandstein: 8 samples from wells GTB Brühl 1, Well B 1, Well B 2, Well A 1 and Well A 2. The real well names cannot be used because of confidentiality issues. Wells A1, A2 and B1, B2 are neighbouring, respectively. Outcrop samples were partly acquired in cooperation with the workgroup for petrophysics from the GeoZentrum Nordbayern and the department for structural geology from the University of Göttingen.

A total of 123 Buntsandstein samples were taken from various natural outcrops and quarries (Cleebourg, Ettlingen, Heidelberg, Hirschhorn, Leistadt, Neckargemünd, Neustadt a.d.W., Rockenau). 70 of these samples were shared with the GeoZentrum Nordbayern, and 2 samples with the University of Göttingen.
All 33 Muschelkalk samples, acquired from the quarry in Nußloch, were shared with the GeoZentrum Nordbayern and 1 with the University of Göttingen.
The Buntsandstein outcrop Ettlingen was surveyed by a bachelor student (Schwab, 2013). Her results were integrated into this thesis, samples were re-evaluated and investigated by additional methods, not included in the BSc thesis.
Prior to project AuGE, two master's theses (Grabowska, 2011; Wasielka, 2012) were supervised by T. Bechstädt at the Jagiellonian University of Krakow. A total of 134 Buntsandstein samples from the Odenwald and Palatinate Forest were acquired within these final year projects. Some of these were reinvestigated to expand the study area and to complement the results from the other outcrops.

2.2 Optical Microscopy

A total of 182 polished, uncovered thin sections were prepared from field and core samples and were studied by optical microscopy. A Carl Zeiss Jena JENALAB POL polarizing microscope and a Carl Zeiss Jena GSZ binocular were used for generic survey of the thin sections. Microscopic thin section imagery was acquired using either a Leica DFC 420C digital microscope camera or an Olympus E-M1 high-end system camera mounted on an Olympus BX51 polarizing microscope.
For the petrographic quantification, the thin sections were subjected to standard point counting, using a Conwy Valley Systems Ltd. stepping stage mounted on an Olympus BX51 petrographic polarizing microscope. The stepping stage was controlled by the PETROG™ digital petrography software with integrated database, allowing the definition of a user-defined number of classes and subclasses. For each sample, 300 points were counted. This is supposed to be an adequate compromise between precision and required time for processing. Detrital grains were classified by their specification (e.g. mono- and polycrystalline quartz, K-feldspar, tourmaline), while authigenic phases were classified by their specification and their textural relationship (e.g. authigenic quartz attached to monocrystalline quartz or illite, grain coating, associated with Fe-oxide). Opaque grain coatings or plugs in pore throats were assumed to be illite associated with Fe-oxide and not pure grain coating or pore filling haematite (Chapter 3.3.1). So-called haematite coatings were usually expressed as a few wt. % Fe in the element spectrum of illite.
For the analysis of the textural composition the image analysis software JMicroVision (Roduit, 2007) was used. For this purpose overlapping images covering an area of 1.5 to 2 cm^2 were acquired and stitched with the PTGui panoramic stitching software. These steps were repeated for each normal and cross-polarized light as well as for cathodoluminescence. After stitching the images were stacked, fit and cut with Adobe® Photoshop® and loaded into JMicroVision. JMicroVision was calibrated using an image of a Leitz Wetzlar micrometer scale. Afterwards the longest diameter of at least 50 detrital grains was measured, using the 1D measuring tool. The grain diameter measured in thin sections is supposed to be smaller than the actual diameter (e.g. determined by sieving), but the precision of this method is sufficient for the purpose of this thesis. The Wentworth classification

(Wentworth, 1922) was used to ease the illustration of grain sizes by using ϕ-units instead of µm according to the modification of Krumbein and Aberdeen (1937). Visual charts were used to determine roundness (Powers, 1953) and sorting (Beard and Weyl, 1973). Point counting raw data and petrography are attached as tables in Appendix 3 and Appendix 4.

2.3 Cathodoluminescence Microscopy

Hot-cathode cathodoluminescence (CL) microscopy was performed with a Lumic HC5-LM modified Olympus microscope. Polished thin sections were coated with gold, using a Cressington Sputter Coater 108auto. The hot-cathode was operated with a vacuum $<10^{-5}$ bar, an acceleration voltage of 14 kV, and beam currents between 0.10 and 0.15 mA. Digital imagery was obtained either using a KAPPA DX40C 285 FW cooled CCD camera or an Olympus E-M1 high-end system camera.
The benefits of CL microscopy are:

- Reliable identification of detrital and authigenic quartz
- Considerably enhanced recognition of feldspars
- Discrimination of carbonate-cement generations
- Recognition of kaolinite-group clay minerals
- Deductions from quartz CL textures and colours on provenance

Quartz types were distinguished by their combined CL and optical features after Bernet and Bassett (2005). The corresponding table is attached in Appendix 2.

2.4 Scanning Electron Microscopy

A large number of samples was subjected to scanning electron microscopy (SEM) and energy-dispersive X-ray spectroscopy (EDS). The analyses were performed at a LEO 440 SEM with an attached Oxford Inca EDS. The LEO 440 SEM allows for the study of rock and mineral textures at high magnification and resolution. EDS was used for the identification of mineral phases by the interpretation of element spectra as well as for element mapping. Processing of element maps and spectra with the Oxford Inca Software allowed for element quantification and thus for distinguished analysis of the measurements. The same polished thin sections as surveyed by optical and CL microscopy were analysed by SEM-EDS and the results were compared. Sample preparation was the same as for CL microscopy. For the acquisition of back scattered electron (BSE) imagery, EDS spectra and element maps, the working distance was set to 23 mm and 10 to 15 nA beam current at 20 kV acceleration voltage. In secondary electron (SE) mode the working distance and beam current were reduced to 5 to 10 millimetres and <2 nA, respectively.

2.5 X-Ray Diffraction Analysis

X-ray diffraction analysis was used for clay mineral identification. For this purpose the clay fraction had first to be separated. Samples were gently crushed with a mortar, 20 to 30 g debris were filled into 50 ml centrifuge tubes and filled up with deionized water. The tubes were put in an ultrasonic bath for a total of 60 minutes to liberate the clay minerals. Afterwards the supernatant suspension was decanted from the settled down sand fraction and centrifuged for 60 seconds at 1000 rpm

using a Hettich ROTANTA 460R centrifuge at the Centre for Organismal Studies of Heidelberg University. This step separates the clay from the silt size fraction (Poppe et al., 2001). The settings for the centrifugation were calculated with a program written by Poppe et al. (1988), which is based on the method published by Hathaway (1956). Both computational methods are based on Stokes' law. After centrifugation 10 ml of the supernatant clay suspension were carefully pipetted in 15 ml tubes and dry frozen for approximately 16 hours. For each sample approximately 4.5 mg clay powder were weighed, mixed with 0.16 ml deionized water and sonicated for 30 minutes to completely disaggregate the clay minerals (modified after Schleicher, 2005). Insulation tape was paste up a glass slide and a square of 1x1 cm was cut into the tape. The suspension was pipetted inside the square and air dried to obtain an oriented aggregate mount (Moore and Reynolds, 1997). After drying the tape was thoroughly removed using a scalpel.
The measurements were conducted using a Siemens D500 X-ray diffractometer with a 1.5406 Å Cu-anode and 30 mA current at 40 kV operating voltage. For clay mineral identification the interval between 3 and 22 °2θ was measured in 0.02° steps with a measurement time of 2 s for each step. Raw data was edited with the Bruker DIFFRAC.EVA XRD-software.
Oriented aggregate mounts were ethylene glycol (EG) and heat-treated. EG is adsorbed by smectite and expands the smectite structure, which becomes visible in XRD analysis (Bradley, 1945). Therefore the samples were put in a large desiccator together with EG and heated to 60 °C over-night (Moore and Reynolds, 1997). Heat treatment was conducted at 375 °C and 550 °C, each for one hour. After heating to 375 °C the mixed-layer illite-smectite diffraction pattern resembles a pure illite (Moore and Reynolds, 1997). Heating to 550 °C causes the collapse of the kaolinite-structure and is thus used for the verification of kaolinite-peaks.

2.6 X-Ray Fluorescence Analysis

X-ray fluorescence (XRF) analyses were conducted using a Siemens SRS303 sequential X-ray spectrometer. Powder samples were prepared to pellets for examination. The results for major elements are plotted as oxides. XRF was used to examine the whole rock composition of sandstones (e.g. bleached vs. non-bleached). The raw data are attached in Appendix 7.

2.7 Whole Rock Geochemistry

Nearly all Buntsandstein samples were subjected to multi-acid ICP to obtain total values especially on metals and trace elements. A 0.25 g split was heated in HNO_3-$HClO_4$-HF to fuming, taken to dryness and the residue was dissolved in HCl for further analysis. The analyses were conducted by a commercial laboratory (AcmeLabs™). The raw data are attached in Appendix 5.

2.8 Fluid Inclusion Microthermometry

Fluid inclusion (FI) microthermometry was conducted on double polished thick sections (approximately 150 µm thick) using a Linkam THMS600 heating and freezing stage. Two-phase (gas bubble + liquid) aqueous fluid inclusions

were measured in syntaxial quartz cements. Homogenization temperature (T_h), nucleation temperature of the bubble ($T_{n\ gas}$), nucleation temperature of the ice ($T_{n\ ice}$), initial ice melting temperature (T_i) and final ice melting temperature ($T_{m\ ice}$) were measured. However, ice nucleation and melting temperatures could only be measured on some samples (compare Chapter 3.6). All measurements were executed three times. Results that could not be reproduced were neglected. Fluid inclusion raw data are attached in Appendix 6.

3 Results

3.1 Lithology and Lithofacies

From the optical appearance of the Buntsandstein, the outcrops at the margins of the Upper Rhine Graben towards the Palatinate forest and the Odenwald can be categorized into three major types:

- Yellowish-light brownish, totally bleached sandstone of the „Haardtrand Fazies“ (Leistadt, Neustadt a.d.W. (quarry „Hanbuch“), wells Well A 1, Well A 2, Well B 1, Well B 2, Figure 5a)
- „Haardtrand Fazies“ adjacent to a major fault zone: mixed “Haardtrand Fazies” with bright white bleached and red sandstone (Cleebourg, Figure 5b)
- Red, non- or subordinately bleached sandstones (Rodalben, Odenwald, Figure 5c)

For the lithological description of the Lower and Middle Buntsandstein the classification of Miall (1977a) was used (Appendix 1). Since the Upper Buntsandstein was not part of this study this unit is not included in the following text. It can also only partly be described by Miall’s classification, because of a major change in depositional environment (Chapter 1.3).

Grain sizes of sandstones as well as sorting only slightly vary in all outcrops sampled. Grain sizes range mostly between fine and medium sand. Coarse sand is most abundant in the Palatinate Forest but rare in the Odenwald. Sorting is rather constant in the sandstones, ranging between moderately to well. Silt- and mudstones were not sampled because of their missing relevance for geothermal reservoirs and difficulties for light-microscopic petrographic analysis. Investigation of the chemistry of siltstones and mudstones or the type of clay minerals was not part of the research plan.

Different fabric types can be distinguished in the field:

- Massive, crudely bedded and/or low angle cross- stratified gravel (Gm, Gp).
- Trough and planar cross-bedded sandstone layers (St, Sp), partly with mudstone intraclasts.
- Sandstones with mudstone clasts up to several cm in diameter (Se).
- Rippled sandstones (Sr).
- Laminated fine sand- to siltstones (Fl).
- Laminated to massive silt- and mudstones (Fsc).
- Mud- and siltstones with desiccation cracks (Fm).
- Planar or trough and tabular cross-bedded, aeolian sandstones (Spe, Ste).

Amongst the outcrops sampled, true gravelly deposits and conglomerates (Gm, Gp) are only present in a section in the Pirmasens area, where the Hauptkonglomerat unit of the Middle Buntsandstein is exposed (Grabowska, 2011; Pucknat, 2011). Although the so-called “Eck´sches-Konglomerat” was recorded at the Molkenkur in Heidelberg, it is represented by a pebbly medium to coarse, cross-bedded sandstone.

Figure 5: (a) Pervasively bleached sandstone, white to yellowish-brown colour. Typical "Haardtrand Fazies". The colours follow the bedding planes. Vertical scale is approximately 1 m. Lower Buntsandstein (Rehberg-Sch.), quarry Hanbuch, Neustadt a.d.W. **(b)** Yellow, red and white sandstones. The colours follow the bedding planes. White bleaching zones are best developed around fractures. Lower Buntsandstein, Cleebourg. **(c)** Red sandstone with minor bleached layers, hardly visible on the weathered surface. This is the most common appearance of the Buntsandstein in South Germany. Vertical scale is approximately 3 m. Lower Buntsandstein, Rockenau.

Most part of the Lower and Middle Buntsandstein is made up of trough and planar cross-bedded sandstones. Grain sizes from fine to coarse and partly pebbly sand were observed in cross-bedded sandstones. Bed thickness varies between a few decimetres up to several meters, when individual sand bodies are amalgamated (e.g. quarries Leistadt and Hanbuch).
Sandstones with mud clasts generally appear at the base of cross-bedded sand bodies or above erosional surfaces and are commonly cross-stratified.
Rippled sandstones were rarely recorded, e.g. in fine sandstones of the Middle Buntsandstein in the Wolfsschlucht (Zwingenberg) along with desiccation cracks (Wasielka, 2012). Climbing ripples were observed in the Middle Buntsandstein around Pirmasens (Pucknat, 2011).
Cross-bedded sandstone bodies are commonly intercalated with laminated fine sand-/siltstones and/or laminated silt-/mudstones. The laminated beds usually exhibit a more or less pronounced erosional surface at the top. Thickness and lateral extent strongly correlate: centimetre -thick beds usually taper out within a few decimetres while beds with a thickness of several decimetres can extend over several tens of meters or exceed the outcrop scale (tens to hundreds of metres).
Desiccation cracks are commonly only preserved as moulds at the base of sandstones because mud beds are usually very thin.
Steeply planar or trough cross-bedded sandstones with tabular cross-stratification were only observed in the area west of the river Rhine. In grain mount the sand grains of these deposits exhibit a frosted surface. In thin section the rims of the grains show numerous small pits and/or inverse grading.
Bleaching is a widespread phenomenon. It was observed in all outcrops as well as in the subsurface, however in strongly differing extent. The scale of bleaching phenomena reached from mm-scale (spots, single laminae) to outcrop and even regional scale (Haardt area). Different types of bleaching could be differed:

1. Bleached spots in red sand- and siltstones (Figure 6a, e, h)
2. Laminar bleaching along bedding planes in red sandstones (Figure 6b, c, g, h)
3. Bleaching associated with fractures (Figure 6c, d)
4. Pervasive bleaching (initial stage in Figure 6c, d)

Types 1 and 2 were commonly observed in red sandstones throughout the study area, on the surface and in the subsurface. Type 3 can be observed in the quarry Cleebourg. Type 4 is typical for the Haardt area, e.g. the quarries in Neustadt a.d.W. and Leistadt. Another phenomenon that can be observed in bleached sandstones is a brown staining, along bedding planes (Figure 6e, f, g) as well as non-stratabound Liesegang rings.

Figure 6: (a) White bleached spots in a very fine sandstone. Vertical scale is approximately 30 cm. Lower Buntsandstein, Hirschhorn. **(b)** Bleaching, which follows complex cross-bedding structures. Lower Buntsandstein, Rockenau. **(c)** Plume-shaped, pervasive bleaching, originating from a fracture and grading into laminar bleaching following the bedding of the sandstone. Vertical scale approximately 30 cm. Lower Buntsandstein, Cleebourg. **(d)** Pervasive bleaching around a fracture. Brown staining (Fe-hydroxide) in direct vicinity to the fracture. Lower Buntsandstein, Cleebourg. **(e)** Strata-bound bleaching with partial brown staining following the bedding of the sandstone. Bleached spots in the overlying red sandstone. Lower Buntsandstein, Cleebourg. **(f)** Almost completely yellowish-brown-stained bleached sandstone. Lower Buntsandstein, Cleebourg. **(g)** Gradual transition from red-bleached to yellowish-brown-bleached sandstone. Lower Buntsandstein, Cleebourg. **(h)** Red clay flakes in a white bleached sandstone. White, circular spots in the red, underlying siltstone. Lower Buntsandstein, Rockenau.

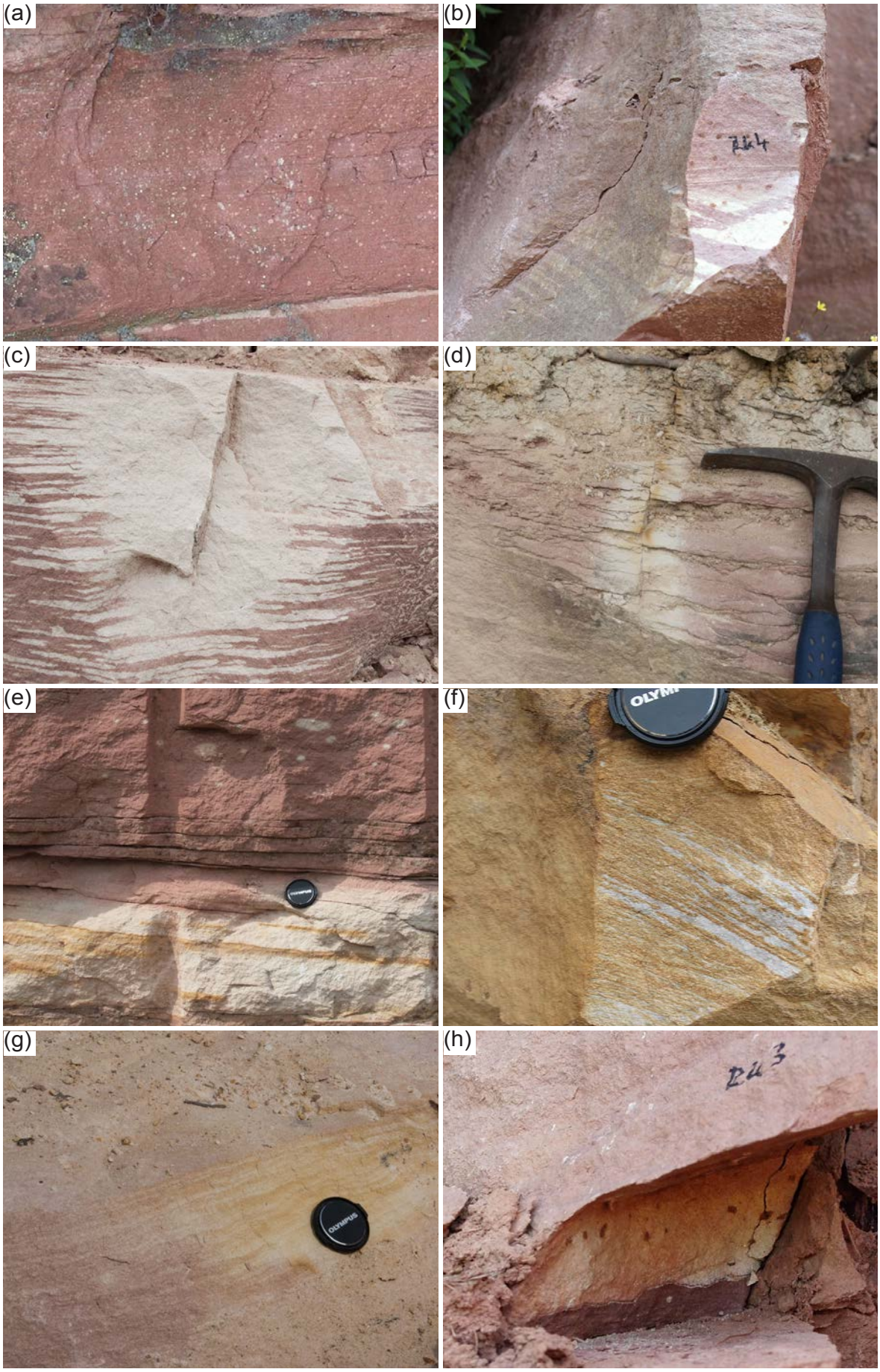
(a)
(b)
(c)
(d)
(e)
(f)
(g)
(h)

3.2 Detrital Mineralogy

The average mineralogical composition can be described as dominantly quartz with K-feldspar content up to 30 % and lithoclast content up to 15 %.
Monocrystalline quartz, strained or unstrained, is the major constituent in almost all samples (52-16 %). The amount of polycrystalline quartz varies between 22 and 2 %. Combined CL and optical characteristics of quartz were surveyed (Chapter 2.3). CL-colours of quartz grains were mostly light or dark violet. Brownish and bright red colours are less common. Monocrystalline quartz frequently exhibits short-lived blue luminescence, as does the quartz from a Variscan granite in Heidelberg. Quartz with strong undulose extinction often appear particularly dark in CL. Monocrystalline quartz commonly contained fluid inclusions, fluid inclusion trails and microcracks. Zoned or patchy CL was occasionally observed particularly in quartz with red CL-colour.
Only orthoclase/microcline (Figure 7a) potassium feldspar was detected. Neither Ca- nor Na-bearing feldspar was found, despite very rare occurrences within lithoclasts. Occurrence of distinctively Ba-bearing alkali feldspar was proven by SEM-EDS. Lithoclasts can be subdivided into intrabasinal and extrabasinal ones. The latter group makes up to 15 % of the whole rock and mostly represent phyllitic or quartz-mica-gneissic and some mylonitic detritus (Figure 7b-e). Pebble-sized, well-rounded, feldspar-free quartzite clasts were rare. Intrabasinal lithoclasts are usually reworked mudrock flakes. These can make up to 24 % of the whole rock. Due to their strongly reduced density compared to other sand-sized detrital grains like quartz and feldspar, clay flakes are always pebble-sized. Smaller sized clay flakes cannot be contemporaneously deposited at the same flow conditions.
Mica (mostly muscovite, subordinately biotite) contents rarely exceed 1 %. Muscovite is significantly more common than biotite. Heavy minerals observed were (in descending order) tourmaline (Figure 7f-g), zircon (Figure 7h-k), magnetite (commonly Ti-bearing), rutile, apatite and monazite.
According to the classification of McBride (1963) most samples plot in the fields of lithic subarkose and subarkose. Fewer samples are classified as arkoses, lithic arkoses, lithic subarkose, lithic arenite, and litharenite (Figure 8).

Figure 7: (a) Crossed twinning in microcline. The feldspar is intermediately weathered. Cross polarized light. Middle Buntsandstein (Upper Felszone), Rodalben. **(b)** Phyllitic lithoclast. This specimen is particularly quartz-rich and almost completely lacks phyllosilicates. Cross polarized light. Lower Buntsandstein (Bausandstein), Rockenau. **(c)-(d)** Mica-schist lithoclast under normal (c) and cross-polarized (d) light. Blue stained resin. Lower Buntsandstein (Bausandstein), Rockenau. **(e)** Quartzose mylonitic lithoclast. Cross-polarized light. Lower Buntsandstein, Cleebourg. **(f)-(g)** Zircon under normal (f) and cross-polarized (g) light. Blue stained resin. Lower Buntsandstein (Bausandstein), Rockenau. **(h)-(i)** Pleochroism in tourmaline: both images show the same specimen turned by 90 degrees. The tourmaline is dark brown in (h) and light greenish brown in (i). Normal polarized light. Blue stained resin. Lower Buntsandstein (Bausandstein), Rockenau. **(j)-(k)** Brown tourmaline under normal (j) and cross-polarized (k) light. Blue stained resin. Lower Buntsandstein (Bausandstein), Rockenau.

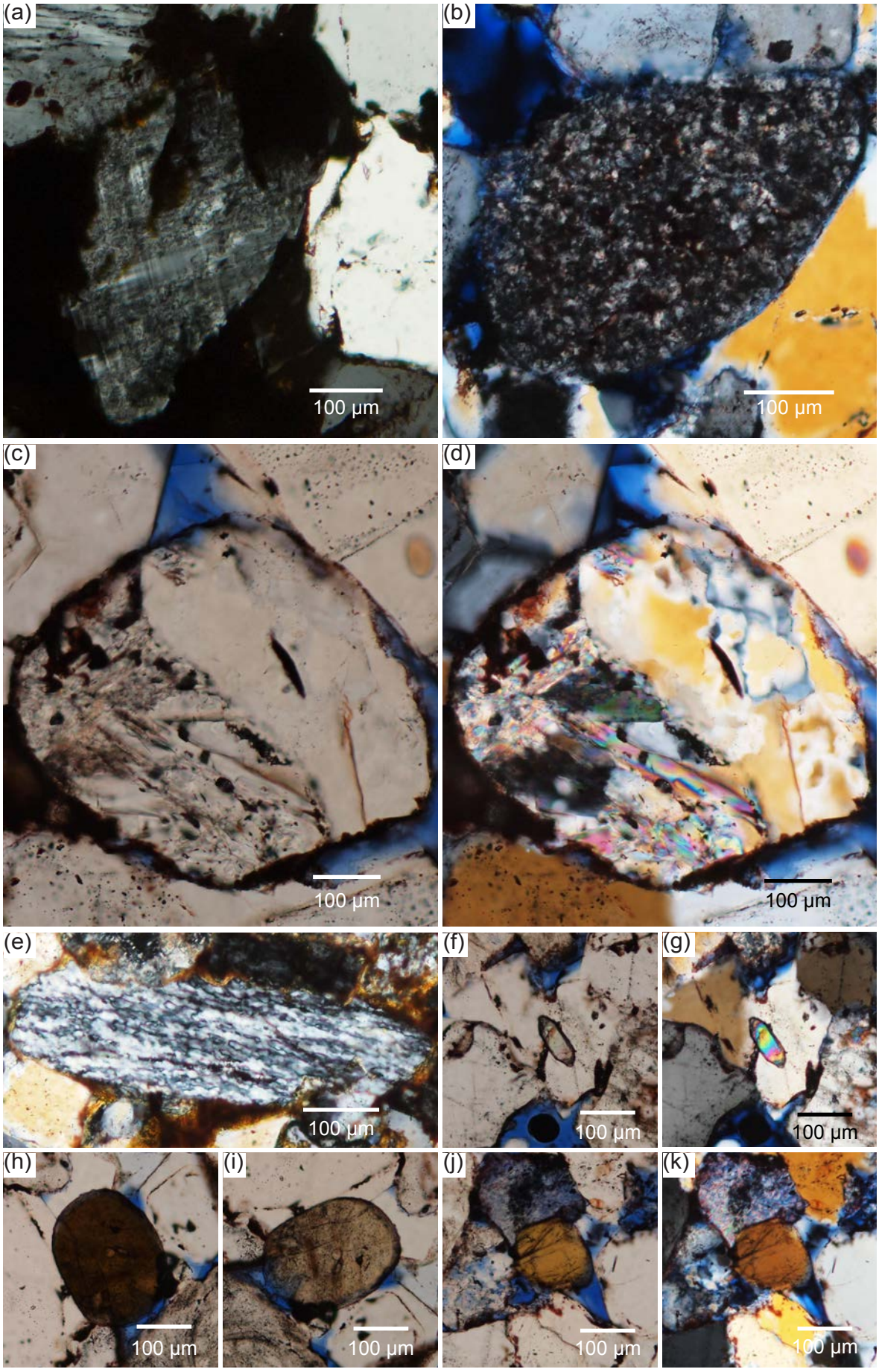
(a)
100 µm
(b)
100 µm
(c)
100 µm
(d)
100 µm
(e)
100 µm
(f)
100 µm
(g)
100 µm
(h)
100 µm
(i)
100 µm
(j)
100 µm
(k)
100 µm

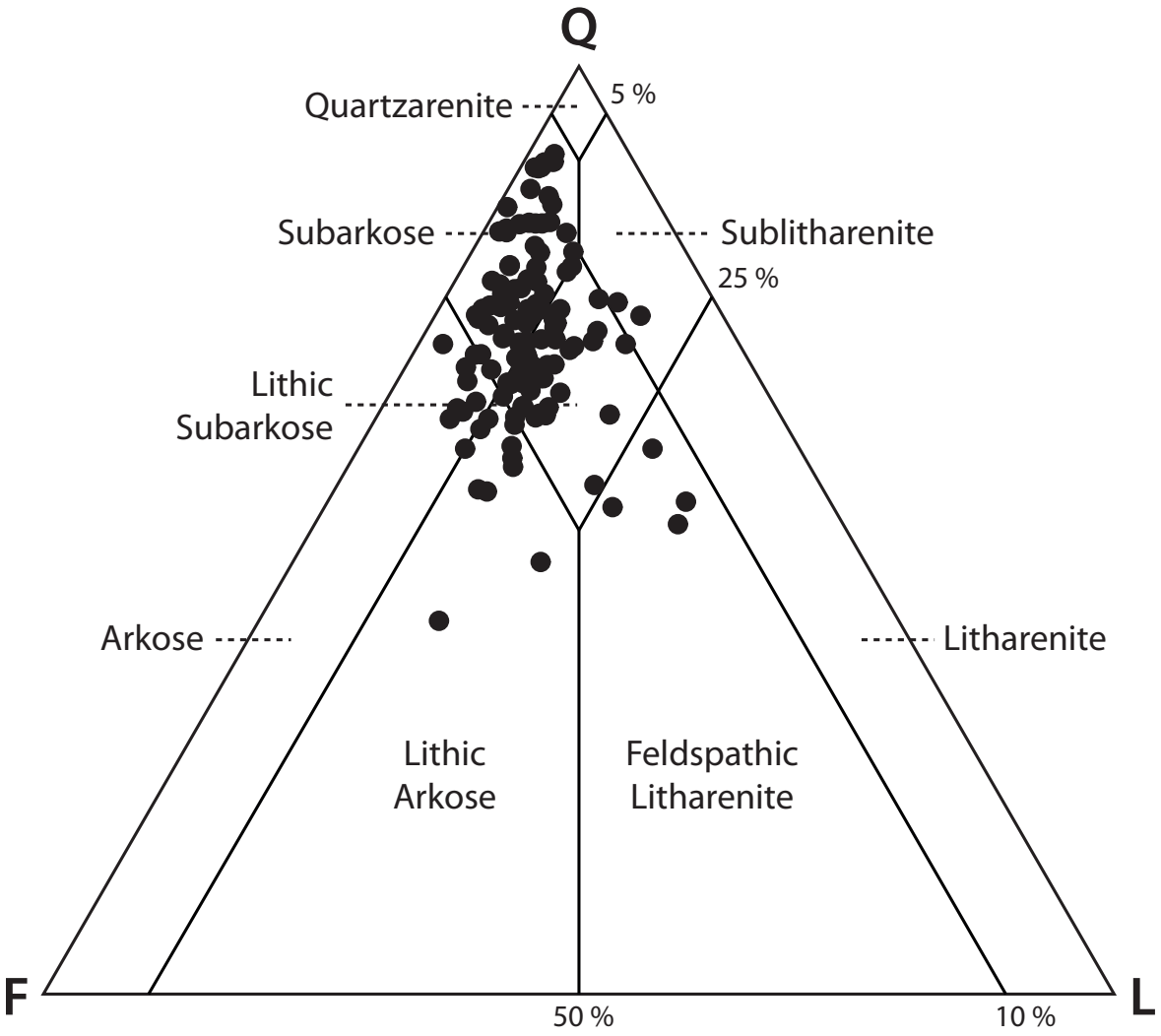

Figure 8: Modal composition of Buntsandstein sandstones surveyed. Most samples are arcosic sandstones. Sandstones with significantly elevated lithoclast contents contain abundant intrabasinal clay flakes rather than lithoclasts derived from the hinterland. Classification after McBride (1963).

3.3 Authigenic Mineralogy

3.3.1 Fe-Oxide and Fe-Hydroxide

The colour of the Buntsandstein is mainly characterized by the presence and the kind of Fe-oxide and/or –hydroxide. Both Fe-oxide and –hydroxide were usually found to be associated with clay minerals (mainly illite), giving them a reddish, brownish or opaque appearance. Massive Fe-hydroxide was detected as fracture infill in the quarry Leistadt. Pure, microscopic authigenic Fe-oxide was rarely found closely associated with weathered ilmenite (Figure 9a).
The Buntsandstein from the "Haardtrand" (Leistadt, Neustadt a.d.W.) is characterized by a yellowish to light brown colour, different from the red colour of non-bleached Buntsandstein. This colour is caused by the presence of goethite and lepidocrocite as shown by XRD analysis (Appendix 8). Reddish-opaque haematite may only be preserved in clay flakes (Figure 6h).

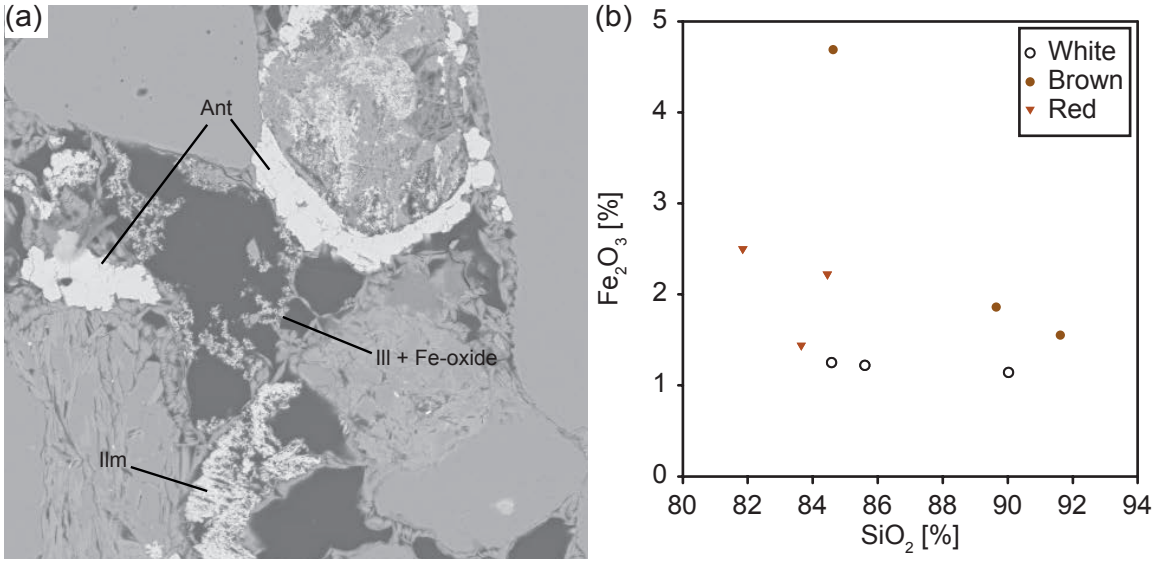

Figure 9: (a) Weathered lithoclast surrounded by authigenic anatase (Ant) and illite coated with Fe-oxide (Ill + Fe-oxide). Most probably the source for both authigenic precipitates is the partly dissolved ilmenite (Ilm) in the lower part of the image. Lower Buntsandstein, Cleebourg. **(b)** The iron content of white, bleached sandstones is usually significantly lower than of red, non-bleached sandstones. Brown sandstones can exhibit highly elevated iron contents. The additional iron is interpreted to be reimported into previously bleached sandstones (Chapter 4.4.8).

The quarry Cleebourg, which is also located within the "Haardtrand" bleaching zone, contains a supposedly large fault. Besides yellowish-brown and red sandstone, white sandstone is present within the fault core and around fractures. With increased distance from the fault, the latter interfingers with red and yellowish-brown-bleached sandstone. The illite in the white sandstone is completely colourless (Chapter 3.3.2.1), and the iron appears to be concentrated in some discrete layers or on fracture planes.
The bulk Fe-content of completely white sandstones is significantly lower than the one of red sandstones. Yellowish-brown samples can reach high Fe-contents (Figure 9b). Fe-oxide in red sandstones exposed in Cleebourg forms opaque to dark red rims around detrital grains and occasionally opaque to dark red pore-filling aggregates. SEM-EDS reveals, that both rims and pore-filling aggregates are a mixture of Fe-oxide and illite.

3.3.2 Clay Minerals

Illite and kaolinite were observed, the former is the most common authigenic clay mineral in the samples examined. Illite/smectite (I/S) mixed-layer clay minerals can be present, but they are not clearly distinguishable microscopically.
The results of XRD analyses from all over the study area are attached in Appendix 8. The grain size fraction <2 µm from 22 samples was separated and analysed by the method described in Chapter 2.5.
The porosity of clay aggregates cannot be quantitatively deduced from thin sections. However, SEM observation suggests, that they usually contain significant microporosity of easily several ten percent. The microporosity in clay aggregates has no positive influence on the quality of a sandstone reservoir, however, it is measured by porosimetry and should therefore be considered.

3.3.2.1 Illite and Smectite

The proportion of smectite versus illite was always distinctly less than 10 % (Chapter 4.4.2.2). Thus, in this chapter illite as well as I/S mixed-layer clay minerals are both summarized under "illite". This mineral occurs in three different morphotypes:

- Pore-lining illite,
- Pore-filling illite or replacing meshwork illite,
- Radial, grain-coating fibrous illite.

Pore-lining illite

Pore-lining illite is the most common type. It mostly appears as grain-coating illite platelets tangential to the detrital grain (Figure 11, Figure 14a, Figure 15a). Tangential clay coatings adjacent to open pore space are most commonly thicker than coatings at grain contacts. In roughly medium sand-sized or coarser-grained sandstones with low compaction, coatings at grain contacts can be absent. Conversely the coatings become significantly more frequent in fine-grained sandstones (Figure 10).

The illite is commonly mixed with Fe-oxide/hydroxide, which significantly control the rock colour: in pure, white sandstones, illite plates are almost colourless (Figure 11a), whereas in yellowish to light brown sandstones they are commonly impregnated with Fe-hydroxide, causing the single platelets to appear dark brown to opaque (Figure 11a, b, c). In red sandstones, single clay crystals are commonly invisible, because there is a dense dark-red to opaque mixture of illite and Fe-oxide/hydroxide (Figure 11d). Especially in red sandstones the total amount of coating illite is presumably overestimated because of the dark colour and the therefore overrated thickness of the coatings by oblique cutting of grain boundaries in thin section. The latter effect becomes particularly obvious contrasting normal light microscopy with CL illumination, where opaque grain coatings are largely eliminated and the true extent of the grain boundaries becomes visible (Figure 12d-e). Illite and Fe-oxide/hydroxide cannot be distinguished by point counting. However, SEM-EDS examination suggests that the amount of Fe-oxide/hydroxide is considerably lower than the one of illite, even in totally opaque coatings. Consequently, coating illite was assigned to three different classes: (i) colourless tangential illite, (ii) dark brown to opaque tangential illite with single illite plates still visible, and (iii) dark red to opaque coatings with no illite aggregates visible.

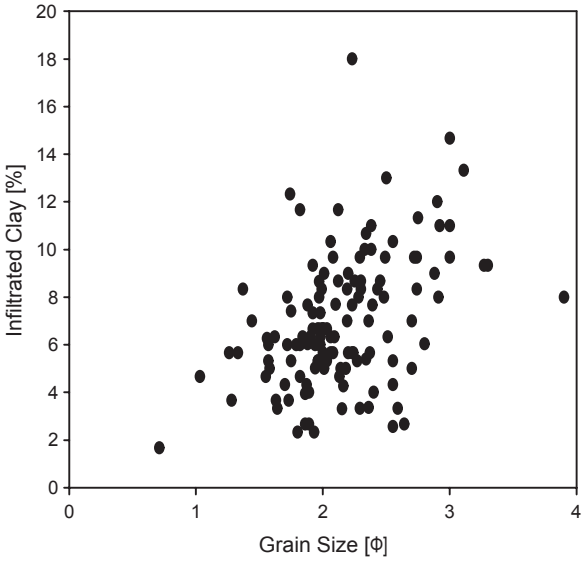

Figure 10: Increasingly fine grained sediments are able to fix increasing amounts of clay from suspension. The actual amount of infiltrated clay is dependent on the amount of clay suspension available and probably the original plagioclase content (Chapter 4.4.2).

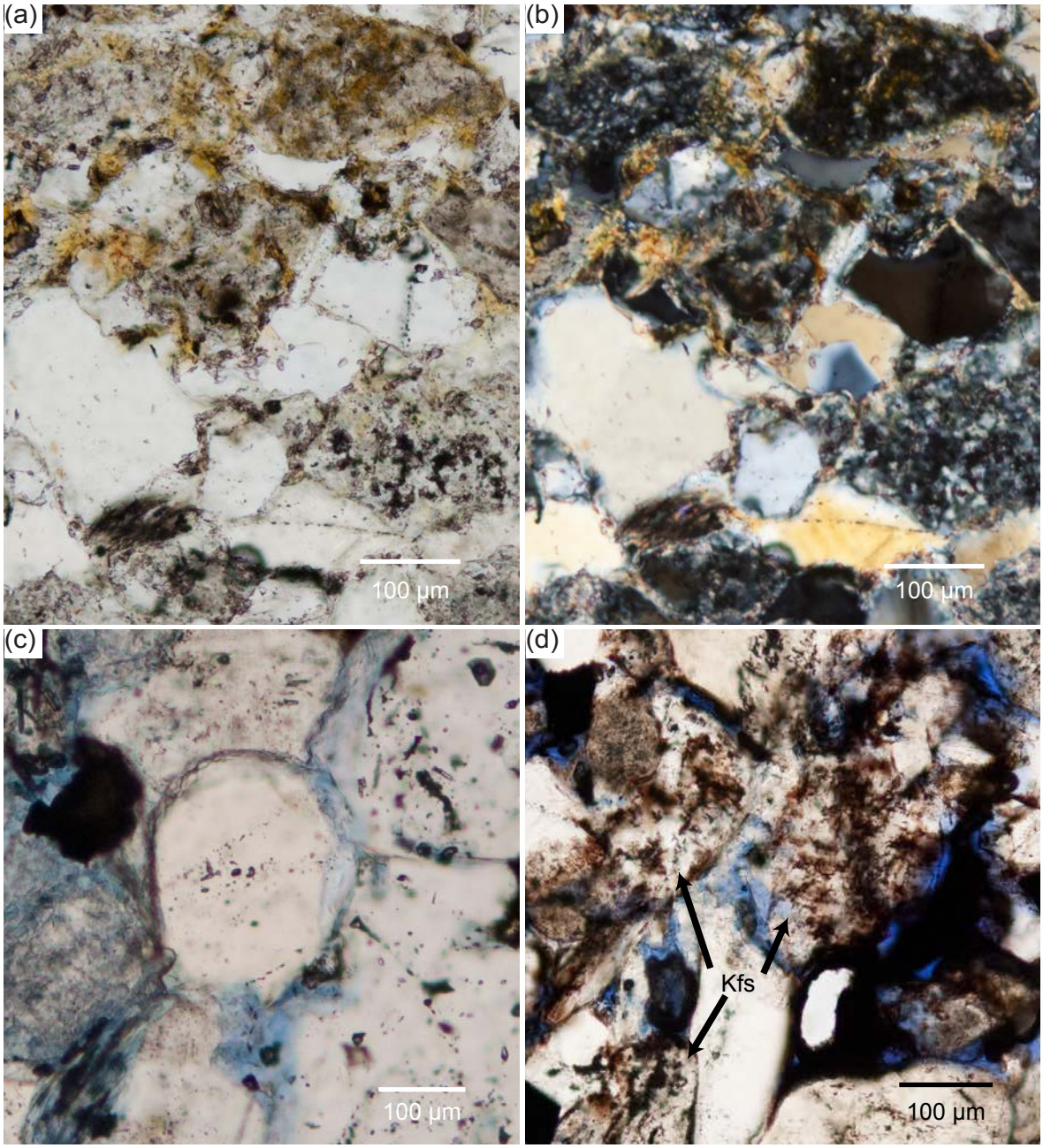

Figure 11: (a)-(b) Illite in a laminar bleached sandstone under normal polarized light (a) and cross polarized light (b). In hand specimen the upper part of the image corresponds to a brown stained lamina and the lower part to a white bleached lamina. Pore-filling illite and tangential illite mixed with Fe-hydroxide in the upper part of the image, indicated by brownish staining of the felt-like illite aggregates. Illite in the bleached lamina is completely colourless and is only revealed by elevated birefringence under cross polarized light. Bleached sandstone. Lower Buntsandstein, Cleebourg. **(c)** Layers of tangential illite plates coating detrital grains. Note the dark staining of the single illite platelets, indicating the association with Fe-hydroxide. Blue stained resin. Bleached sandstone, normal polarized light. Lower Buntsandstein, Cleebourg. **(d)** Opaque to dark red, grain-coating and pore-filling illite mixed with Fe-oxide/hydroxide. Reddish colour indicates the presence of haematite. Mineralogical composition of opaque aggregates can only be revealed by scanning electron microscopy. Note the pervasive growth of illite + Fe-oxide/hydroxide on K-feldspar grains (Kfs) indicating incipient illitization of the feldspars. Blue stained resin. Red sandstone, normal polarized light. Lower Buntsandstein (Bausandstein), Rockenau.

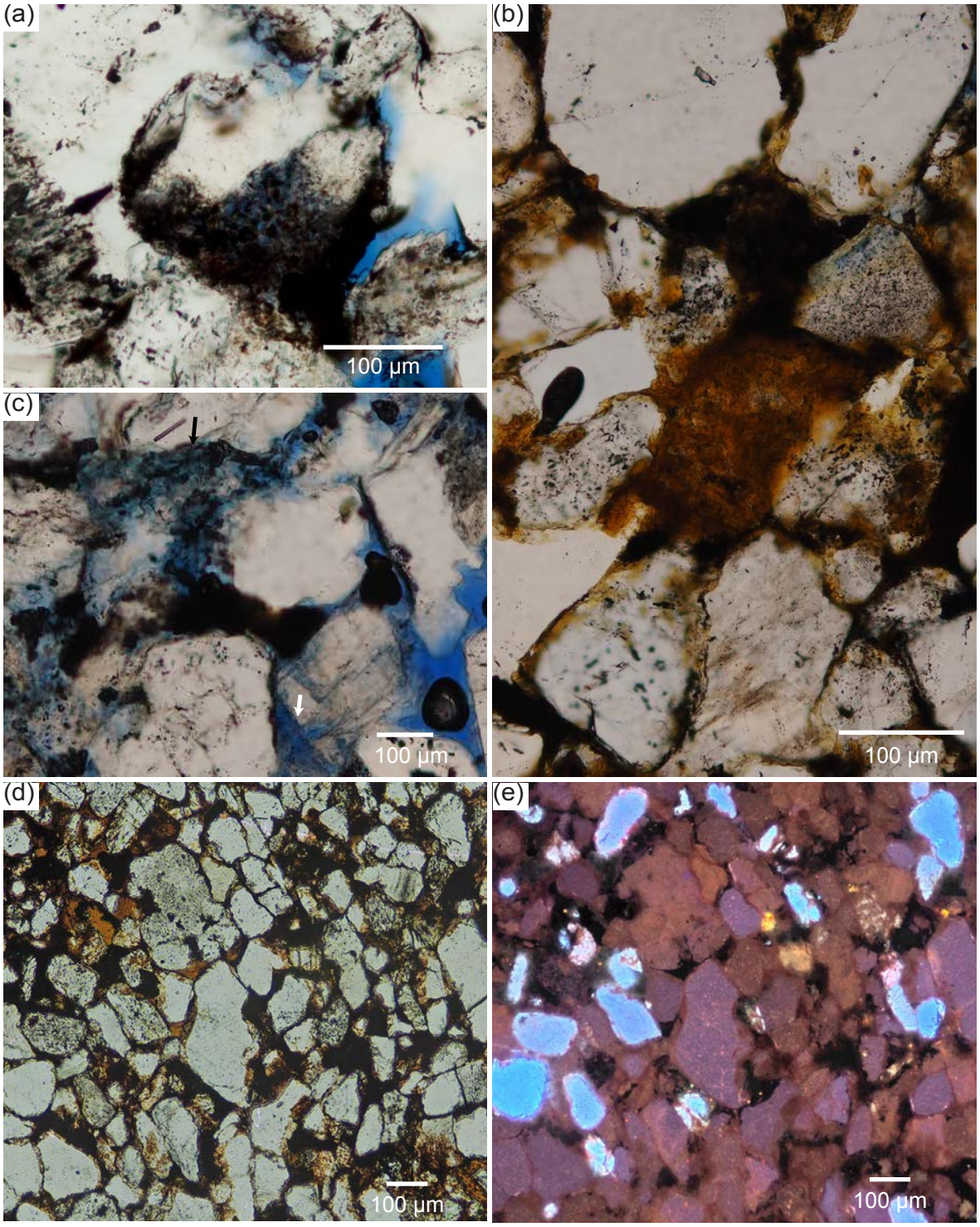

Figure 12: (a) A mixture of illite, quartz and Fe-oxide/hydroxide. Illite replaces K-feldspar as is revealed by SEM-EDS (compare Figure 13c and d; Figure 13c shows approximately the same image section as this figure). Red sandstone. Lower Buntsandstein (Bausandstein), Neckargemünd. **(b)** A mixture of illite and Fe-oxide/hydroxide partially replaces a clast in a red sandstone. Lower Buntsandstein, Cleebourg. **(c)** K-feldspar is replaced by a mixture of illite and Fe-oxide/hydroxide (top, black arrow). On the bottom of the image feldspar dissolution without or with minor illite precipitation can be observed (white arrow). Lower Buntsandstein, Cleebourg. **(d)-(e)** Identical section of a red sandstone in normal transmitted light (a) and CL (b). Note that many grains in transmitted light are partially (e.g. the feldspar in the lower centre with blue CL) or completely (e.g. the zircon in the upper centre with yellow CL) occluded by an opaque mixture of illite and Fe-oxide. Middle Buntsandstein (Karlstal Sch.), Rodalben.

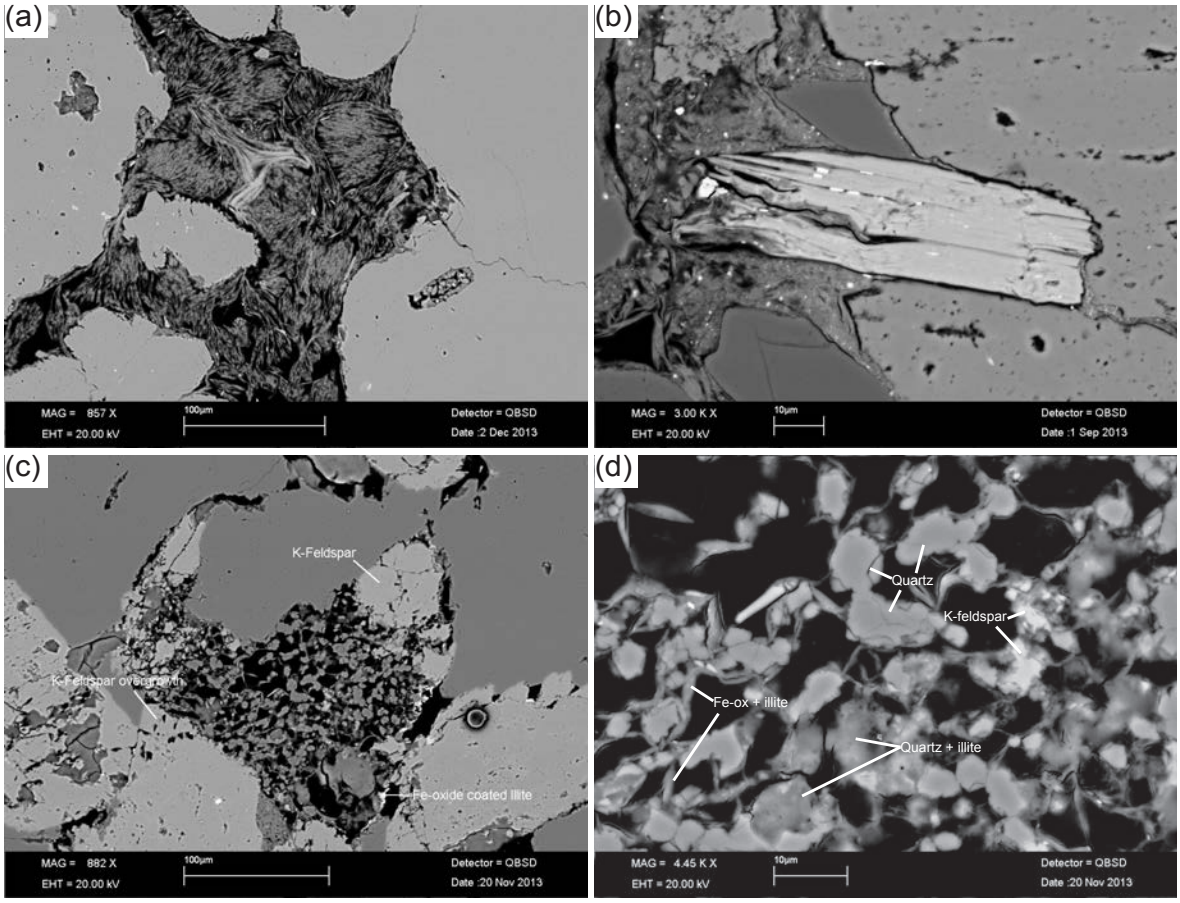

Figure 13: (a) Backscattered SEM image showing kaolinite intergrown with and replaced by illite. Kaolinite is characterized by "booklet" structure. Bleached sandstone. Lower Buntsandstein (Rehberg Schichten), quarry Hanbuch, Neustadt a.d.W. **(b)** A biotite flake is heavily weathered and replaced by illite on the side, which extends into the pore space. Illite replacement propagates along the layers of the sheet silicate. Around the right side of the biotite, the adjacent K-feldspar grain is dissolved ("pressure solution"), without deformation of the biotite. Red sandstone. Lower Buntsandstein (Bausandstein), Riesenstein, Heidelberg. **(c)** A K-feldspar grain is partially leached and replaced by a mixture of illite, Fe-(hydr)oxide, quartz and K-feldspar. Adjacent feldspar overgrowths have irregular surfaces, caused by incipient dissolution. Figure 12a shows the same image section in transmitted light. Detailed view of the replacing mineral composition in Figure 13d. Red sandstone. Lower Buntsandstein (Bausandstein), Neckargemünd. **(d)** Detailed view of the mineral composition replacing the detrital K-feldspar in Figure 13c. Illite flakes are mixed with Fe-oxide/hydroxide giving the opaque appearance in transmitted light on Figure 12a. Red sandstone. Lower Buntsandstein (Bausandstein), Neckargemünd.

The total content of coating illite varies between 3 and 18 % with the gross of the samples plotting between 3 and 10 %. Illite coatings are considerably more frequent in fine- to very fine-grained sandstones. Chemically the grain coating illite is commonly Mg-bearing, corroborating a smectite component and/or a smectitic precursor.

Pore-filling illite or replacing meshwork illite

A transitional type between pore-lining and pore-filling illite are plugs at pore throats (Figure 14b). The distinction from meshwork illite using light microscopy is often difficult, especially if the illite aggregates are associated with Fe-oxide/hydroxide causing an opaque appearance. Only SEM imagery can facilitate a

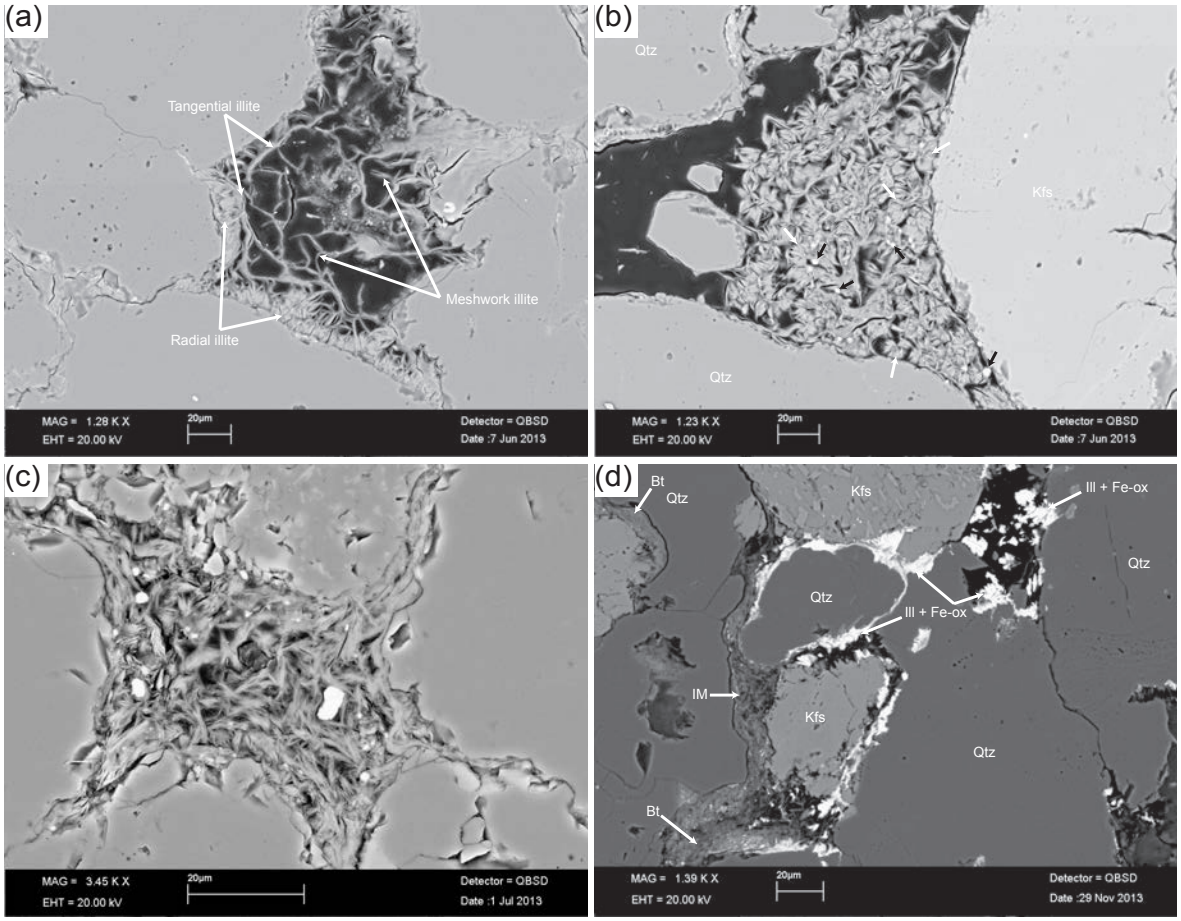

Figure 14: (a) Three generations of illite can be observed: The earliest generation is tangential illite, which is, in this case, detached from the grain surface by dense, fibrous radial illite. The open pore space (black) is filled by loose meshwork illite. Meshwork illite is tied in tangential and radial illite. Detrital grains are quartz. Red sandstone. Middle Buntsandstein (Geröllsandstein), Ettlingen. **(b)** Meniscal bridge of illiteat a pore throat. Illite platelets commonly resemble the kaolinite "booklet" structure (white arrows). Hence, illite replaces a former kaolinite precipitate. Detrital grains are quartz (Qtz) and K-feldspar (Kfs). Bright crystals, <5 µm in size, are Ba-phosphate (black arrows). Red sandstone. Middle Buntsandstein (Geröllsandstein), Ettlingen. **(c)** Dense, felt-like pore-filling illite. The illite is apparently squeezed between grain contacts and in pore throats. Laminar bleached red sandstone. Lower Buntsandstein, Cleebourg. **(d)** Grain-coating and pore-filling illite strongly impregnated with Fe-oxide (Ill + Fe-ox), indicated by the very bright colour and by SEM-EDS analysis. Under optical light this illite type forms opaque grain-coatings and pore-fillings. Another generation of meshwork illite (IM, see arrow left centre) replaces a strongly weathered biotite (Bt, see arrow lower left). Detrital grains are quartz (Qtz), K-feldspar (Kfs) and biotite (Bt). The K-feldspar in the centre has a strongly etched surface. Red sandstone. Lower Buntsandstein (Bausandstein), Rockenau.

distinction but is not suitable for the handling of large sample numbers. Thus, illite appearing as plugs was recorded together with meshwork illite during petrographic analysis. Further discussion on the probable occurrence of each is provided in Chapter 4.4.2.2.

Plugging and pore-filling illite can be particularly observed in most fine to very fine grained sandstones. Pore-filling illite is generally less common than coating illite with contents between 0 and 12 %. Pore-filling illite shows various morphologies. Most commonly it appears as a rather loose platy meshwork or as dense hairy aggregates. Like coating illite, pore-filling illite also tends to be mixed with Fe-

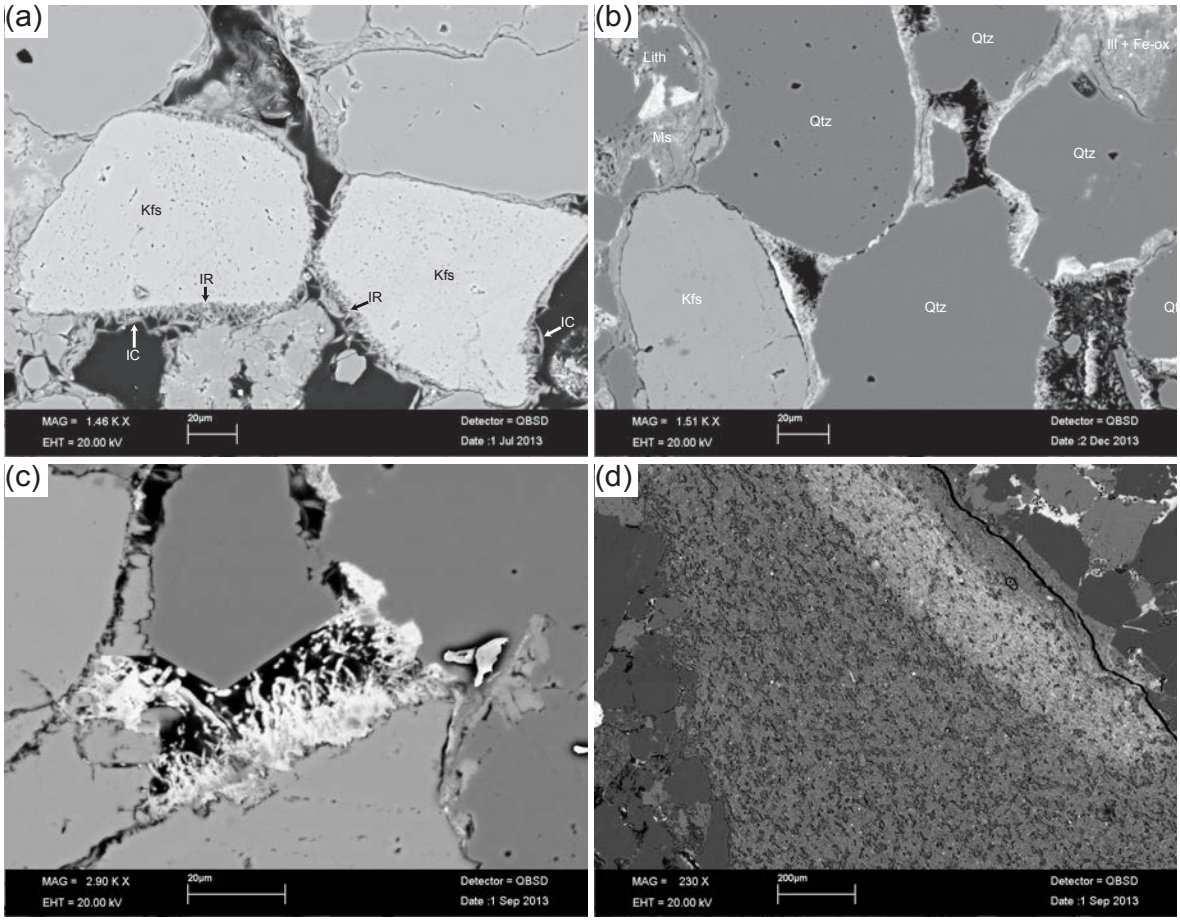

Figure 15: (a) Fibrous radial illite (IR) grows on detrital K-feldspar (Kfs) and detaches earlier grain-coating tangential illite (IC) from the grain surface. The feldspar grains are etched, probably because radial illite grows in expense of K-feldspar. Bleached sandstone. Lower Buntsandstein, Cleebourg. **(b)** Radial illite grows on both K-feldspar (Kfs) and quartz (Qtz) grains. Illite is strongly impregnated with Fe-oxide/hydroxide, particularly near the grain surface, as is revealed by the bright colour. On the top right there is a very dense aggregate of illite and Fe-oxide/hydroxide (Ill + Fe-ox). Other detrital grains are lithoclasts (Lith) and muscovite (Ms). Partly bleached sandstone. Lower Buntsandstein, Cleebourg. **(c)** Radial illite, strongly impregnated with Fe-oxide/hyrdoxide. Red sandstone. Lower Buntsandstein (Bausandstein), Riesenstein, Heidelberg. **(d)** Detrital clay flake in sandstone. Dense mixture of crytpocrystalline clay minerals and very fine grained quartz, clearly distinguishable from authigenic clay. Red sandstone. Lower Buntsandstein (Bausandstein), Riesenstein, Heidelberg.

oxide/hydroxide (Figure 11a, Figure 12a). Hence, three different types were distinguished conforming to the classification of coating illite: (i) colourless pore-filling illite, (ii) dark brown to opaque illite with single crystals visible, and (iii) opaque aggregates of illite together with Fe-oxide/hydroxide. As stated before, if mixed with Fe-oxide or -hydroxide, meshwork illite and infiltrated illite plugs could hardly be distinguished by optical microscopy. Both are summarized under "pore-filling illite".

However, unlike coating illite and illite plugs, meshwork illite not only occurs in pore spaces but also replaces detrital grains. Most commonly feldspar is replaced as shown by feldspar remnants within illite meshwork, detected under SEM-EDS (Figure 12a, c, Figure 13c, d). Meshwork illite replacing feldspar exhibits a distinct appearance under the light microscope: either illite plates are mixed

with opaque Fe-oxide rich spots, or, when illitization is incomplete, former grain boundaries can still be deduced. However, it is not clear in every case, whether illite replaced K-feldspar or plagioclase. For further details compare Chapter 4.2.3 and Chapter 4.4.2.2 as well as Figure 40.
Pseudomorphs of illite after kaolinite were commonly observed under SEM (Figure 13a, Figure 14b), corroborating the replacement of kaolinite by illite. They cannot be observed under transmitted light.
Subordinately illite replaces mica (preferably biotite, Figure 13b, Figure 14d) and feldspar-bearing lithoclasts. Illite, which clearly replaces detrital grains, was counted separately from pore-filling illite during point counting.
Pore-filling illite aggregates are often squeezed between adjacent detrital grains (Figure 14c) and might therefore be the weathering product of a former detrital grain. However, without any remnants of a detrital precursor, this assumption remains speculative. The inability to clearly distinguish between primary pore-filling and secondary pore-filling (i.e. detrital mineral-replacing) clay minerals complicates or prohibits the assessment of the intergranular volume (IGV) and the compactional index (ICOMPACT) in clay-rich sandstones (see Chapter 3.4).
Detrital clay can usually be easily distinguished from infiltrated and authigenic clay (Figure 15d).

Radial, grain-coating fibrous illite
Radial, fibrous illite is the least common illite type with contents usually below 1 %. This type consists of µm-scaled illite plates that radially grow on the surface of detrital grains. Radial illite preferably grows on K-feldspar, but also on quartz grains. It is commonly developed below tangential illite plates. It can therefore detach tangential illite coatings from the detrital host (Figure 14a, Figure 15a, b, c).

3.3.2.2 Kaolinite

Kaolinite was found in most samples examined by SEM but usually in low proportions. It is therefore often not recorded by point counting. In the samples analysed, average contents are well below 2 %. At the Haardtrand, no isolated kaolinite was found, it was always associated with illite (Figure 13a). In the Odenwald kaolinite was commonly found to replace K-feldspar or to precipitate in vicinity to dissolved K-feldspar (Figure 17, Figure 18). Pure kaolinite postdates significant compaction, whereas mixed illite-kaolinite is commonly squeezed in the pore throats (Figure 14b, Figure 40 on page 58). Kaolinite is characterized by the typical booklet-like alignment of the crystal plates and by a lower birefringence than illite. However, due to the mixture of kaolinite and illite aggregates, these distinctive features are hardly visible under polarized light and can only be reliably determined by scanning electron microscopy.

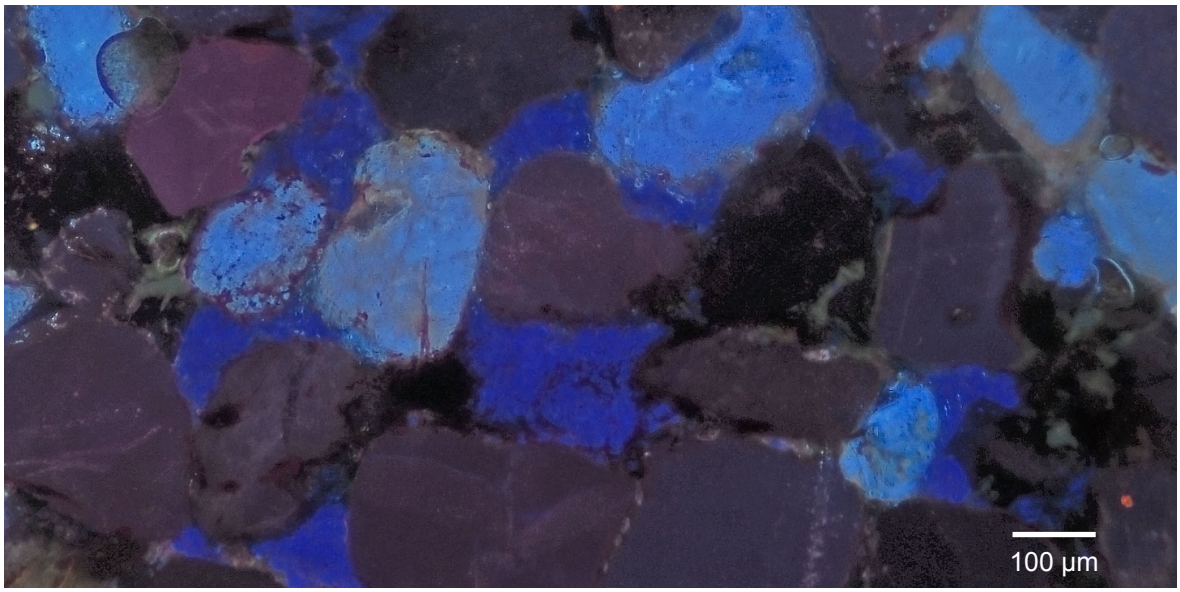

Figure 16: Dark blue luminescent pore filling and replacing kaolinite. Bright blue detrital K-feldspar and violet to glowing red detrital quartz grains. The pale beige-rose rim on the feldspar grain on the uppermost left is authigenic K-feldspar. The image includes the section on Figure 18a. Red sandstone. Lower Buntsandstein (Bausandstein), Neckargemünd.

3.3.2.3 Chlorite

Different from previous descriptions (Hoppe, 1927; Valeton, 1953), no chlorite was found microscopically. It could only be detected under SEM and XRD (Clauer et al., 2008), where it forms rare trace amounts. XRD analysis of the clay fraction from 22 samples (Appendix 8) corroborates the absence of chlorite in sandstones studied. Chlorite was only detected in siltstones from the Upper Buntsandstein (Appendix 8: Chart 9, Chart 11).

3.3.3 Quartz and amorphous silica

Authigenic quartz always appears as syntaxial overgrowth on quartz grains, possessing the same crystallographic orientation as the detrital grain. Cement overgrowths on monocrystalline quartz are clearly preferred with respect to polycrystalline grains. In the latter case, the different crystallographic orientation of the growing quartz crystals soon interferes with one another, which inhibits further growth. The thickness of the quartz overgrowths from the Palatinate forest usually does not exceed 100 µm. With increasing thicknesses, the overgrowths develop sharp crystal edges resembling idiomorphic quartz crystals. Quartz cements grew therefore in open pore spaces. In the samples from the Palatinate forest, only patchy cements randomly grew on grain surfaces. No continuous quartz overgrowths were detected, coating whole detrital grains. The content of quartz cement in these samples ranges from 0 to 9 %. Appearance and amount of quartz overgrowths is clearly triggered by three factors: grain size, illite coatings, and presence of mudrock clasts.
Generally quartz cement is considerably more common in sandstones with coarser grain size. This means that samples with grain sizes ranging from fine-medium to

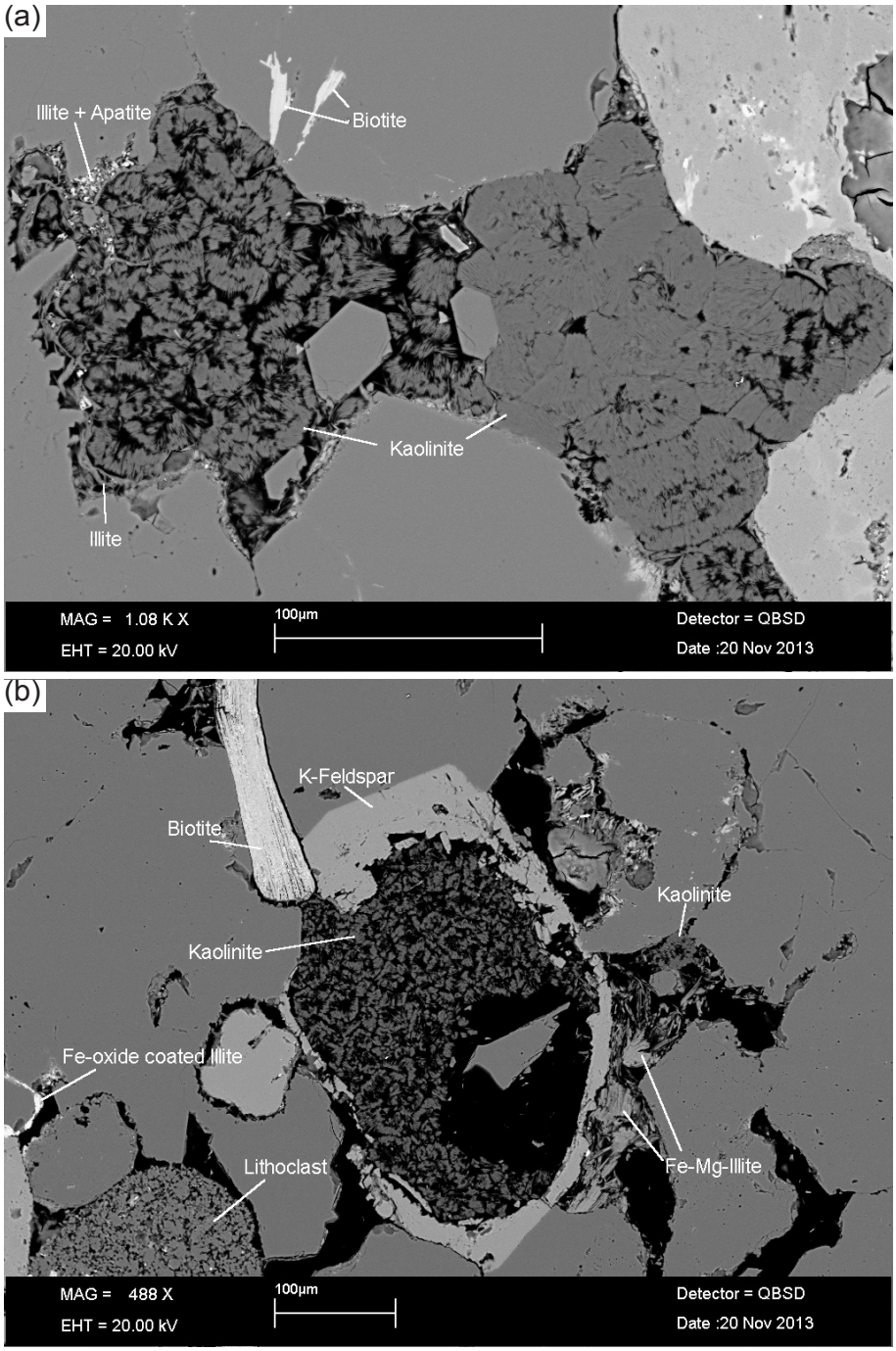

Figure 17: (a) Pore-filling kaolinite showing distinctively different morphology within one connected pore. On the right side of the pore adjacent to detrital K-feldspar grains (light grey) the kaolinite platelets are at least twice the size of the ones on the left side, where the pore is surrounded by detrital quartz grains. The kaolinite aggregate on the right side is very dense, whereas the one on the left reveals a considerable amount of microporosity (black). Tangential illite coatings around detrital grains are visible but no intergrowth of authigenic illite and kaolinite is observed. The image reveals an enlarged section in the lower left of Figure 18a (black frame). Red sandstone. Lower Buntsandstein (Bausandstein), Neckargemünd. **(b)** K-feldspar in the centre of the image contains a dissolved core, which is in large parts filled with a loose aggregate of replacing kaolinite, characterized by typical “booklet” structure. On both the upper and the lower side of the feldspar grain there are syntaxial overgrowths covered by authigenic quartz (Figure 18b). The surfaces of the overgrowths are not etched. In the pore space adjacent to the feldspar grain there is more kaolinite and Fe-oxide/hydroxide-stained illite, which replaced kaolinite (Fe-Mg-illite). The image shows a similar area as Figure 18b. Red sandstone. Lower Buntsandstein, Neckargemünd.

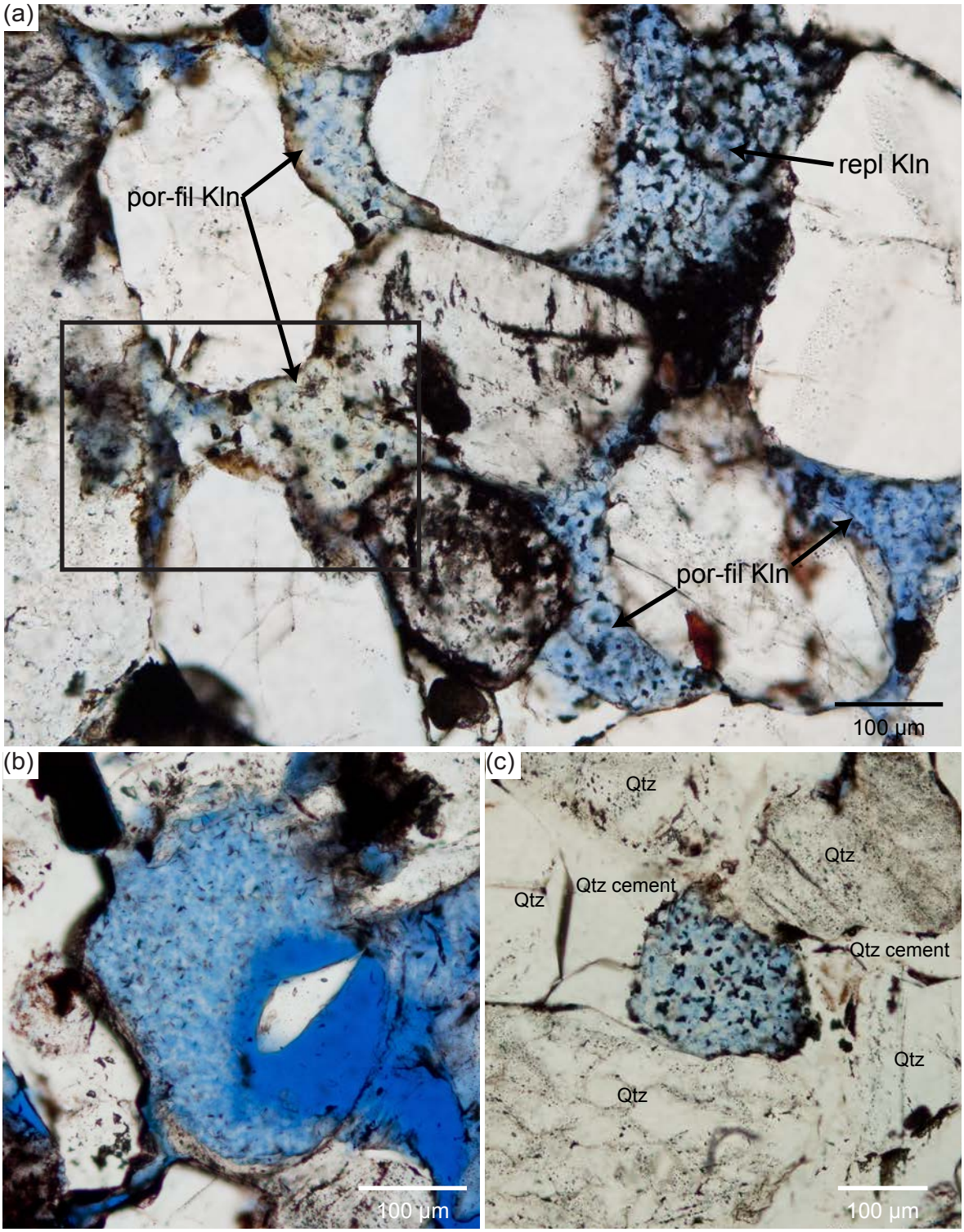

Figure 18: (a) Pore-filling (por-fil Kln) and replacing (repl Kln) kaolinite in a red sandstone. Replacing kaolinite yields opaque patches, which are probably Fe-oxide/hydroxide coated illites. Detrital grains are coated by a reddish-brown mixture of illite and Fe-oxide/hydroxide. The frame corresponds to the image section in Figure 17a. Blue stained dye. Red sandstone. Lower Buntsandstein (Bausandstein), Neckargemünd. **(b)** Kaolinite replaces a detrital grain, still marked by the ferrous former illite coating. The image shows a similar area as Figure 17b. Blue stained resin. Red sandstone. Lower Buntsandstein (Bausandstein), Neckargemünd. **(c)** Kaolinite replacing K-feldspar surrounded by authigenic and detrital quartz (Qtz). The ferrous illite coating of the replaced detrital grain is still visible. Dark patches within the kaolinite aggregate are possibly Fe-oxide stained illites. Red sandstone. Lower Buntsandstein (Bausandstein), Neckargemünd.

Figure 19: (a)-(b) Red, translucent carnelian under normal (a) and cross-polarized (b) light. Middle Buntsandstein, Wolfsschlucht, Zwingenberg. **(c)** Dark to medium purple and non-luminescent, zoned quartz overgrowths. Probably the latter initially exhibited short-lived blue luminescence. Feldspars are overexposed due to the weak luminescence of the cements. Porosity is black. Lower Buntsandstein (Rehberg-Sch.), Leistadt. **(d)-(f)** Chalcedony under normal (d), cross-polarized (e) light and CL (f). Chalcedony exhibits a concentric texture under transmitted light and CL and radial extinction under cross-polarized light. Epoxy resin in (d) is brown due to CL electron bombardment. Lower Buntsandstein (Rehberg-Sch.), Leistadt. **(e)-(f)** Sandstone with quartz overgrowths under transmitted light (e) and CL (f). The overgrowths exhibit short-lived blue luminescence with some zonation. Most quartz grains equally exhibit short-lived blue luminescence while some grains remain non-luminecent. Lower Buntsandstein (Rehberg-Sch.), quarry Hanbuch, Neustadt a.d.W.

medium sand frequently exhibit considerable contents of quartz cement, whereas samples with grain sizes smaller than 2.5 Phi usually comprise no or little quartz cement.

As mentioned in Chapter 3.3.2.1, the frequency of illite coatings is considerably higher in fine- to very fine-grained sandstones, quartz cementation is less strong in these sediment types. If illite coatings were not continuous, quartz overgrowths, which started from uncoated spots, incorporated the illite coatings. Quartz cements have not been found in pores where no detrital quartz was present. In contrast, if detrital clay appears as macroscopic clay flakes, quartz cement is readily observed. Cathodoluminescence colours of quartz vary between non-luminescent, blue and dark to medium purple (Figure 19c, h). Some cements exhibit zonation patterns. Blue luminescence is usually very short lived and can be easily missed (Figure 21). In the stage of the short-lived luminescence, these cements may also exhibit complex zonation. Once vanished, the short-lived luminescence does not recur. This type of luminescence was found throughout the study area.

The extent of quartz cementation shows a clear regional trend. None of the analysed samples from the western flank of the Upper Rhine Graben exceeds 10 % quartz cement, while samples from the eastern flank reach >30 % (Figure 20). This trend is

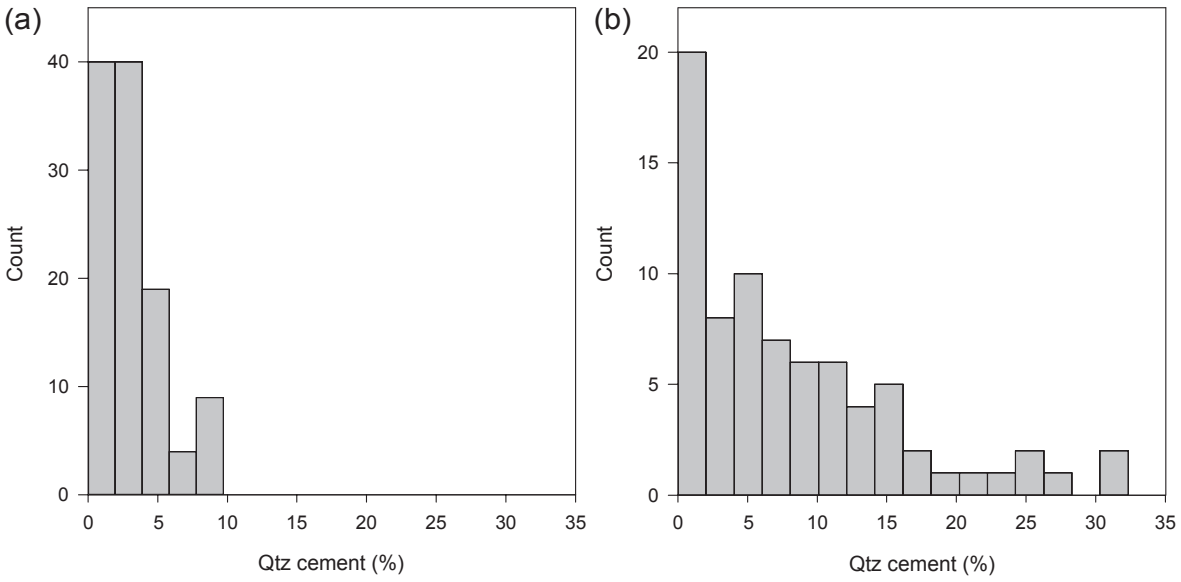

Figure 20: Regional distribution of the observed percentages of intergranular quartz cement on the (a) western and (b) eastern flank of the URG. While quartz cement contents >10 % were commonly observed on the eastern flank, no sample exceeding 10 % quartz cement was observed on the western flank.

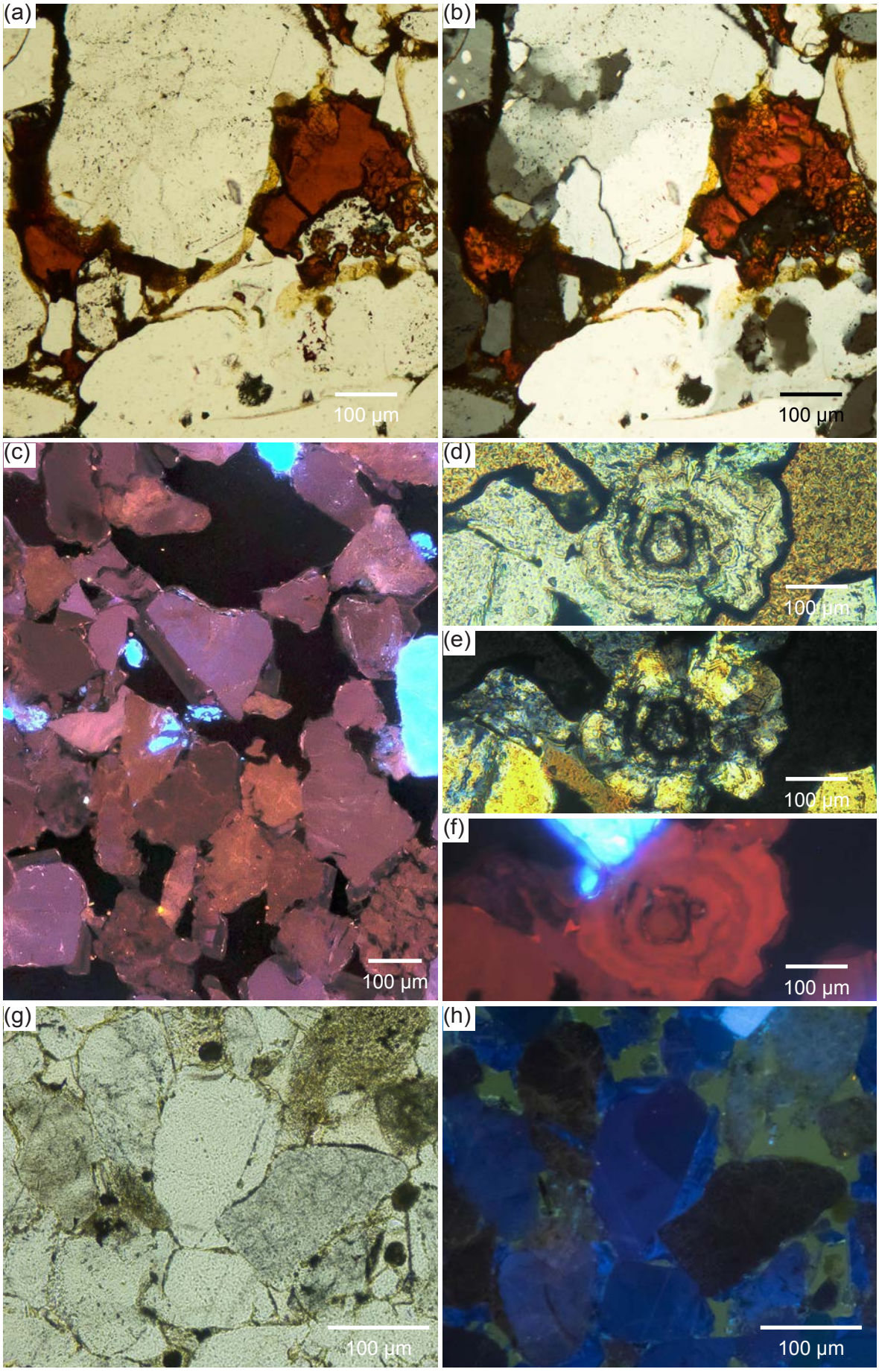
(a)
100 µm
(b)
100 µm
(c)
100 µm
(d)
100 µm
(e)
100 µm
(f)
100 µm
(g)
100 µm
(h)
100 µm

Figure 21: (a)-(c) Short-lived blue luminescence in quartz after one second (a), four seconds (b) and one minute (c) exposure to the hot-CL electron beam. The white arrows exemplary indicate two quartz overgrowths. Note how the blue luminescence of the left overgrowth is already hardly visible on image (b). After one minute (c) all overgrowths appear completely non-luminescent. Note that most detrital quartz grains also exhibit a short-lived blue luminescence, which subsequently fades into a reddish-brownish-violet colour. The same behaviour was observed on magmatic quartz in a granite from Russenstein, Heidelberg. The green, fading luminescence is caused by the epoxy, i.e. it indicates porosity. Bright blue luminescence indicates K-feldspar. Lower Buntsandstein (Rehberg-Sch.), Leistadt. **(d)-(e)** Zoned, short-lived blue luminescent quartz overgrowths after one second (d) and after some seconds (e) electron bombardment under CL. Note the initial short-lived blue luminescence in detrital grains. Bright blue luminescence by K-feldspar. Green luminescence by epoxy resin. Middle Buntsandstein (Geröllsandstein), Ettlingen.

already observable in the field: Buntsandstein rocks east of the URG are commonly very hard and splintery, while the rocks in the west often crumble and are sandy. Carnelian (Figure 19a-b) and chalcedony (Figure 19d-f) were rarely detected. They can appear cumulative in specific dolomite-carnelian and/or dolomite-chalcedony beds together with dolomite nodules.

3.3.4 Feldspar

Authigenic feldspar overgrowths on detrital K-feldspar are present in almost all samples (Figure 22). SEM-EDS analysis reveals the cements to chemically conform to an orthoclase end-member and form rhomb shaped overgrowths. Usually the cement surfaces are etched and commonly overgrown by radial illite, like the ones of detrital K-feldspar. Unaltered K-feldspar cement is only preserved, when overgrown by authigenic quartz. However, the detrital grain is always more readily dissolved than the cement. The most obvious explanation for this phenomenon is, that the solubility of the cement, because of its pure orthoclase composition, is lower than the one of the detrital grain. Although K-feldspar cements are common, they usually constitute less than 1-2 % of the whole rock.

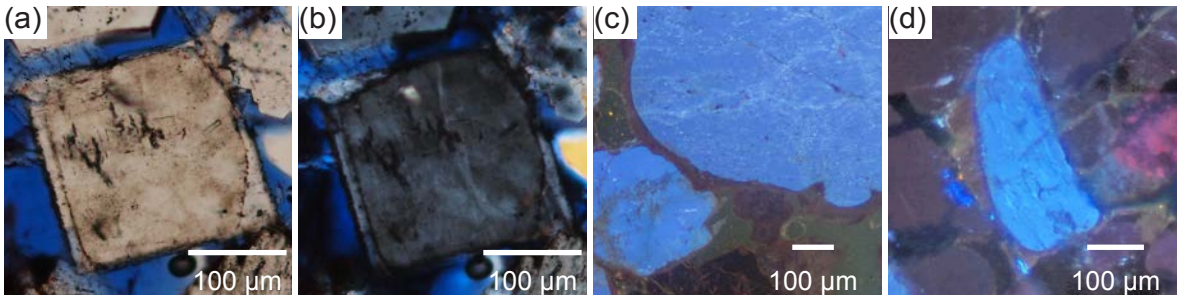

Figure 22: (a)-(b) Authigenic K-feldspar overgrowth on detritic K-feldspar under normal (a) and cross-polarized (b) light. The overgrowths are rhomb-shaped and grow in optical continuity to the detrital grain (b). Red sandstone. Lower Buntsandstein (Bausandstein), Rockenau. **(c)** Poorly developed K-feldspar overgrowth. The K-feldspar overgrowth has a violet luminescence colour and is yet too thin to develop the typical rhomb-shape. Under cathodoluminescence it can be clearly distinguished from the bright blue luminescent detrital host. Cathodoluminescence image. Red sandstone. Upper Buntsandstein (Zwischenschichten), Rodalben. **(d)** Well developed, rhomb-shaped K-feldspar overgrowth on the grain in the centre (bright blue luminescence). The brownish colour is typical for most of the K-feldspar overgrowths observed. Cathodoluminescence image. Red sandstone. Lower Buntsandstein (Bausandstein), Rockenau.

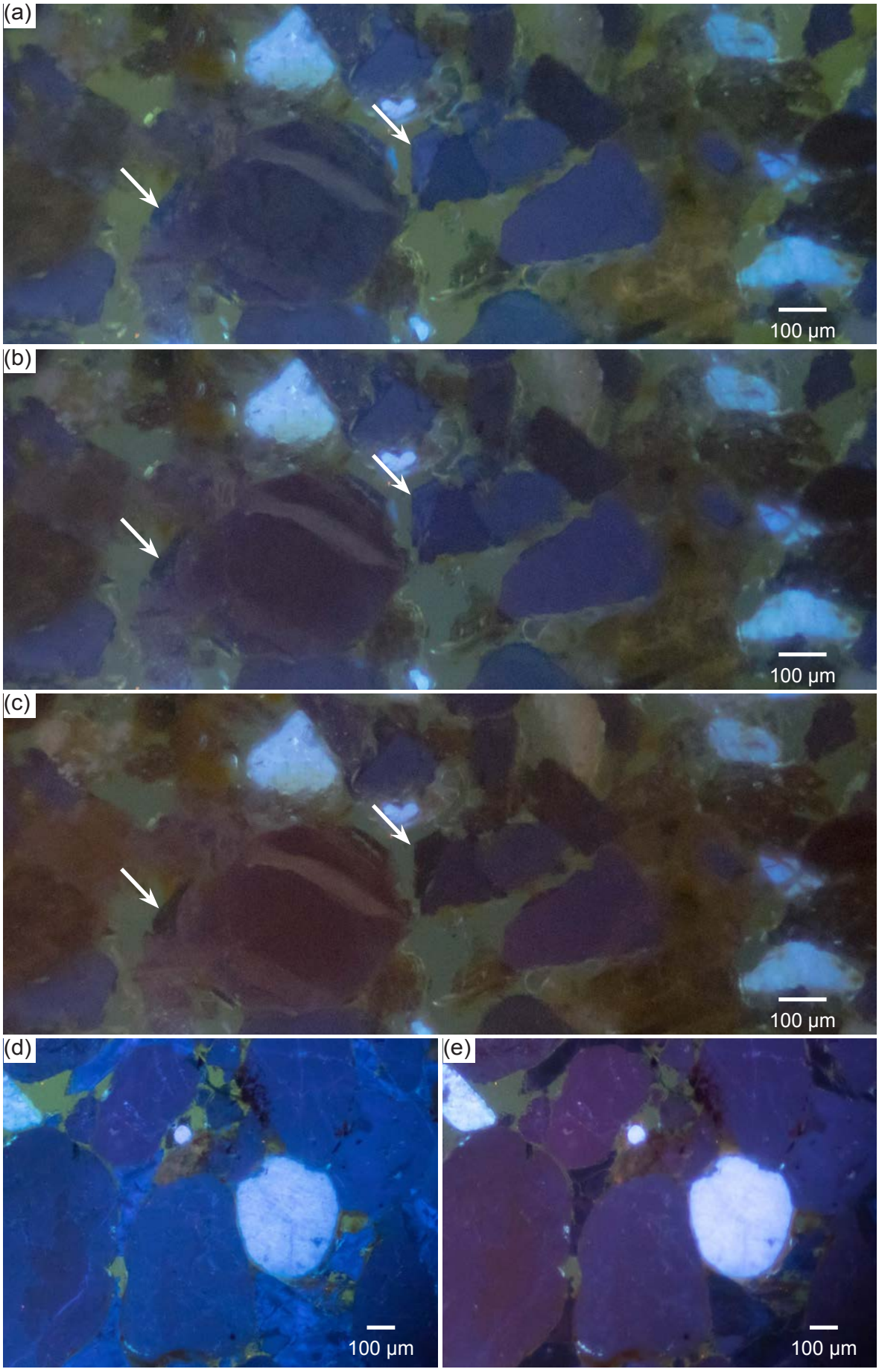
(a)
100 µm
(b)
100 µm
(c)
100 µm
(d)
100 µm
(e)
100 µm

3.3.5 Carbonates

In the outcrops investigated, calcite and dolomite only occur in the Middle and Upper Buntsandstein. Carbonate cements are rare overall and occur either as calcitic/dolomitic pore-filling cement (Figure 24a-b, Figure 26, Figure 27), dolomitic nodules (Figure 24c-d), dolomite replacing K-feldspar (Figure 24a-b), or as calcite, filling secondary porosity (usually due to feldspar leaching, Figure 24a). In a sample from well Well A 2 an iron free, pore-filling dolomite cement was largely replaced by a Mg-Fe-bearing zoned calcite cement (Figure 27). The calcite cement overgrows syntaxial quartz cement, and the surfaces of quartz cement and especially quartz grains are etched at the contact to the calcite cement. Other than dolomite cements, calcite cements commonly exhibit complex zonation patterns in CL and/or in BSE-SEM (Figure 27a). Calcite from the graben flanks exhibits zoned yellow CL (Wasielka, 2012), calcite from the URG subsurface is non-luminescent (Figure 27b).

3.3.6 Barite

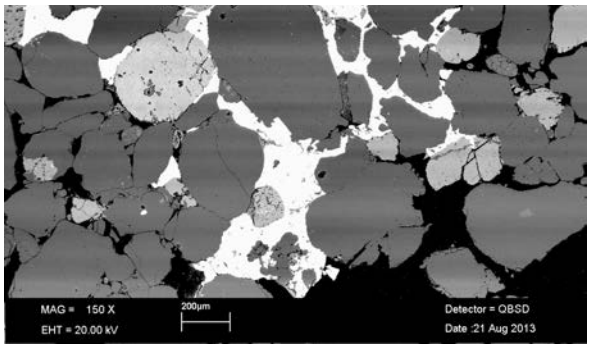

Figure 23: Highly-porous (porosity is black) weakly cemented sandstone with patchy intergranular barite (white). Multiple grains exhibit microcracks, which indicate brittle deformation. Buntsandstein, Well A 2.

Barite cementation of intergranular porosity is very rare. Amongst the outcrops in this study it was only observed in the quarry Leistadt. In the latter outcrop barite was particularly common as fracture mineralization together with Fe-hydroxide (Chapter 3.5).
Intergranular barite is more common in core samples from the URG (wells GTB1 Brühl, Well A 1, Well A 2) than in outcrops (Figure 23). It is not evenly distributed but forms isolated prismatic crystals or patches, which may incorporate some sand grains.

3.3.7 Accessory Minerals

Mn-Fe-oxides commonly appear on fracture planes and can be macroscopically observed as black, dendritic, very thin precipitates. Under the SEM these may appear as grainy aggregates (Figure 28f).
Sample R2/1 IIb from Riesenstein, Heidelberg, contains a Fe-rich, Zn-bearing mineral (Zn-bearing Fe-oxide?). It forms aggregates of elongate, zoned crystals, probably due to association with illite (Figure 28b). In whole rock chemistry this sample showed a significantly elevated Zn-content, still as low as 146 ppm.
Authigenic, Ti-bearing Fe-oxide was detected in various samples (Figure 28c). It forms aggregates of more or less elongate crystals, probably due to association with illite. Ti-content is below 2 atomic percent according to SEM-EDS.
In Cleebourg an authigenic aluminium phosphate-sulphate mineral was detected by SEM-EDS (Figure 28a), filling the open pore space. However the core apparently

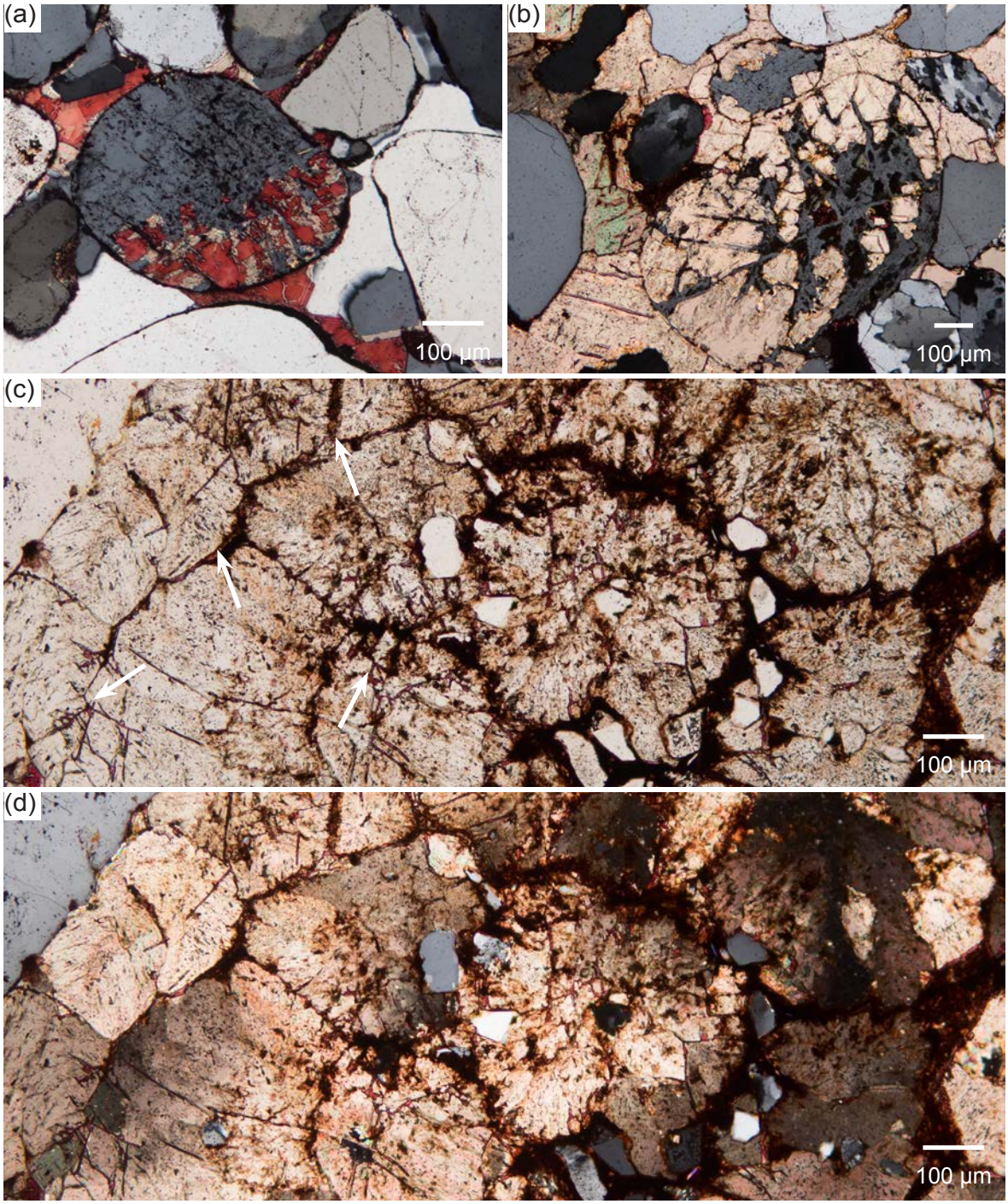

Figure 24: (a) Red-stained calcite fills intergranular porosity and intragranular in K-feldspar. Occasional dolomite (not stained, elevated birefringence colours) may have been replaced by calcite. Cross-polarized light, calcite stained with Alizarinred-S. Middle Buntsandstein, Wolfsschlucht, Zwingenberg. **(b)** Dolomite replaced K-feldspar at the rim of a dolomite nodule. Red-stained calcite in the centre may be an initial stage of dolomite replacement by calcite. Cross-polarized light, calcite stained with Alizarinred-S. Middle Buntsandstein, Wolfsschlucht, Zwingenberg. **(c)-(d)** Dolomite nodule under normal (c) and cross-polarized (d) light. Hardly visible in (c) due to common oxide/hydroxide, red-stained calcite borders the dolomite crystals (white arrows). The dolomite crystals exhibit a vague radial fabric. Some silt-sized quartz grains were incorporated in the centre of the nodule. Calcite stained with Alizarinred-S. Middle Buntsandstein, Wolfsschlucht, Zwingenberg.

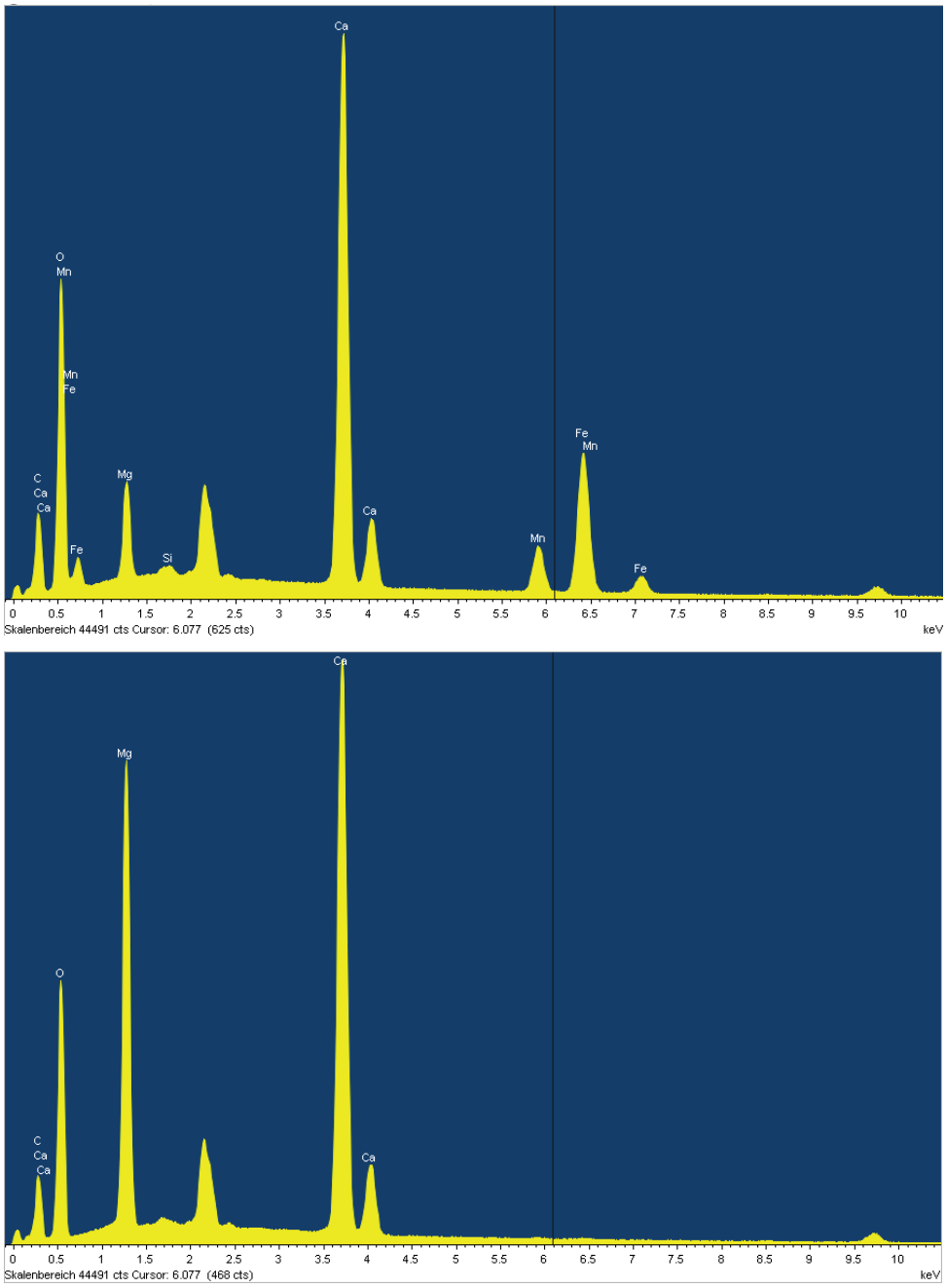

Figure 25: EDS-spectra corresponding to Figure 26a. **Spectrum 1:** Fe-Mn-Calcite. The quantification of the spectrum resulted in 6.33 atom % iron, 2.16 atom % magnesium and 1.04 atom % manganese. **Spectrum 2:** Iron-free dolomite. Peaks are labelled with the corresponding elements. Unlabelled peaks correspond to the gold-coating.

Figure 26: (a) Mg-Fe-Mn calcite (EDS-spectrum 1, Figure 25) replaced iron-free dolomite (EDS-spectrum 2, Figure 25). SEM-EDS proved a gradual transition from dolomite to calcite. The dolomite is usually first replaced by calcite along the grain-boundaries. Other than authigenic quartz, detrital quartz is commonly etched at the contact to the calcite cement (black arrows). White arrows indicate the lower boundary of the quartz grain in the upper left part of the image. Buntsandstein, well Well A 2. **(b)** Calcite postdates authigenic quartz. Detrital quartz as well as authigenic quartz are etched at the contact to the calcite cement (black arrows). Buntsandstein, well Well A 2.

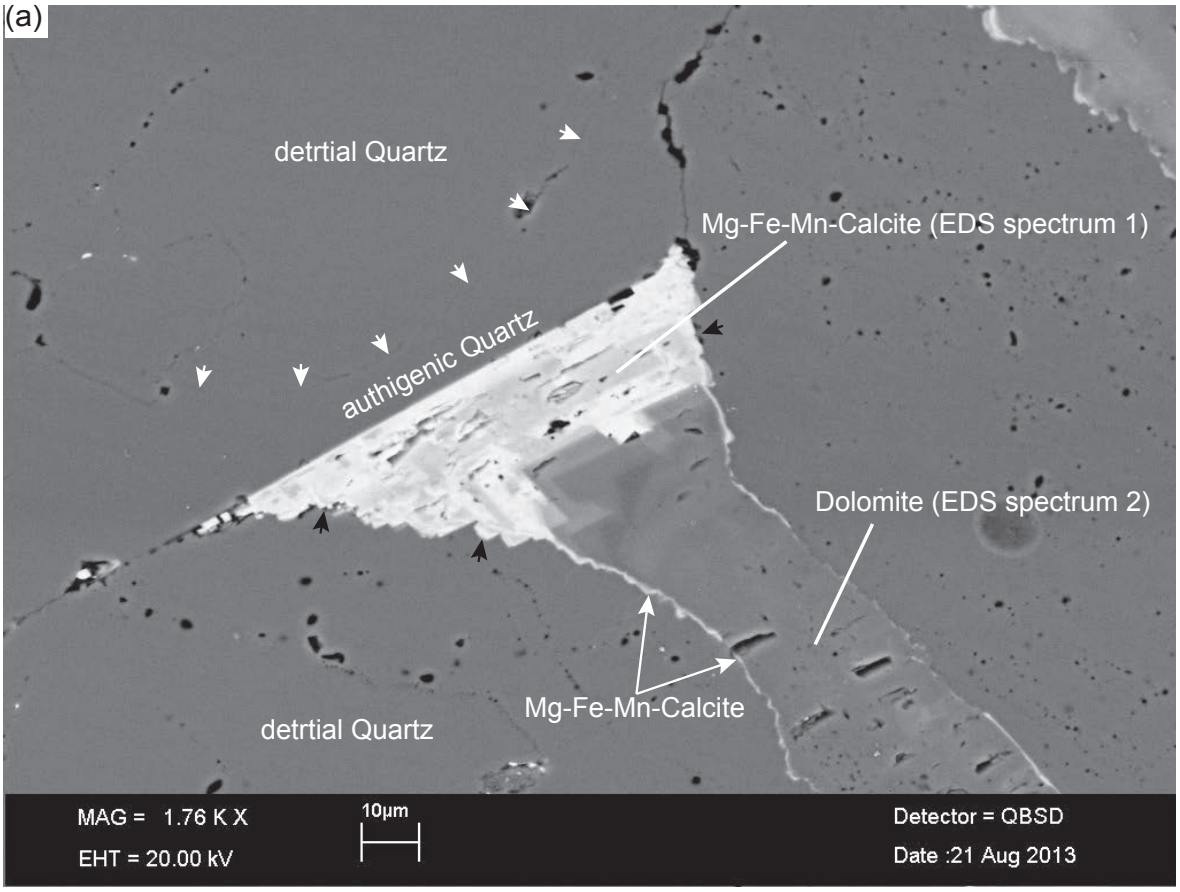
(a)
detrtial Quartz
Mg-Fe-Mn-Calcite (EDS spectrum 1)
authigenic Quartz
Dolomite (EDS spectrum 2)
Mg-Fe-Mn-Calcite
detrtial Quartz
MAG = 1.76 K X
EHT = 20.00 kV
10µm
Detector = QBSD
Date :21 Aug 2013

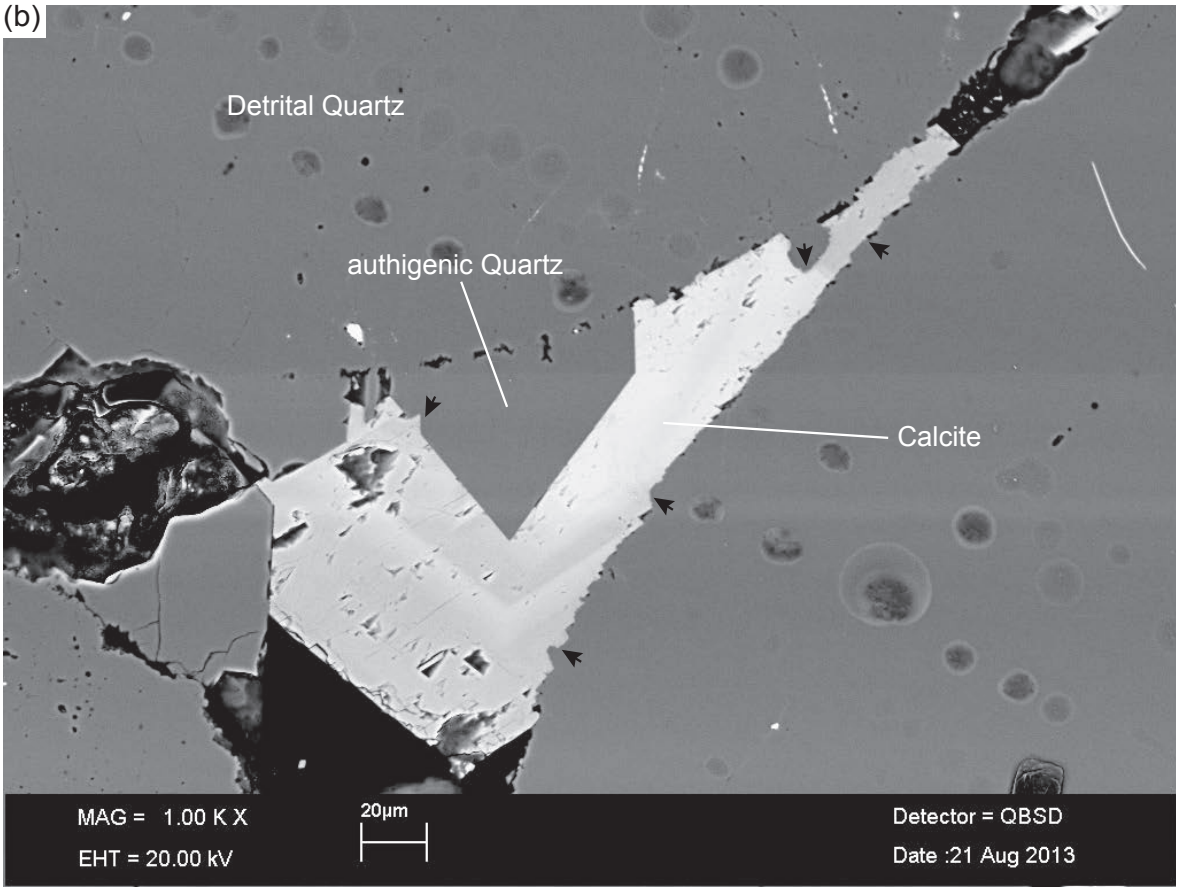
(b)
Detrital Quartz
authigenic Quartz
Calcite
MAG = 1.00 K X
EHT = 20.00 kV
20µm
Detector = QBSD
Date :21 Aug 2013

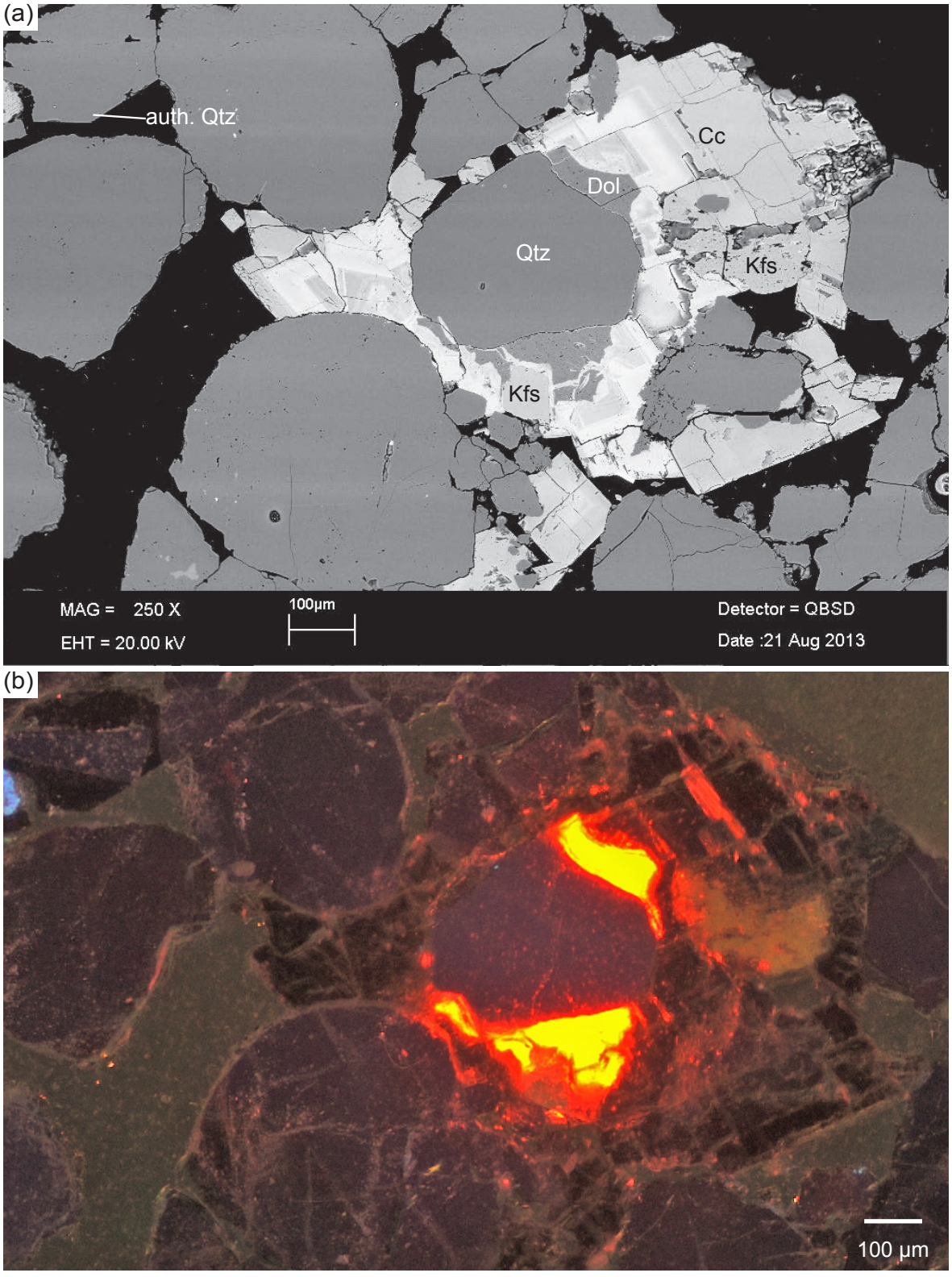

Figure 27: (a) Ferrous, zoned calcite (Cc) replaces dolomite (Dol). The sandstone is made up of detrital K-feldspar (Kfs) and quartz (Qtz). Quartz overgrowths (auth Qtz) cannot be deduced from the SEM image but only in comparison with the CL image (b). Buntsandstein, well Well A 2. **(b)** CL image of (a). Dolomite cement has a bright orange luminescence. Ferrous calcite is non-luminescent. Authigenic quartz cement (compare a; upper left) is also non-luminescent. The K-feldspar surrounded by calcite cement lost its blue luminescence and is brown to non-luminescent instead. Buntsandstein, well Well A 2.

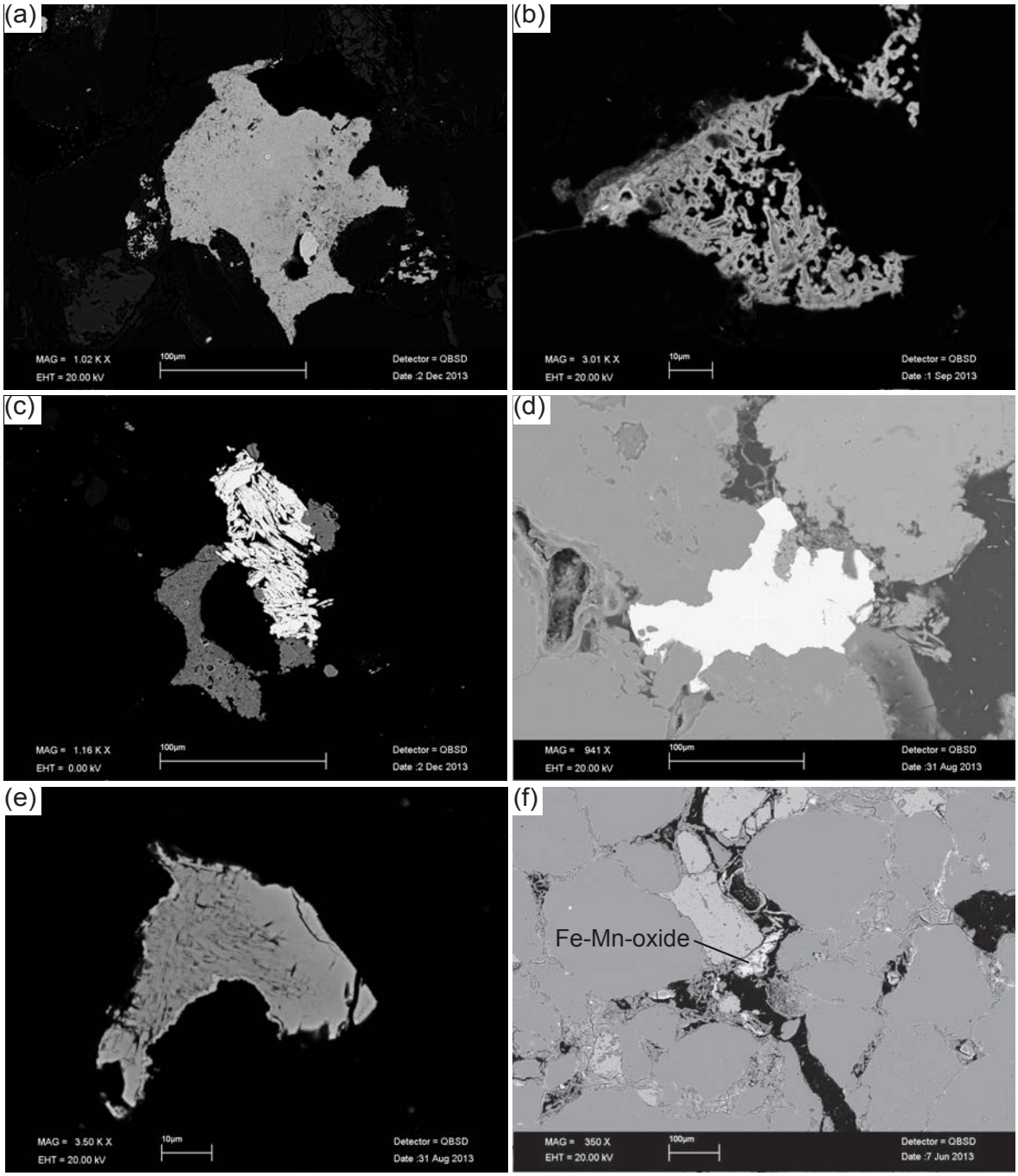

Figure 28: (a) Aluminium-phosphate-sulphate (APS) mineral. Possibly replacement of a more solid detrital grain in the central part. The brightness of the image had to be strongly reduced to display the APS mineral. Therefore surrounding quartz and feldspar grains are almost black. Lower Buntsandstein, Cleebourg. **(b)** Zoned, Zn-bearing Fe-oxide. EDS-spectra suggest that the oxide precipitated on illite. This also explains the elongate crystals. Zn-Fe-oxide thus postdates illite. Lower Buntsandstein (Bausandstein), Riesenstein, Heidelberg. **(c)** Ti-bearing Fe-oxide (white) and apatite (grey). The texture of the Fe-oxide aggregate corroborates the precipitation around illite crystals. The Ti-content indicates biotite and/or ilmenite as a primary source. Lower Buntsandstein, Cleebourg. **(d)** As-Ni-bearing pyrite. Buntsandstein, well Well B 2. **(e)** As-bearing pyrite. Buntsandstein, well Well B 1. **(f)** Colloform Mn-Fe-oxide that precipitated along a fracture. Middle Buntsandstein (Geröllsandstein), Schöllbronner Steig, Ettlingen.

replaces a precursor mineral, which no longer can be identified. The elemental composition of the mineral is rather complex. Besides Al, P and S it comprises Sr, K, Ca, Ba, Fe, As, Ce and Nd.
In samples from the wells Well B 1 and Well B 2 pyrite with trace amounts of As and Ni (each <2 atomic percent) was detected (Figure 28d, e). The sandstones on both wells are bleached.

3.4 Porosity and Compaction

Porosity and permeability was measured on 70 shared rock samples at the GeoZentrum Nordbayern by M. Fensterer. The measured porosity data usually exceed the values determined in this study by point counting (Figure 29). This discrepancy is mostly caused by microporosity (e.g. in clay minerals) and edge effects by grain curvature in a 20-30 µm thick thin section (Halley, 1978). Porosimetry was performed on merely a part of the samples examined. Only point-counting porosity data are used in this study, to allow for comparability of the results. Consequently, there are no quantitative permeability data available from this method. Permeability could only be evaluated qualitatively by the description of the interconnection between pores and the estimation of pore throat diameters. Porosity was assigned to three classes: (i) primary intergranular porosity, (ii) secondary porosity caused by dissolution, as well as (iii) by fracturing. Most secondary porosity was observed by detrital grain (mostly feldspar) dissolution. Porosity caused by fracturing was only subordinately observed in thin section scale. In the outcrops investigated, secondary porosity is, with an average percentage of 1-3 %, only a minor constituent of total porosity. Primary intergranular porosity reaches up to 22 %.

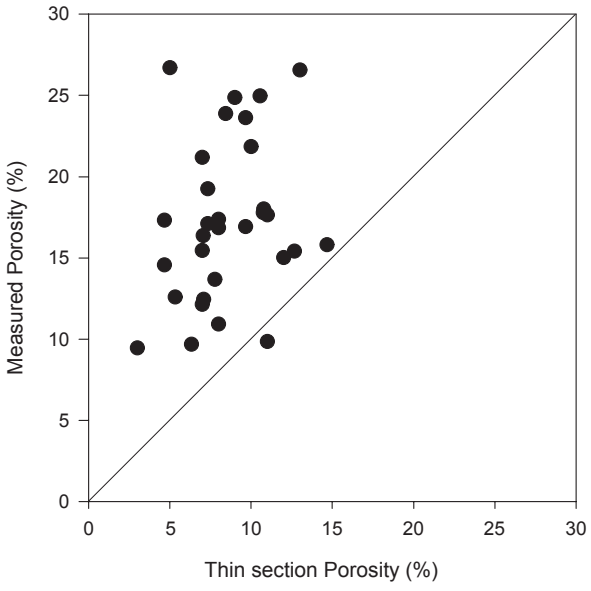

Figure 29: Porosity values derived from porosimetry (measured porosity) and point counting (thin section porosity) can significantly differ. To some extent microporosity, which is not recorded during point counting, is definitely responsible for the deviation. However, deviations >>10 % can only be explained by strong heterogeneities of the measured samples or measuring errors.

Compaction in sandstones can be identified by the Intergranular Volume (IGV), which is the sum of all cement and remaining primary porosity (Houseknecht, 1987). The term is synonymous with minus-cement porosity (Rosenfeld, 1949; Heald, 1956). The concept is based on the assumption that three major diagenetic processes modify the intergranular porosity of sands and sandstones: mechanical and chemical compaction as well as cementation. These three processes are clearly defined by Houseknecht (1987). According to his definitions, compaction basically describes processes, which reduce the bulk volume of a rock. (i) Mechanical compaction comprises reorientation

and repacking, fracture and plastic deformation of ductile grains. (ii) Chemical compaction means bulk volume loss by framework grain dissolution at grain contacts and stylolitization. (iii) Cementation is defined as a process, which reduces intergranular pore space by the occlusion with authigenic minerals, but does not reduce the bulk volume of a rock. The examination of both IGV and cementation therefore allows to understand the relative importance of each process for intergranular porosity reduction and/or conservation (Houseknecht, 1987). Clean, well-sorted, unconsolidated sand is often estimated to possess approximately 40 % porosity at the depositional surface (Fraser, 1935; Hamilton and Menard Jr., 1956; Beard and Weyl, 1973; Pryor, 1973). However, porosity measured in recent sands by the above-mentioned authors and thin section porosity data can considerably vary; the values are more qualitative and not strictly quantitative. This technique was only applied to samples with overall clay and opaque contents below 15 %. If applied to samples with high clay and opaque (in the following summarized as "clay") contents, the results can be distinctly different (Figure 30). The positive excursion of the IGV in samples with high clay content can be explained, if some samples with high clay content originally contained abundant plagioclase or other minerals, which were transformed into clay minerals. Clay minerals from in-situ (e.g. plagioclase) weathering precipitated in secondary porosity and should therefore not be considered for the calculation of the IGV. However, under the light microscope they can usually not be distinguished from infiltrated clay, especially if they are mixed with opaque. The secondary porosity from early weathering processes can hardly be identified, because it was deformed and thus occluded by compaction.

The original porosity of wet sand considerably varies with sorting (Lundegard, 1992; Ehrenberg, 1995). Therefore only medium well- or better-sorted samples were considered for the assessment of compaction.

The degree of compaction decreases with increasing quartz cementation (Figure 30a). The values commonly vary between 20 and 30 % with minimum values around 15 % and maximum values around 35 %.

To further investigate the contribution of compaction to porosity loss, the cementational porosity loss (CEPL) and compactional porosity loss (COPL) were used to calculate the compactional index (ICOMPACT) according to Lundegard (1992).

The indexes are defined as follows:

$$COPL = \frac{P_i - (100 - P_i) \cdot IGV}{100 - IGV}$$

$$CEPL = (P_i - COPL) \cdot \frac{C}{IGV}$$

$$ICOMPACT = \frac{COPL}{COPL + CEPL}$$

ICOMPACT is a measure for the role compaction played in porosity loss. A value of 1.0 implies that all porosity loss is due to compaction and a value of 0.0 that all porosity loss is due to cementation.

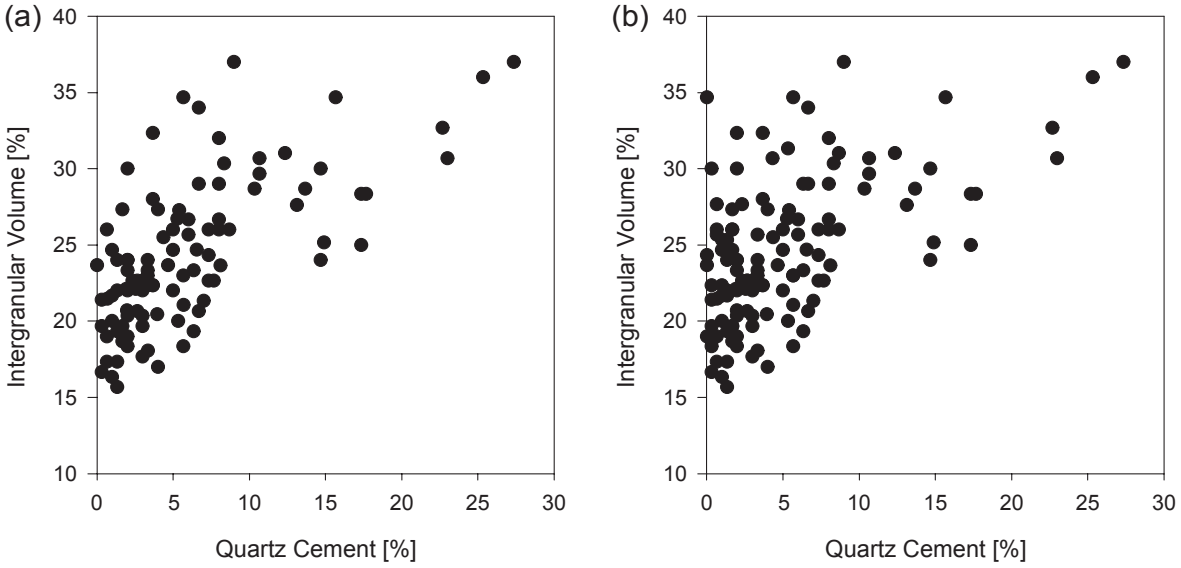

Figure 30: Intergranular volume (IGV) plotted versus quartz cement. **(a)** Plot of selected samples with clay + opaque contents below 15 %. In some cases, quartz cement contents even below 5 % support the framework against compaction. However, the effect is most obvious at quartz cement contents above 10 %. **(b)** Plot of all samples from the study area. The unfiltered data partly exhibit unusually elevated IGV at very low quartz cement contents and were therefore neglected for the interpretation of the IGV. See text below for a probable explanation of the effect.

As an estimate, an initial porosity (Pi) of 40 % was assumed and IGV is the sum of total optical porosity and pore-filling cement (c). The results for the observed outcrops and wells are plotted in Figure 32 and in Figure 53 on page 87. Within the standard deviation ICOMPACT generally vary between 0.5 and 0.7.
Compaction can additionally be assessed by the study of grain contacts (for a review compare Pettijohn et al. (1987)). Grain contact types on numerous samples were counted. They were classified as floating, point, long, concavo-convex and sutured (Figure 31). Stylolites were not observed at all. Grain contacts indicating grain-grain dissolution (concavo-convex, sutured) were observed on quartz and K-feldspar grains. Weighted Contact Packing (WCP) was calculated to define the detrital framework of the sandstones (Hoholick et al., 1982):

$$WCP = \frac{a + 2b + 4c + 8d + 16e}{a + b + c + d + e}$$

a = floating
b = point
c = long
d = concavo-convex
e = sutured

The latter authors recommend to use the formula preferably for quartz arenites, because ductile lithoclasts or soluble carbonate grains may distort the results. Both types of clasts are rare to absent in the examined sandstones. Despite the often elevated feldspar content, the results are supposed to be comparable within the study area. The separate examination of the outcrops exhibits several trends (Figure 33): (i) WCP decreases with increasing quartz cementation; (ii) WCP can increase with increasing content of grain-coating illite; (iii) WPC generally increases with decreasing grain size. These trends are best expressed in the outcrops near the main fault of the URG (Cleebourg, Ettlingen, Heidelberg, Leistadt, Neustadt a.d.W.). Most exceptional are the samples from Neustadt a.d.W., which consistently exhibit strongly elevated WCP, i.e. strongly increased dissolution at grain contacts. However, the sample with the highest WCP is from Cleebourg. The WCP of the samples from

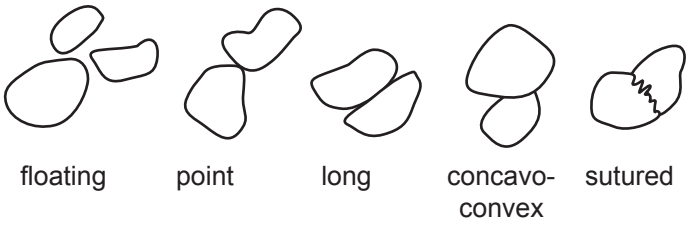

Figure 31: Illustration of grain contact types after Hoholick et al. (1982).

the Neckar valley (Hirschhorn, Neckargerach, Neckargemünd, Rockenau) and the Palatinate Forest (Rodalben) is less affected by quartz cementation, grain-coating illite and grain size. To ensure the significance of this observation, the descriptions of Grabowska (2011) and Wasielka (2012) were embraced. None of the latter authors quantitatively surveyed grain contacts but reported a subjective description of the amount of grain-grain dissolution observed. The thin sections from these studies were available and new CL imagery was acquired, which was optically compared with our quantified imagery. Grabowska (2011) reported low to intermediate grain-grain dissolution (WCP approximately 3-6), which could be confirmed. Amongst 66 samples none

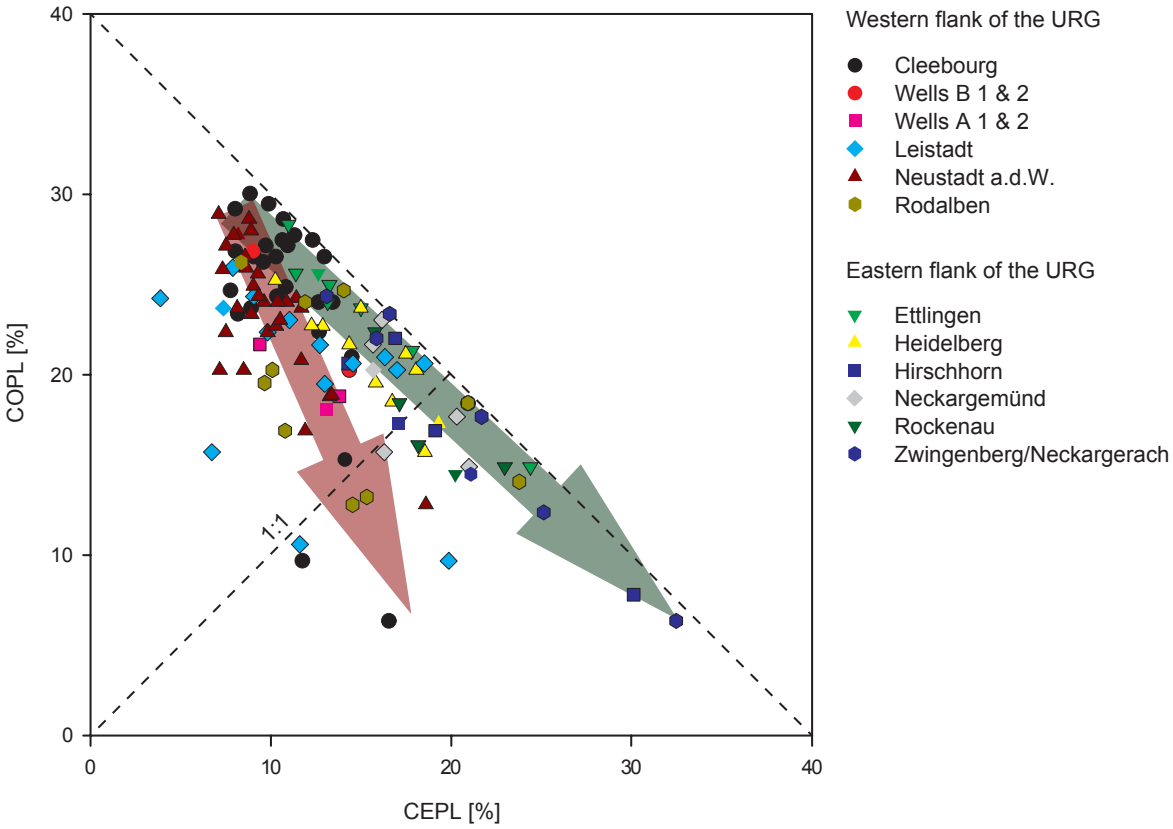

Figure 32: Cementational porosity loss (CEPL) plotted versus compactional porosity loss (COPL), indicating the relative importance of each process on total porosity loss. The bisectrix marks equal proportions. In most sampled sandstones COPL prevails. These samples are clay-rich sandstones, which hardly allowed for framework cementing cementation. With increasing, framework supporting cementation two regional trends develop, indicated by the red (western flank of the URG) and green (eastern flank of the URG) arrows. The red arrow shows that framework supporting quartz cementation counteracted compaction and thus preserved some intergranular porosity. The green arrow shows that quartz cement equally constrained compaction but advanced further, destroying intergranular porosity. Samples from Rodalben, located within the green arrow (at about 21 and 25 % CEPL, respectively) lost their porosity due to intense haematite cementation, not by intergranular quartz cement.

was found to exhibit dissolution at grain contacts comparable to samples from e.g. Neustadt a.d.W. Sandstones, which were reported to exhibit high to very high grain-grain dissolution by Wasielka (2012), turned out to exhibit intermediate to high WCP (approximately 5-7), still lower than most samples from Neustadt. The results for compaction are discussed in Chapter 4.7.

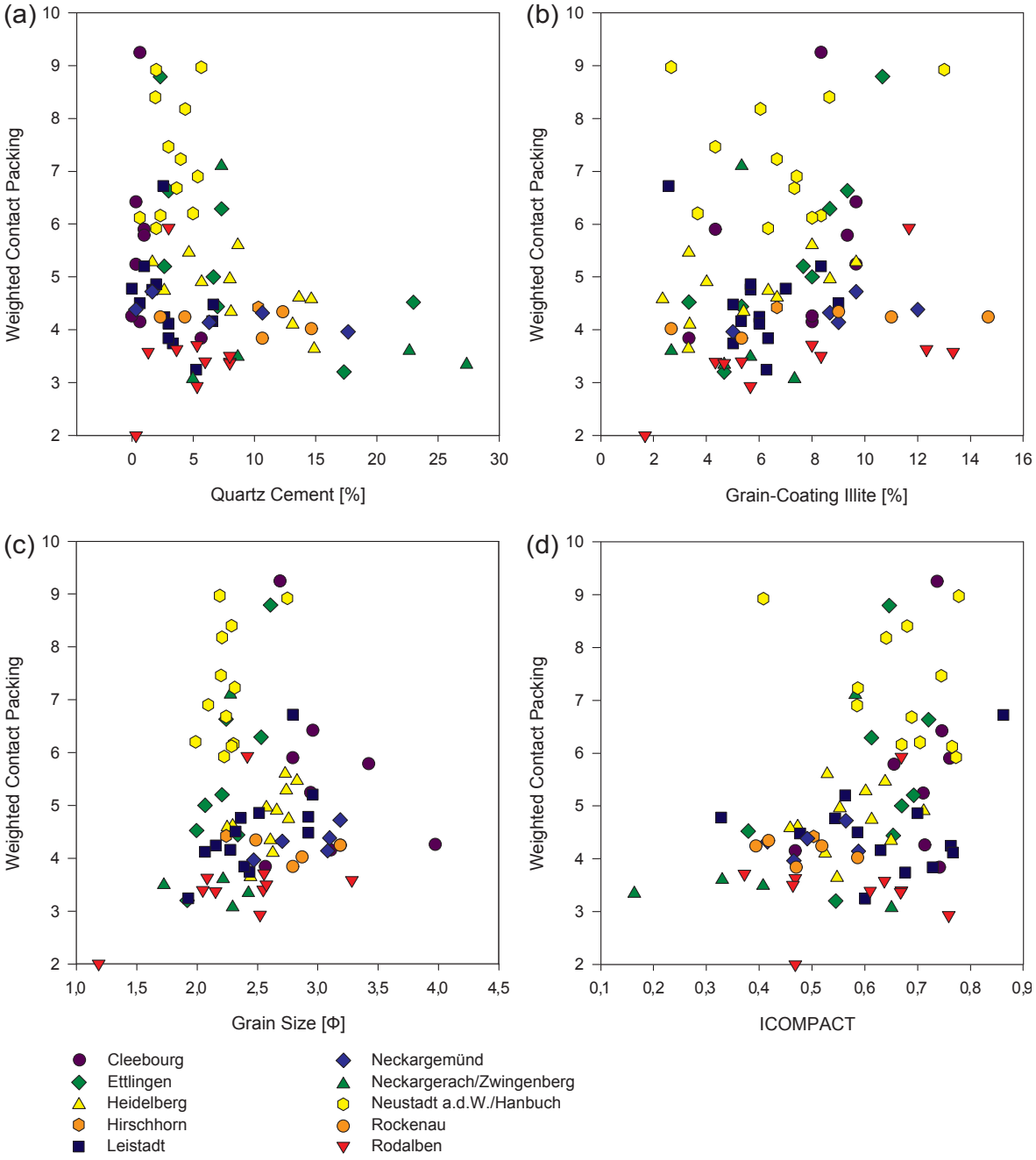

Figure 33: Weighted Contact Packing (WCP) plotted versus **(a)** quartz cement; **(b)** coating illite; **(c)** grain size; **(d)** compactional index.

3.5 Fractures and Fracture Mineralization

Joints, fractures and/or deformation bands were observed in all outcrops and cores. Fracture mineralization was, however, rather uncommon. Most fractures observed were non-mineralized or exhibited thin, dendritic Mn-oxide. The latter could be analytically proved by SEM-EDS. Other fracture planes were irregularly coated with black and brown oxides and hydroxide (probably Fe-hydroxide and Mn-oxide; Figure 34a).

The only outcrop of this study with considerable fracture mineralization is the quarry in Leistadt. Barite and Fe-hydroxide commonly mineralized extension fractures. Strongly mineralized fractures have apertures up to several centimetres. Other fractures are filled with host rock debris (up to several centimetres in diameter), irregularly cemented with barite. Barite in the first type of fractures shows multiple generations, starting with cryptocrystalline aggregates on the fracture walls developing to elongate barite prisms growing perpendicular to the fracture wall. In CL fracture-mineralizing barite exhibits multiple zones (Figure 36a), indicating repeated, episodical growth. Macroscopically, the barite cements form undulating, radial aggregates of strongly elongated crystals (Figure 36b).

Fe-oxide/hydroxide forms crusts up to several millimetres thick, precipitated on preceding cements of barite, which reach a thickness up to one centimetre (Figure 36b). The fractures were usually incompletely cemented from both sides, leaving them partly open. Under SEM the cements turn out to be amorphous and colloform aggregates. Fe-hydroxide adjacent to earlier barite cement commonly exhibit colloform and framboidal shapes (Figure 36c). To the centre of the fracture the Fe-hydroxide contains increasing porosity, host rock debris and finely broken barite pieces as well as minor authigenic barite (Figure 36d, e). For further information on Fe-hydroxide see Chapter 3.3.6.

In the quarry Cleebourg the relationship between bleaching and fracturing can be observed (Figure 6 on page 16). Bleaching patterns show a gradual transition

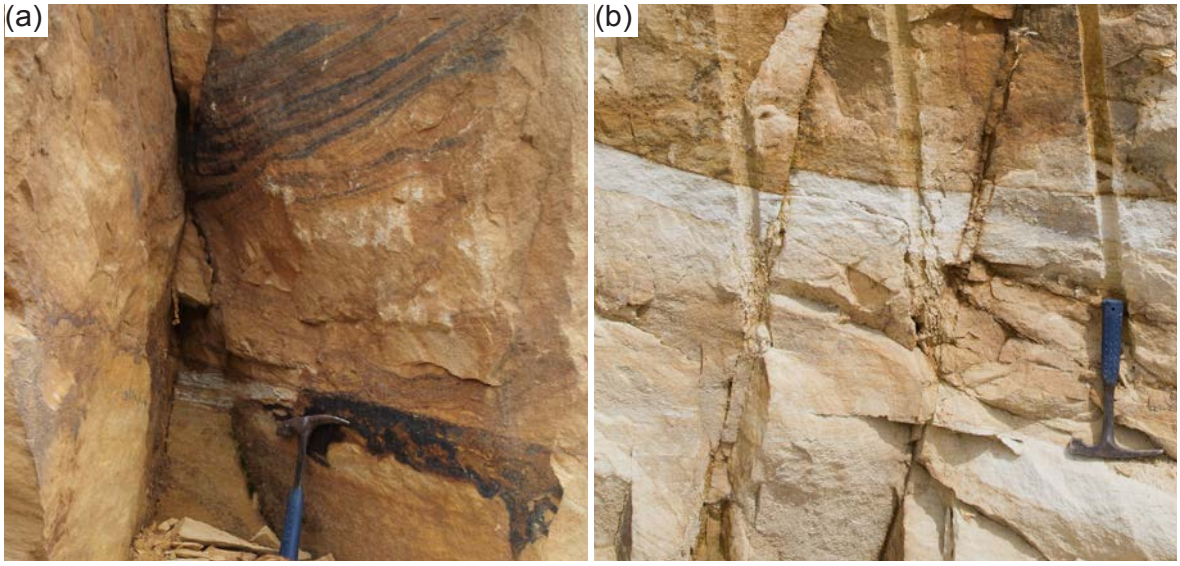

Figure 34: (a) Precipitation of black and brown Fe-hydroxide and probably Mn-oxide on a fracture plane. Lower Buntsandstein, Cleebourg. **(b)** Offset of bleached layers at normal fault planes. Lower Buntsandstein, Cleebourg.

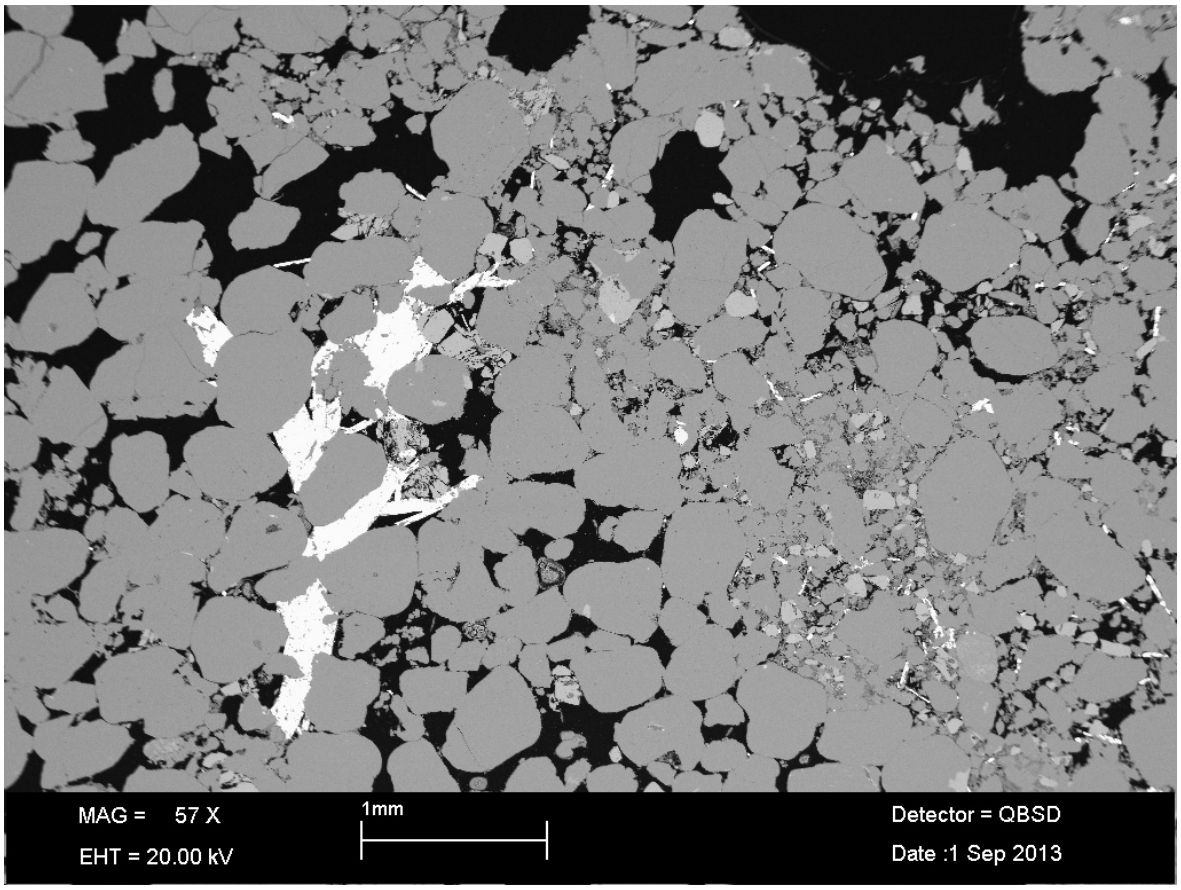

Figure 35: Deformation band with fine debris on the right side of the BSE-SEM image. Needle-shaped barite (white) and authigenic illite (felt-like grey) precipitated in the deformation band. The host rock is highly porous (porosity is black). Long-prismatic barite precipitated in the pore space directly adjacent to the deformation band. Some sand grains exhibit non-healed microcracks. Buntsandstein, Well A 1.

in colour from red to yellowish to pure white. Bleached layers are offset at fault planes (Figure 34b).

In samples from subsurface wells of the URG, comparable to the samples from the quarry Leistadt, barite was primarily found along fractures and only subordinately pore-filling within the sandstone. Other than in Leistadt, the fracture apertures in the core samples do not exceed a few millimetres and the fractures are probably rather shear than extension fractures ("deformation bands"; Aydin, 1978; Aydin and Johnson, 1978, 1983, Fossen et al., 2007). Thus, the fractures are filled with fine debris with common barite needles in the pore space (Figure 35). Barite was proved in the wells GTB 1 Brühl, Well A 1 and Well A 2.

3.6 Fluid Inclusions

A total of 31 aqueous fluid inclusions were measured on six samples from four outcrops on both flanks of the URG. All fluid inclusions measured were trapped in syntaxial quartz overgrowths. Syntaxial K-feldspar overgrowths and barite veins were unsuccessfully checked for fluid inclusions. Fluid inclusions in quartz cements were either trapped at the boundary between grain surface and syntaxial overgrowth or within the overgrowth. Within the overgrowth only isolated fluid

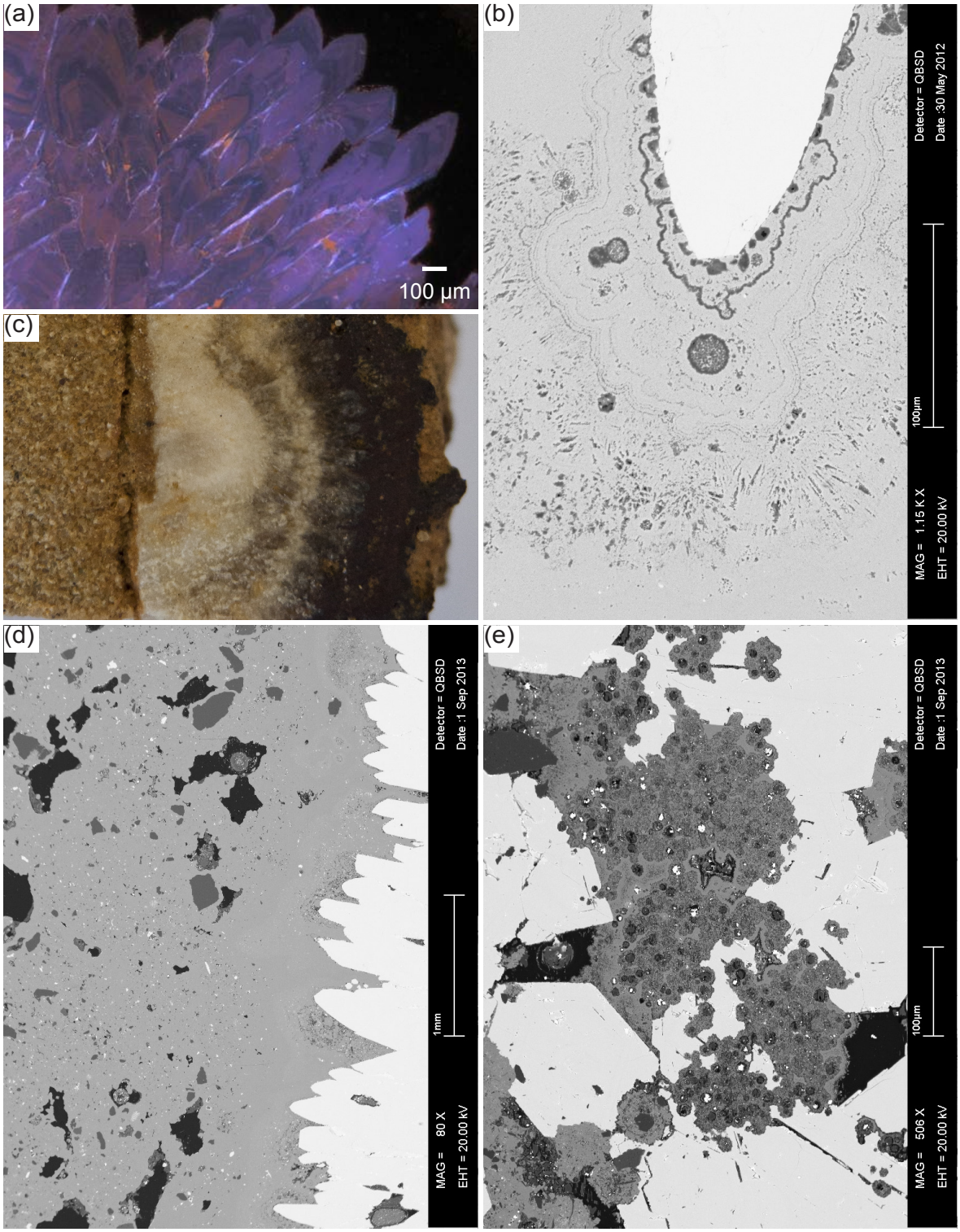

Figure 36: (a) CL image of fracture-filling barite in (c). Multiply zoned, elongate crystals. Fracture porosity is black. **(b)** Barite (white crystal on the top) surrounded by Fe-hydroxide. Colloform, zoned texture, framboids and microporosity in the Fe-hydroxide. Scale bar is 100 µm. **(b)** Perpendicular cut through a barite-Fe-hydroxide fracture mineralization. Host rock (brown sandstone) to the left. Acicular white to translucent barite is followed by Fe-hydroxide. Horizontal scale 1 cm. **(c)** Transition from acicular barite (white crystals on the right) to dense, rather pure Fe-hydroxide to porous (porosity is black), debris-bearing (quartz is dark grey) Fe-hydroxide. Scale bar is 1 mm. **(d)** Colloform texture in Fe-hydroxide, intergrown with barite. Scale bar is 100 µm. All images are from the Lower Buntsandstein, Leistadt.

inclusions were measured. Inclusions that were obviously aligned along trails were neglected, because they may be affected by "necking down", which may alter the properties of the original inclusion (Goldstein, 2001). All fluid inclusions where small with diameters of 10 to 15 µm and below. This fact complicated the measurement of temperatures, particularly the ice melting temperature ($T_{m\ ice}$). Namely, for all the 31 inclusions measured the homogenization temperature (T_h) could be determined but Tm could only be measured on eight inclusions.

Homogenization temperatures (T_h) provide information on the minimum fluid temperatures at the time of cementation. To obtain a more precise trapping temperature (T_t) of a fluid inclusion, a pressure correction of T_h should be conducted. Frequent problem as in this case is the lack of information on the burial depth during cementation. No pressure correction was performed therefore. However, assuming a hydrostatic pressure of 150 to 200 bar at an estimated maximum burial depth between 1500 and 2000 m, T_t would exceed T_h values only around 10 °C (Roedder and Kopp, 1975; Potter, 1977). This variation is negligible for the purpose of this research work. Thus, T_h is assumed to be the minimum fluid temperature at the time of cement precipitation.

Besides the fluid inclusions measured by the author of this thesis, the results of previous work was integrated in this study (Figure 37). Each of the four histograms comprises data from different outcrops and thus represents a specific area rather than a single location. The histograms are aligned in the way that in the top row Palatinate Forest and Haardt represent the western margin of the study area and the western flank of the URG and in the bottom row Heidelberg and Odenwald represent the eastern flank of the URG and the eastern margin of the study area, respectively.

No information on the chemical composition of the fluids trapped in the fluid inclusions was obtained, because this was outside of the scope of this research. However, there is data published on geothermal brines from the Soultz-sous-Forêts site, which were produced from granite but are supposed to be derived from the Buntsandstein (Sanjuan et al., 2010). These brines are NaCl dominated but exhibit additionally a complex composition of trace metals and sulphates (Sanjuan et al., 2010; Nitschke et al., 2014).

As mentioned before, basically two sets of fluid inclusions were measured: one trapped at the grain boundary and one trapped isolated within the cement. These sets appear more or less pronounced as two populations within the histograms. Inclusions trapped between detrital grain and overgrowth cement exhibited T_h below approximately 150 °C, isolated inclusions within the overgrowths are usually (partly distinctly) above 150 °C. The homogenization temperatures measured at the grain-cement boundary are largely consistent throughout the study area. Variations in the significance of the low temperature population are caused by varying occurrence of measured and/or measurable inclusions at the grain-cement boundary.

The high temperature inclusions (>150 °C), mainly located isolated within the syntaxial overgrowths, show a broad variation in T_h with a distinct regional pattern. T_h increase from 150-175 °C near Pirmasens to 175-200 °C in the Haardt to 250-275 °C in the Odenwald near Zwingenberg and Neckargerach. There are too few values available from Heidelberg to point out an average temperature. However,

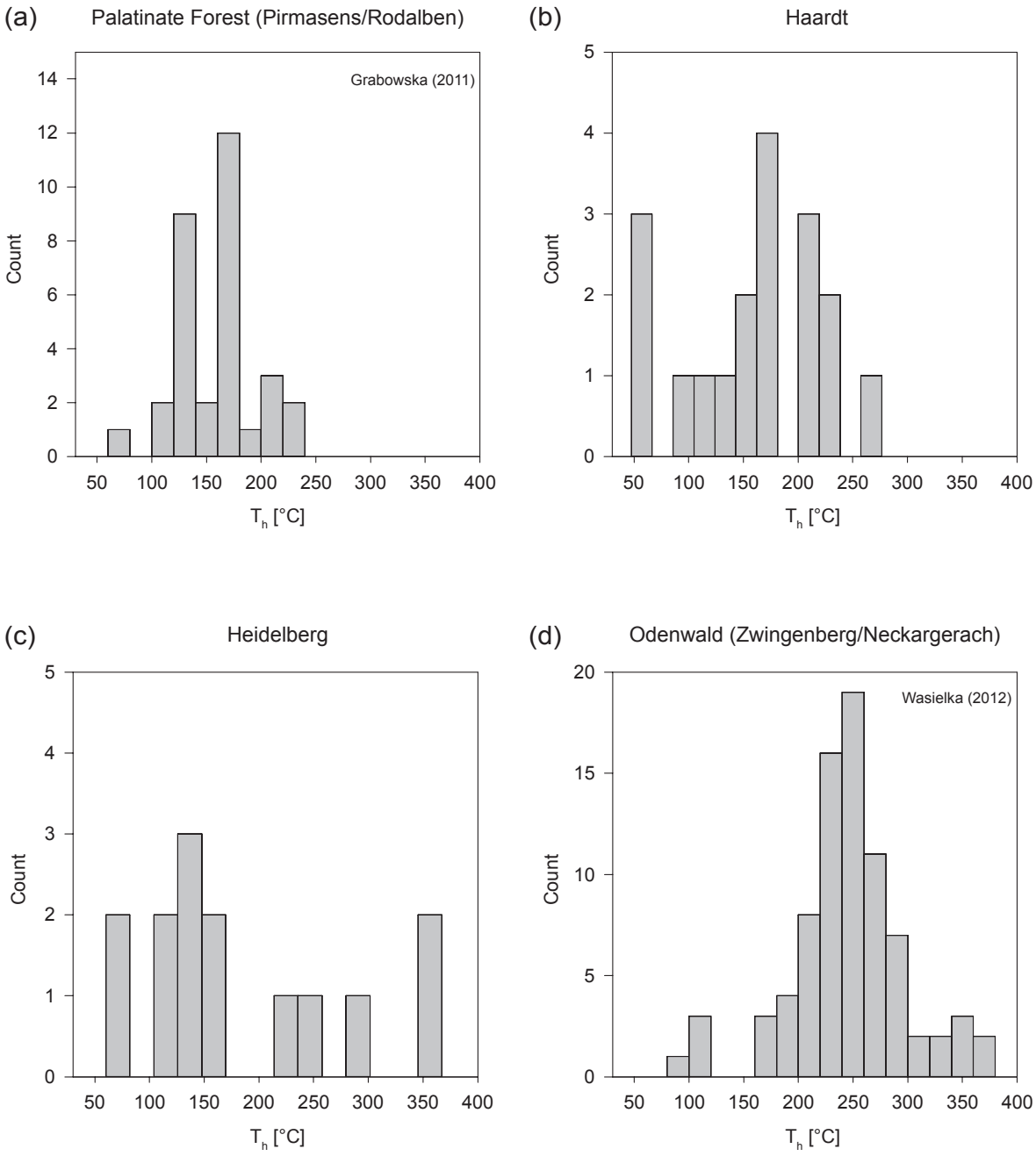

Figure 37: Histograms of fluid inclusion homogenization temperatures (T_h) measured in syntaxial quartz cements. The graph 'Haardt' comprises measurements from the quarries Leistadt, Neustadt a.d.W. and Cleebourg. Data from the Palatinate Forest and Odenwald were taken from Grabowska (2011) and Wasielka (2012), respectively.

measured temperatures beyond 350 °C clearly indicate the continuation of the observed temperature-trend also for the Heidelberg area. T_h measured west of the URG are hardly above 250 °C, whereas T_h measured east of the URG commonly exceed 250 °C and reach up to >350 °C.

Ice melting temperatures were measured to obtain information on the salinity of the fluid. Due to their small size, $T_{m\ ice}$ could only be measured on a total of eight inclusions. Most of these measurements definitively have a distinct error of

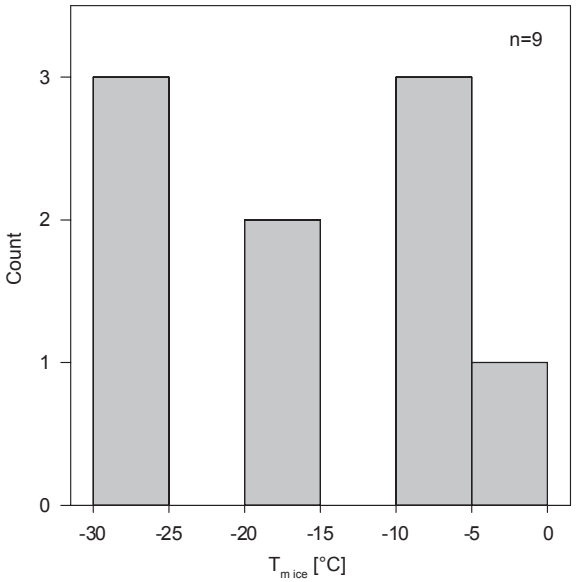

Figure 38: Final ice melting temperatures of aqueous fluid inclusions trapped in quartz cements in the Buntsandstein, Haardt and Heidelberg area.

several degrees Celsius: most fluids exhibit gradual melting, i.e. there is a temperature interval between initial melting and final melting of the ice. The temperature for complete melting could hardly be determined, even after repeated measurements, and was thus estimated within a few degrees Celsius. Only one $T_{m\ ice}$ could be measured on an inclusion at the grain-cement boundary with a final melting temperature of -0.01 °C. All other values were measured on isolated inclusions trapped in a quartz overgrowth. Other than T_h there was no information on ice melting temperatures in Grabowska (2011) or Wasielka (2012). The results from the Haardt and Heidelberg areas are plotted in Figure 38.

4 Discussion

4.1 Lithology, Lithofacies and Depositional Environment

The following lithofacies types were recorded. For further details see Chapter 3.1.

(a) Massive, crudely bedded and/or cross-stratified gravel (Gm, Gt, Gp).
(b) Trough and planar cross-bedded sandstone layers (St, Sp), partly with mud stone intraclasts.
(c) Sandstones with mudstone clasts up to several cm in diameter (Se).
(d) Rippled sandstones (Sr).
(e) Laminated fine sand- to siltstones (Fl).
(f) Laminated to massive silt- and mudstones (Fsc).
(g) Mud- and siltstones with desiccation cracks (Fm).
(h) Steeply planar or trough and tabular cross-bedded sandstones (Spe, Ste).

Many authors (Füchtbauer, 1967; Backhaus, 1974, 1975; Dachroth, 1985) interpreted the Lower and the Middle Buntsandstein in South Germany as predominantly fluvial and minor lacustrine and aeolian deposits. Haematite coatings on sand grains, which cause the common red colour of the Buntsandstein, were interpreted as indicator for arid or semiarid climate during deposition (Valeton, 1953). Hence, the depositional environment was interpreted as a wadi-like braided river system (Backhaus, 1974). The classification of lithofacies types according to Miall (1977a) corroborates this interpretation. However, the paleoenvironment during deposition of the Buntsandstein cannot be compared to

the climate in recent desert areas. Despite the overall semiarid climate, frequent cycles with significantly increased precipitation rates, up to monsoonal climate (Parrish, 1993; Feist-Burkhardt et al., 2008; Paul and Puff, 2014) occurred.
Mostly massive or crudely-bedded gravel, showing some internal horizontal bedding and/or imbrication of clasts are interpreted as longitudinal bars. If these beds show a large lateral extent, they may also be regarded as lag deposits. Cross-stratified gravel is interpreted as channel fills and bars.
Sandstones with mud clasts were commonly observed at the base of sandy trough cross-bedded channel fills. Channels with mud clast-bearing sandstones often exhibit a pronounced erosional basal surface. These mud clasts are the result of reworking of rip-up of semi-lithified mud rocks.
Different types of rippled sandstones were observed. Climbing ripples indicate increasing rates of net deposition with increasing climb angle of the ripples (Allen, 1971a, b; Ashley et al., 1982; Leeder, 2011). In a fluvial-alluvial depositional environment they occur in overbank, crevasse splay and point bar deposits (Allen, 1964; Miall, 1977b; Díaz-Molina, 1993).
Laminated fine sand- and siltstones as well as massive mud- and siltstones probably represent overbank, backswamp and/or flood deposits (Allen, 1964; Miall, 1977b). In case of the Upper Buntsandstein, these sediments were partly also deposited in a brackish to shallow marine environment. Episodic marine incursions are revealed by the appearance of marine molluscs (Backhaus, 1974). In the Middle and especially the Upper Buntsandstein fine clastic, so-called violet horizons ("Violette Horizonte") represent paleosols (Müller, 1954a, b; Ortlam, 1967, 1974; Dachroth, 1985; Backhaus and Heim, 1995). These commonly possess, besides the violet colour, dolomite concretions, and more rarely carnelians and rootlets (Dachroth, 1985). Within this research work no further investigation was carried out on these fine clastic sediments. Therefore the silt- and mudstones of the Lower and Middle Buntsandstein were generally defined as floodplain deposits.
Tabular cross-stratified sandstones with steeply inclined planar or trough cross-stratification are interpreted as aeolian dune deposits (Dachroth, 1985; Pye and Tsoar, 2009; Grabowska, 2011; Pucknat, 2011). Microscopic survey of these samples corroborates this interpretation, because sand grains have a frosted surface in grain mount caused by small surface-pits and are often inversely graded. These pits are caused by saltation during aeolian transport. Sand dunes were only observed in the Palatinate Forest, however, well sorted fine to medium sandstones may indicate aeolian transport in the Odenwald as well (Backhaus, 1975).
The facies assemblage of the Lower and Middle Buntsandstein coincides in large parts with Miall's cyclic sandy braided river deposits ("South Saskatchewan type"). In the Pirmasens/Rodalben area and probably other parts of the Palatinate Forest some facies assemblages represent cyclic distal gravelly river deposits ("Donjek type"), indicating a more proximal depositional environment (Steingötter, 2005; Grabowska, 2011; Pucknat, 2011). Within the Lower and Middle Buntsandstein, the investigated outcrops at the Haardt, the Odenwald and the Northern Black Forest exhibit mainly the same "South Saskatchewan type" facies associations. Therefore the subsurface facies of the URG of the same stratigraphic interval is considered to be largely consistent with the investigated facies at the flanks of the URG. Aeolian deposits as well as very coarse conglomerates, cropping out at the eastern part of

the Palatinate Forest (e.g. Rodalben) are explicitly excluded from this statement.
Following two regressive cycles in the Lower and Middle Buntsandstein, a transgressive cycle represented by pronounced fine-grained sediments characterize the depositional environment of the Upper Buntsandstein (Eisbacher and Fielitz, 2010). In the Odenwald and the Palatinate Forest, due to differences in paleogeography, the facies associations of this interval now differ (Bindig and Backhaus, 1995), in contrast to the Lower and Middle Buntsandstein. The lower part of the Upper Buntsandstein is still a mainly fluvial succession similar to the Lower and Middle Buntsandstein, although grain size decreases upwards (Backhaus, 1968, 1974; Dachroth, 1985). The "Röt" in the upper part of the Upper Buntsandstein is already influenced by the transgression of the Muschelkalk sea and is mostly built up by parallel bedded clay and silt stones (Backhaus, 1968, 1975).

4.2 Detrital Mineralogy

4.2.1 Quartz

The combined CL and optical characteristics of detritral quartz were interpreted according to Bernet and Bassett (2005) (Appendix 2)
Monocrystalline quartz with non-undulose to slightly-undulose extinction, fluid inclusions, fluid inclusion trails and microcracks are from plutonic origin. Randomly oriented microcracks form because of thermal stress in the crystal during postmagmatic cooling, not due to tectonic stress (Moss and Green, 1975; Sprunt and Nur, 1979; Bernet and Bassett, 2005). The latter is can cause oriented cracks, which were less common, though. Oriented cracks indicate brittle deformation. Such quartz grains are thus derived from brittle fault zones.
Quartz grains with undulose extinction and dark to black CL colours were frequently observed and interpreted as metamorphic quartz. Equally, polycrystalline mosaic-like quartz grains are originally metamorphic.
Zoned or patchy CL and commonly bright red luminescence colours characterize volcanic quartz (Matter and Ramseyer, 1985; Ramseyer et al., 1988). Under normal polarized light it exhibits a clear appearance, and sharp extinction under cross-polarized light.
The ratio of the mentioned quartz types varies between the different outcrops and along the stratigraphic profile. For further results see Chapter 4.3.

4.2.2 K-Feldspar

In this study K-feldspar varieties were not further determined. Previous authors already observed the low abundance of twinned K-feldspars (Valeton, 1953; Heim, 1974). From optical mineralogical data, the former author inferred an average composition of 10 % twinned microcline, 50 % untwinned microcline and 40 % orthoclase. The lack of twinning in microcline is an indicator for crystallisation temperatures below approximately 300 °C (Nesse, 2004). Thus, a high abundance of untwinned microcline (Valeton, 1953) would be difficult to explain in terms of the Variscan provenance. If we compare the optical mineralogical parameters published in Valeton (1953) with the specifications given in Nesse (2004), the

untwinned “microcline” of Valeton (1953) represents most likely orthoclase. A strong domination of orthoclase is also corroborated by X-ray diffraction analysis (Heim, 1974).

4.2.3 Plagioclase

The major difference in the primary mineralogy between the marginal Buntsandstein in Southern Germany and the distal Buntsandstein in the North German Basin is the preservation of plagioclase in the latter and the absence in the former (Füchtbauer, 1967; Heim, 1974). Considering the Variscan source area of the Buntsandstein, which consists of mostly igneous and metamorphic rocks, the complete absence of Na- and Ca-bearing feldspars (alkali feldspar and plagioclase) can only be explained by diagenetic processes, selective dissolution and/or replacement by clay minerals. There are essentially three mechanisms possible (or a combination of these), which can account for the plagioclase loss and preservation of orthoclase: (1) in-situ weathering in bedrock and regolith, (2) mechanical and chemical weathering during transport, and (3) weathering/ dissolution after deposition.
Plagioclase tends to exhibit significantly higher weathering rates than K-feldspar already in the host rock and its regolith (Figure 39; Banfield and Eggleton, 1990; Nesbitt et al., 1997). The former might convert to kaolinite in depths up to several meters in granitic bedrock, while K-feldspar is still stable (White et al., 2001). Authigenic illite can form from plagioclase during weathering under hot semiarid conditions (Betard et al., 2009). (Semi)-arid to sub-humid conditions allow for the formation of smectite from plagioclase (Bestland et al., 1997; Ryu and Niem, 1999; McKinley et al., 2003).
To explain the above mentioned differences in plagioclase content, Füchtbauer (1967) and Heim (1974) assume transport of plagioclase-bearing sediment from the north, east and west into the North German Basin, and supply of material without plagioclase from the south. In the Unterschmeien 1 well in Bavaria, an area at the southern margin of the German Basin, the transition from Lower Buntsandstein to weathered Variscan granite was drilled. In the regolith of the Variscan basement at this site, plagioclase is strongly sericitized, while K-feldspar is almost fresh (Drong, 2003). However, weathering and diagenetic alteration of the basement probably continued after the deposition of the Buntsandstein. The observation of Drong (2003) is therefore only proof for the selective weathering of plagioclase near the surface under the given climatic conditions and after burial, but not for a plagioclase-free sediment source. Plagioclase content might have been diminished by early weathering, but it is very unlikely, that totally plagioclase-free sediments originated from such sources.
Distinct differences in climatic conditions between the source areas surrounding the southern German basin are unlikely (Bohemian Massif and Vindelician High in the east and southeast, Armorican Massif in the southwest, London-Brabant Massif and Rhenish Massif in the west and northwest). Climate further to the north, in present Scandinavia and Scotland might have been somewhat more humid, favouring the preservation of plagioclase. However, it is highly improbable that all plagioclase in the central German basin is derived from source areas in the north. Sediments originated from the Fennoscandian Shield were deposited in the

northern part of the German Basin (Mader, 1982). There is no reason to assume transport of plagioclase-bearing sediment from northern areas in contrast to plagioclase-free transport from southern areas. In addition, weathering conditions would not have changed much along the fluvial transport and after deposition, still preferably weathering plagioclase, and exposition to weathering during fluvial transport was distinctively shorter than in the bedrock.

Aggregates of mixed illite and K-feldspar were observed in our samples under SEM and were compared to the plagioclase of a Variscan granite from Heidelberg (Figure 40a, b), because Variscan granites were major sediment sources for the Buntsandstein (Drong, 2003; Paul et al., 2008). The illite–K-feldspar aggregates are believed to represent remnants of the plagioclase-type observed in the Variscan granite. There are well-founded arguments, which corroborate this interpretation:

(i) The clay aggregates exhibit tangential clay coatings (Figure 40c), which proof their detrital origin (see Chapter 4.4.2.2 for details on clay coating formation).

(ii) In the current state, the aggregates could impossibly be transported, i.e. they must replace a solid precursor. The illite, making up most of the clay aggregates, commonly exhibits typical kaolinite booklet-structures (Figure 40c, Figure 40d). Kaolinite, though, is a common weathering product of plagioclase (Chapter 4.4.2.1).

(iii) Both the igneous plagioclase and the illite aggregates contain similarly distributed patches of K-feldspar (Figure 40). The size of the single patches is 5-10 µm in the granite and 1-5 µm in the clay aggregates. This difference can be well explained by weathering of the K-feldspar in the clay aggregate. The weathering of plagioclase compared to K-feldspar is discussed later in this chapter. The illite-K-feldspar aggregates are always significantly deformed by compaction (Figure 40c). This important observation proves, that the dissolution of plagioclase occurred before the framework-supporting quartz-cementation.

The mentioned observations corroborate that (i) plagioclase was transported by ephemeral rivers from the south, comparable to rivers from the west, east and north; (ii) plagioclase was originally deposited in the continental, fluvial depositional environment at the southern margin of the German Basin; (iii) in contrast to the northern German Basin, weathering of plagioclase continued after deposition in the marginal areas. The most likely reason for the lack of plagioclase in the southern, marginal Buntsandstein and preservation in the northern, basinal Buntsandstein is the different depositional environment. Weathering conditions in the southern part of the basin remained essentially the same along the course of the different rivers (braided channels with longer, subaerial exposition) and thus promoted plagioclase weathering. Plagioclase can be transformed to kaolinite by meteoric water, flushing the sediment (see Chapter 4.4.2.1). This process was probably favoured by the Triassic intensive Pangean monsoon (Parrish, 1993). In the north, constant water coverage was common, partly of brackish/marine up to saline conditions (Füchtbauer, 1967; Feist-Burkhardt et al., 2008). Such standing saline waters are able to promote the preservation of plagioclase (Bjørlykke and Aagaard, 1992). Furthermore the sediments in the North German Basin are usually silt- to clay-sized and sandstones occur only subordinately. This has a strongly negative impact on the permeability of the succession. Pore waters cannot circulate easily and would become saturated with respect to the weathered minerals. The saturation of acidic meteoric water with respect to albite is reached after only 0.66 g/L of albite

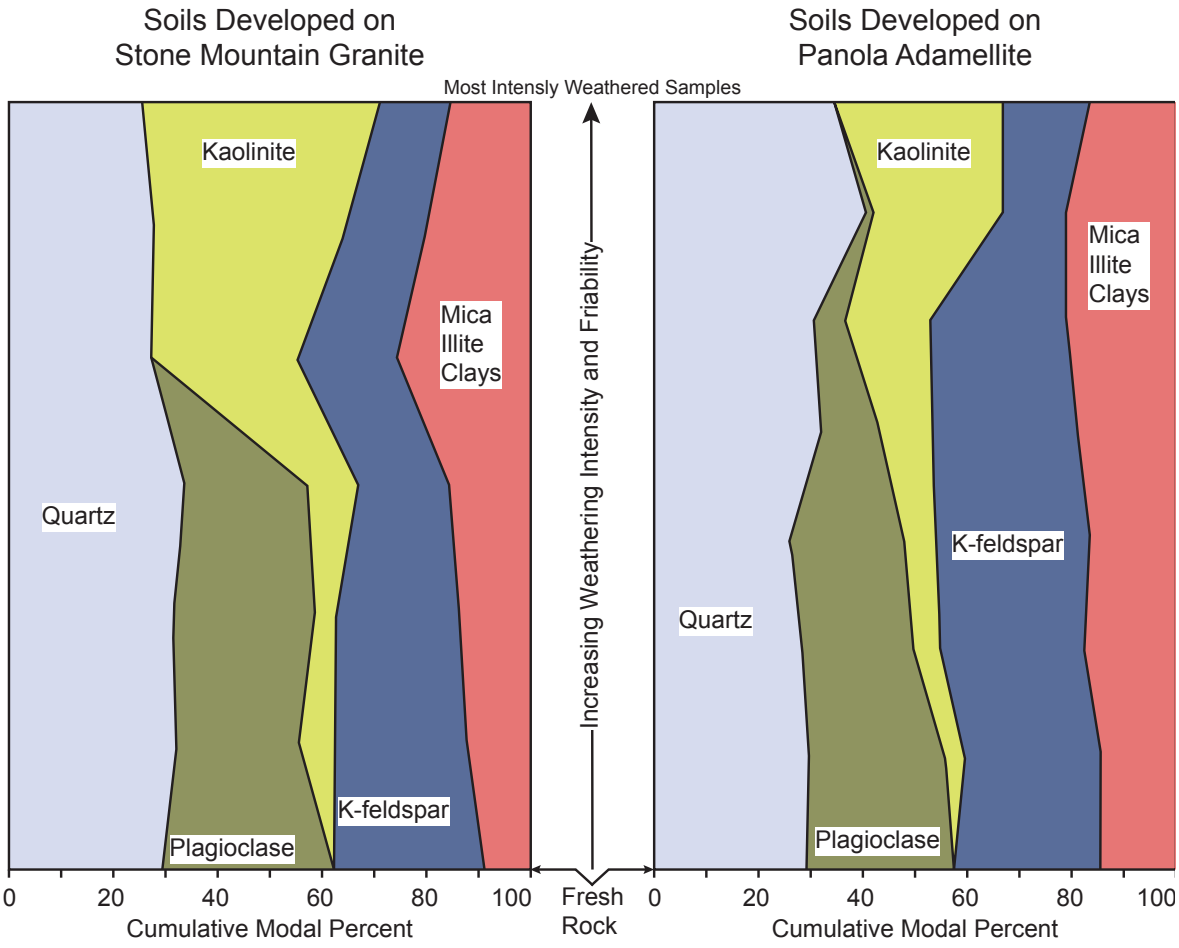

Figure 39: Change of the modal composition along a weathering profile of the regolith from two different granites. K-feldspar is significantly weathered not until almost all plagioclase is dissolved/ transformed to kaolinite (modified from Nesbitt et al., 1997).

are dissolved (Nesbitt et al., 1997). Therefore, a perpetual substitution of pore water with fresh meteoric water is required to achieve considerable plagioclase dissolution. This setting is characteristic for highly permeable regolith or fluvial sand in the south, but is most unlikely for low- or impermeable silts and clays in the north, which were constantly or at least most of the time covered by standing, often saline water. Consequently, the lack of plagioclase at the southern margins of the German Basin is caused by the different weathering and environmental conditions in this area compared to the basinal area in the North.

The proof of plagioclase in the Upper Buntsandstein in the south by XRD analyses (Backhaus, 1975, 1979, 1981) further corroborates this model: In the Upper Buntsandstein the depositional environment changes from a continental to a brackish-marine setting (Röttransgressions, Szulc 2000), hydrologically comparable to the depositional environment in the Central German Basin (Backhaus, 1981). In the Late Buntsandstein time, in contrast to the Early and Middle Buntsandstein, there is uplift in the north and subsidence in the south (Mader, 1982; Feist-Burkhardt et al., 2008). Similar observations regarding plagioclase content were made in the Alpine Buntsandstein in Austria and Switzerland, where this feldspar is absent in the lower continental succession and appears in the marine-brackish

Figure 40: (a) Backscattered electron (BSE) image of a Variscan granite from Heidelberg. The granite is mainly composed of quartz (Qtz), plagioclase (Pl), K-feldspar (Kfs), biotite (Bt) and apatite (Ap). The BSE contrast between quartz and plagioclase is low but the latter exhibits a perforated texture, probably due to incipient weathering. Vugs in K-feldspar are also probably caused by weathering. BSE-image. Granite, Russenstein, Heidelberg. **(b)** Plagioclase from a Variscan granite. Detailed view of a plagioclase in (a) (black frame). Albite is grey and K-feldspar (probably orthoclase) is light grey. Patchy distribution of K-feldspar caused by exsolution (e.g. black arrows). Note considerable microporosity of the albite (black "dots"), probably due to incipient weathering. BSE-image. Granite, Russenstein, Heidelberg. **(c)** Probable detrital plagioclase grain replaced by illite. The presence of a former detrital grain is indicated by tangential illite (white arrows). Small pieces of K-feldspar (light grey, some are exemplarily marked by black arrows) resemble the texture of plagioclase observed in a Variscan granite (compare b). The rest of the detrital grain is replaced by illite. Booklet structures suppose a kaolinitic precursor to illite. The grain was clearly deformed by compaction, indicating that the replacement took place before or during compaction, e.g. by weathering. For this particular grain the following diagenetic sequence is proposed: (i) Deposition of a detrital plagioclase grain; (ii) Infiltration of detrital clay → tangential illite; (iii) Weathering of the albite component of the detrital plagioclase → formation of kaolinite, preservation of K-feldspar; (iv) Deformation by compaction; (v) Transformation of kaolinite to illite. Lower Buntsandstein, Cleebourg. **(d)** Original kaolinite transformed to illite (note common booklet structures, e.g. black arrows). Abundant fragments of K-feldspar (light grey, some indicated by white arrows) are probably an indicator of the former presence of plagioclase (compare b, Variscan granite). Lower Buntsandstein, Cleebourg.

transition to fully marine carbonates (Stingl, 1984, 1987; Ramseyer et al., 1988).
Telogenetic weathering of plagioclase might also be considered. If telogenetic dissolution of plagioclase grains would have occurred, vugs after plagioclase should frequently be present because of the preceding quartz cementation. Dissolution vugs are, however, only rarely present and are probably not telogenetic but much earlier in origin. In addition, if this process would have occurred, it should have taken place almost exclusively outside the URG, because the overburden inside the URG is considerably high and fluids are strongly saline. The conditions in the subsurface of the graben would hardly allow for the required meteoric water flushing. Present saline formation waters would preserve plagioclase, if any was still present. The fact that no plagioclase was detected in wells Well A 1, 2 and Well B 1 and 2 suggests that plagioclase was already completely leached during eodiagenesis, inside- and outside the graben.
In summary, the lack of plagioclase was most probably promoted by a combination of weathering processes in the hinterland, as well as after deposition, and only subordinately during transport. The reason for the lack of plagioclase in the southern marginal German Basin contrary to the Central German Basin is the advanced weathering after deposition under continental conditions.

4.3 Provenance

The provenance interpretation within this study is based on petrographic and cathodoluminescence observations as well as on geochemical data. Only a general characterization of the hinterland is given, a detailed provenance study is outside the focus of this thesis.
The quartz types identified by cathodoluminescence microscopy (Chapter 4.2.1) and the always-observed mixed mono- and polycrystalline composition corroborate a mixed igneous-metamorphic source. The occasional oriented cracks in quartz grains indicate brittle deformation, i.e. faulting and/or thrusting in the hinterland.

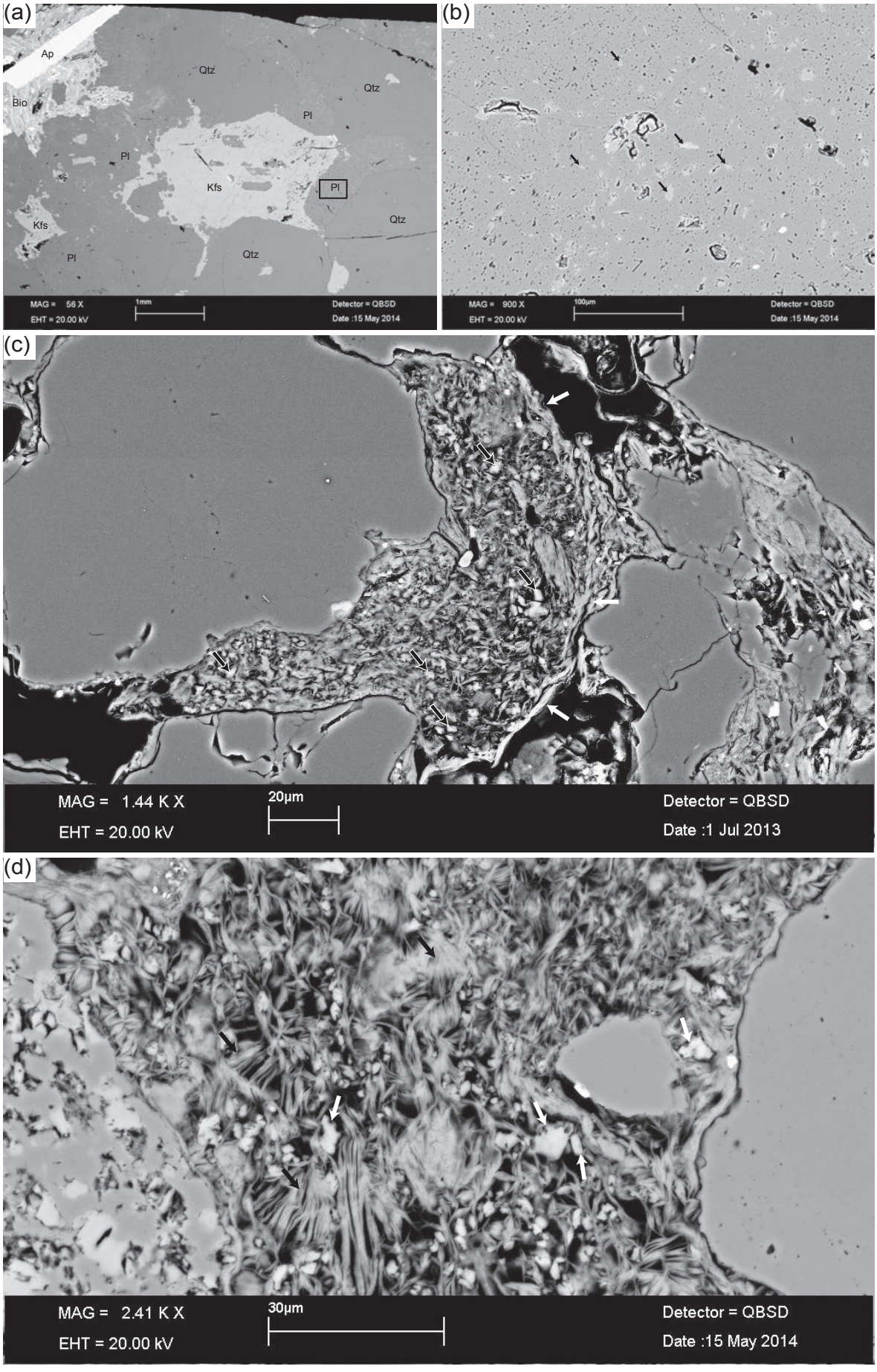
(a)
Ap
Qtz
Qtz
Bio
Pl
Pl
Kfs
Pl
Kfs
Qtz
Pl
Qtz
MAG = 56 X
EHT = 20.00 kV
1mm
Detector = QBSD
Date :15 May 2014
(b)
MAG = 900 X
EHT = 20.00 kV
100µm
Detector = QBSD
Date :15 May 2014
(c)
MAG = 1.44 K X
EHT = 20.00 kV
20µm
Detector = QBSD
Date :1 Jul 2013
(d)
MAG = 2.41 K X
EHT = 20.00 kV
30µm
Detector = QBSD
Date :15 May 2014

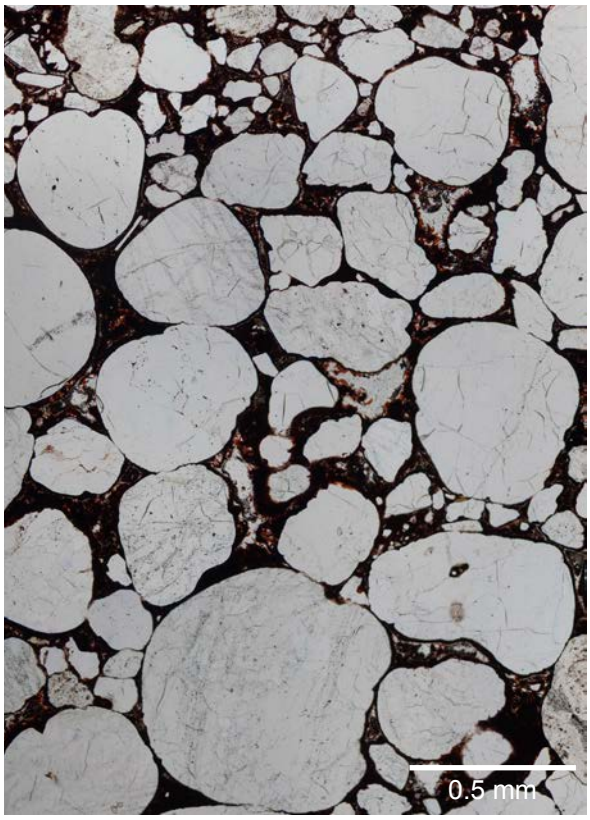

Figure 41: Very well rounded grains from reworked sediment together with subangular to subrounded grains. Middle Buntsandstein (Upper Karlstal Sch.), Rodalben.

The appearance of red luminescing volcanic quartz was qualitatively analysed along two stratigraphic profiles: Rodalben (Middle to Upper Buntsandstein) and Zwingenberg/ Wolfsschlucht (Lower to Upper Buntsandstein). In Rodalben, volcanic quartz is almost absent in the Upper Buntsandstein, whereas there are two distinct clusters in the lower parts of the Upper Felszone and the Upper Karlstal-Schichten (both Middle Buntsandstein), respectively. In Zwingenberg, volcanic quartz was observed throughout the Lower Buntsandstein. It occurs also in the lowest and in upper parts of the Middle Buntsandstein, but is absent in between. This observation shows, that the source areas for the Buntsandstein sediments east and west of the URG where somewhat different and evolved through time.

Phyllitic lithoclasts are derived from low-grade metamorphic rocks. Muscovite and biotite could be derived from both igneous and low- to high-grade metamorphic rocks. The common occurrence of polycrystalline quartz corroborates the presence of medium- to probably high- grade metamorphic rocks and mylonites (Passchier and Trouw, 2005) in the hinterland.

The proportion of quartz, K-feldspar and plagioclase in the sediment is often able to corroborate the source area composition (Figure 42). Quartzite pebbles and very well rounded quartz and feldspar grains (Figure 41) indicate the reworking process. The lack of plagioclase may be partly due to the reworking of previously weathered (meta)sediments. However, the quartz-plagioclase-K-feldspar proportions plotted in the ternary diagrams in Figure 42b corroborate a generally granitic composition of the source area. The weathering degree of the Buntsandstein is intermediate to high.

4.4 Postdepositional Processes

Whatever the original content in the rocks of the source area, plagioclase is the most prominent example of depletion due to weathering, and loss of the remaining content after deposition. In the following subchapter the transformation of detrital and neoformation of authigenic minerals are discussed together with other postdepositional processes, like compaction or bleaching. Of importance is also the relative timing of these processes, which is assigned to eo-, meso- and telodiagenesis sensu Choquette and Pray (1970). Eodiagenesis includes processes during progressive burial, telodiagenesis during uplift. Eo- and telogenetic

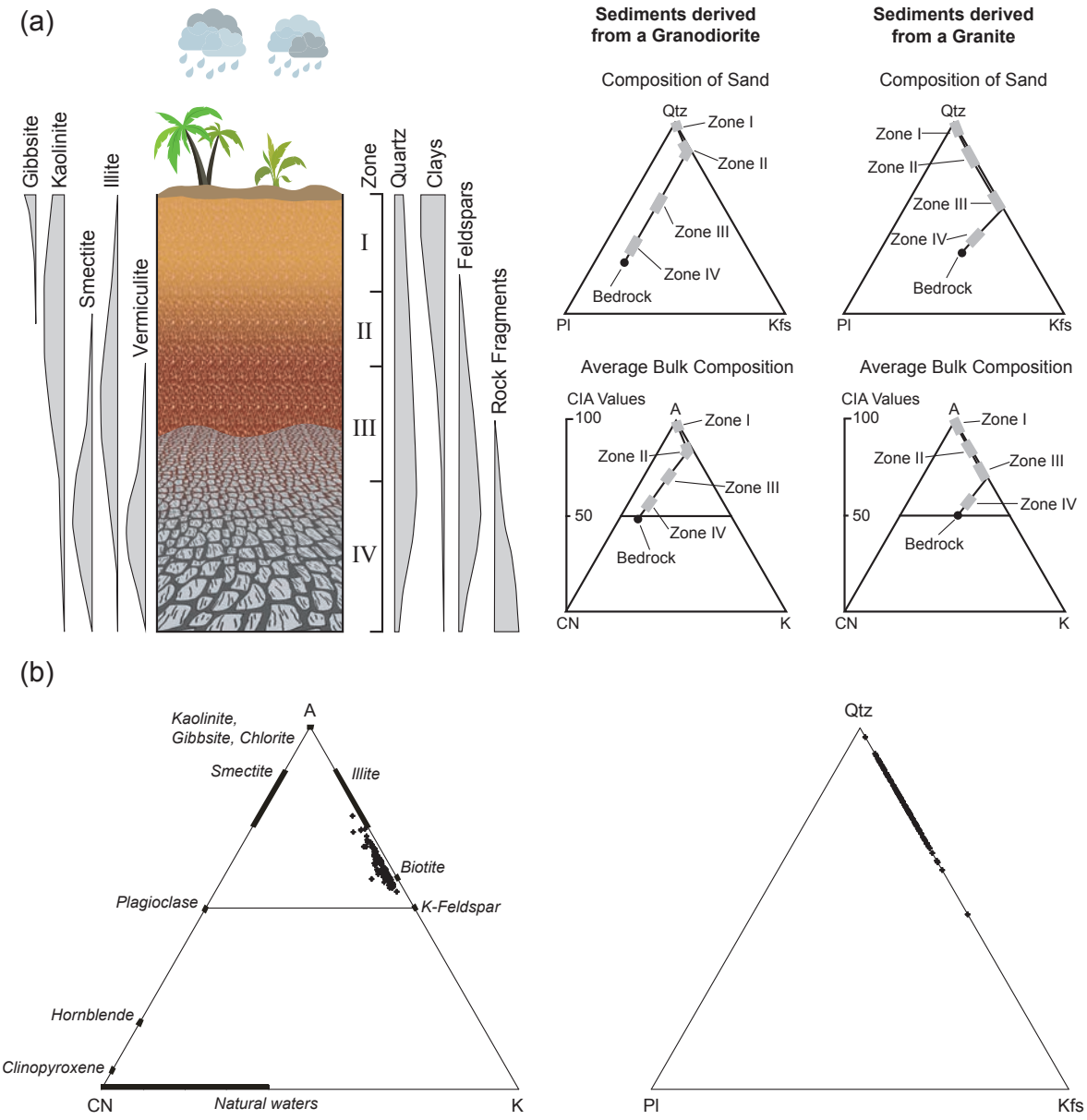

Figure 42: (a) Weathering zones in a granitic bedrock. Ternary diagrams plot the average mineralogical (plagioclase – Pl, K-feldspar – Kfs, quartz – Qtz) and chemical ($CaO + Na_2O$ – CN, K_2O – K, Al_2O_3 – A) composition of a sediment derived from a weathered granite. Only the CaO content of the silicate (not carbonate) fraction is considered (modified after Nesbitt et al., 1997); **(b)** Mineralogical and chemical composition of the Buntsandstein samples (modified after Li and Yang, 2010), resembling weathering zones III and II sensu Nesbitt et al. (1997). The shift towards the K-feldspar indicates an initially enriched sediment source, possibly by the presence of older sediments, which were already depleted in plagioclase.

reactions are related to the influence of surface waters (i.e. meteoric, marine or mixed marine-meteoric waters), whereas evolved formation waters are involved in mesogenetic processes (Morad et al., 2000).

4.4.1 Fe-Oxide and Fe-Hydroxide

The colour of the typical red Buntsandstein is caused by haematite. Haematite forms during early diagenesis from Fe-hydroxide (Walker, 1967; Van Houten, 1968;

Berner, 1969). Yellow or brown colour is caused by the presence of Fe-hydroxide. The abundance of goethite in Leistadt (detected by XRD diffraction, Appendix 8, Chart 8) suggests a link to the barite-Fe-(hydr)oxide fracture fills, which are characteristic for this outcrop. As discussed in Chapter 4.4.6, these veins are hydrothermal and Fe-(hydr)oxide originally precipitated as siderite. Obviously, the hydrothermal fluid hardly penetrated the host rock but was constrained to the fractures. The yellow rock colour must be caused therefore by a telogenetic redistribution of part of the iron released during the transformation from siderite to Fe-(hydr)oxide (mostly goethite). This process is not related to the mesogenetic bleaching. In bleached rocks, neither haematite, nor Fe-hydroxide is present, giving the rock a bright white appearance. For further details on the bleaching process compare Chapter 4.4.8.

4.4.2 Clay Minerals

The most prominent clay minerals are kaolinite and the even more frequent illite. Smectite is rare, its occurrence is discussed together with the one of illite. Chlorite was only detected in a siltstone from the Upper Buntsandstein.
In our samples, the probability for abundant clay minerals generally increases with decreasing grain size. There is no rule of thumb that fine sandstones are generally rich in clay minerals, however, no coarse sandstones with elevated clay mineral content were observed (Figure 10 in Chapter 3.3.2.1). As discussed in the following subchapters, clay minerals were generally emplaced either by (i) infiltration of detrital clay shortly after deposition or (ii) mineral reactions including clay mineral authigenesis during weathering and possibly all stages of diagenesis.

(Ad i) Finer sand was probably able to filter detrital clay more effectively than coarser grained sand during clay infiltration.

(Ad ii) In the South German Basin detrital plagioclase was weathered and replaced by clay minerals (Chapters 4.2.3). Plagioclase is reported to be more abundant in fine grain size fractions in the North German Basin (Füchtbauer, 1967). Its weathering may thus have contributed to elevated clay mineral contents in fine sandstones.

4.4.2.1 Kaolinite

Kaolinite appears as pore filling and replacing clay mineral. “Early” and “late” kaolinite seems to occur. Much of the kaolinite represents a precursor to illite. This interpretation is corroborated by illite-kaolinite intergrowths and illite pseudomorphs after the typical booklet structure of kaolinite (Figure 13 on page 25, Figure 14 on page 26, Figure 40c, Figure 40d). The texture of replacing, illitized, mixed kaolinite-K-feldspar aggregates commonly resembles the one of igneous plagioclase (Chapter 4.2.3). Early kaolinite preferably formed in expense of albite rather than K-feldspar:

$$4\,NaAlSi_3O_8(s) + 4H^+ + 18\,H_2O\,(l) = Si_4Al_4O_{10}(OH)_8\,(s) + 8\,Si(OH)_4 + 4Na^+$$

albite *kaolinite* **R01** (Sposito, 2008)

Besides mixed illitic-kaolinitic clay aggregates, pore filling and K-feldspar replacing pure kaolinite was observed (Figure 16 on page 29, Figure 17 on page 30, Figure 18 on page 31). The formation and preservation of this non-altered kaolinite can be due to (i) shielding of kaolinite from hot, saline burial fluids, e.g. caused by the impermeability of the host rock, or (ii) a later telogenetic generation of kaolinite. It is difficult or impossible to distinguish petrographically between early and late (telogenetic) pure kaolinite, as both precipitate at similar temperatures and chemical conditions. Both scenarios are possible, for the margins of the Upper Rhine graben a telogenetic formation seems more likely, and unlikely for the graben subsurface, as discussed below. In any case, kaolinite is supposed to have formed under the influence of meteoric water (Dunoyer de Segonzac, 1970; Bjørlykke and Aagaard, 1992).

Early kaolinite formation: As discussed before, at least some grains of plagioclase were present in the sediment shortly after deposition. Kaolinite would then rather grow in expense of albite than of K-feldspar (Figure 43). In the aquifers early after deposition, recharge of meteoric water was high and salinity was low (Bjørlykke and Aagaard, 1992).

Late kaolinite formation: Probably due to Tertiary and Cenozoic uplift of the graben shoulders, kaolinite may have formed, again due to the influx of meteoric water. Since all plagioclase was leached during eodiagenesis (see Chapter 4.2.3), this reaction ran exclusively in expense of K-feldspar (Figure 43a). The replacement of K-feldspar by non-illitized kaolinite, as is shown in Figure 17 on page 30 and Figure 18 on page 31, was only observed in outcrop samples outside the graben, not in the subsurface, where highly saline brines occur. However, the number of samples from the subsurface was extremely limited and may not be representative.

4.4.2.2 Illite and Smectite

Illite occurs as tangential grain-coating, radial grain-coating, pore-lining and pore-filling clay mineral (see Chapter 3.3.2.1). The different morphologies indicate differing conditions and ages of mineral formation. Illite, which appears as tangential clay coatings or plugs of pore throats presumably formed during weathering of the hinterland, whereas illite covering cement crystal surfaces is a later product. Presently, the illite precursor smectite occurs only very rarely, due to temperatures in the subsurface and duration of burial, as discussed below.

Early illite/smectite
Numerous authors discussed the mechanical and electrokinetic processes leading to the formation of clay coatings. For an overview on published experimental studies see Matlack et al. (1989). In sedimentologic literature, four major modes for the input of clay minerals into sands during or shortly after deposition have been established. (i) Contemporaneous deposition of the clay and sand fractions. This is hydrodynamically only possible if a very rapid drop of the flow velocity occurs. In terms of depositional environments this can only be the case in turbidite, glacial and debris-flow systems (Morad et al., 2003). (ii) Detrital grains can pick up clay minerals during transport. This mode is characterized by clay coatings,

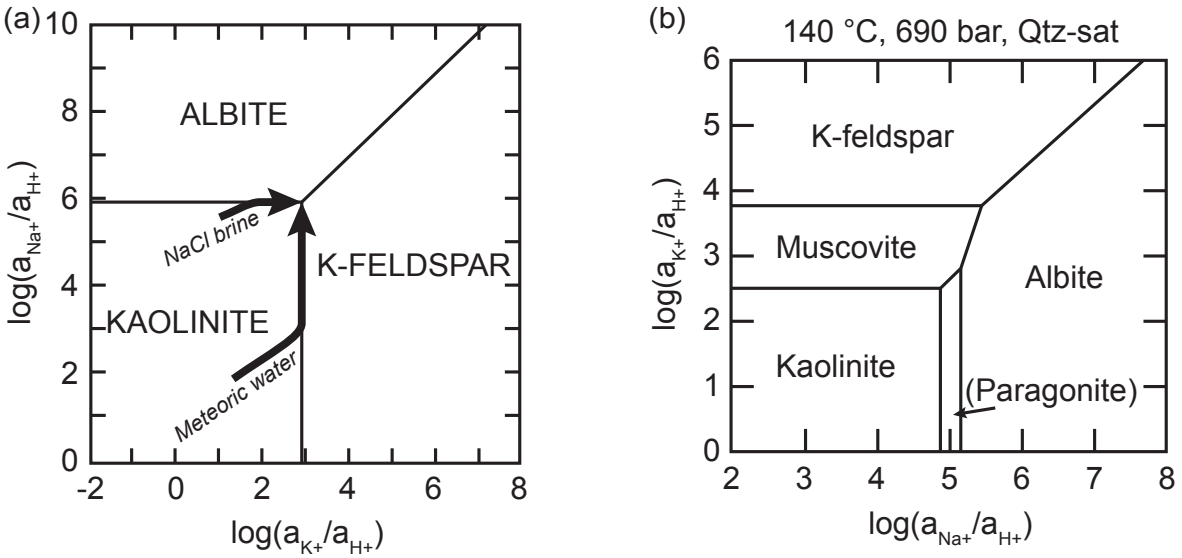

Figure 43: Stability diagrams and phase relationships in feldspathic sandstones. Figures and subsequent figure captions from Bjørlykke and Aargaard (1992), thermodynamic data from Helgeson et al. (1978). **(a)** Reaction paths of aqueous solutions reacting with feldspathic sandstone at 25 °C and 1 bar are indicated by arrows. An equal amount of albite and K-feldspar is assumed released into solution during hydrolysis. The reacting waters, "meteoric water" and "NaCl-brine" (1M), were originally charged with CO_2 at a partial pressure of 10-15 bar. In both cases, kaolinite will be the first to precipitate. The "NaCl-brine" will soon reach equilibrium with albite, whereas the meteoric water will approach equilibrium with K-feldspar first. Thus, meteoric water will tend to dissolve more albite than K-feldspar and NaCl brines will stabilize albite and dissolve K-feldspar. **(b)** Kaolinite and K-feldspar cannot coexist at 140 °C, 690 bar and excess quartz. Illite (muscovite) will precipitate instead.

which most commonly occur within embayed surfaces of sand particles, and/or appear at point contacts between detrital grains. Other characteristics are widely varying rim thicknesses, absence on diagenetic mineral surfaces, and preferential occurrence in sediments deposited from lower energy sedimentary environments (Pittman et al., 1992; Wilson, 1992; Morad et al., 2003). (iii) "Sieve deposits" contain different types of clay mineral arrangements, which are caused by muddy water infiltrating into sand (Wilson and Pittman, 1977; Walker et al., 1978; Matlack et al., 1989; Azmon, 1990). Result are pore-lining clay minerals parallel to sand grain surfaces ("clay coatings"), plugs of randomly oriented clay minerals at pore throats ("meniscal bridges"), and absence of clay coatings at the preexisting point contacts between sand grains. In addition, Walker et al. (1978) described the concentration of infiltrated clay minerals on the top of beds with low permeability, serving as barriers to further downward migration of the influent surface waters. (iv) Bioturbation might also cause clay rim formation (Needham et al., 2005).

Regarding the depositional environment and the sedimentary fabrics of the Buntsandstein, the first and the last option can be ruled out. Considering the texture of the grain-coating and pore-lining clay minerals, most were either picked up during transport, or indicate infiltration shortly after deposition.

Depositional and early diagenetic tangential clay coatings are assumed to have an essential influence on quartz cementation by covering quartz grain surfaces and thus blocking syntaxial quartz overgrowth (see Chapter 3.3.3 and Chapter 4.2.1). The tangential illite crystals may themselves only slightly decrease the permeability

of large pores, but the effect on the amount of cementation and compaction and thereby the poroperm properties can be dramatic. The formation of plugs at the pore throats due to infiltration of clay minerals may also strongly impair rock permeability.
As discussed in Chapter 4.2.3, illite neoformation can occur during weathering of plagioclase under semiarid conditions (Betard et al., 2009). Another probable weathering process was the transformation of mica into smectite (Fordham, 1990). XRD analyses prove the presence of a smectitic precursor to illite in some samples (Figure 46). Fluvial depositional environment, semiarid climatic conditions, hot temperatures, poor/episodic drainage and low relief during Buntsandstein times (Valeton, 1953; Backhaus, 1974; Dachroth, 1985; Bindig and Backhaus, 1995; Paul and Puff, 2014) might have strongly promoted smectite formation during weathering of the hinterland as well as of freshly deposited sandstones (Bjørlykke and Aagaard, 1992; Stern et al., 1997; Hartmann et al., 1999; McKinley et al., 2003). SEM-EDS analyses commonly revealed trace contents of magnesium within the clay coatings, probably caused by the presence of minor mixed layer illite/smectite. Smectite authigenesis occurs in volcaniclastic litharenites (Carrigy and Mellon, 1964; Galloway, 1974) and plagioclase-rich arkoses and litharenites (Ryu and Niem, 1999; McKinley et al., 2003). Assuming that quite some plagioclase was deposited originally in the sediment (see Chapter 4.2.3), smectite authigenesis as described by the latter authors may also have occurred. The observation (Füchtbauer, 1967) that clay minerals are persistent in the plagioclase-free sandstones in the southern part of the German Basin and are less frequent in the plagioclase bearing sandstones in the north may further corroborate this hypothesis.
All mentioned results corroborate the detrital origin of a large part of the illite/smectite observed. A significant part of today's illite most probably formed during burial diagenesis from a smectitic precursor.

Late illite/smectite
During burial diagenesis, illitization of smectite was favoured due to at least episodically elevated burial temperatures (Chapter 4.6) and sufficient K^+ supply from (sub)arkoses (Figure 44). Besides temperature and fluid composition, time is another main parameter for diagenetic reactions. The degree of smectite to illite conversion can be predicted from sedimentation age together with burial history (Velde, 1995). In Figure 45 (adapted from Rügner, 2000) the hypothetical burial history of the overlying Lower Muschelkalk at a geothermal gradient of 30 °C/km is compared to the time-depth (i.e. temperature) relationship of the smectite-illite transformation proposed by Velde (1995). According to this model, the proportion of illite in the overlying Lower Muschelkalk is supposed to be around 98 %. Approximately the same ratio may be expected for the underlying Buntsandstein. If a geothermal gradient higher than 30 °C/km for at least part of the burial history is assumed, virtually no smectite should have remained. Considering the paleofluid temperatures during burial diagenesis, which were commonly well above 200 °C or higher (Chapter 3.6), the smectite-illite transformation may have occurred in time scales between 10,000 to even 10 years (Table 2 after Pytte & Reynolds, 1989).
I/S mixed layer clay minerals were only detected in wells from the subsurface of the URG (Well A 1, 2 and Well B 1, 2) and in the quarry Cleebourg. Analyses of the XRD-patterns consistently resulted in illite proportions >>90 % (Table 3).

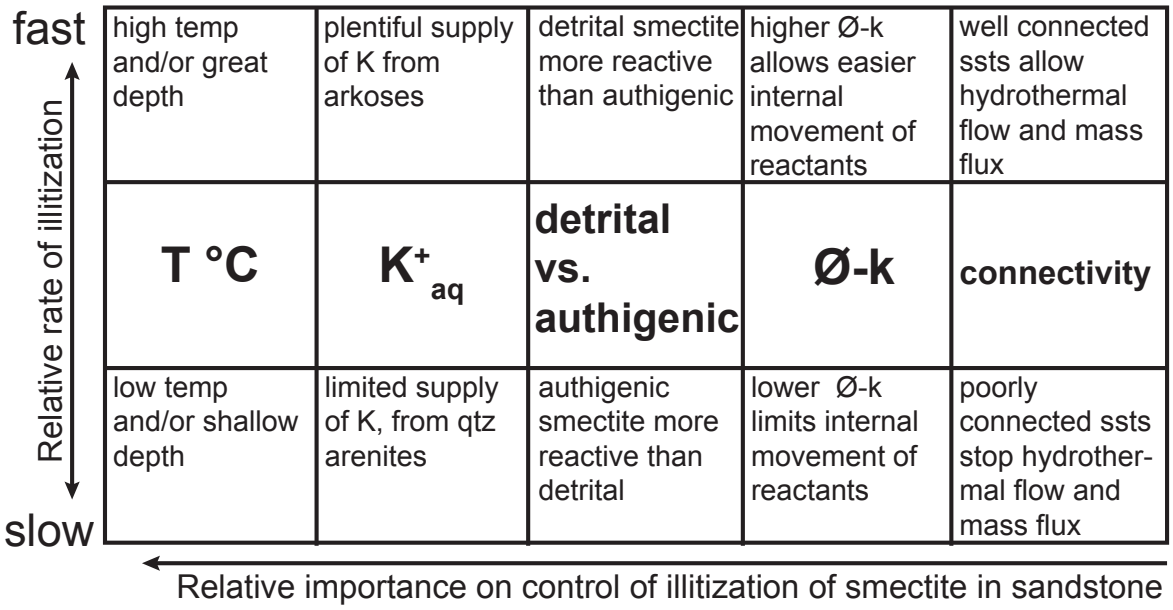

Figure 44: Factors controlling the illitization of smectite in sandstones (McKinley, 2003).

Samples from the subsurface as well as from the surface (Cleebourg) are derived from the direct vicinity of faults. Hydrothermal I/S neoformation may therefore have occurred (Inoue, 1995). I/S minerals in the URG wells could just as well be introduced from overlying Tertiary beds during drilling. Considering the abundance of illite throughout the Buntsandstein and assuming that a large part of the illite was initially smectite, the smectite-illite transformation could represent a major sink for potassium derived from feldspar dissolution and a major silica source for quartz cementation (Chapter 4.4.3).

Illite neoformation

Illite neoformation in expense of kaolinite and K-feldspar was observed as well as pore-filling (meshwork illite) and pore lining (radial illite) precipitates without an obvious relationship to a precursor mineral.

The illitization of kaolinite has been described by two chemical reactions. The first one is a pH-neutral, isochemical, kinetically-controlled process (Bjørlykke and Aagaard, 1992; Gaupp et al., 1993; Morad et al., 2003):

$$Kaolinite + K\text{-}Feldspar \rightarrow Illite + 2\ Quartz + H_2O \qquad \textbf{R02}$$

Table 2: Time-temperature relationship of the smectite-illite transformation. Approximate times at temperatures exceeding 90 % of peak values for the transformation of pure smectite into I/S with 80 % illite in argillaceous rocks (Pytte & Reynolds, 1989).

Approximate time	Estimated peak temperature (°C)	Geological conditions	Reference
10 yr	250	Contact metamorphism	Reynolds (1981)
10,000 yr	150	Hydrothermal well	Jennings & Thompson (1986)
1 my	127	Burial diagenesis	Perry & Hower (1972)
10 my	100	Burial diagenesis	Perry & Hower (1972)
300 my	70	Burial diagenesis	Środoń & Eberl (1984)
450 my	70	K-Bentonite	Huff & Turkmenoglu (1981)

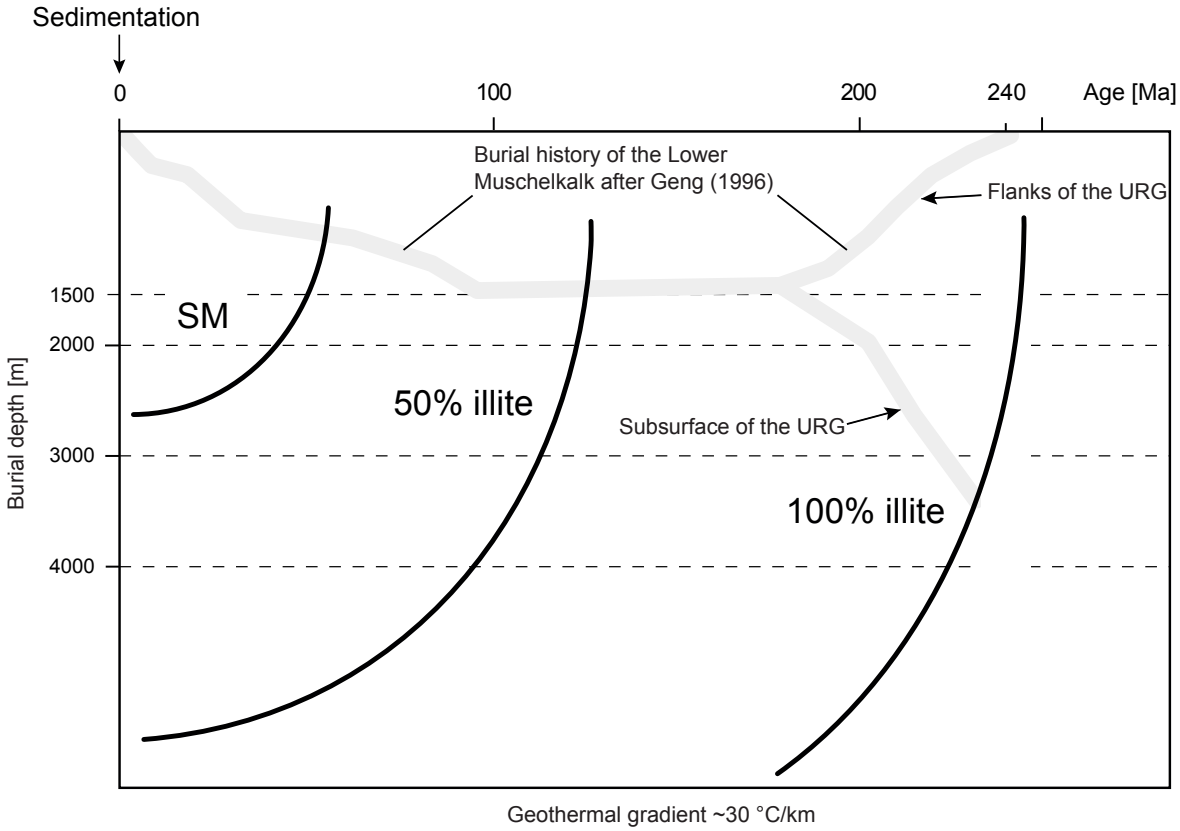

Figure 45: Smectite-illite transformation with time and depth after Velde (1995). The burial history of the Lower Muschelkalk is plotted in the graph (according to Geng, 1996), resulting in illite contents of nearly 100 % for both the flanks and the subsurface of the URG. Plot modified according to Rügner (2000).

A reaction without the involvement of K-feldspar but an external source of K^+, e.g. adjacent evaporites, should also be considered (Rossel, 1982; Lanson et al., 1996; Gaupp and Okkerman, 2011):

$$Kaolinite + \frac{2}{3}\,K^+ \rightarrow \frac{2}{3}\,Illite + \frac{2}{3}\,H^+ + H_2O \qquad \textbf{R03}$$

The following reaction leading to the replacement of K-feldspar by illite was described by Platt (1993) and McAulay et al. (1993):

$$3\,K\text{-}Feldspar + H_2O + 2\,H^+ \rightarrow Illite + 6\,Quartz + 2\,K^+ \qquad \textbf{R04}$$

This reaction needs a source of acidity, possibly provided by the influx of organic-acid bearing formation water (Morad et al., 2003) or by migration and dissociation of CO_2 (Barclay and Worden, 2000).
Reactions R02 and R04 most probably account for the formation of diagenetic illite within the study area. Kaolinite as well as K-feldspar are both common constituents of the Buntsandstein, and are the assumed sources of Al and K for this reaction. The observed intergrowth of kaolinite and illite, as well as of K-feldspar, illite and quartz (Figure 13 on page 25) supports this assumption. Reaction R03 cannot be disproved by petrographic observation but an external source of K^+, related to

Table 3: (a) Δ2θ (CuKα) values using 001/002 (near 9-10° 2θ) and 002/003 (near 16-17° 2θ) positions of illite/EG-solvated smectite for estimating percent illite in illite/ethylene-glycolated-smectite (Moore, 1997). **(b)** Δ2θ (CuKα) values measured on samples with distinct smectite peak. According to table (a) illite contents are consistently beyond 90 %.

(a)

% Illite	Reichweite	° Δ2θ
10	0	5.49
20	0	5.68
30	0	5.94
40	0	6.16
50	0	6.52
60	1	7.01
70	1	7.38
80	1	7.88
90	3	8.83

(b)

Sample	Outcrop	° Δ2θ
L7602	Landau 76	8.61
L7601	Landau 76	8.62
Cl1	Cleebourg	8.64
Cl19	Cleebourg	8.81
En01	Edenkoben 1	8.85

adjacent evaporite deposits, is unlikely in the Buntsandstein of southern Germany (in contrast to the area in the north). In the study area some evaporite deposits of the clay-bearing Middle Muschelkalk occur, but are separated from the Buntsandstein by the thick Lower Muschelkalk, and consist of sulphates (anhydrite, gypsum) only. Na-chlorides occur in some distance further to the east (Heilbronn) and southeast (Haigerloch-Stetten).

Meshwork illite might form preferentially close to faults and fractures: numerous samples from the quarry Cleebourg, where a major fault is exposed, show elevated contents of meshwork illite. SEM examination of fractured rocks from well Well A 1 also revealed pronounced illite growth within and around fractures (Figure 47).

Radial illite is a later precipitate than tangential illite as can be deduced from the growth relationship (Figure 14a, Figure 15a). Radial illite preferably grows on K-feldspar. This supports the earlier discussed assumption that K-feldspar is the main K^+ source for the formation of authigenic illite, according to reactions R02 and R04.

K-feldspar and kaolinite coexist at temperatures below 130 °C in a metastable state. According to reaction R02 (Bjørlykke and Aagaard, 1992), after a threshold between 130 °C and 140 °C, illite formation is initiated in expense of kaolinite as well as K-feldspar. This reaction continues as long as the temperatures stay at or above 130 °C to 140 °C. The observed kaolinite-illite intergrowths imply therefore longer lasting burial temperatures not exceeding 130 °C to 140 °C. A telogenetic reaction, transforming illite back to kaolinite is less probable, because it requires intense weathering under warm, humid climate conditions (Bjørlykke, 1998), which is not applicable for the Triassic deposits of southern Germany. Neither petrographic observation nor the chemical index of alteration (Chapter 4.3) indicate the weathering intensity required for this reaction. The picture is slightly modified if we assume reaction R04: in this case illite formation requires temperatures higher than 60 °C but mostly exceeding 100 °C (Platt, 1993).

Whatever reaction is assumed, illite neoformation took place under mesogenetic conditions. The elevated temperatures required cannot easily be explained by a normal geothermal gradient associated with subsidence during the Triassic and

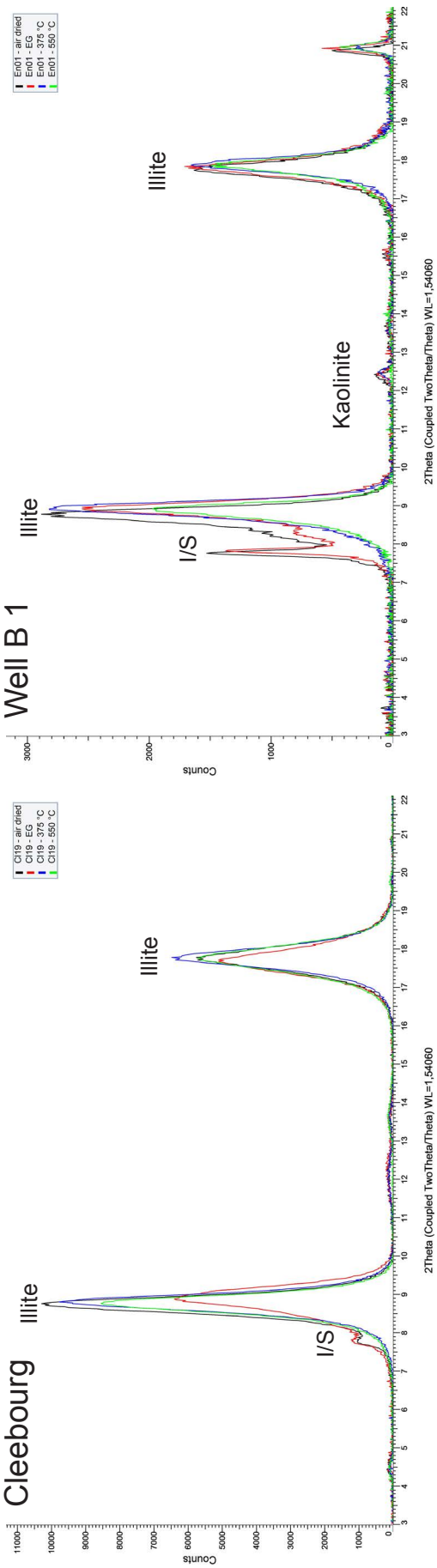

Figure 46: XRD diffractograms of smectite-bearing Buntsandstein samples from the quarry Cleebourg as well as wells Well B 1 and Well A 2. The two peaks with the capture "Illite" were used for the calculation of Δ2θ. Note the sharpening of the 001 reflection and disappearance of the I/S-"hook" after heating to 375 °C. The kaolinite 001 peak, if present before, disappears after heating to 550 °C.

thereafter, achieving burial depths probably less than 1500 m (Chapter 4.6). The required temperatures are more straightforwardly explained by hydrothermal activity. K/Ar dating of authigenic illites (Clauer et al., 2008) corroborates this assumption: illite formed in several age-intervals (mainly 210 – 185 Ma, 175 – 155 Ma, 110 – 95 Ma). Clauer et al. (2008) analysed samples from outcrops and well cores in the area between the northern Vosges in the west and Strasbourg in the east. Illite datings from the Black Forest and the Odenwald also give Jurassic to Cretaceous ages (Brockamp et al., 1994; Meyer et al., 2000; Lippolt and Leyk, 2004; Schleicher et al., 2005). Different pulses of hydrothermal activity were made responsible for the episodic formation of authigenic illite. However, the different hydrothermal events were never recorded together at one single location, suggesting that the thermal history of the URG is complex and locally constrained, probably due to migrating tectonic activity (Clauer et al., 2008).

4.4.3 Quartz

The quartz cementation of the Buntsandstein is discussed quite contradictorily in literature, regarding timing and silica sources. A group of authors, e.g. Valeton (1953), Dachroth (1985) supposed precipitation of silica at or near the surface. Valeton (1953) assumed silica dissolution in depth and subsequent upwelling of a silica-rich fluid leading to precipitation of quartz near the surface. Possible evidence and mechanisms listed by this author are a) the less tight fabric of quartz-cemented rocks compared to weakly or non-quartz-cemented sandstones, b) the occurrence of silcretes and carnelian-crusts, c) pronounced ascension of groundwater into coarse-grained, porous sandstones and further pronounced evaporation, and d) grain-contact-solution between quartz and feldspar grains, which are only possible under burial conditions. Some of the observations and interpretations of Valeton (1953) are in agreement with the results of this study, others can be disproved as discussed subsequently. Carnelian surfaces are rarely present, but they are distinctly different from the quartz cements of the sandstones and should not be intermingled with one another.

Dachroth (1985) as well did not distinguish between locally occurring (carnelian) silcretes and the much more common quartz cements. According to this author there is variability in the amount of quartz cementation between fine-grained to laminated sandstones ("Dünnschichten", interpreted as aeolian dune sands, interdune deposits and playa sediments), and coarse-grained sandstones ("Felssandsteine", interpreted as fluvial channel deposits). The reasons for this variability are, as assumed by Dachroth (1985), selective silicification at or near the surface of fluvial channel deposits ("Felssandsteine") within an overall fluvial depositional environment. As assumed proof for surficial quartz cementation, Dachroth (1985) described fossil ventifacts. The wind-exposed side was said to be grinded, leaving it devoid of authigenic overgrowths, whereas overgrowths were conserved on the lee side. No pictures or detailed mineralogical descriptions of these specimens were given, however. Even if such ventifacts would occur, they would represent a part of the sparse carnelian silcretes but cannot be taken as proof of surficial precipitation of quartz cement. From approximately 150 sandstone samples thoroughly observed within this study, none exhibited a texture as described by Dachroth (1985). A main argument against a near-surface (in terms

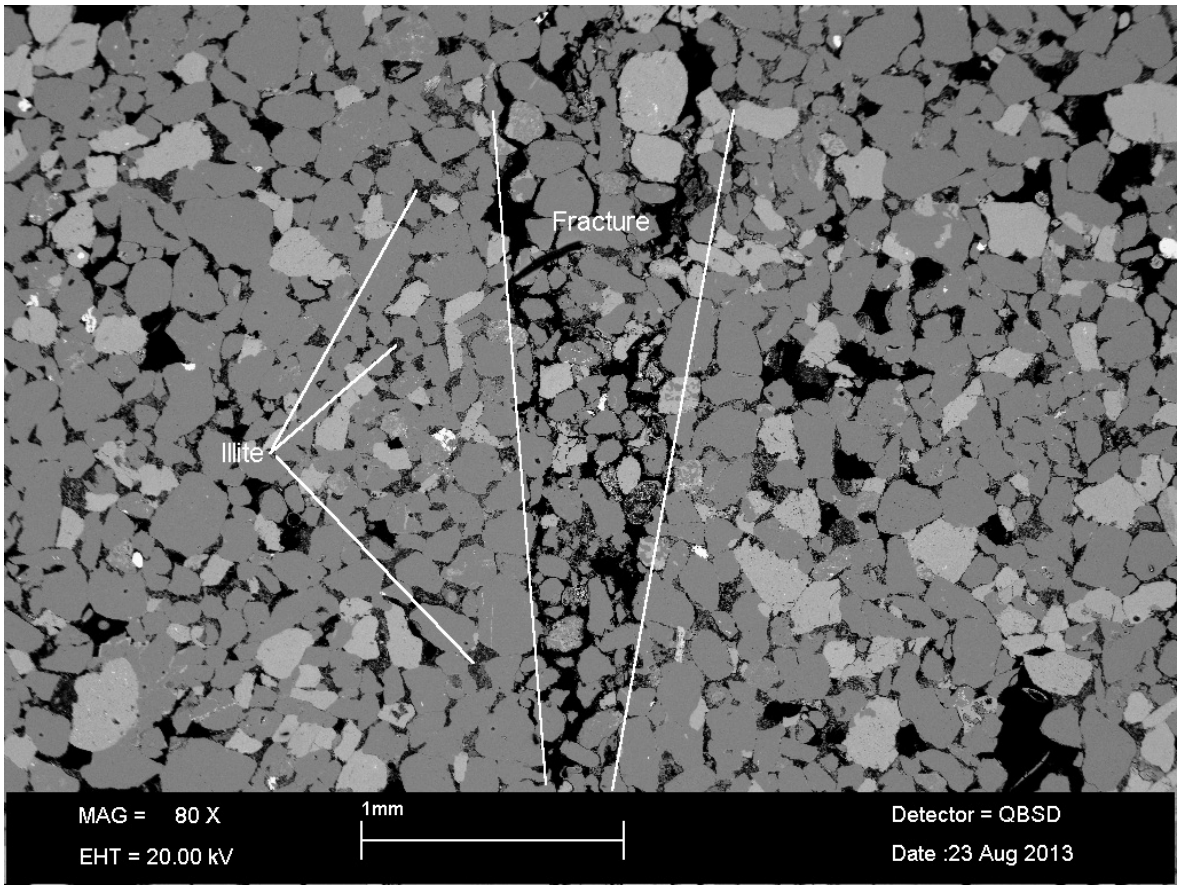

Figure 47: Fracture (outlined by white lines) in fine sandstone. Meshwork illite (felt like intergranular aggregates) precipitated preferably in and directly adjacent to the fracture. Three illite aggregates are exemplarily marked. Dark grey grains are detrital quartz, light grey grains are K-feldspar. Heavy minerals (barite, zircon, apatite, anatase) are white. BSE-SEM image. Buntsandstein, well Well A 2.

of decimetres to metres) quartz cementation is the result of microthermometry (Chapter 3.6). Apart from this, a hypothesis for the silica source of all the quartz cements is missing in his publication.

The amount of authigenic quartz overgrowths is triggered by the physical and compositional sediment properties prior to the quartz cementation. A distinct dependency on lithofacies types could not be established. The appearance and amount of syntaxial quartz cement is mostly dependent on the abundance of pore-lining and grain-coating clay minerals and on grain size as well as on fluid temperature during cementation.

Coating by illite can very effectively prevent precipitation of quartz overgrowths, because it inhibits the ion exchange between pore fluid and detrital grain surface (Heald and Larese, 1974; Pittman et al., 1992). Only at high burial temperatures quartz cements are able to grow below and possibly break through clay coatings (Ajdukiewicz and Larese, 2012). Incomplete coatings can be overgrown by quartz cement, indicating that the illite (or a predecessor) grew or was infiltrated earlier in diagenetic history than quartz. Quartz cementation is not present in pores without detrital quartz grains. Laminated sandstone successions consisting of different grain sizes often show strongly heterogeneous cementation of the different laminae or interbeds, as already observed by Dachroth (1985). According to Füchtbauer (1967), investigating the North German Basin, quartz cement favours finer sandstones, and

anhydrite prefers coarser sandstones. Fine sandstones, largely lacking clay coatings, might promote quartz cementation due to their increased specific detrital quartz surface, compared to coarser sandstones. In our Buntsandstein samples, medium- to coarse-grained sandstones are in contrast prone to quartz cementation. This effect is most probably coupled with the higher abundance of illite coatings in the fine and very fine sandstones of our working area. Our own and Füchtbauers (1967) observations are not necessarily inconsistent with each other, because the latter author analysed a different facies, the more distal, brackish-lagoonal, partly saline environment of the northern part of the German Basin. Our samples represent marginal deposits of this basin. One major difference is the amount of clay coatings, crucial for quartz cementation. Füchtbauer (1967) described only "small amounts" of detrital clay minerals in the sandstones and slightly elevated contents in siltstones, which "not uncommonly" form tangential coatings around detrital grains. He also mentioned, that phyllosilicates are restricted to the estuaries of the two main rivers east and west of the Rhenish Massif. The samples in our study, however, are often rich in phyllosilicates. Because the presence and amount of tangential clay coatings are adjudged a key trigger controlling the subsequent quartz cementation, this difference is the most probable reason for the only at first sight controversial observations.
The amount of quartz cement has a massive influence on the amount of compaction and the poroperm values. Authigenic quartz was the first framework-supporting cement: quartz-cemented sandstones show the highest Intergranular Volumes (IGVs), i.e. the lowest compaction. The quartz cementation initiated at a depth of about 1300-1500 m, which is also the maximum burial to be assumed (Chapter 4.6). This is an extraordinarily shallow burial depth regarding the high amount of quartz cement observed (up to >25 vol. %, with an average around 5 vol. %, Chapter 3.3.3). In numerous examples from oil and gas fields worldwide (McBride, 1989; Giles et al., 2000), a content of more than 5 vol. % of authigenic quartz cement is usually assigned to burial depths of more than 2500 m, whereas contents higher than 20 vol. % indicate depths exceeding 3000 to 4000 m burial.

Silica supply and quartz cementation
Silica sources are discussed by numerous authors, e.g. McBride (1989) and Giles et al. (2000). Introduction of silica by an oversaturated external pore fluid is not feasible according to the latter authors. It can only induce localized cementation. This is the main result of their reactive fluid flow models. Internal silica sources must therefore account for distinct, more than local quartz cementation.
The most likely sources are:

(1) Feldspar dissolution with associated clay mineral authigenesis,

$$4\,Albite + 4\,H^+ + 18\,H_2O \rightarrow Kaolinite + 8\,Si(OH)_4 + 4\,Na^+$$ **R01** (Chapter 4.4.2.1)

$$Kaolinite + K\text{-}Feldspar \rightarrow Illite + 2\,Quartz + H_2O$$ **R02** (Chapter 4.4.2.2)

$$3\,K\text{-}Feldspar + H_2O + 2\,H^+ \rightarrow Illite + 6\,Quartz + 2\,K^+$$ **R04** (Chapter 4.4.2.2)

(2) Smectite-illite transformation of dispersed smectite clay minerals and/or of interbedded mudstones,

$$Smectite + K^+ + Al^{3+} \rightarrow Illite + Quartz + H^+$$ **R05** (Bjørlykke, 1983)

(3) Quartz dissolution at grain contacts (Giles and Marshall, 1986).

(Ad 1) The dissolution of plagioclase to form kaolinite (R01) or illite can only subordinately account for silica enrichment of the pore water, despite the fact, that the degree of this transformation is considered to be very high and significant plagioclase is supposed to have been originally deposited. An ongoing reaction of this type needs meteoric water flushing, otherwise it would cease (Bjørlykke and Aagaard, 1992). Hence, the silica formed by this transformation is constantly removed already during weathering and/or early diagenesis, even if the process affected larger amounts of grains. This might have contributed to the formation of carnelian, but not of quartz. Chalcedony (carnelian crusts) precipitated only locally at or close to the surface (Ortlam, 1967; Backhaus, 1975). Quartz formed from these amorphous silica would have a chert-like appearance (Bjørlykke and Egeberg, 1993), which was not observed in our samples. A precipitation of quartz under surface conditions only possible under specific circumstances with inclusions of hydroxides and chert (Harder and Flehmig, 1970) or the formation process is very slow (Heydemann, 1964; Mizutani, 1970). Significant quartz cementation in sedimentary basins usually occurs at temperatures exceeding 90 °C (McBride, 1989; Bjørlykke and Egeberg, 1993; Lander et al., 2008).
Reactions R02 and R04, involving clay minerals and K-feldspar, probably contributed to the silica supply for quartz cementation. Both reactions are kinetically controlled and require temperatures above 130 to 140 °C (Bjørlykke and Aagaard, 1992) and 100 °C (Platt, 1993), respectively, to achieve considerable reaction rates (see Chapter 4.4.2.2 for further details). Fluid inclusion temperatures in quartz cements are well within and above this temperature range (Chapter 3.6).

(Ad 2) The amount of silica produced by smectite-illite transformation is unknown, because the original proportion of smectite on the entire amount of clay is unknown as well. Nevertheless, there are several indications, that originally there was a considerable amount of smectite in the sediment (Chapter 4.4.2.2). The process might therefore have been a significant silica source. Since smectite – illite transformation is a kinetically driven process, it might be jointly responsible for the regional differences in quartz cementation observed (Chapter 4.7). An example is given by millimetre- to centimetre-sized detrital clay flakes (=components of clay assemblages), which can locally enhance quartz cementation. The effect is restricted to the direct vicinity (up to a few millimetres) of mud rip-up clasts. Only with abundant mud clasts present, quartz cementation can be locally extensive. Siltstones contain high detrital clay contents and therefore have the potential to produce significant silica from smectite – illite transformation. Unstable Al-bearing silicates (amphibole, pyroxene, biotite, feldspar, garnet) were probably the source for dissolved Al.

(Ad 3) Medium- to coarse-grained sandstones with little grain-grain dissolution and elevated quartz cement content are considered silica importers. Fine, clay-rich sandstones are usually low on quartz cement, occasionally exhibit increased quartz dissolution at grain contacts, and represent therefore silica exporters. The amount of quartz cementation due to grain-grain dissolution could not be quantified. But siltstones may represent again a major SiO_2 source for intergranular quartz cementation: The clay content enables pronounced quartz dissolution at contacts between grains.

To sum up: Fine to very fine sandstones rather exported silica, whereas coarser grained sandstones rather imported. This hypothesis is based on the following observations:

1. Fine to very fine sandstones often reveal pronounced quartz dissolution in contrast to coarser grained sandstones. This trend may be caused by the elevated abundance of grain-coating illite in fine sandstones, which promote quartz dissolution at grain contacts (Bjørkum, 1996).
2. The amount of quartz cement in fine-grained sandstones is significantly less than in coarser grained sandstones, caused by the abundance of quartz cement-inhibiting clay coatings in fine sandstones.
3. The content of detrital and infiltrated clay (now illite) is significantly elevated in fine-grained sandstones. Much of this illite likely formed from a smectitic or kaolinitic precursor through a silica-releasing reaction.
4. Interbedded mudstones, similar to local accumulations of clay rip-up clasts, may have contributed to the quartz cementation of adjacent sandstones by smectite-illite transformation and dissolution of silt and clay sized quartz grains.

The mentioned three possible sources for quartz precipitation, regardless of primary rock composition, porosity, permeability, etc., primarily depend on temperature and pH (Bjørkum, 1996; McKinley et al., 2003). The controlling factors of the smectite-illite transformation were already discussed (Chapter 4.4.2.2). Similarly the dissolution of quartz (or other detrital grains) at grain contacts only requires the presence of mica (Figure 13 on page 25) or illitic clay between the grain contacts and elevated fluid temperatures (Thomson, 1959; Bjørkum, 1996; Bjørkum et al., 1998; Sheldon et al., 2003; Kristiansen et al., 2011). Under these conditions quartz dissolution may already take place at pressures below 10 bar (100 m overburden). The commonly used expression “pressure solution” should be avoided for this process (Bjørkum, 1996). As mentioned before, regarding the assumed maximum burial depth of only about 1500 m, the Buntsandstein is exceptionally well cemented with quartz compared to published data on reservoir sandstones elsewhere.

The reactions responsible for silica supply as well as quartz cementation are both mainly temperature- and not pressure-dependent. Highly elevated temperatures are needed for precipitation, which can hardly be achieved by a reasonable geothermal gradient at the time of maximum burial mentioned above. The strong influence of hydrothermal fluids on quartz precipitation is corroborated by fluid inclusion microthermometry (see Chapter 3.6). Hydrothermal activity was also deduced from illite age determinations and apatite/zircon fission track analysis carried out in the surroundings of the URG by various authors (see Chapter 4.6 for further details).

The quartz overgrowths commonly show highly complex cathodoluminescence zonation and purple or short-lived blue luminescence colour (Figure 19, Figure 21). The appearance of such differently luminescing zones in quartz cements are attributed to variations in aluminium and trace element content (Matter and Ramseyer, 1985; Ramseyer et al., 1988; Ramseyer and Mullis, 1990). Various authors relate the formation of such complex zonation patterns to variations in crystal growth rate, fluid chemistry, or discrete phases of over-regional cementation (Zinkernagel, 1978; Land et al., 1987; Marshall, 1988; McBride, 1989). Fractionation of the fluid-phase in water-rich and volatile-rich components can also cause cyclic growth of quartz; this type of quartz commonly exhibits zoned, short-lived blue CL (Ramseyer and Mullis, 1990), which was commonly observed in our samples. The phase separation may be caused by a sudden pressure drop, induced by active tectonics (Mullis, 1987). The occurrence of both zoned and non-zoned luminescing overgrowths within the same outcrop (e.g. Leistadt) and the impossibility of regional correlation of CL zones argue against over-regional variations in fluid chemistry. In our samples, the zones could not even be correlated in thin section scale. In addition to the fluid inclusion data these are important arguments for laterally strongly fluctuating hydrothermal imprints onto formation waters as well as distinctly variable concentration gradients of Si.
The co-occurrence of zoned as well as uniform quartz cements (in CL) indicates that different processes contributed to the silica-delivery. If fluctuating aluminium supply was the main cause for zonation patterns in quartz, reaction R05 (smectite-illite transformation) likely describes the process (dissolved aluminium is mandatory for this reaction).
Uniform luminescence of quartz cements probably formed due to dissolution at grain contacts. Even though mica and/or clay minerals are involved in this process, they act like a catalyst and remain unaffected (Bjørkum, 1996; Kristiansen et al., 2011), i.e. there is no Al necessary for or liberated by this reaction. Aluminium may of course be already present in the pore fluid, but the CL zonation patterns can be better explained by the involvement of the Al-consuming reaction R05.
Burley et al. (1992), and Graham et al. (1996) reported significant variations in $\delta^{18}O$ across single quartz overgrowths. However, Sullivan et al. (1997) and Kelly et al. (2007) showed, that oxygen isotopes measured with a high-resolution ion probe exhibited no significant shifts related to the quartz overgrowth zonation. Kelly et al. (2007) investigated the same sandstone formation as Graham et al. (1996) and attributed the differing results to poorer precision and larger spot size of the microprobe used in 1996 and hence failure to identify measurements that included both quartz cement and detrital grains. Also the results of Burley et al. (1992) are doubtful therefore. In our study, high-resolution $\delta^{18}O$ ion probe analysis could not be undertaken.

4.4.4 Feldspar

The shape of the feldspar overgrowths suggests, that they grew into open pore space and are therefore an eo- to early mesogenetic phase. Subsequent overgrowth by authigenic quartz was observed (Figure 17 on page 30). Authigenic K-feldspar formed therefore prior to at least part of the syntaxial quartz cement.

Potassium, aluminium and silicon were most probably provided by intrastratal dissolution of unstable silicates such as hornblende, pyroxene and plagioclase (Walker, 1976; Walker et al., 1978; Waugh, 1978; Turner, 1980; Ali and Tuner, 1982). Tatsumoto and Patterson (1980) corroborated the process of detrital feldspar dissolution and re-precipitation as authigenic feldspar, because lead isotopes in detrital grains and overgrowths are similar. Due to dissolution, the concentrations of potassium, sodium, aluminium and silicon in the pore fluid increased. These fluids probably migrated downward and precipitation of K-feldspar occurred. The scarcity of authigenic K-feldspar either implies, that the supersaturation of the pore fluid with respect to K-feldspar was very low and/or that the diagenetic (especially thermal) conditions changed and promoted the formation of illite instead of K-feldspar (see Chapter 4.4.2.2). The overall low K^+ activity was probably caused by the subsequent transformation of smectite to illite, which consumed K^+ and was initiated during eodiagenesis (Velde, 1995). But also etching of K-Feldspar is observed, commonly accompanied by illite neoformation. Hence, the pore fluid changed from a (super)saturated composition with respect to K-feldspar during eo-/early mesodiagenesis to an undersaturated composition during later mesodiagenesis, causing dissolution of K-feldspar.

4.4.5 Carbonates

No remnants of extensive early diagenetic carbonate or evaporite cements were detected. Nodular dolomite or dolocrete rarely occur and often appear together with carnelian. K-feldspar in vicinity to dolomite nodules is occasionally replaced by dolomite (Figure 24 on page 37). These particular beds are called ‘violet horizons’ (‘Violette Horizonte’, VH) by some authors (Ortlam, 1967, 1974; Dachroth, 1985). Another phenomenon caused by carbonate cementation are carbonate-cemented, concretionary spheres (Straßer, 1907; Hoppe, 1927). For a summary of the various formation processes and a digest on relevant literature see Chen et al. (2002) and Morad et al. (2000). VHs are restricted to the Middle and Upper Buntsandstein. The sources for Ca, Mg and Si are most likely feldspar and other weathered silicates. Carnelian and dolomite probably precipitated from highly saturated fluctuating groundwater (Backhaus, 1975; Mader, 1982). There may be a link to the ingression of the Röt sea, considering the more frequent appearance towards the Upper Buntsandstein (Langbein, 1974).
Calcite was additionally found to replace dolomite (dedolomitization, Figure 24 on page 37, Figure 26 on page 38, Figure 27 on page 40) and to precipitate in vugs resulting from K-feldspar leaching (Figure 24 on page 37). Dedolomitization occurs under near-surface conditions (Evamy, 1967; Abbott, 1974; Back et al., 1983; Escorcia et al., 2013) as well as under burial diagenetic (Mattavelli et al., 1969; Budai et al., 1984; Stoessell et al., 1987) and other conditions (e.g. contact metamorphism, fault-related; Wood and Armstrong, 1975; Longman and Mench, 1978). Because of this variety of conditions, Smit and Swett (1969) recommend to avoid the term “dedolomitization”, which pretends a single process. Nevertheless it is still commonly used in recent literature. Calcite, the product of dedolomitization in our samples from well Well A 2, was found to postdate quartz cement (Figure 26 on page 38); an eogenetic formation of calcite can therefore be excluded. The calcite contains significant iron and manganese. Because the

replaced dolomite was found to be iron-free, it can be excluded as iron-source as is suggested e.g. by Evamy (1963). Similarly to the studies of Back et al. (1983) and Stoessell et al. (1987), the dedolomitization in the URG presumably took place involving Na-Ca-Cl brines. The formation water in the URG has a Na-Ca-Cl, often ferrous, composition (Sanjuan et al., 2010; Stober and Jodocy, 2011).
The late calcite inside and outside the URG probably represent calcite E1 and E2 as defined by Geng (1996) in the overlying Muschelkalk limestone. Brightly orange luminescent dolomite as shown on Figure 27 on page 40 was not described by the latter author. Analyses of its isotopic composition would be necessary to better constrain the origin of this dolomite.

4.4.6 Fracture Mineralization

The barite-Fe-(hydr)oxide mineralization in the quarry near Leistadt are interpreted as hydrothermal. Obviously the hydrothermal fluid hardly penetrated the host rock, since no barite was observed cementing the sandstone. The age of the barite cannot be determined and very little has been published on hydrothermal barite veins of the Palatinate Forest. The only larger occurrence known is the former barite mine Clarashall in the Hunsrück near Baumholder (Blume and Kohn, 1962), which is in quite a distance. However, there are several publications on hydrothermal mineral deposits in the Black Forest and the Odenwald (Joachim, 1984; Behr and Gerler, 1987; Lüders, 1994; Werner and Dennert, 2004; Baatartsogt et al., 2007; Staude et al., 2009; Pfaff et al., 2010). A hypothetical correlation can be drawn between the Leistadt and the Neuenbürg mineralization (Northern Black Forest). The mineralogical composition of the latter is characterized by barite, goethite, minor haematite, psilomelane, siderite and quartz. Siderite represents the primary hydrothermal Fe-bearing precipitate, which was transformed to oxides and hydroxides by circulating meteoric waters (Joachim, 1984). The major difference between the two mineralizations is the extent and the size of the fractures. In Leistadt the width hardly exceeds a few centimetres, whereas the Neuenbürg mineralizations span more than two meters (Joachim, 1984). Hydrothermal mineralizations in south-west Germany formed during the final Variscan stages (Permo-Carboniferous), in Jurassic, Paleogene and Miocene time (Staude et al., 2009). As in Neuenbürg, the orientation of the fractures in Leistadt follows the recent regional stress field. Therefore, one can assume that also the Leistadt mineralization formed in the same way and at the same time as the hydrothermal barite-siderite bodies of Miocene age, which are related to URG extensional tectonics (Werner and Dennert, 2004). There is no direct evidence (‘crack-seal’ structures sensu Laubach, 2003) for repeated, synkinematic barite precipitation in Leistadt. The barite texture indicates episodical growth from both fracture walls towards the centre of an open fracture. Open fractures must already have existed before the first barite mineralization. The debris in the central, oxidic part of these fractures (compare Figure 36 on page 49) can however be best explained by brittle deformation; i.e. there was brittle deformation before and coeval with fracture mineralization.

4.4.7 Accessory Minerals

The occurrence of Zn-bearing minerals in the Heidelberg area is most probably related to the Wiesloch Zn-Pb-Ag deposit occurring in the Muschelkalk (Pfaff et al., 2010).
A Ti-bearing, prismatic Fe-oxide was detected in vicinity to weathered ilmenite, and is thus probably a weathering product. During weathering, iron may be oxidized and leached from ilmenite (Lynd, 1960) and precipitate as the observed Fe-oxide. Nucleation of Fe-oxide preferably occurs on the surface of clay minerals (Figure 9 on page 21, Figure 14 on page 26).
Aluminium phosphates and sulphates (APS), detected in a sample from Cleebourg, are usually a rare phase in sandstones (Dill, 2001). The EDS element spectrum points to the mineral svanbergite ($SrAl_3(PO_4/SO_4)(OH)_6$), which is part of the woodhouseite solid solution series (Switzer, 1949). APS minerals in sandstones can be an early diagenetic precipitate due to interaction with meteoric water. In this case PO_4^{2-} could be derived from weathered apatite, Al^{3+} and Sr^{2+} from weathered feldspar and SO_4^{2-} from oxidized sulphides (Spötl, 1990). These conditions would be in good agreement with those proposed for early diagenetic kaolinite formation and plagioclase dissolution. However, a telogenetic formation cannot be excluded.
As-bearing pyrite was only detected in wells from the subsurface of the URG. Studies on arsenic pyrite associated with bituminous coal deposits in the US, point to a deposition from hydrothermal fluids (Kolker et al., 2000; Ding et al., 2001). The occurrence of nickel in the same pyrites also strongly corroborates a hydrothermal origin from a fluid circulating within crystalline basement, from where the nickel could have been sourced. The relative timing of pyrite precipitation is unclear. It has been found only in the subsurface of the URG and could be linked with the migration of hydrocarbons. However, pyrite in the sandstones outside the URG might have been present, but it could have been dissolved by surface processes.
The formation of dendrites is a telogenetic process. Experimental work showed that Fe-Mn-oxide precipitates as dendrites on joint planes under surface conditions (Swartzlow, 1934).

4.4.8 Bleaching

Considering that the Buntsandstein west of the SSW-NNE striking Haardt bleaching zone has a red colour, it is obvious that the bleaching is a diagenetic process that took place after the red staining of the Buntsandstein. The vicinity to the recent western margin of the URG suggests a link to the fault zones, striking the same direction. The Buntsandstein in the wells Well B 1 & 2 and Well A 1 & 2 was also bleached. Bleaching is considered in literature an “old” phenomenon, not connected to Tertiary URG tectonics and related HC migration (Gaupp et al., 1998; Baaske, 1999).
As was shown in Chapter 3.1, four bleaching types were differentiated:

1. Bleached spots in red sandstones (Figure 6a, e, h)
2. Laminar bleaching along bedding planes in red sandstones (Figure 6b, c, g, h)
3. Bleaching associated with fractures (Figure 6c, d)
4. Pervasive bleaching (initial stage in Figure 6c, d)

Type 1 reduction spots can form around organic particles or other isolated reductants. If only relict haematite occurs within the reduction spots, haematite

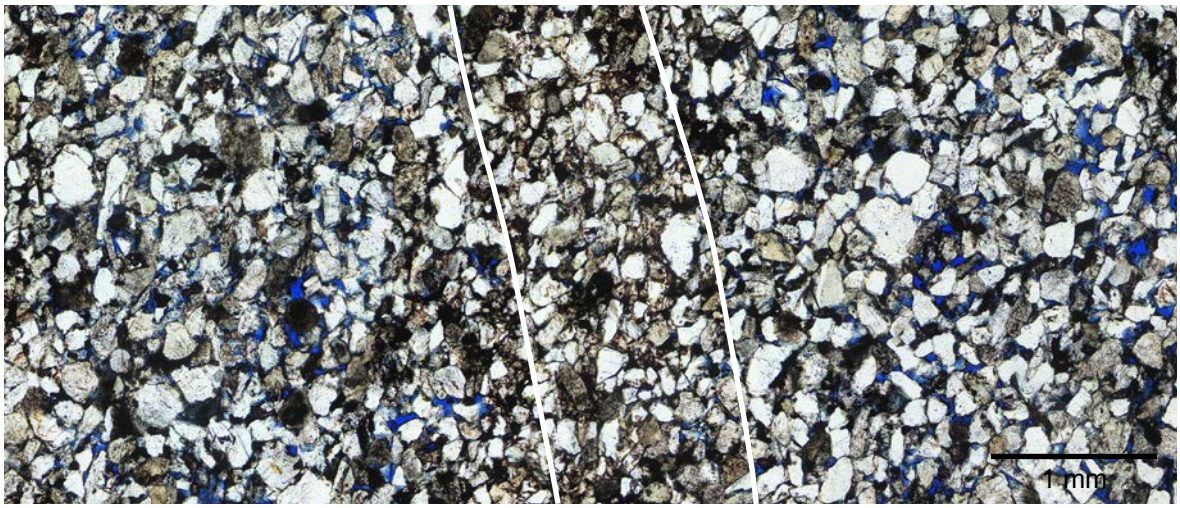

Figure 48: A red lamina in the centre is outlined by white lines. The sandstone on each side is bleached white. Note the difference between red and white sandstone in (i) grain size, (ii) clay mineral content and (iii) porosity (blue). Lower Buntsandstein, Rockenau.

precipitation was either prevented or the reduction spots formed after haematite.
Type 2 laminar bleaching along bedding planes develops due to the dissolution of haematite caused by migration of reducing fluids preferentially along the more permeable bedding planes. Bleached laminae are commonly more porous, exhibit coarser grain size and/or contain less clay than adjacent red laminae (Figure 48). Relict haematite within bleached laminae corroborates the relative timing of the bleaching, which took place after formation of the red beds.
Type 3 bleaching along fractures is basically the same process as the bleaching along bedding planes. Reducing fluids migrated into the sediment along fracture planes to cause laminar bleaching. In the Cleebourg quarry this was obviously the case, however, no direct link was observed in the other outcrops.
Type 4 pervasive bleaching was observed in the quarries in Leistadt and Neustadt a.d.W. and is typical for the Haardt area. The latter bleaching zone is restricted to the eastern margin of the Palatinate Forest, corresponding to the SW-NE striking western margin of the URG. Presumably, the pervasive bleaching is, like in the quarry in Cleebourg, also initially fracture related. Today the Haardt sandstones are usually yellowish-brown. The original white colour, caused by bleaching, is not preserved. Fluids migrating during the Tertiary along URG-related structures reimported iron in the form of siderite (Chapter 4.4.6). The siderite was subsequently dissolved due to meteoric water influx. The iron was redistributed throughout the rock and precipitated as Fe-hydroxide, which causes the yellowish-brown colour.
The exact timing of the bleaching in the Haardt area cannot be determined. Most probably it occurred before the formation of the first authigenic illite (Baaske, 1999), which show mean ages around 180 ma. In Neustadt a.d.W. Carboniferous organic-rich rocks are exposed, which may have caused the bleaching by maturation and associated release of organic acids (pers. comm. R. Gaupp, 2013). Accordingly, later bleaching in the URG could also be caused by the maturation of Jurassic and Tertiary source rocks.

4.5 Diagenetic Sequence

The diagenetic sequence (Figure 49) is divided in eodiagenesis, mesodiagenesis 1 and 2, as well as telodiagenesis (Choquette and Pray, 1970; Morad et al., 2000). Mesodiagenesis 1 comprises processes before the formation of the URG, and mesodiagenesis 2 processes related to the formation of the URG. All diagenetic processes identified were integrated into a cement stratigraphy. As discussed in the introduction of Chapter 4.4, the distinction between eo- meso- and telogenetic processes is based on (1) the kind of fluids involved (surface vs. burial fluids) and (2) on the temporal sequence of the processes. It should be considered, however, that telodiagenesis and mesodiagenesis 2 are both related in time to the formation of the URG and are thus partly coexistent. There is no spatial constriction of telo- and mesogenetic processes to flanks and subsurface of the URG, respectively. For example the mesogenetic barite vein formation was observed both in the quarry Leistadt and in the wells Well A 1 and 2 (flank of the URG and subsurface of the URG, respectively).

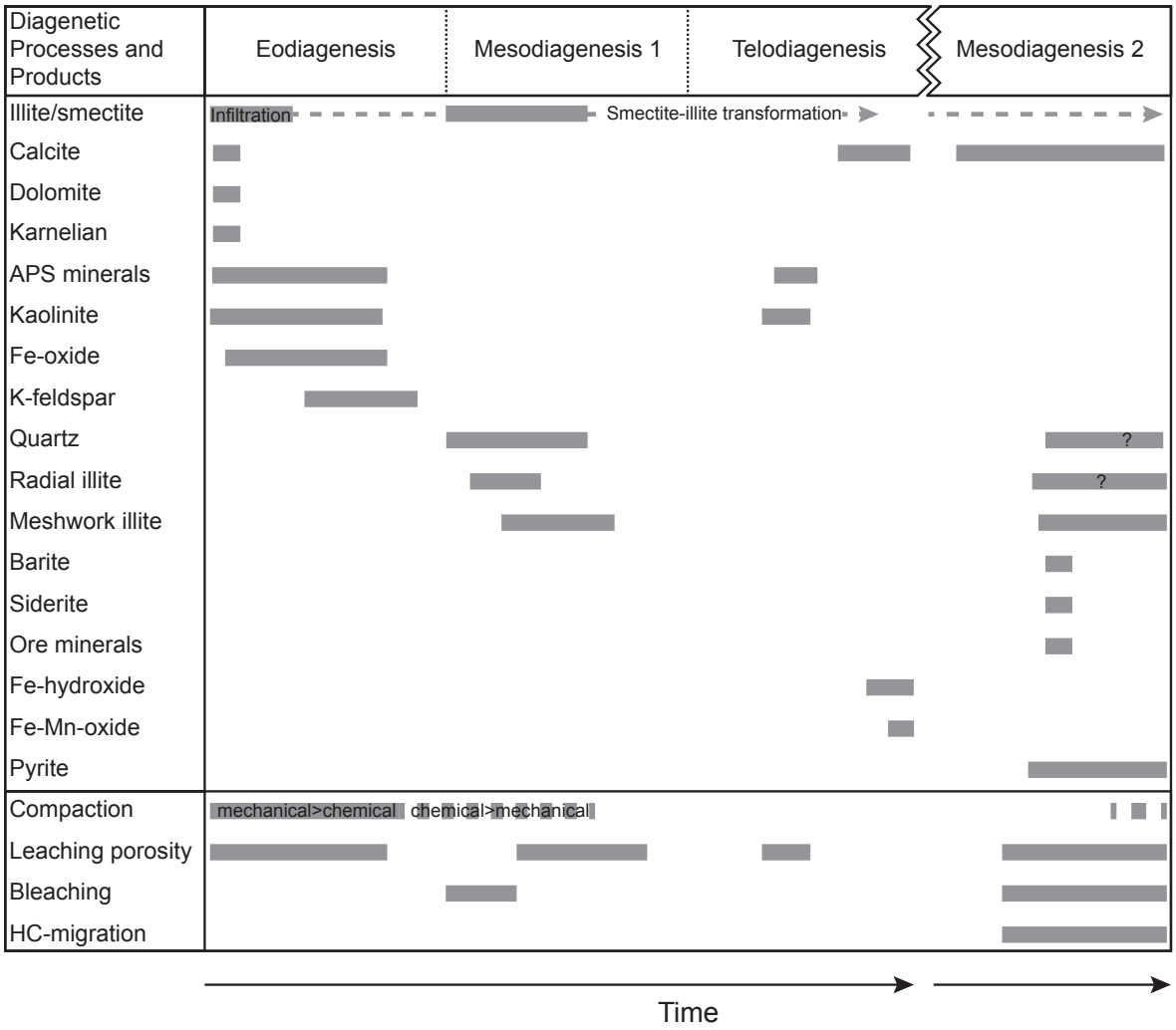

Figure 49: Diagenetic sequence of the Buntsandstein in the study area. Telodiagenesis and Mesodiagenesis 2 have to be considered as coexistent. Note that this is a schematic diagram, comprising data from the whole study area, i.e. not every diagenetic process can be observed in any location. See text for detailed explanation.

Figure 50: Incision of a wadi conglomerate ('Hauptkonglomerat') into aeolian sandstone ('Kugelfelszone'), Middle Buntsandstein, Drachenfels SW of Bad Dürkheim. The eroded sandstone was semilithified at the time of deposition of the conglomerate. (Backhaus, 1974)

Postdepositional processes

The first process in the Lower and Middle Buntsandstein after deposition was the infiltration of clay minerals. Amongst others, Backhaus (1974) showed that the Buntsandstein succession must have been weakly lithified shortly after deposition (Figure 50). Dolomite precipitation, which can be found in the form of concretions in the Middle and Upper Buntsandstein, cannot account for this extent of lithification. Dolocrete and nodular dolomite/calcretes are only local eogenetic precipitates. Therefore, the partial lithification must be related to the infiltration of clay minerals. Numerous samples, e.g. from Cleebourg, show, that even with virtually no quartz cement present, clay-rich, fine-grained sandstones can still be considerably rigid. XRD-analysis revealed that at least part of the detrital clay minerals had originally a smectitic composition and formed during weathering of the hinterland. However, the sandstones in Cleebourg underwent burial and thus significant compaction. An early calcitic cementation cannot be categorically ruled out. Very similar sediment structures were observed in semi-lithified Pleistocene sands on Fuerteventura (Soyk, 2010). The sands are weakly cemented with carbonate and probably clay minerals but can be crumbled by hand. Conglomerates and breccias, composed of well rounded sandstone intraclasts and/or angular debris from the surrounding volcanic and igneous rocks (Figure 51b) cut into the semi-lithified sand (Figure 51a) and often created scours.

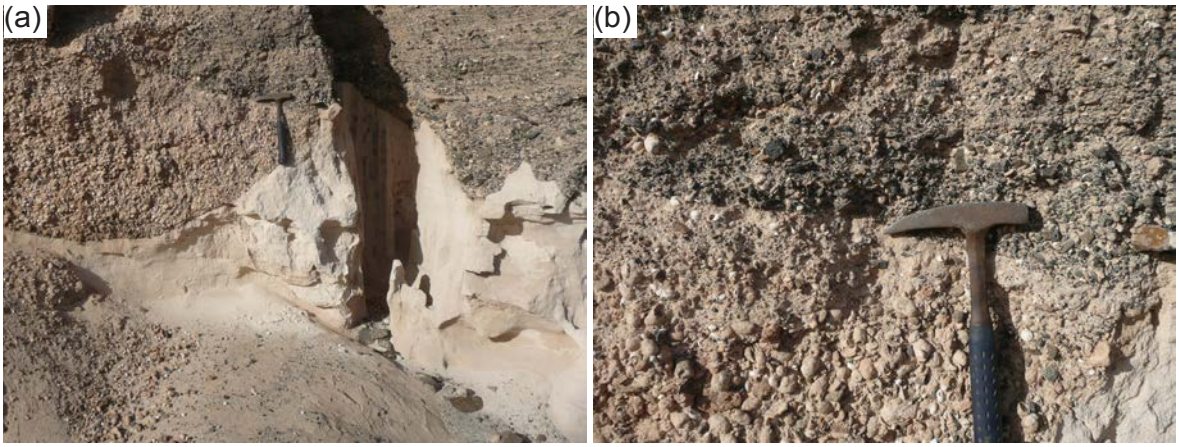

Figure 51: (a) Conglomerates/breccias cut into semi-lithified sand. Pleistocene sand, northern Fuerteventura. **(b)** The lower conglomerate is composed of well rounded intraclast of semi-lithified sand, fossils (gastropods and solitary bee nests) and minor dark, angular volcanic or igneous lithoclasts. In the overlying breccia dark, angular volcanic and igneous lithoclasts prevail. (Soyk, 2010)

Other smectite formed in-situ due to plagioclase-weathering. Because plagioclase in the Buntsandstein is only present in the northern, more distal part of the German Basin (Füchtbauer, 1967), a constriction of plagioclase dissolution to the hinterland and the transport are considered unlikely, as discussed earlier. Thus, both pre- and postdepositional leaching of plagioclase by meteoric water flushing and/or semiarid conditions is proposed.

Eogenetic processes

The formation of haematite, causing the characteristic staining of the Buntsandstein red beds, is considered an eogenetic, near surface process. Both Fe-oxide and -hydroxide were almost always associated with clay minerals. Thus, the introduction of Fe-hydroxide into the sediment together with the infiltration of clay minerals is the major source for later haematite formation. A minor source is the in situ weathering of iron-rich minerals (e.g. ilmenite, biotite).

Dolocrete, calcrete and nodular dolomite are eogenetic precipitates. Only some authigenic quartz was initiated during eodiagenesis, whereas most is mesogenetic. The in situ weathering of plagioclase in the sediment did not cause dissolution vugs, because the process occurred before mesogenetic framework stabilization by quartz. Plagioclase dissolution probably contributed to the formation of eogenetic kaolinite and smectite. The eogenetic formation of the former is proven by its intergrowth with mesogenetic illite. Authigenic K-feldspar is supposed to be an eogenetic rather than a mesogenetic phase. Earliest illite is due to the transformation from smectite, this process may have already started during eodiagenesis.

Mesogenetic processes

The formation of authigenic quartz is mostly mesogenetic. The evolution from eogenetic to mesogenetic quartz is reported by fluid inclusion microthermometry. Earliest FI located between cement and rims of detrital grains exhibit temperatures between 50 °C up to above 100 °C. Homogenization temperatures measured on FI trapped within the overgrowths were hardly below 150 °C. In contrast to the Muschelkalk (Geng and Zeeh, 1995; Geng, 1996), no saddle dolomite was observed, which would further corroborate relatively elevated precipitation temperatures.

Mechanical compaction ceased with the precipitation of the first framework supporting quartz cement. Rocks lacking framework stabilisation may still be subject to mechanical compaction in the subsurface of the URG. However, from a depth of approximately 2 km downward there is only a marginal increase in mechanical compaction (Paxton et al., 2002). The more prevalent process has been chemical compaction since the beginning of mesodiagenesis 1.

Fluid temperature and composition during mesodiagenesis promoted the formation of illite instead of K-feldspar. This is most obvious from the mesogenetic dissolution of K-feldspar, which is closely associated with the formation of authigenic illite. K-feldspar is supposed to be unstable under acid, saline pore fluid conditions and illite may precipitate under elevated temperature conditions (Chapter 4.4.4). Mesogenetic K-feldspar dissolution accounts for the bulk of secondary porosity. In contrast to plagioclase dissolution this occurred after the framework supporting quartz cementation. Vugs after dissolved detrital K-feldspar grains are therefore still preserved.

The earliest illite is due to the transformation from smectite. The process may have been initiated during eodiagenesis, it remained active throughout the burial of

the Buntsandstein. The precipitation of authigenic illite is a mesogenetic process, fibrous, radial crystals apparently were the first ones to precipitate. Fibrous illite preferentially appears around detrital K-feldspar grains, probably marking the above mentioned switch from K-feldspar to illite stability and -precipitation. Pore-filling meshwork illite precipitated later and/or contemporaneously with radial illite. Meshwork illite is partly tied in radial illite (Figure 14a). Clauer et al. (2008) and many others (see earlier discussion) assigned authigenic illite formation mainly to the early Jurassic to late Cretaceous. Illite neoformation during mesodiagenesis 2 is possible, if not probable.
Hydrothermal veins consisting of barite and Fe-(hydr)oxide probably formed during the Miocene and are therefore a syn-rift product. This process most probably was also responsible for the local precipitation of several Zn minerals, which might be synchronous with the fairly important Pb-Zn ore concentrations deposited during Miocene at the nearby Wiesloch mining site (15 km south of Heidelberg).
As-bearing Pyrite was only detected in samples from hydrocarbon wells inside the URG. The pyrite formed possibly in association with the maturation of organic material and/or the migration of hydrocarbons.
The exact timing of the bleaching cannot be constrained, but it represents a mesogenetic process. Bleaching is related with reducing fluids, possibly associated with the maturation of organic-rich shales and/or the migration of hydrocarbons. As discussed in Chapter 4.4.8, the first bleaching is supposed to have occurred before the formation of authigenic illite, i.e. during mesodiagenesis 1. Because the migration of hydrocarbons has been active at least since the Neogene (Rückheim, 1989), bleaching may be still active locally in the subsurface of the URG.
Dedolomitization in the URG probably occurred involving Na-Ca-Cl brines, i.e. during mesodiagenesis 2. Minor etching of quartz was observed in association with dedolomitization.

Telogenetic processes
Telogenetic kaolinite was identified in several samples, in addition to eogenetic kaolinite. However, this does not imply that one or both generations appear throughout the study area. Telogenetic kaolinite supposedly grew in expense of K-feldspar, due to the total loss of plagioclase until this diagenetic stage. Calcite, which precipitated in vugs (commonly derived by leached feldspar) is probably telogenetic and postdates mesodiagenesis. The formation of accessory APS minerals is favoured by meteoric water conditions. It remained ambiguous, if their formation is an eo- or telogenetic process.

4.6 Burial and Thermal History

In the study area, thicknesses of the overlying strata are known or could be extrapolated up to the Middle to Upper Jurassic (Table 4), because, depending on the region, an erosional unconformity cuts the succession.
Quartz cement is the only framework supporting cement within the study area, clearly illustrated by the correlation between the compactional index and the intergranular volume, indicating the extent of quartz cementation (Figure 52a). The methods for measuring intergranular volume (IGV) and compactional index (ICOMPACT) are both described in Chapter 3.4. After precipitation of approximately

Table 4: Published values on minimum pre-Tertiary overburden above the Buntsandstein. The Jurassic is cut by an erosional unconformity in all areas. There is particularly no information on the thickness of possible Cretaceous successions or if they were deposited at all.

	Odenwald (Rupf & Nitsch, 2008)	**Northern Black Forest** (Rupf & Nitsch, 2008)	**Haardt** (Steingötter, 2005)
Middle Jurassic	400 m	300-360 m	>30 m
Lower Jurassic	170 m	130-150 m	150 m
Keuper	300-350 m	250 m	200 m
Muschelkalk	200 m	200 m	185 m
Total	1070-1120 m	880-960 m	565 m

8 % quartz cement, the observed sandstones are usually not (or almost not) further compacted, i.e. their IGVs remain constant. Comparing the IGVs of the investigated sandstones with an empirical compaction curve (Paxton et al., 2002; Figure 52b), the depths where compaction ceased can be estimated. Accordingly, in exceptional cases framework supporting quartz cementation in the Buntsandstein may have occurred at less than 1000 m burial depth. However, only few samples had IGVs above 30 to 35 % and the error is unknown, because the true initial porosity of the sand is unknown. An error of ±2 % at an IGV of 35 % would cause an error of ±350 m in depth! In most cases framework supporting quartz cementation probably occurred deeper than 1000 m.

Only in the Odenwald area the proposed thickness of the overburden nearly reaches the minimum burial depth of the Buntsandstein deducted from the lowest compaction status. Two conclusions can be drawn from these observations. 1) Framework supporting cementation did presumably not occur before Jurassic, and 2) significant Middle/Upper Jurassic and possibly Cretaceous sediments, not preserved today, contributed to advanced compaction.

Apatite fission track data from Variscan igneous rocks from the Odenwald corroborate a cooling below 150 °C between 170 ma in the north and 120 ma in the south (Wagner, 1975). These data corroborate a preceding Mesozoic heating event, probably during the Jurassic. Various studies from the surroundings of the URG and all over Europe further confirm a considerable hydrothermal event at that time, followed by a prolonged phase of elevated temperatures (Brockamp et al., 1994; Zwingmann et al., 1998; Meyer et al., 2000; Lippolt and Leyk, 2004; Timar-Geng et al., 2004; Timar-Geng et al., 2006; Clauer et al., 2008; Dresmann et al., 2010; Brockamp et al., 2011; Zielinski et al., 2012; Brockamp and Clauer, 2013; Środoń et al., 2014). The fluid inclusion temperatures above 150 °C measured in this study have therefore most likely a Jurassic age. Since all temperatures below 150 °C were measured at the grain-cement boundary, they likely reflect the initial intrusion of hydrothermal fluids and mixture with cooler formation waters.

The Late Cretaceous to Paleocene volcanic activity of the Katzenbuckel in the Odenwald most likely did not or only locally cause significant heating of the surroundings, since fission track ages of the Katzenbuckel postdate all other cooling ages in the Odenwald (Wagner, 1975).

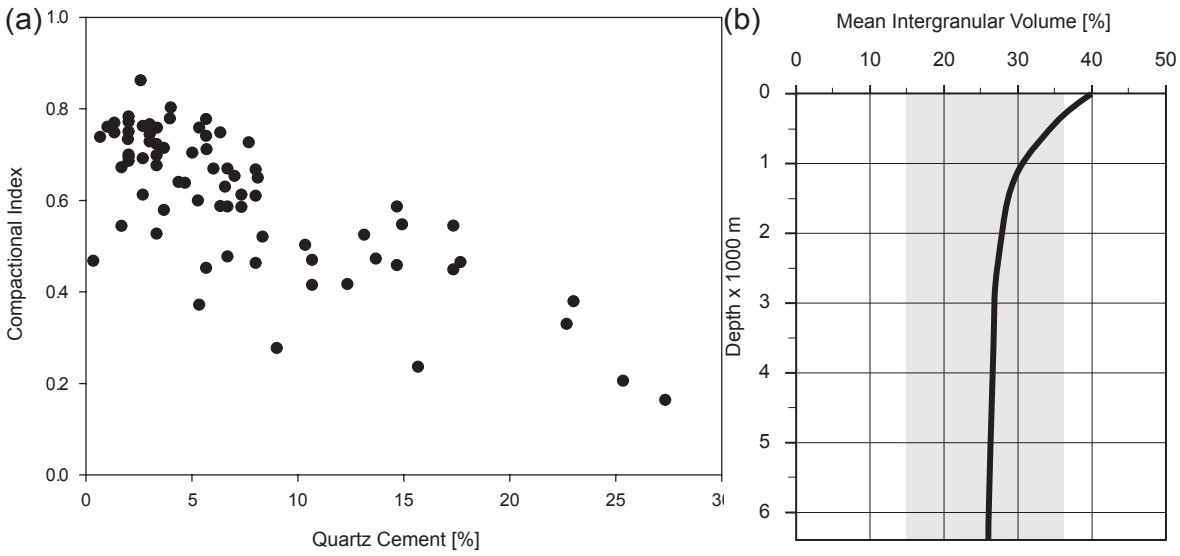

Figure 52: (a) This diagram illustrates, how increasing quartz cementation counteracts further compaction of the sandstones. There is a vague threshold around 8 % quartz cement, enabling the preservation of very low compaction states. Samples with relatively low compactional indexes around 0.4 and quartz cement percentages below about 8 % are additionally cemented by early carbonate and/or haematite cements. **(b)** Empirical compaction curve for relatively uncemented rigid-grain sandstones (modified after Paxton et al., 2002). The grey box represents the range of IGVs observed in this study.

4.7 Regional Diagenesis

Depositional environment and facies primarily control quartz cementation (see Chapter 4.2.1). However, samples with comparable primary composition show different diagenetic characteristics on each side of the URG, indicating regional variations of diagenesis. Most characteristic are the differences in average rigidity between the Buntsandstein east and west of the URG. In the Odenwald and the Black Forest the Buntsandstein is frequently very hard, while its counterpart in the Haardt and the Palatinate Forest is commonly crumbling and sanding. This characteristic divergence is caused by a different degree of quartz cementation (Chapter 3.3.3). The results of the fluid inclusion thermometry in quartz cements also show a regional trend with increasing T_h from west to east (3.6). Therefore a link between T_h and the amount of quartz cementation is assumed.
In addition to Th, the primary composition of the sediment was most important for the development and amount of quartz cements. Since quartz grains were always available as nucleation centres, the occurrence of grain coating clay minerals primarily controlled the formation of quartz overgrowths (Chapter 4.2.1). Likewise early carbonate cements would have prevented intergranular quartz cementation, but they were only detected in a very small fraction of the samples. They cannot account for the regional varying quartz cement distribution. The amount of quartz cementation was somehow less sensitive to cementation-inhibiting phases in the east (Figure 54a). The higher saturation of the fluids in the east, probably caused by rapid smectite-illite transformation, enabled quartz nucleation also on less favourable surfaces and led to a generally more extensive quartz cementation compared to the west.

IGVs on the eastern and the western flank of the URG are largely consistent, although IGVs below 20 % are more common on the western flank (Figure 54b). The minimum value of the IGV possibly reached by mechanical compaction of rigid grains is about 26 %. Further compaction can only be achieved by chemical compaction (grain-grain dissolution) or ductile grain deformation (Fraser, 1935; Graton and Fraser, 1935; Paxton et al., 2002). However, the Buntsandstein largely lacks ductile grains. IGV values below 26 % are thus caused by grain-grain dissolution, increased values west of the URG do not indicate diverging burial depths. The phenomenon seems to correlate with the less developed framework-supporting quartz cementation in the west. As discussed in Chapter 4.6, compaction usually ceased after precipitation of >8 % quartz cement. Only few sandstones on the western flank exceed this threshold; accordingly, in this area, compaction is slightly further advanced (Figure 53), but still preserves significant intergranular porosity. A large proportion of samples from the western flank exceed 10 % porosity, some even 20 %, and measured porosities (inclusive of microporosity) are even higher (Chapter 3.4). In contrast, on the eastern flank and further to the east, quartz cement commonly almost completely occludes intergranular porosity, resulting in intergranular porosity values <<10 %. Likewise, permeabilities strongly differ regionally. Permeability values from the western flank partly exceed 1000 mD, in contrast to values from the eastern areas, which hardly exceed 20 mD (pers. comm. M. Fensterer, 2014).

To understand the regionally differing amounts of cementation, quartz solubility has to be discussed. The solubility of SiO_2 in water depends on temperature, pressure, pH, and salinity (Correns, 1968; Xie and Walther, 1993; Newton and Manning, 2000). Pressure and pH of the formation waters are assumed to have had no or only negligible influence on the observed differences in quartz cementation:

- Compaction data do not indicate significantly differing burial depths for both areas.
- Below pH 9, SiO_2-solubility is almost independent from pH but significantly increases above. Modern (i.e. post Archean) hydrothermal fluids have an acid to neutral composition (Barnes, 1997; Shibuya et al., 2010). Only in special cases alkaline compositions up to pH 7 may occur (Smith et al., 2010). An impact of pH on SiO_2 solubility is therefore unlikely.

Salinities are highly variable on both sides of the URG, as is inferred from ice melting temperatures in fluid inclusions. Salinity is hence comparably ambiguous in both regions. Increasing molality of a NaCl solution can both increase ("salting-in") and decrease ("salting-out") the solubility of SiO_2, depending on P-T conditions. At constant pressure the solubility behaviour changes from salting-out at low temperatures to salting-in at high temperatures. At constant temperature the solubility increases with increasing pressure (Xie and Walther, 1993; Newton and Manning, 2000). There is no data available for a fluid pressure below 0.5 kbar, which is significantly higher than the hydrostatic pressure expected in the Buntsandstein during maximum burial (>>0.3 kbar). Hence, the influence of salinity on local SiO_2 solubility remains unclear, but was probably not relevant.

Temperature is assumed to represent the major determinant for SiO_2 solubility in the pore fluid during burial diagenesis. The amount of dissolved silica positively correlates with increased temperature (Kennedy, 1950; Morey et al., 1962).

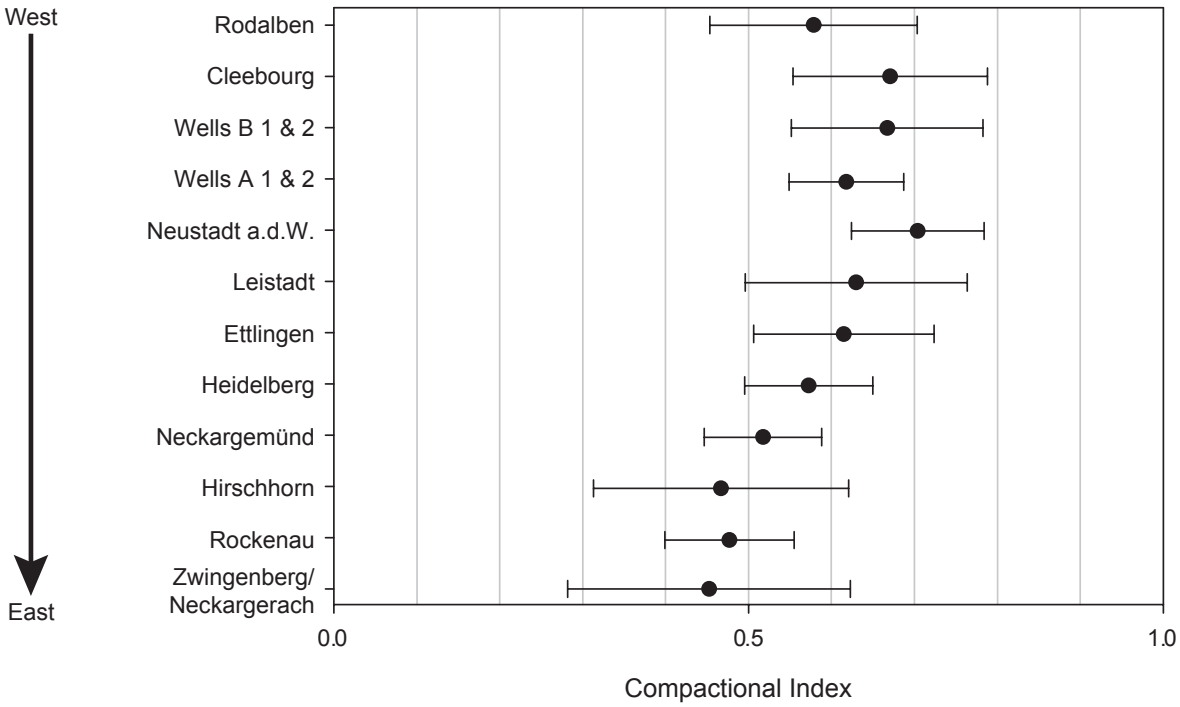

Figure 53: Compactional indexes for each sampled outcrop/well. Error bars represent one standard deviation. Note that compactional indexes on the eastern flank of the URG (Ettlingen, Heidelberg, Hirschhorn, Neckargemünd, Rockenau, Zwingenberg/Neckargerach) are generally slightly lower than on the western flank.

Conversely, if being cooled to the same final temperature, a fluid with an initial temperature of 350 °C would become more supersaturated with respect to quartz than a fluid with an initial temperature of 250 °C. More quartz cement would consequently precipitate from the hotter fluid during cooling.

In Chapter 4.2.1 two major sources for dissolved silica were figured out. (a) Smectite-illite transformation and (b) grain-grain dissolution. At least one of the two must vary between the eastern and western flank of the URG, to account for the quartz cement distribution pattern observed.

Ad (a) The rate of the smectite – illite transformation may have played a major role for the silica supply. As discussed in Chapter 4.4.2.2, its reaction rate is very sensitive to kinetics (Table 2 on page 66): At a fluid temperature of 150 °C an illite – smectite ratio of 4:1 may be achieved within 10,000 years, whereas the same ratio may be achieved within 10 years at a fluid temperature of 250 °C. In the "hot area" east of the URG, the smectite – illite transformation may therefore have rapidly expelled large amounts of SiO_2, causing significant supersaturation of the pore fluid. In the cooler area west of the URG, the reaction rate was probably slower by some orders of magnitude, allowing for the removal of part of the SiO_2 by flushing. East of today's URG the saturation of the fluids in dissolved silica was therefore most likely higher than in the area west of it.

Ad (b) Grain-grain dissolution was assessed by the calculation of the Weighted Contact Packing (WCP, Chapter 3.4). Three general trends were observed, which

Figure 54: (a) Quartz cement inhibitors are primarily clay coatings around detrital grains and rare matrix and early carbonate cements. With decreasing cement inhibitors the increase in quartz cement on the eastern flank (green arrow) significantly outperforms the one on the western flank (red arrow), i.e. the quartz cementation process on the eastern flank was less sensitive to cement inhibitors and/or dissolved silica available on the western flank was not sufficient for further cementation. **(b)** Houseknecht diagram of Buntsandstein samples from the entire study area. Black symbols indicate samples from the western flank, white symbols samples from the eastern flank of the URG. Note that destruction of original porosity by cementation is by far more pronounced on the eastern flank. This is caused by elevated quartz cementation. In extreme cases there was almost no porosity lost due to compaction but it was almost completely occluded by quartz cement. On the western flank, increasing quartz cementation led to decreasing compaction, same as on the eastern flank. However, quartz cementation is significantly less pronounced, allowing for the preservation of distinct intergranular porosity. These regional diagenetic trends on the eastern and the western flank of the URG are indicated by the green and red arrows, respectively.

are best visible in the area around the main faults, and less or not developed in samples away from these.

1. More quartz cement, less grain-grain dissolution;
2. More illite coatings, more grain-grain dissolution;
3. Smaller grain size, more grain-grain dissolution.

Trend (1) can best be explained by early precipitation of framework-supporting quartz cement, which constrained grain displacement/grain dissolution within the framework. (2) Illite coatings hinder framework-supporting early quartz cementation, promote therefore grain-grain dissolution, and depend themselves on (3) grain size (Chapter 4.4.3, Chapter 4.4.2.2).

The data exhibit some regional characteristics, however, no distinct east-west trend comparable to the one for the amount of quartz cementation and the fluid inclusion thermometry was observed (Figure 55). Positive anomalies follow the main faults on the eastern and on the western side of the URG (Chapter 3.4). The outcrops, which exhibited increased quartz dissolution at grain-grain contacts, are

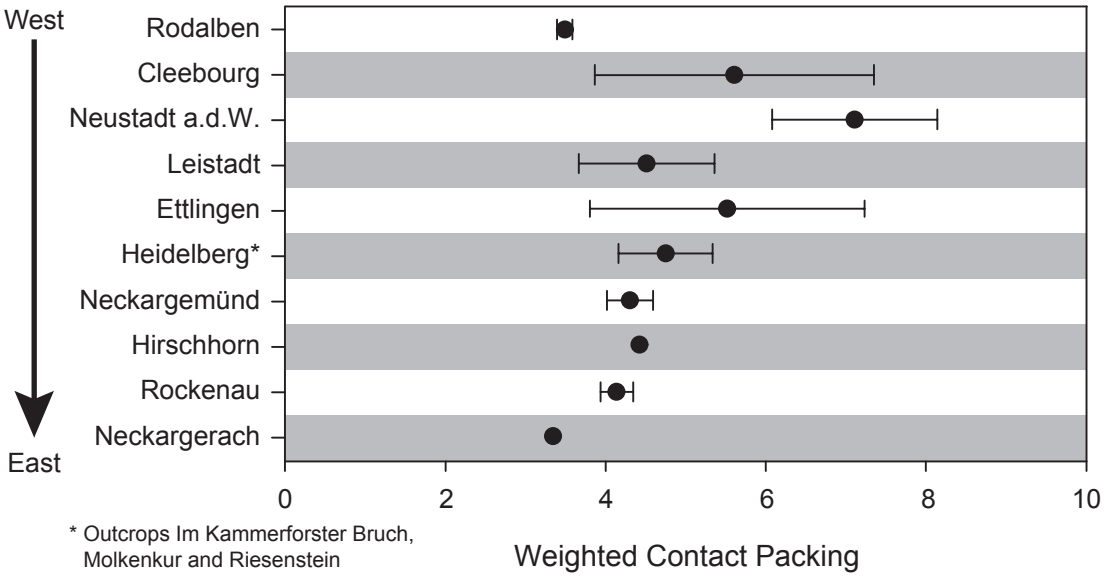

Figure 55: Mean values of WCP from all outcrops. The error bars represent one standard deviation.

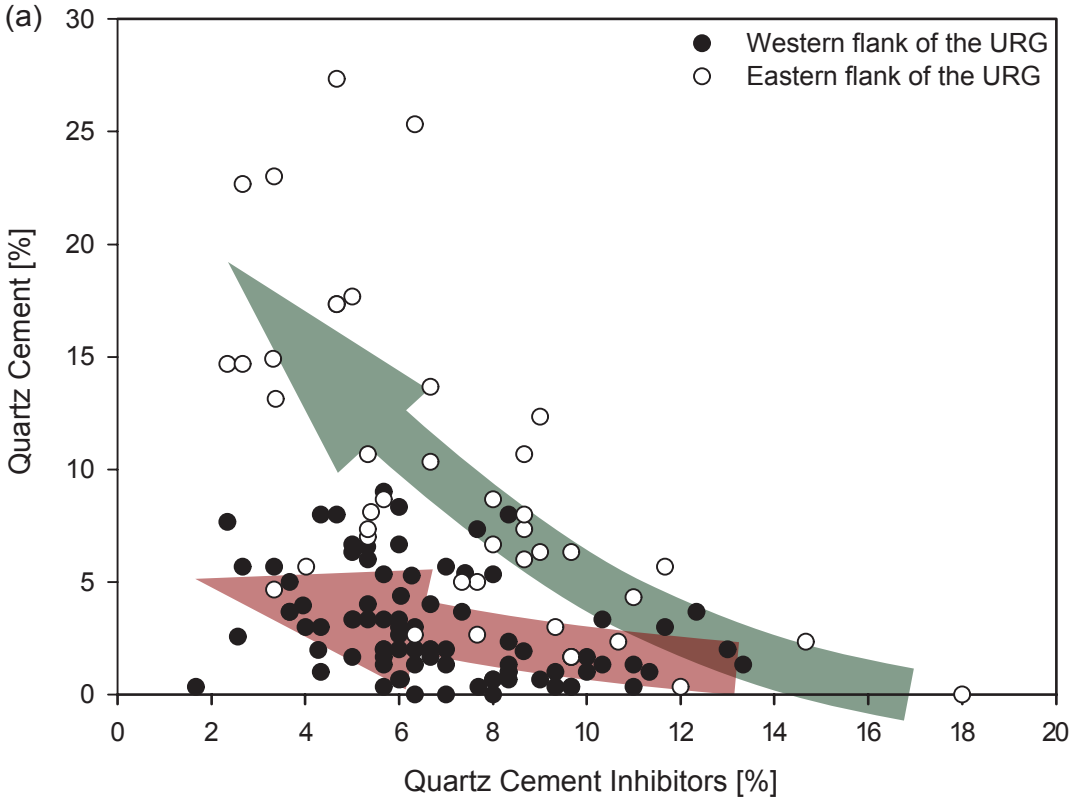
(a)
Western flank of the URG
Eastern flank of the URG
Quartz Cement [%]
Quartz Cement Inhibitors [%]
0
5
10
15
20
25
30
0
2
4
6
8
10
12
14
16
18
20

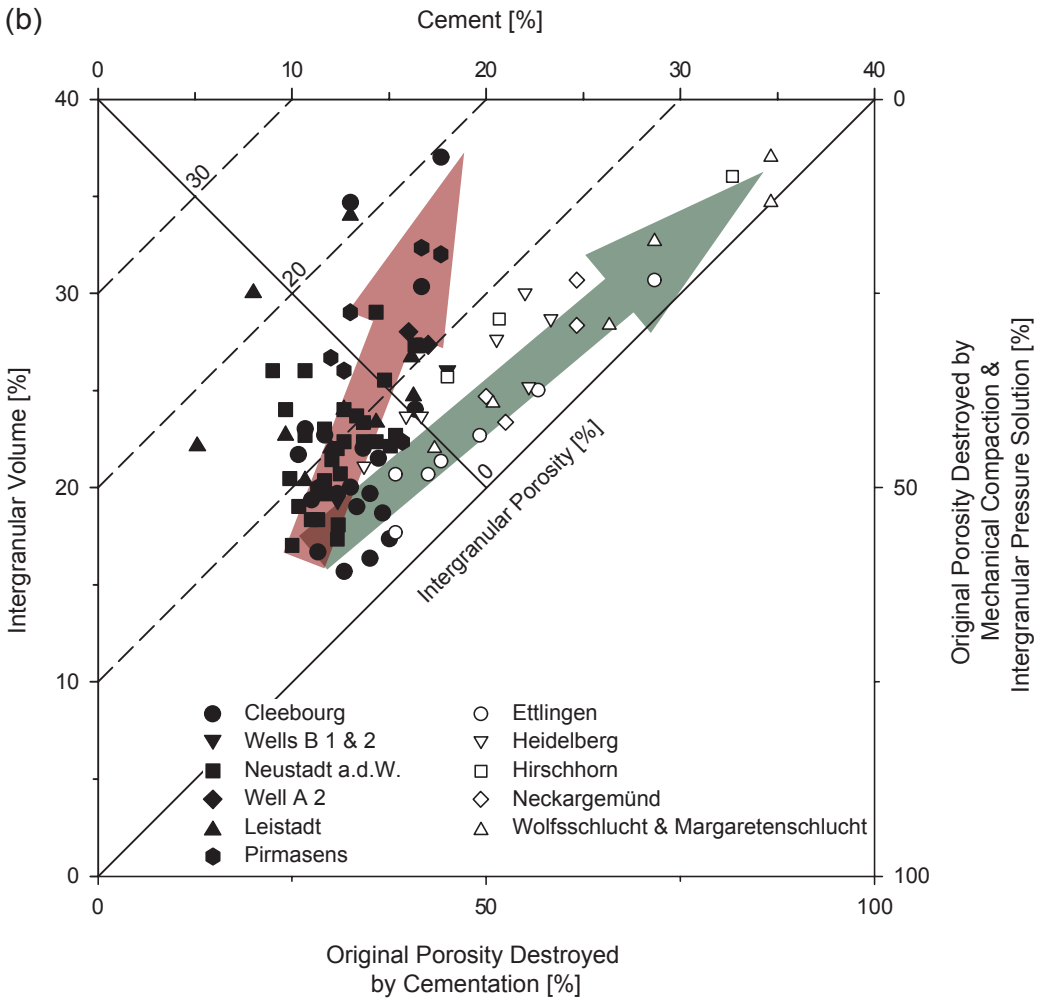
(b)
Cement [%]
Intergranular Volume [%]
Original Porosity Destroyed by Mechanical Compaction & Intergranular Pressure Solution [%]
Original Porosity Destroyed by Cementation [%]
Intergranular Porosity [%]
30
20
0
Cleebourg
Wells B 1 & 2
Neustadt a.d.W.
Well A 2
Leistadt
Pirmasens
Ettlingen
Heidelberg
Hirschhorn
Neckargemünd
Wolfsschlucht & Margaretenschlucht

less than a few hundred meters away from the URG main fault. However, no positive anomaly in the content of quartz cement was observed in the same outcrops, i.e. the dissolved silica did not contribute substantially to in-situ quartz cementation. The enhanced grain-grain dissolution is therefore considered to be a process later than mesodiagenesis 1, when most of the quartz cementation took place. Possibly it occurred during mesodiagenesis 2 in the Tertiary, when the faulting of the URG was active. Hot fluid circulation and tectonic stress along the main faults may have induced grain-grain dissolution. At that time, smectite had already changed to illite, this source of Si was no longer available. Illite and mica are both reported to strongly promote quartz dissolution at grain contacts, smectite, which was probably still present during mesodiagenesis 1, is not reported to do so (Bjørkum, 1996). In addition, URG-related fluids where probably undersaturated with respect to quartz (no fracture-filling quartz was observed), which might have further promoted quartz dissolution, but and the silica gained was mostly exported. The sandstones along the western flank were less cemented with quartz and were probably more prone to dissolution. The silica dissolved may have contributed to the partly intense silicification of Tertiary beds, e.g. near Heppenheim, which is located at the eastern margin of the URG (pers. comm. G. Kowalczyk, 2014).

4.8 Reservoir quality

Matrix

The matrix reservoir quality of the Buntsandstein is controlled by three major rock properties: (i) degree of quartz cementation, (ii) clay mineral content, and (iii) degree of compaction. All three may have a strong effect on porosity and permeability.

The formation of quartz overgrowths is closely related to the presence or absence of (particularly grain coating) clay minerals. Clay coatings around quartz grains inhibit quartz cement growth. There are essentially two extreme cases: (1) clay minerals completely inhibit the formation of quartz cement, and (2) quartz cement can grow unhindered due to the lack of clay minerals. Both cases principally have a negative influence on the reservoir quality.

In case (1) there is no framework supporting cement, enabling increased compaction, i.e. porosity destruction. Clay minerals plug pore throats and thus reduce permeability. This sandstone type can be found all over the study area, however, it is particularly common in the quarry Hanbuch in Neustadt a.d.W. (west of the Rhine graben). Because of the correlation between grain size and abundance of clay coatings, this sandstone type is most common in fine and less common in medium sandstones (Chapter 3.3.2.1).

In case (2), porosity is destroyed by the precipitation of quartz cement, although subsequent porosity reduction by compaction is minimized. Particularly in sandstones with rip-up clay clasts, extensive quartz cements, which almost completely destroyed the porosity, were observed (Chapter 3.3.3, Chapter 4.2.1). Additionally, the degree of quartz cementation was controlled by fluid temperature during quartz cementation. Very hot fluids during quartz cementation enabled to override the inhibition-effect of clay coatings. As a result, sandstones can be well

cemented with quartz, despite significant clay coatings. Because of the regional variation of fluid temperature, generally higher in the east, quartz cements are by far more common on the eastern flank of the URG than on the western margin. The potential for porosity preservation is therefore much smaller on the eastern flank (Chapter 4.7).

The conditions to achieve optimal reservoir properties are consequently: (i) an intermediate amount of clay coatings to allow for framework supporting quartz cementation but to impede porosity destruction by extensive quartz cement growth; (ii) low fluid temperatures during quartz cementation, to avoid porosity destruction by extensive quartz cementation. These conditions were particularly present in the quarry in Leistadt. Porosities commonly exceed 20 % and permeabilities reach up to several Darcy (pers. comm. M. Fensterer, 2014).

A reliable correlation of facies with reservoir quality exists only for a few cases. Sandstones with rip-up clay clasts (Se; see Appendix 1 for the list of abbreviations) consistently exhibit elevated quartz cement around the clay clasts, which negatively influence local porosity and permeability. Fine-grained overbank deposits (Fl, Fsc, Fm) may exhibit considerable porosity, but permeability is insufficient due to the high clay contents. Rippled sandstones (Sr) were also commonly found to be fine-grained and clay-rich and thus also exhibit rather unfavourable reservoir properties. The reservoir quality prediction for the significantly most common facies – trough cross bedded (St) and planar cross bedded (Sp) sandstones – is, however, by far more inaccurate. Because the maximum clay content of these sandstones depends on their grain size, the probability to find good reservoir conditions is generally higher in coarse-grained sandstones than in fine ones. However, fine sandstones can but do not have to contain more clay minerals. Unfortunately, lateral and vertical continuity of these facies is usually not well developed.

Another uncertainty is the degree of compaction. The quarries Neustadt a.d.W. and Leistadt are good examples for differences in chemical compaction. Both outcrops are comparable in terms of stratigraphy, petrography and facies. Nevertheless, the permeability in Leistadt is one to two orders higher than those in Neustadt (pers. comm. M. Fensterer, 2014). The main difference is the dissimilar degree of compaction. Dissolution at grain contacts is a common phenomenon in Neustadt, whereas it is rather rare in Leistadt. This has a minor effect on porosity, however, it strongly affects the geometry of the pore throats. Because of frequent long, concavo-convex and sutured grain contacts, the pore throats in Neustadt are much tighter than in Leistadt, resulting in a massive drop of permeability. It remains unclear, however, what causes the different degree of compaction in both outcrops. A link may exist with the adjacent URG main fault (Chapter 4.7), but both outcrops are around 100 to 200 m away from the fault. A reliable prediction for grain-grain dissolution along the regional faults is not yet possible.

K-feldspar dissolution may contribute to secondary porosity. In the outcrops studied, this phenomenon was commonly observed on the eastern flank of the URG. In the wells Well A 1, Well A 2, Well B 1 and Well B 2 K-feldspar dissolution was also occasionally detected. K-feldspar dissolution can be enhanced by organic acids (Bevan and Savage, 1989). In the subsurface of the URG organic acids may be derived from the maturation of Jurassic or Tertiary source rocks. Particularly in the outcrop samples, K-feldspars were occasionally replaced in-situ by kaolinite, or

kaolinite precipitated in intergranular (primary) pores near the dissolved feldspar grains. Isolated patches of clay minerals like the described occurrences of kaolinite have only a minor effect on permeability (Heald and Larese, 1974). An enhancement of reservoir quality due to K-feldspar dissolution can only be expected, if the dissolution products were removed (Bjørlykke, 1984; Giles and Marshall, 1986).
Summarizing these observations, the Lower and the Middle Buntsandstein in the western (and central?) part of the URG have the potential for a good to excellent reservoir rock, whereas good porosity and permeability values can hardly be expected for the Buntsandstein on the eastern side of the URG. Organic acids from maturation of organic material and acidic formation waters may have further improved the reservoir quality by K-feldspar dissolution, if newly generated clay minerals were not emplaced in direct vicinity of dissolution, giving a negative effect on the generated porosity and permeability, its amount depending on the type of clay minerals formed.
Injection of fresh water into a reservoir can cause the swelling of smectite and mixed layer I/S (Jones, 1964). However, the overall smectite proportion is very low (Chapter 4.4.2.2) and no peculiar swelling of clay minerals caused by flushing with low saline water during drilling or production should occur. During the production of a deep geothermal reservoir, formation water is re-injected and thus should cause small changes of subsurface equilibrium conditions only.

Fractures
Fractures are important in hydrocarbon and geothermal production because they can significantly improve the permeability of a reservoir. The porosity of a fracture network is less important. Aperture, roughness, spacing and connectivity mainly characterize the quality of a fracture networks (National Research Council, 1996). Diagenesis has some direct and indirect influence on these factors. Within the AuGE project, the assessment of fractures was outside the scope of this study, but some observations are given here.
The fractures in Leistadt commonly exhibit apertures between some millimetres up to more than a centimetre or large, well-connected vugs (Chapter 3.5), i.e. they considerably increase reservoir permeability. Fracture apertures in the other outcrops were always in the sub-centimetre-scale (Bauer et al., 2013, in press), still allowing for enhanced fluid flow.
Fracture mineralization may have a negative effect on aperture and roughness of a fracture, however, meniscal bridges may prop open fractures and preserve the aperture (Laubach, 2003). Additionally, fracture cements can be particularly unfavourable for petroleum reservoirs, because they can prevent the fluid flow between fractures and matrix and act as lateral flow barriers (National Research Council, 1996). The barite-cemented fracture walls, which were commonly observed in Leistadt, would hardly allow for fluid flow between matrix and fractures. However, their lateral continuity is unknown. The occasional fracture mineralization in Cleebourg is usually much thinner and patchy, still allowing for fluid flow between matrix and fracture.
In contrast to mineralization on fracture planes, synkinematic, rock-stiffening cementation of the matrix can prevent fractures from closing due to a re-orientation of the stress field (Laubach et al., 2004). The latter authors concluded from

crack-seal structures in quartz-sealed fractures on coeval, synkinematic quartz cementation of the matrix. However, in our samples no quartz mineralization of fractures was observed at all. The only noteworthy fracture cements were the barite-Fe-hydroxide mineralization in Leistadt (Chapter 3.5). These cements hardly penetrated the host rock and thus did not increase the stiffness of the whole rock. The texture of the barite-Fe-hydroxide mineralization indicates a synkinematic formation (Chapter 4.4.6).
Fracture spacing mainly depends upon bed thickness and rigidity of the fractured and the surrounding layers (Hobbs, 1967; Pollard and Aydin, 1988; Bai and Pollard, 2000). In sandstones the latter is strongly affected by the kind and extent of intergranular cement. The regionally different quartz cementation east and west of the URG (Chapter 4.7) most probably has implications on the respective fracture behaviour. In contrast to the overlying Muschelkalk and Keuper, the formation permeability of the Buntsandstein in the URG is highly variable (Stober and Jodocy, 2009). The latter authors did not observe a distinct regional distribution but observed a generally significant formation permeability for the Buntsandstein. None of the surveyed wells from their study is located in our study area.

Aqueous Fluid
The composition of the aqueous reservoir fluid is particularly important for geothermal reservoirs. Formation water of the Mesozoic in the URG is usually a NaCl-brine. It is often CO_2-rich and commonly contains a large variety of other solvents (Sanjuan et al., 2010; Stober and Jodocy, 2011; Stober and Bucher, 2014). Scalings and corrosion in geothermal power plants are thus major technical challenges and the prediction of the fluid composition is desired (Kohl et al., 2013; Mundhenk et al., 2013a; Mundhenk et al., 2013b; Scheiber et al., 2013; Scheiber et al., 2014). We can hardly contribute to the solution of this problem, because we almost exclusively surveyed surface outcrops in our study and therefore have no information on recent conditions in the subsurface. The only relevant observation we made was barite in deformation bands in the Wells A 1 and A 2, which possibly indicates elevated Ba^{2+} and SO_4^{2-} contents in this area. In the Soultz-sous-Forêts geothermal power plant the precipitation of barite scalings in the production facilities (Nitschke et al., 2014) occurs. Although the Soultz-sous-Forêts geothermal power plant produces from a Variscan granite, the fluid is derived from the Buntsandstein (Sanjuan et al., 2010). This indicates a comparable fluid chemistry in the recent to the fluid infilling fractures and part of the formation in the past.

5 Conclusions

The diagenetic processes, which control in addition to the depositional facies the reservoir quality of the Buntsandstein, where surveyed with several analytical methods. According to our data, mesogenetic processes, which predate the URG formation, primarily defined the reservoir quality of the sandstones. However, we had only limited access to subsurface samples, particularly from depths exceeding 1000 m.

The reservoir quality of the matrix (poroperm) primarily depends on the extent of (a) quartz cementation, the abundance of (b) clay minerals, and subordinately on (c) feldspar dissolution.

Ad (a):

- (i) A lack of quartz cement causes enhanced compaction and thus contributes to the destruction of porosity and particularly permeability. (ii) Intermediate quartz cementation (5 to 10 %) prevents further compaction and preserves considerable porosity. If clay mineral content is low, permeabilities in the Darcy-scale (e.g. Leistadt) are possible. (iii) Extensive quartz cementation (>>10 %) still prevents further compaction but destroys porosity and particularly permeability, when quartz overgrowths cement pore throats and thus prevent the interconnection of the pores (Chapter 4.6, Chapter 4.8).
- Tangential clay coatings on detrital quartz grains restrained or prevented the precipitation of quartz overgrowths (Chapter 4.4.3). A correlation between grain size and the abundance of clay coatings was observed (Chapter 3.3.2.1). Thus, quartz overgrowths are generally more abundant in coarse-grained than in fine-grained sandstones.
- The study of fluid inclusion homogenization temperatures (FI-T_h) in quartz overgrowths exhibits a correlation between T_h and the extent of quartz cementation. The sandstones with low to intermediate T_h (50 to 250 °C) generally have quartz cement contents below 10 %. In sandstones with high T_h (250 to >350 °C) quartz cement frequently occludes almost the entire primary porosity (Chapter 4.7).

Ad (b):

- Most of the clay minerals observed were either (i) infiltrated shortly after deposition or a product of (ii) feldspar (particularly plagioclase) weathering (Chapter 4.4.2).
- Infiltrated clay minerals were illite and probably significant smectite, which formed tangential coatings around detrital grains and/or plugs in pore throats (Chapter 3.3.2.1, Chapter 4.4.2.2). The latter have a significantly negative effect on the matrix permeability.
- Kaolinite from plagioclase weathering is largely transformed to illite (Chapter 4.4.2.2). Booklet structures within illite aggregates indicate the kaolinitic precursor. Plagioclase weathering occurred before significant compaction. Therefore the clay aggregates are often squeezed and plug adjacent pore throats, having a negative effect on the permeability (Chapter 4.2.3).

Ad (c):

- In outcrop, dissolved K-feldspar was usually either (i) in-situ replaced by kaolinite, or (ii) kaolinite precipitated in adjacent intergranular porosity (Chapter 3.3.2.2). In both cases the positive effect on reservoir quality by the formation of secondary porosity is counteracted by the negative effect of kaolinite precipitation.
- In cores from the subsurface of the URG (Well A, Well B), K-feldspar dissolution without nearby kaolinite precipitation was observed. In this case, the reservoir quality would be enhanced. However, due to the scarcity of core samples this observation is not representative.

- Plagioclase was partly dissolved already at the source, and the plagioclase arriving at the depositional site was replaced by kaolinite or went into solution before quartz cementation (Chapter 4.2.3). The former existence can only be assumed, compaction must have closed the originally present dissolution vugs. Plagioclase dissolution did therefore hardly contribute to the present porosity/ permeability.

The distribution of FI homogenization temperatures and thus the distribution of quartz cement exhibited a clear regional pattern:

- Mean values of T_h in quartz overgrowths continuously rise from Pirmasens/ Rodalben (180 °C) in the west across the Haardt area (200 °C) and Heidelberg (~230 °C) to Zwingenberg/Neckargerach (260 °C) in the east (Chapter 3.6).
- The burial depth of the Buntsandstein probably hardly exceeded 1500 m before the formation of the URG (Chapter 4.6). The FIs in the quartz cements are hydrothermal.
- The age of the main hydrothermal event was constrained by many authors between 180 and 150 ma (Chapter 4.6).
- The amount of quartz cement in our samples is always below 10 % on the western flank and commonly exceeds 15 to 20 % on the eastern flank (Chapter 4.7).
- Core samples exhibit characteristics comparable to the western URG flank. However, all core samples available were derived from (i) direct vicinity to the western graben flank and from (ii) depths hardly exceeding 1000 m.
- Well quartz-cemented rock chips were observed in the cuttings from GTB1 Brühl (>3500 m depth). This well is situated about 12 km west of the eastern margin of the URG. The strong quartz cementation of the eastern URG flank might therefore have extended westwards more than 10 kms into the URG.

The silica sources for the quartz cementation were internal and were caused by (a) clay mineral transformation, and (b) quartz dissolution at grain contacts.

Ad (a):

- A significant amount of the observed illite was originally probably kaolinite and/or smectite (Chapter 4.4.2.2). Both smectite-illite and kaolinite-illite transformations release silica (Chapter 4.4.3).
- Smectite-illite transformation is a non-linear, temperature-sensitive process. The reaction rate of this process increases exponentially with increasing temperature. Clay mineral transformations therefore most probably caused the observed correlation between FI-T_h and quartz cementation (Chapter 4.4.2.2, Chapter 4.7).
- Clay-rich fine sand- and siltstones were probably additional major silica-suppliers.

Ad (b):

- Petrographic observation revealed that quartz dissolution at grain contacts ("pressure dissolution") is particularly common in clay-rich sandstones (Chapter 3.4). Although siltstones were not subject to petrographic observation they have ideal prerequisites for increased grain-grain dissolution (usually clay-rich, large number of grain contacts) and might have supplied significant silica from grain-grain dissolution.

- Although quartz dissolution at grain contacts is a particularly temperature-sensitive process, no correlation with FI-T_h was observed. Temperature-related dissolution can therefore not account for the observed differences in the regional quartz cementation pattern (Chapter 4.7).
- Increased quartz dissolution at grain contacts was often but not everywhere observed in outcrops along the main faults of the URG (Chapter 4.7). Stronger dissolution in certain areas might have contributed to local silicification of other successions (e.g. of Tertiary beds).

The regional distribution of quartz cement causes a regional pattern of reservoir quality:

- Porosities measured in thin sections hardly exceed 10 % on the eastern flank of the URG.
- On the western flank the thin section porosities are commonly above 10 % and occasionally exceed 20 %.
- The distribution of permeabilities is more complex and is assessed by M. Fensterer in an on-going research within project AuGE.
- In our study area the Lower and Middle Buntsandstein have a considerable potential for a high-quality matrix reservoir near the western flank and become less favourable towards the eastern flank of the URG (Chapter 4.8).

For geothermal production, fractures and the composition of the formation water are highly important:

- Most observed fractures were non- or hardly mineralized.
- Mineralized fractures were coated with barite and Fe-hydroxide (former siderite). No quartz mineralization was observed (Chapter 3.5).
- The fracture mineralization is related to the formation of the URG (Chapter 4.4.6). It may therefore somehow reflect the composition of today's formation water in the area. Barite, Fe-hydroxide/oxide and carbonate can cause severe damage to the production facilities of a geothermal power plant. The probable occurrence of these minerals should therefore be considered: Scaling formation and corrosion because of the high saturation of the formation water is a major challenge for geothermal production from the Buntsandstein. Barite preferably precipitates in the heat exchanger and both reduces the pipe diameter and acts as an insulator (e.g. Soultz-sous-Forêts). Carbonates precipitate due to pressure drop and CO_2 degassing (e.g. Bruchsal, Chapter 4.8).
- The regional quartz cementation probably causes a regionally varying fracture behaviour (existing fracture network, induced by stimulation). This effect was not in the scope of this study but further research might enhance the reservoir quality prediction in geothermal exploration.

In summary the Lower and Middle Buntsandstein in the URG are promising reservoir successions for both (a) geothermal and (b) hydrocarbon exploration:

Ad (a):

- Fracture permeability is more important for geothermal production than matrix permeability. Potential reservoir sandstones are therefore both in the east and in the west of the URG, irrespective of regional quartz cementation.

- Neither fracture healing nor fracture sealing with quartz was observed, which would decrease the fracture aperture and thus permeability.
- No crack-seal textures in barite fracture mineralizations were observed, i.e. the fractures were not completely sealed at any time but always open for fluid flow during local barite precipitation.
- Siderite has the potential to seal wider (>1 cm) fractures. In outcrop (Leistadt) siderite was replaced by highly porous Fe-hydroxide, still allowing for significant fluid flow (Chapter 3.5, Chapter 4.8).

Ad (b):

- Potential source rocks in the subsurface of the URG are Tertiary and Jurassic black shales.
- Clay successions in the Upper Buntsandstein ("Röttone") and/or shaly Lower Muschelkalk are potential seals.
- The regional distribution of the quartz cementation makes the Buntsandstein in the western part of the URG more favourable for hydrocarbon exploration. Fractured, amalgamated fluvial channel deposits with porosities above 20 % and permeabilities up to several Darcy, like the ones observed near the URG main fault in Leistadt, would make up an excellent hydrocarbon reservoir.

6 References

Abbots, I. L. (ed.), 1991, UK Oil and Gas Fields, 25 Years Commerative Volume, Geological Society, London, Memoir 14, 582 pp.

Abbott, P. L., 1974, Calcitization of Edwards Group dolomites in the Balcones Fault Zone aquifer, south-central Texas: Geology, v. 2, no. 7, p. 359-362.

Aigner, T. and Bachmann, G. H., 1992, Sequence-stratigraphic framework of the German Triassic: Sedimentary Geology, v. 80, no. 1–2, p. 115-135.

Ajdukiewicz, J. M. and Larese, R. E., 2012, How clay grain coats inhibit quartz cement and preserve porosity in deeply buried sandstones: Observations and experiments: American Association of Petroleum Geologists Bulletin, v. 96, no. 11, p. 2091-2119.

Ali, A. D. and Tuner, P., 1982, Authigenic K-feldspar in the Bromsgrove sandstone formation (Triassic) of central England: Journal of Sedimentary Research, v. 52, no. 1, p. 187-197.

Allen, J. R. L., 1964, Studies in fluviatile sedimentation: Six cyclothems from the Lower Old Red Sandstone, Anglowelsh Basin: Sedimentology, v. 3, no. 3, p. 163-198.

Allen, J. R. L., 1971a, Instantaneous sediment deposition rates deduced from climbing-ripple cross-lamination: Journal of the Geological Society, v. 127, no. 6, p. 553-561.

Allen, J. R. L., 1971b, A theoretical and experimental study of climbing-ripple cross-lamination, with a field application to the Uppsala Esker: Geografiska Annaler. Series A, Physical Geography, v. 53, no. 3/4, p. 157-187.

Ashley, G. M., Southard, J. B. and Boothroyd, J. C., 1982, Deposition of climbing-ripple beds: a flume simulation: Sedimentology, v. 29, p. 67-79.

Assmann, P., 1933, Die Stratigraphie der oberschlesischen Trias: Jahrbuch der preußischen geologischen Landesanstalt zu Berlin, v. 53, p. 731-757.

Aydin, A., 1978, Small faults formed as deformation bands in sandstone: Pure and Applied Geophysics, v. 116, p. 913-930.

Aydin, A. and Johnson, A. M., 1978, Development of faults as zones of deformation bands and as slip surfaces in sandstones: Pure and Applied Geophysics, v. 116, p. 931-942.

Aydin, A. and Johnson, A. M., 1983, Analysis of faulting in porous sandstones: Journal of Structural Geology, v. 5, p. 19-31.

Azmon, E., 1990, Emplacement of clay into sand by infiltration - discussion: Journal of Sedimentary Petrology, v. 60, no. 1, p. 173-174.

Baaske, U., 1999, Untersuchungen zur Diagenese des Buntsandsteins am Westrand des Rheingrabens (Region Bad Dürkheim/Neustadt a.d.W.) [Diploma thesis]: Johannes Gutenberg Universität Mainz, 105 pp.

Baatartsogt, B., Schwinn, G., Wagner, T., Taubald, H., Beitter, T. and Markl, G., 2007, Contrasting paleofluid systems in the continental basement: a fluid inclusion and stable isotope study of hydrothermal vein mineralization, Schwarzwald district, Germany: Geofluids, v. 7, no. 2, p. 123-147.

Back, W., Hanshaw, B. B., Plummer, L. N., Rahn, P. H., Rightmire, C. T. and Rubin, M., 1983, Process and rate of dedolomitization: Mass transfer and 14C dating in a regional carbonate aquifer: Geological Society of America Bulletin, v. 94, no. 12, p. 1415-1429.

Backhaus, E., 1960, Zur Neugliederung des Odenwälder Buntsandsteins und ein Vergleich mit Nordhessen und Thüringen: Neues Jahrbuch für Geologie und Paläontologie, no. 3, p. 292-313.

Backhaus, E., 1968, Fazies, Stratigraphie und Paläogeographie der Solling-Folge (Oberer Buntsandstein) zwischen Odenwald-Rhön und Thüringer Wald: Oberrheinische Geologische Abhandlungen, v. 17, p. 1-164.

Backhaus, E., 1974, Limnische und fluviatile Sedimentation im südwestdeutschen Buntsandstein: Geologische Rundschau, v. 63, no. 3, p. 925-942.

Backhaus, E., 1975, Der Buntsandstein im Odenwald: Der Aufschluß, Sonderband 27, p. 299-320.

Backhaus, E., 1979, Zur Sedimentologie und Sedimentpetrographie des Buntsandsteins und Unteren Muschelkalks im Odenwald: Fortschritte der Mineralogie, v. 57 (Beih. 2), p. 3-22.

Backhaus, E., 1981, Der marin-brackische Einfluß im Oberen Röt Süddeutschlands: Zeitschrift der Deutschen Geologischen Gesellschaft, v. 132, p. 361-382.

Backhaus, E., 1994, Der Einfluß der Tektonik und des skythisch-anisischen Meeresspiegelanstiegs auf die Faziesgliederung des Oberen Buntsandsteins im Germanischen Triasbecken: Zeitschrift der Deutschen Geologischen Gesellschaft, v. 145, p. 325-342.

Backhaus, E. and Heim, D., 1995, Die fluvio-lakustrine Fazies des Übergangsbereichs Plattensandstein/Rötquarzit (Oberer Buntsandstein) im mittleren Odenwald unter besonderer Berücksichtigung der Violetten Zone: Geologisches Jahrbuch Hessen, v. 123, p. 49-68.

Backhaus, E., Rawanpur, A. and Zirngast, M., 1974, Das Schollenmosaik des nördlichen Michelstädter Grabens, *in* Illies, J. H., ed., Approaches to Taphrogenesis, Schweizerbart, Stuttgart, p. 303-309.

Backhaus, E. and Reul, K., 1971, Der Mittlere und Obere Buntsandstein im Bereich der Rhön-Schwelle: Notizblätter des hessischen Landesamtes für Bodenforschung, v. 99, p. 142-192.

Bai, T. and Pollard, D. D., 2000, Fracture spacing in layered rocks: a new explanation based on the stress transition: Journal of Structural Geology, v. 22, no. 1, p. 43-57.

Banfield, J. F. and Eggleton, R. A., 1990, Analytical transmission electron-microscope studies of plagioclase, muscovite and K-feldspar weathering: Clays and Clay Minerals, v. 38, no. 1, p. 77-89.

Barclay, S. A. and Worden, R. H., 2000, Effects of reservoir wettability on quartz cementation in oil fields, *in* Worden, R. H. and Morad, S., eds., Quartz Cementation in Sandstones, International Association of Sedimentologists, Special Publications 29, Blackwell Publishing Ltd., Oxford, p. 103-117.

Barnes, H. L., 1997, Geochemistry of Hydrothermal Ore Deposits, 3rd ed., John Wiley & Sons, 992 pp.

Bauer, J. F., Meier, S. and Philipp, S. L., 2013, Infrastructure and mechanical properties of a fault zone in Bunter sandstone (Lower Triassic) in the Upper Rhine Graben, *in* Philipp, S. L. and Acocella, V., eds., Rock Fractures in Geological Processes: Abstracts of the Presentations of the Symposium, London, 26-27 November 2013: Universitätsdrucke Göttingen, Universitätsverlag Göttingen, p. 41-44.

Bauer, J. F., Meier, S. and Philipp, S. L., in press, Architecture, fracture system, mechanical properties and permeability structure of a fault zone in Lower Triassic sandstone, Upper Rhine Graben: Tectonophysics.

Beard, D. C. and Weyl, P. K., 1973, Influence of texture on porosity and permeability of unconsolidated sand: American Association of Petroleum Geologists Bulletin, v. 57, no. 2, p. 349-369.

Behr, H. J. and Gerler, J., 1987, Inclusions of sedimentary brines in post-Variscan mineralizations in the Federal Republic of Germany — A study by neutron activation analysis: Chemical Geology, v. 61, no. 1–4, p. 65-77.

Berner, R., 1969, Goethite stability and the origin of red beds: Geochimica et Cosmochimica Acta, v. 33, no. 2, p. 267-273.

Bernet, M. and Bassett, K., 2005, Provenance analysis by single-quartz-grain SEM-CL/optical microscopy: Journal of Sedimentary Research, v. 75, no. 3, p. 492-500.

Bestland, E. A., Retallack, G. J. and Swisher, C. C., 1997, Stepwise climate change recorded in Eocene-Oligocene paleosol sequences from central Oregon: The Journal of Geology, v. 105, no. 2, p. 153-172.

Betard, F., Caner, L., Gunnell, Y. and Bourgeon, G., 2009, Illite neoformation in plagioclase during weathering: Evidence from semi-arid Northeast Brazil: Geoderma, v. 152, no. 1-2, p. 53-62.

Beutler, G., 1991, Zur Frage der Eichsfeld-Schwelle im Keuper: Zeitschrift für Geologische Wissenschaften, v. 19, no. 1, p. 79-89.

Beutler, G. and Szulc, J., 1999, Die paläogeographische Entwicklung des Germanischen Beckens in der Trias und ihre Verbindung zur Tethys, *in* Hauschke, N. and Wilde, V., eds., Trias - Eine ganz andere Welt, Verlag Dr. Friedrich Pfeil, München, p. 71-81.

Bevan, J. and Savage, D., 1989, The effect of organic acids on the dissolution of K-feldspar under conditions relevant to burial diagenesis: Mineralogical Magazine, v. 53, p. 415-425.

Bifani, R., 1986, Esmond Gas Complex, *in* Brooks, J., Goff, J. C. and van Hoorn, B., eds, Habitat of Palaeozoic Gas in N.W. Europe.: Geological Society, London, Special Publications, 23, p. 209-221.

Bindig, M. and Backhaus, E., 1995, Rekonstruktion der Paläoenvironments aus den fluviatilen Sedimentkörpern der Röt-Sandsteinfazies (Oberer Buntsandstein) Südwestdeutschlands: Geologisches Jahrbuch Hessen, v. 123, p. 59-105.

Bjørkum, P. A., 1996, How important is pressure in causing dissolution of quartz in sandstones?: Journal of Sedimentary Research, v. 66, no. 1, p. 147-154.

Bjørkum, P. A., Oelkers, E. H., Nadeau, P. H., Walderhaug, O. and Murphy, W. M., 1998, Porosity prediction in quartzose sandstones as a function of time, temperature, depth, stylolite frequency and hydrocarbon saturation: American Association of Petroleum Geologists Bulletin, v. 82, no. 4, p. 637-648.

Bjørlykke, K., 1983, Diagenetic reactions in sandstones, *in* Parker, A. and Sellwood, B. W., eds., Sediment Diagenesis: NATO Advanced Study Institutes Series 115, NATO Scientific Affairs Division, Dordrecht/Boston/Lancaster, p. 169-214.

Bjørlykke, K., 1984, Formation of secondary porosity: How important is it?: Part 2. Aspects of porosity modification, *in* MacDonald, D. A. and Surdam, R. C., eds., Clastic Diagenesis: American Association of Petroleum Geologists Memoir 37, p. 277-286.

Bjørlykke, K., 1998, Clay mineral diagenesis in sedimentary basins - a key to the prediction of rock properties. Examples from the North Sea Basin: Clay Minerals, v. 33, no. 1, p. 15-34.

Bjørlykke, K. and Aagaard, P., 1992, Clay minerals in North Sea sandstones, *in* Houseknecht, D.W. and Pittman, E.D., eds., Origin, Diagenesis and Petrophysics of Clay Minerals in Sandstones, SEPM Society for Sedimentary Geology, Special Publication, 47, p. 65-80.

Bjørlykke, K. and Egeberg, P. K., 1993, Quartz cementation in sedimentary basins: American Association of Petroleum Geologists Bulletin, v. 77, no. 9, p. 1538-1548.

Blume, H. P., and Kohn, K. J., 1962, Grube Clarashall, Baumholder/Pfalz: Der Aufschluß, v. 13, no. 1, p. 10-12.

Bourquin, S., Peron, S. and Durand, M., 2006, Lower Triassic sequence stratigraphy of the western part of the Germanic Basin (west of Black Forest): Fluvial system evolution through time and space: Sedimentary Geology, v. 186, no. 3-4, p. 187-211.

Bradley, W. F., 1945, Molecular associations between montmorillonite and some polyfunctional organic liquids: Journal of the American Chemical Society, v. 67, p. 975-981.

Brockamp, O. and Clauer, N., 2013, Hydrothermal and unexpected diagenetic alteration in Permian shales of the Lodève epigenetic U-deposit of southern France, traced by K–Ar illite and K-feldspar dating: Chemical Geology, v. 357, p. 18-28.

Brockamp, O., Clauer, N. and Zuther, M., 1994, K-Ar dating of episodic Mesozoic fluid migrations along the fault system of Gernsbach between the Moldanubian and Saxothuringian (northern Black-Forest, Germany): Geologische Rundschau, v. 83, no. 1, p. 180-185.

Brockamp, O., Schlegel, A. and Clauer, N., 2011, Mesozoic hydrothermal impact on Rotliegende and Bunter immature sandstones of the High Rhine trough and its adjacent eastern area (southern Black Forest, Germany): Sedimentary Geology, v. 234, no. 1-4, p. 76-88.

Budai, J. M., Lohmann, K. C. and Owen, R. M., 1984, Burial dedolomite in the Mississippian Madison Limestone, Wyoming and Utah thrust belt: Journal of Sedimentary Research, v. 54, no. 1, p. 276-288.

Buness, H., Gabriel, G. and Ellwanger, D., 2008, The Heidelberg Basin drilling project: Geophysical pre-site surveys: Quaternary Science Journal, v. 57, no. 3-4, p. 338-366.

Burley, S. D., Lyon, I. C., and McKeever, P. J., 1992, Microbeam oxygen isotope mass-spectrometry of authigenic quartz using the VG Isolab 54 Ion Probe, 31st Annual Meeting of the British Sedimentological Research Group, University of Southampton.

Cameron, T. D. J., Crosby, A., Balson, P. S., Jeffery, D. H., Lott, G. K., Bulat, J. and Harrison, D. H., 1992, United Kingdom offshore regional report: The Geology of the Southern North Sea: HMSO for the British Geological Survey, London, 152 pp.

Carrigy, M. A. and Mellon, G. B., 1964, Authigenic clay mineral cements in Cretaceous and Tertiary sandstones of Alberta: Journal of Sedimentary Research, v. 34, no. 3, p. 461-472.

Chen, X. Y., Lintern, J. and Roach, I., 2002, Calcrete: Characteristics, Distribution and Use in Mineral Exploration, Cooperative Research Centre for Landscape Environments and Mineral Exploration, 160 pp.

Choquette, P. W. and Pray, L. C., 1970, Geologic nomenclature and classification of porosity in sedimentary carbonates: American Association of Petroleum Geologists Bulletin, v. 54, no. 2, p. 207-250.

Clauer, N., Liewig, N., Ledesert, B. and Zwingmann, H., 2008, Thermal history of Triassic sandstones from the Vosges Mountains-Rhine Graben rifting area, NE France, based on K-Ar illite dating: Clay Minerals, v. 43, no. 3, p. 363-379.

Correns, C. W., 1968, Einführung in die Mineralogie: (Kristallographie u. Petrologie), Springer, Berlin, Heidelberg, 485 pp.

Cumming, A. D. and Wyndham, C. L., 1975, The geology and development of the Hewett gas field, *in* Woodland, A. W., ed., Petroleum and the Continental Shelf of N.W. Europe, Volume 1, Applied Science Publishers, London, p. 313-325.

Dachroth, W., 1985, Fluvial sedimentary styles and associated depositional environments in the Buntsandstein west of river Rhine in Saar area and Pfalz (F.R. Germany) and Vosges (France), *in* Mader, D., ed., Aspects of fluvial sedimentation in the Lower Triassic Buntsandstein of Europe: Lecture Notes in Earth Sciences 4, Springer, Berlin, Heidelberg, p. 197-248.

Dèzes, P., Schmid, S. M. and Ziegler, P. A., 2004, Evolution of the European Cenozoic rift system: interaction of the Alpine and Pyrenean orogens with their foreland lithosphere: Tectonophysics, v. 389, no. 1–2, p. 1-33.

Díaz-Molina, M., 1993, Geometry and lateral accretion patterns in meander loops: Examples from the Upper Oligocene–Lower Miocene, Loranca Basin, Spain, *in* Marzo, M., Puigdefabregas, C., eds., Alluvial Sedimentation, International Association of Sedimentologists, Special Publication 17, Blackwell Publishing Ltd., p. 115-131.

Dill, H. G., 2001, The geology of aluminium phosphates and sulphates of the alunite group minerals: a review: Earth-Science Reviews, v. 53, no. 1–2, p. 35-93.

Ding, Z., Zheng, B., Long, J., Belkin, H. E., Finkelman, R. B., Chen, C., Zhou, D. and Zhou, Y., 2001, Geological and geochemical characteristics of high arsenic coals from endemic arsenosis areas in southwestern Guizhou Province, China: Applied Geochemistry, v. 16, no. 11–12, p. 1353-1360.

Dresmann, H., Keulen, N., Timar-Geng, Z., Fügenschuh, B., Wetzel, A. and Stünitz, H., 2010, The south-western Black Forest and the Upper Rhine Graben Main Border Fault: thermal history and hydrothermal fluid flow: International Journal of Earth Sciences, v. 99, no. 2, p. 285-297.

Drong, H. J., 2003, Das kristalline Grundgebirge in Bohrungen des nordwestlichen Alpenvorlandes: Geologica Bavarica, v. 108, p. 13-110.

Dunoyer de Segonzac, G., 1970, The transformation of clay minerals during diagenesis and low-grade metamorphism: a review: Sedimentology, v. 15, no. 3-4, p. 281-346.

Ehrenberg, S. N., 1995, Measuring sandstone compaction from modal analyses of thin sections: How to do it and what the results mean: Journal of Sedimentary Research, v. 65, no. 2a, p. 369-379.

Eisbacher, G. H. and Fielitz, W., 2010, Karlsruhe und seine Region: Nordschwarzwald, Kraichgau, Neckartal, Oberrhein-Graben, Pfälzerwald und westliche Schwäbische Alb, Sammlung geologischer Führer, Borntraeger, Stuttgart, v. 103, 342 p.

Escorcia, L. C., Gomez-Rivas, E., Daniele, L. and Corbella, M., 2013, Dedolomitization and reservoir quality: insights from reactive transport modelling: Geofluids, v. 13, no. 2, p. 221-231.

Evamy, B. D., 1963, The application of a chemical staining technique to a study of dedolomitisation: Sedimentology, v. 2, no. 2, p. 164.

Evamy, B. D., 1967, Dedolomitization and the development of rhombohedral pores in limestones: Journal of Sedimentary Research, v. 37, no. 4, p. 1204-1215.

Evans, D. J., Rees, J. G. and Holloway, S., 1993, The Permian to Jurassic stratigraphy and structural evolution of the central Cheshire Basin: Journal of the Geological Society, v. 150, no. 5, p. 857-870.

Feist-Burkhardt, S., Götz, A. E., Szulc, J., Borkhataria, R., Geluk, M., Haas, J., Hornung, J., Jordan, P., Kempf, O., Michalik, J., Nawrocki, J., Reinhardt, L., Ricken, W., Röhling, H.-G., Rüffer, T., Török, A. and Zühlke, R., 2008, Triassic, *in* McCann, T., ed., The Geology of Central Europe: Mesozoic and Cenozoic, Geological Society, London, p. 749-821.

Feldrappe, H., Obst, K. and Wolfgramm, M., 2008, Die mesozoischen Sandsteinaquifere des Norddeutschen Beckens und ihr Potential für die geothermische Nutzung: Zeitschrift für Geologische Wissenschaften, v. 36, no. 4-5, p. 199-222.

Filomena, C. M. and Stollhofen, H., 2011, Ultrasonic logging across unconformities - outcrop and core logger sonic patterns of the Early Triassic Middle Buntsandstein Hardegsen unconformity, southern Germany: Sedimentary Geology, v. 236, no. 3-4, p. 185-196.

Fordham, A. W., 1990, Weathering of biotite into dioctahedral clay-minerals: Clay Minerals, v. 25, no. 1, p. 51-63.

Fossen, H., Schultz, R. A., Shipton, Z. K. and Mair, K., 2007, Deformation bands in sandstone: a review: Journal of the Geological Society, v. 164, p. 755-769.

Fraser, H. J., 1935, Experimental study of the porosity and permeability of clastic sediments: The Journal of Geology, v. 43, no. 8, p. 910-1010.

Füchtbauer, H., 1967, Der Einfluss des Ablagerungsmilieus auf die Sandsteindiagenese im Mittleren Buntsandstein: Sedimentary Geology, v. 1, p. 159-179.

Gall, J.-C., 1971, Faunes et Paysages du Grès à Voltzia du Nord des Vosges. Essai paléoécologique sur le Buntsandstein Supérieur., Mémoires du Service de la Carte géologique d'Alsace et de Lorraine, Strasbourg,318 pp.

Galloway, W. E., 1974, Deposition and diagenetic alteration of sandstone in northeast Pacific arc-related basins: Implications for graywacke genesis: Geological Society of America Bulletin, v. 85, no. 3, p. 379-390.

Gaupp, R., Clauer, N., Bauer, A., von Eynatten, H., Baaske, U. and Mezger, J., 1998, Untersuchung des Einflusses von Diagenese im Bereich von Störungen anhand von Oberflächen-Aufschlüssen: Unpubl. report: Geowissenschaftliches DGMK-Forschungsprojekt Nr. 545, 107 pp.

Gaupp, R., Matter, A., Platt, J., Ramseyer, K. and Walzebuck, J., 1993, Diagenesis and fluid evolution of deeply buried Permian (Rotliegende) gas-reservoirs, northwest Germany: American Association of Petroleum Geologists Bulletin, v. 77, no. 7, p. 1111-1128.

Gaupp, R. and Okkerman, J. A., 2011, Diagenesis and reservoir quality of Rotliegend sandstones in the northern Netherlands—a review, *in* Grötsch, J. and Gaupp, R., eds., The Permian Rotliegend of the Netherlands, SEPM Society for Sedimentary Geology, Special Publication 98, p. 193-226.

Geluk, M. C. and Röhling, H.-G., 1997, High-resolution sequence stratigraphy of the Lower Triassic "Buntsandstein" in the Netherlands and northwestern Germany: Geologie en Mijnbouw, v. 76, p. 227-246.

Geng, A., 1996, Diagenesis of the Middle Triassic Muschelkalk, Southwestern Germany [Doctoral thesis]: Ruprecht-Karls-Universität Heidelberg, 86 pp.

Geng, A. and Zeeh, S., 1995, Diagenesis of Middle Triassic Muschelkalk carbonate rocks of the Rhine graben and adjacent areas (southwest Germany): Zeitschrift der Deutschen Geologischen Gesellschaft, v. 146, p. 372-385.

Giles, M. R., Indrelid, S. L., Beynon, G. V. and Amthor, J., 2000, The origin of large-scale quartz cementation: Evidence from large data sets and coupled heat–fluid mass transport modelling, *in* Worden, R. H., Morad, S., Quartz Cementation in Sandstones, International Association of Sedimentologists, Special Publications 29, Blackwell Publishing Ltd., Oxford, p. 21-38.

Giles, M. R. and Marshall, J. D., 1986, Constraints on the development of secondary porosity in the subsurface: Re-evaluation of processes: Marine and Petroleum Geology, v. 3, no. 3, p. 243-255.

Glennie, K. W., 1997, History of exploration in the southern North Sea, *in* Ziegler, K., Turner, P. and Draines, R.R., eds., Petroleum Geology of the Southern North Sea: Future Potential, Geological Society, London, Special Publications, 123, p. 5-16.

Goldstein, R. H., 2001, Fluid inclusions in sedimentary and diagenetic systems: Lithos, v. 55, no. 1-4, p. 159-193.

Grabowska, A., 2011, Buntsandstein west of the Upper Rhine Valley (Pirmasens area): facies and diagenesis [M.Sc. Master thesis]: Jagiellonian University Krakow, 157 pp.

Graham, C. M., Valley, J. W., and Winter, B. L., 1996, Ion microprobe analysis of $^{18}O/^{16}O$ in authigenic and detrital quartz in the St. Peter Sandstone, Michigan Basin and Wisconsin Arch., USA: Contrasting diagenetic histories: Geochimica et Cosmochimica Acta, v. 60, p. 5101-5116.

Graton, L. C. and Fraser, H. J., 1935, Systematic packing of spheres: With particular relation to porosity and permeability: The Journal of Geology, v. 43, no. 8, p. 785-909.

Haffen, S., Géraud, Y. and Diraison, M., 2015, Geothermal, structural and petrophysical characteristics of Buntsandstein sandstone reservoir (Upper Rhine Graben, France), *in* Proceedings World Geothermal Congress, Melbourne, Australia, 19-25 April 2015, p. 1-11.

Haffen, S., Géraud, Y., Diraison, M. and Dezayes, C., 2013, Fluid-flow zones in a geothermal sandstone reservoir: localization from thermal conductivity and temperature loge, borehole EPS 1 (Soultz-sous-Forêts, France) and 3D models, *in* Proceedings Thirty-Eighth Workshop on Geothermal Reservoir Engineering, Stanford University, Stanford, California, February 11-13, 2013, SGP-TR-198.

Halley, R. B., 1978, Estimating pore and cement volumes in thin section: Journal of Sedimentary Research, v. 48, no. 2, p. 642-650.

Hamilton, E. L. and Menard Jr., H. W., 1956, Density and porosity of seafloor surface sediments off San Diego, California: American Association of Petroleum Geologists Bulletin, v. 40, p. 754-761.

Harder, H. and Flehmig, W., 1970, Quarzsynthese bei tiefen Temperaturen: Geochimica et Cosmochimica Acta, v. 34, no. 3, p. 295-305.

Hartmann, B. H., Bodnár, K. J., Ramseyer, K. and Matter, A., 1999, Effect of Permo-Carboniferous climate on illite-smectite, Haushi Group, Sultanate of Oman: Clays and Clay Minerals, v. 47, no. 2, p. 131-143.

Hasemann, W., 1928, Erläuterungen zu Blatt Eberbach (Nr. 24) der Geologischen Spezialkarte von Baden:, Herder, Freiburg im Breisgau, 62 p.

Hasemann, W., 1930, Erläuterungen zu Blatt Zwingenberg (Nr. 25) der Geologischen Spezialkarte von Baden: Herder, Freiburg im Breisgau, 58 p.

Hathaway, J. C., 1956, Procedure for clay mineral analyses used in the sedimentary petrology laboratory of the U.S. Geological Survey: Clay Minerals, v. 3, no. 15, p. 8-13.

Heald, M. T., 1956, Cementation of Simpson and St. Peter sandstones in parts of Oklahoma, Arkansas and Missouri: Journal of Geology, v. 64, p. 16-30.

Heald, M. T. and Larese, R. E., 1974, Influence of coatings on quartz cementation: Journal of Sedimentary Research, v. 44, no. 4, p. 1269-1274.

Heim, D., 1974, Über die Feldspäte im Germanischen Buntsandstein, ihre Korngrößenabhängigkeit Verbreitung und paläogeographische Bedeutung: Geologische Rundschau, v. 63, no. 3, p. 943-970.

Helgeson, H. C., Delaney, J. M., Nesbitt, H. W. and Bird, D. K., 1978, Summary and critique of the thermodynamic properties of rock forming minerals, American Journal of Science, v. 278-A, 229 pp.

Heydemann, A., 1964, Untersuchungen über die Bildungsbedingungen von Quarz im Temperaturbereich zwischen 100 °C und 250 °C: Beiträge zur Mineralogie und Petrographie, v. 10, no. 2, p. 242-259.

Hinze, C., 1967, Der Obere Buntsandstein (Röt) im niedersächsischen Bergland: Geologisches Jahrbuch, v. 84, p. 637-716.

Hobbs, D. W., 1967, The formation of tension joints in sedimentary rocks: an explanation: Geological Magazine, v. 1046, p. 550-556.

Hoholick, J. D., Metarko, T. A. and Potter, P. E., 1982, Weighted contact packing - improved formula for grain packing of quartz arenites: The Mountain Geologist, v. 19, no. 3, p. 79-82.

Hoppe, W., 1927, Beiträge zur Geologie und Petrographie des Buntsandsteins im Odenwald II: Petrographie, 1, Struktur des Buntsandsteins und ihre Beziehungen zur Einkieselung und Bleichung, - Notizblätter des Vereins für Erdkunde hessische geologische Landesanstalt für 1926, 9, Darmstadt, p. 80–103, 1 Taf.

Houseknecht, D. W., 1987, Assessing the relative importance of compaction processes and cementation to reduction of porosity in sandstones: American Association of Petroleum Geologists Bulletin, v. 71, no. 6, p. 633-642.

Huff, W. D. and Turkmenoglu, A. G., 1981, Chemical characteristics and origin of Ordovician K-Bentonites along the Cincinnati Arch: Clays and Clay Minerals, v. 29, p. 113-123.

Hüttner, R., 1991, Bau und Entwicklung des Oberrheingrabens, Ein Überblick mit historischer Rückschau: Geologisches Jahrbuch E, v. 48, p. 17-42.

Illies, J. H., 1965, Bauplan und Baugeschichte des Oberrheingrabens; ein Beitrag zum 'Upper Mantle Project'. Oberrheinische Geologische Abhandlungen, v. 14, p. 1-54.

Illies, J. H., ed., 1974, Approaches to Taphrogenesis, Schweizerbart, Stuttgart, 460 pp.

Inoue, A., 1995, Formation of clay minerals in hydrothermal environments, *in* Velde, B., ed., Origin and Mineralogy of Clays, Springer, Berlin, Heidelberg, New York, p. 268-329.

Jennings, S. and Thompson, G. R., 1986, Diagenesis of Plio-Pleistocene sediments of the Colorado River delta, southern California: Journal of Sedimentary Petrology, v. 56, p. 89-98.

Joachim, H., 1984, Mineralogische Untersuchung der manganhaltigen Brauneisen-Baryt-Gänge des Neuenbürger Reviers (nördlicher Schwarzwald). [Diploma thesis]: Karlsruhe University, 133 p.

Jones Jr., F. O. 1964. Influence of Chemical Composition of Water on Clay Blocking of Permeability: Journal of Petroleum Technology, vol. 16, no. 4, p. 441-446.

Kelly, J. L., Fu, B., Kita, N. T. and Valley, J. W., 2007, Optically continuous silcrete quartz cements of the St. Peter Sandstone: High precision oxygen isotope analysis by ion microprobe: Geochimica et Cosmochimica Acta, v. 71, no. 15, p. 3812-3832.

Kennedy, G. C., 1950, A portion of the system silica-water: Economic Geology, v. 45, no. 7, p. 629-653.

Kohl, T., Blum, P., Mutschler, T., Schilling, F., Müller, B., Gaucher, E., Bucher, K., Joswig, M., Doherr, D. and Koenigsdorff, R., 2014, Basisdaten für tiefe Geothermievorhaben in Baden-Württemberg: Geothermale Fluide, tektonische Spannungen und Seismizität. Unpublished report, Umweltforschung in Baden-Württemberg, Abschlussbericht, 83 pp.

Kolker, A., Huggins, F. E., Palmer, C. A., Shah, N., Crowley, S. S., Huffman, G. P. and Finkelman, R. B., 2000, Mode of occurrence of arsenic in four US coals: Fuel Processing Technology, v. 63, no. 2–3, p. 167-178.

Krämer, F. and Kunz, H., 1969, Leithorizonte und Schichtausfälle im Buntsandstein Hessens und Thüringens: Oberrheinische Geologische Abhandlungen, v. 18, p. 67-76.

Kristiansen, K., Valtiner, M., Greene, G. W., Boles, J. R. and Israelachvili, J. N., 2011, Pressure solution – The importance of the electrochemical surface potentials: Geochimica et Cosmochimica Acta, v. 75, no. 22, p. 6882-6892.

Krumbein, W. C. and Aberdeen, E., 1937, The Sediments of Barataria Bay: Journal of Sedimentary Petrology, v. 7, no. 1, p. 3-17.

Kürschner, W. M. and Herngreen, G. F. W., 2010, Triassic palynology of central and northwestern Europe: a review of palynofloral diversity patterns and biostratigraphic subdivisions: Geological Society, London, Special Publications, 334, no. 1, p. 263-283.

Land, L. S., Milliken, K. L. and McBride, E. F., 1987, Diagenetic evolution of Cenozoic sandstones, Gulf-of-Mexico sedimentary basin: Sedimentary Geology, v. 50, no. 1-3, p. 195-225.

Lander, R. H., Larese, R. E. and Bonnell, L. M., 2008, Toward more accurate quartz cement models: The importance of euhedral versus noneuhedral growth rates: American Association of Petroleum Geologists Bulletin, v. 92, no. 11, p. 1537-1563.

Langbein, R., 1974, Zur Petrologie der Karneole des thüringischen Chirotheriensandsteins (Solling Folge): Chemie der Erde, v. 33, p. 301-325.

Lanson, B., Beaufort, D., Berger, G., Baradat, J. and Lacharpagne, J.-C., 1996, Illitization of diagenetic kaolinite-to-dickite conversion series; late-stage diagenesis of the Lower Permian Rotliegend Sandstone reservoir, offshore of the Netherlands: Journal of Sedimentary Research, v. 66, no. 3, p. 501-518.

Laubach, S. E., 2003, Practical approaches to identifying sealed and open fractures: American Association of Petroleum Geologists Bulletin, v. 87, no. 4, p. 561-579.

Laubach, S. E., Olson, J. E. and Gale, J. F. W., 2004, Are open fractures necessarily aligned with maximum horizontal stress?: Earth and Planetary Science Letters, v. 222, no. 1, p. 191-195.

Leeder, M. R., 2011, Sedimentology and Sedimentary Basins: From Turbulence to Tectonics, 2nd ed., Wiley-Blackwell, Chichester, 768 pp.

Li, C. and Yang, S., 2010, Is chemical index of alteration (CIA) a reliable proxy for chemical weathering in global drainage basins?: American Journal of Science, v. 310, p. 111-127.

Lippolt, H. J. and Leyk, H. J., 2004, Alteration ages of the Heidelberg Granite based on studies of clay mineral enrichments from a mine on the Branich in Schriesheim, southwestern Odenwald: Jahreshefte des Landesamts für Geologie, Rohstoffe und Bergbau Baden-Württemberg, v. 40, p. 187-230.

Longman, M. W. and Mench, P. A., 1978, Diagenesis of Cretaceous limestones in the Edwards aquifer system of south-central Texas: A scanning electron microscope study: Sedimentary Geology, v. 21, no. 4, p. 241-276.

Lüders, V., 1994, Geochemische Untersuchungen an Gangmineralen aus dem Bergbaurevier Freiamt-Sexau und dem Badenweiler-Quarzriff (Schwarzwald): Abhandlungen des Geologischen Landesamtes Baden-Württemberg, v. 14, p. 173-190.

Lundegard, P. D., 1992, Sandstone porosity loss; a "big picture" view of the importance of compaction: Journal of Sedimentary Research, v. 62, no. 2, p. 250-260.

Lynd, L. E., 1960, Study of the mechanism and rate of ilmenite weathering: American Institute of Mining and Metallurgical Engnineers Transactions, v. 217, p. 311-318.

Mader, D., 1982, Genese des mitteleuropäischen Buntsandsteins: Naturwissenschaften, v. 69, no. 7, p. 311-325.

Marshall, D. J., 1988, Cathodoluminescence of geological materials, Allen & Unwin, Boston, 146pp.
Matlack, K. S., Houseknecht, D. W. and Applin, K. R., 1989, Emplacement of clay into sand by infiltration: Journal of Sedimentary Petrology, v. 59, no. 1, p. 77-87.
Mattavelli, L., Chilingarian, G. V. and Storer, D., 1969, Petrography and diagenesis of the Taormina formation, Gela oil field, Sicily (Italy): Sedimentary Geology, v. 3, no. 1, p. 59-86.
Matter, A. and Ramseyer, K., 1985, Cathodoluminescence microscopy as a tool for provenance studies of sandstones, *in* Zuffa, G. G., ed., Provenance of arenites, Reidel, Dordrecht, p. 191-211.
McAulay, G. E., Burley, S. D. and Johnes, L. H., 1993, Silicate mineral authigenesis in the Hutton and NW Hutton fields: implications for sub-surface porosity development: Geological Society, London, Petroleum geology of northwest Europe, Proceedings of the 4th conference, v. 4, p. 1377-1394.
McBride, E. F., 1963, A classification of common sandstones: Journal of Sedimentary Research, v. 33, no. 3, p. 664-669.
McBride, E. F., 1989, Quartz cement in sandstones - a review: Earth-Science Reviews, v. 26, no. 2, p. 69-112.
McKinley, J. M., Worden, R. H. and Ruffell, A. H., 2003, Smectite in sandstones: A review of the controls on occurrence and behaviour during diagenesis, *in* Worden, R. H., and Morad, S., eds., Clay Mineral Cements in Sandstones, Special Publication 34 of the International Association of Sedimentologists ,Blackwell Publishing Ltd., p. 109-128.
Menning, M. and German Stratigraphic Commission, 2002, A geologic time scale 2002, *in* German Stratigraphic Commission, ed., Stratigraphic Table of Germany 2002.
Meyer, M., Brockamp, O., Clauer, N., Renk, A. and Zuther, M., 2000, Further evidence for a Jurassic mineralizing event in central Europe: K–Ar dating of hydrothermal alteration and fluid inclusion systematics in wall rocks of the Käfersteige fluorite vein deposit in the northern Black Forest, Germany: Mineralium Deposita, v. 35, no. 8, p. 754-761.
Miall, A. D., 1977a, Lithofacies types and vertical profile models in braided river deposits: a summary, *in* Miall, A.D., ed., Fluvial Sedimentology, Memoir 5, Canadian Society of Petroleum Geologists, Calgary, Alberta, Canada, p. 597-604.
Miall, A. D., 1977b, A review of the braided-river depositional environment: Earth-Science Reviews, v. 13, no. 1, p. 1-62.
Mizutani, S., 1970, Silica minerals in the early stage of diagenesis: Sedimentology, v. 15, no. 3-4, p. 419-436.
Moore, D. M. and Reynolds, R. C., 1997, X-Ray Diffraction and the Identification and Analysis of Clay Minerals, 2nd ed., Oxford University Press, Oxford, 396 pp.
Morad, S., Ketzer, J. M. and De Ros, L. F., 2000, Spatial and temporal distribution of diagenetic alterations in siliciclastic rocks: implications for mass transfer in sedimentary basins: Sedimentology, v. 47, p. 95-120.
Morad, S., Worden, R. H. and Ketzer, J. M., 2003, Oxygen and hydrogen isotopic composition of diagenetic clay minerals in sandstones: a review of the data and controls, *in* Worden, R. H. and Morad, S., eds., Clay Mineral Cements in Sandstones, Special Publication 34 of the International Association of Sedimentologists, Blackwell Publishing Ltd., p. 63-91.
Morey, G. W., Fournier, R. O. and Rowe, J. J., 1962, The solubility of quartz in water in the temperature interval from 25° to 300° C: Geochimica et Cosmochimica Acta, v. 26, no. 10, p. 1029-1043.
Moss, A. J. and Green, P., 1975, Sand and silt grains: Predetermination of their formation and properties by microfractures in quartz: Geological Society of Australia, Journal, v. 22, p. 485-495.
Müller, E. M., 1954a, Beiträge zur Kenntnis der Stratigraphie und Paläogeographie des Oberen Buntsandsteins im Saar-Lothringischen Raum: Annales Universitatis Saraviensis: Scientia, v. 3, p. 176-200.
Müller, E. M, 1954b, Die Ausbildung und Mächtigkeit der Zwischenschichten im Saar-Lothringischen Raum: Annales Universitatis Saraviensis: Scientia, v. 3, p. 68-74.
Mullis, J., 1987, Fluid inclusion studies during very low grade metamorphism, *in* Frey, M., ed., Low Temperature Metamorphism, Blackie & Son, Glasgow and London, 351 pp.
Mundhenk, N., Huttenloch, P., Kohl, T., Steger, H. and Zorn, R., 2013a, Metal corrosion in geothermal brine environments of the Upper Rhine graben – Laboratory and on-site studies: Geothermics, v. 46, p. 14-21.

Mundhenk, N., Huttenloch, P., Sanjuan, B., Kohl, T., Steger, H. and Zorn, R., 2013b, Corrosion and scaling as interrelated phenomena in an operating geothermal power plant: Corrosion Science, v. 70, p. 17-28.

National Research Council, 1996, Rock Fractures and Fluid Flow: Contemporary Understanding and Applications, National Academy Press, Washington DC, 568 pp.

Nawrocki, J., 1997, Permian to Early Triassic magnetostratigraphy from Central European Basin in Poland: implications on regional and worldwide correlations: Earth and Planetary Science Letters, v. 152, p. 37-58.

Needham, S. J., Worden, R. H. and McIlroy, D., 2005, Experimental production of clay rims by macrobiotic sediment ingestion and excretion processes: Journal of Sedimentary Research, v. 75, no. 6, p. 1028-1037.

Nesbitt, H. W., Fedo, C. M. and Young, G. M., 1997, Quartz and feldspar stability, steady and non-steady-state weathering and petrogenesis of siliciclastic sands and muds: Journal of Geology, v. 105, no. 2, p. 173-191.

Nesse, W. D., 2004, Introduction to Optical Mineralogy, 3rd ed., Oxford University Press, New York, Oxford, 348 pp.

Newton, R. C. and Manning, C. E., 2000, Quartz solubility in H_2O-NaCl and H_2O-CO_2 solutions at deep crust-upper mantle pressures and temperatures: 2–15 kbar and 500–900 °C: Geochimica et Cosmochimica Acta, v. 64, no. 17, p. 2993-3005.

Nitschke, F., Scheiber, J., Kramar, U. and Neumann, T., 2014, Formation of alternating layered Ba-Sr-sulfate and Pb-sulfide scaling in the geothermal plant of Soultz-sous-Forêts: Neues Jahrbuch für Mineralogie – Abhandlungen (Journal of Mineralogy and Geochemistry), v. 191, no. 2, p. 145-156.

Ortlam, D., 1967, Fossile Böden als Leithorizonte für die Gliederung des Höheren Buntsandsteins im nördlichen Schwarzwald und südlichen Odenwald: Geologisches Jahrbuch, v. 84, p. 485-590.

Ortlam, D., 1974, Inhalt und Bedeutung fossiler Bodenkomplexe in Perm und Trias von Mitteleuropa: Geologische Rundschau, v. 63, no. 3, p. 850-884.

Parrish, J. T., 1993, Climate of the Supercontinent Pangea: Journal of Geology, v. 101, no. 2, p. 215-233.

Passchier, C. W. and Trouw, R. A. J., 2005, Microtectonics, 2nd ed., Springer, Berlin; Heidelberg, 366 pp.

Paul, J., 1999, Oolithe und Stromatolithen im Unteren Buntsandstein, *in* Hauschke, N. and Wilde, V., eds., Trias - Eine ganz andere Welt, Verlag Dr. Friedrich Pfeil, München, p. 263-271.

Paul, J. and Puff, P., 2014, Das Klima des Buntsandstein: Schriftenreihe der Deutschen Gesellschaft für Geowissenschaften, v. 69, p. 213-221.

Paul, J., Wemmer, K. and Ahrendt, H., 2008, Provenance of siliciclastic sediments (Permian to Jurassic) in the Central European Basin: Zeitschrift der Deutschen Gesellschaft für Geowissenschaften, v. 159, no. 4, p. 641-650.

Paxton, S. T., Szabo, J. O., Ajdukiewicz, J. M. and Klimentidis, R. E., 2002, Construction of an intergranular volume compaction curve for evaluating and predicting compaction and porosity loss in rigid-grain sandstone reservoirs: American Association of Petroleum Geologists Bulletin, v. 86, no. 12, p. 2047-2067.

Perry, E. A. and Hower, J., 1972, Late-stage dehydration in deeply buried pelitic sediments: American Association of Petroleum Geologists Bulletin, v. 56, p. 2013-2021.

Pettijohn, F. J., Potter, P. E. and Siever, R., 1987, Sand and Sandstone, 2nd ed., Springer, New York, Berlin, Heidelberg, 576 pp.

Pfaff, K., Hildebrandt, L. H., Leach, D. L., Jacob, D. E. and Markl, G., 2010, Formation of the Wiesloch Mississippi Valley-type Zn-Pb-Ag deposit in the extensional setting of the Upper Rhinegraben, SW Germany: Mineralium Deposita, v. 45, no. 7, p. 647-666.

Pflug, R., 1982, Bau und Entwicklung des Oberrheingrabens, Darmstadt, Wissenschaftliche Buchgesellschaft, Erträge der Forschung; 184, 145 pp.

Pittman, E. D., Larese, R. E. and Heald, M. T., 1992, Clay coats: occurence and relevance to preservation of porosity in sandstones, *in* Houseknecht, D. W. and Pittman, E. D., eds., Origin, Diagenesis and Petrophysics of Clay Minerals in Sandstones, SEPM Society for Sedimentary Geology Special Publication 47, p. 241-255.

Platt, J. D., 1993, Controls on clay mineral distribution and chemistry in the Early Permian Rotliegend of Germany: Clay Minerals, v. 28, no. 3, p. 393-416.

Pollard, D. D. and Aydin, A., 1988, Progress in understanding jointing over the past century: Geological Society of America Bulletin, v. 100, no. 8, p. 1181-1204.

Poppe, L. J., Fredericks, J. J. and Hathaway, J. C., 1988, A computer program to calculate centrifugation parameters for sedimentation analyses: Computers & Geosciences, v. 14, no. 4, p. 541-545.

Poppe, L. J., Paskevich, V. F., Hathaway, J. C. and Blackwood, D. S., 2001, A laboratory manual for X-ray powder diffraction: United States Geological Survey Open-File Report 2001-41, One CD-ROM.

Potter, R., 1977, Pressure corrections for fluid-inclusion homogenization temperatures based on the volumetric properties of the system NaCl-H_2O: Journal of Research of the U.S. Geological Survey, v. 5, no. 5, p. 603-607.

Powers, M. C., 1953, A new roundness scale for sedimentary particles: Journal of Sedimentary Research, v. 23, no. 2, p. 117-119.

Pryor, W. A., 1973, Permeability-porosity patterns and variations in some Holocene sand bodies: American Association of Petroleum Geologists Bulletin, v. 57, p. 162-189.

Pucknat, S., 2011, Sedimentologie und Fazies des Mittleren und Oberen Buntsandsteins (Raum Pirmasens) [Diploma thesis]: Heidelberg University, 136 pp.

Pye, K. and Tsoar, H., 2009, Aeolian Sand and Sand Dunes, 2nd ed., Springer, Berlin, Heidelberg, 458 pp.

Pytte, A. M., and Reynolds, R. C., 1989, The thermal transformation of smectite to illite, *in* Naeser, N. and McCulloh, T., eds., Thermal History of Sedimentary Basins, Springer, New York, p. 133-140.

Radies, D., Stollhofen, H., Hollmann, G. and Kukla, P., 2005, Synsedimentary faults and amalgamated unconformities: Insights from 3D-seismic and core analysis of the Lower Triassic Middle Buntsandstein, Ems Trough, north-western Germany: International Journal of Earth Sciences, v. 94, p. 863-875.

Ramseyer, K., Baumann, J., Matter, A. and Mullis, J., 1988, Cathodoluminescence colors of α-quartz: Mineralogical Magazine, v. 52, no. 368, p. 669-677.

Ramseyer, K. and Mullis, J., 1990, Factors influencing short-lived blue cathodoluminescence of α-quartz: American Mineralogist, v. 75, p. 791-800.

Reicherter, K., Froitzheim, N., Jarosinski, M., Badura, J., Franzke, H.-J., Hansen, M., Hübscher, C., Müller, R., Poprawa, P., Reinecker, J., Stackebrandt, W., Voigt, T., von Eynatten, H. and Zuchiewicz, W., 2008, Alpine tectonics north of the Alps, *in* McCann, T., ed., The Geology of Central Europe, p. 1233-1285.

Rettig, B., 1996, Die Solling-Folge (Mittlerer Buntsandstein) im Grenzgebiet Niedersachsen - Thüringen - Hessen: Mitteilungen aus dem Geologischen Institut der Universität Hannover, v. 35, p. 1-105.

Reynolds, R. C., Mixed-layered illite-smectite in a contact metamorphic environment, Eighteenth Annual Meeting of the Clay Minerals Society, University of Illinois at Urbana-Champaign, Urbana, IL, 1981, p. 5.

Richter-Bernburg, G., 1974, Stratigraphische Synopsis des deutschen Buntsandsteins: Geologisches Jahrbuch A, v. 25, p. 127-132.

Roduit, N., 2007, JMicroVision: un logiciel d'analyse d'images pétrographiques polyvalent [Doctoral thesis]: Université de Genève, 116 pp.

Roedder, E. and Kopp, O. C., 1975, A check on the validity of the pressure correction in inclusion geothermometry, using hydrothermally grown quartz: Fortschritte Mineralogie, v. 52, p. 431-446.

Roos, B. M. and Smits, B. J., 1983, Rotliegend and Main Buntsandstein Gas Fields in Block K/13 — A Case History, *in* Kaasschieter, J. P. H. and Reijers, T. J. A., eds., Petroleum Geology of the Southeastern North Sea and the Adjacent Onshore Areas, Springer Netherlands, The Hague, p. 75-82.

Rosenfeld, M. A., 1949, Some aspects of porosity and cementation: Producers Monthly, v. 13, p. 39-42.

Rossel, N. C., 1982, Clay mineral diagenesis in Rotliegend aeolian sandstones of the southern North Sea: Clay Minerals, v. 17, p. 69-77.

Rückheim, J., 1989, Migrations- und Akkumulationsgeschichte der Erdöle des nördlichen Oberrheingrabens und deren Beziehung zur Diagenese der klastischen Speichergesteine [Doctoral thesis]: RWTH Aachen, 282 pp.

Rügner, O., 2000, Tonmineral-Neubildung und Paläosalinität im Unteren Muschelkalk des südlichen Germanischen Beckens [Doctoral thesis]: Heidelberg University, 189 pp.

Rupf, I. and Nitsch, E., 2008, Das geologische Landesmodell von Baden-Württemberg: Datengrundlagen, technische Umsetzung und erste geologische Ergebnisse, Landesamt für Geologie, Rohstoffe und Bergbau Baden-Württemberg, Freiburg im Breisgau, 81 pp.

Ryu, I. C. and Niem, A. R., 1999, Sandstone diagenesis, reservoir potential and sequence stratigraphy of the Eocene Tyee basin, Oregon: Journal of Sedimentary Research, v. 69, no. 2, p. 384-393.

Sanjuan, B., Millot, R., Dezayes, C. and Brach, M., 2010, Main characteristics of the deep geothermal brine (5 km) at Soultz-sous-Forêts (France) determined using geochemical and tracer test data: Comptes Rendus Geoscience, v. 342, no. 7-8, p. 546-559.

Scheiber, J., Seibt, A., Birner, J., Cuenot, N., Gentner, A. and Moeckes, W., 2014, Barite scale control at the Soultz-sous-Forêts (France) EGS site, *in* Proceedings Thirty-Eighth Workshop on Geothermal Reservoir Engineering, Stanford University, Stanford, California, February 24-26, 2014, SGP-TR-202.

Scheiber, J., Seibt, A., Birner, J., Gentner, A. and Moeckes, W., 2013, Application of a scaling inhibitor system at the geothermal power plant in Soultz-sous-Forêts: Laboratory and on-site studies, European Geothermal Congress: Pisa, Italy, p. 1-12.

Schleicher, A. M., 2005, Clay mineral formation and fluid-rock interaction in fractured crystalline rocks of the Rhine rift system [Doctoral thesis]: Heidelberg University, 104 pp.

Schleicher, A. M., Warr, L. N. and Pluijm, B. A., 2005, Fluid focusing and back-reactions in the uplifted shoulder of the Rhine rift system: a clay mineral study along the Schauenburg Fault zone (Heidelberg, Germany): International Journal of Earth Sciences, v. 95, no. 1, p. 19-33.

Schwab, M. S., 2013, Ein Aufschlussanalog für geothermische Reservoirgesteine: Diagenese und Fazies des Mittleren Buntsandsteins bei Ettlingen (Baden) [B.Sc. thesis]: Heidelberg University, 101 pp.

Sheldon, H. A., Wheeler, J., Worden, R. H. and Cheadle, M. J., 2003, An analysis of the roles of stress, temperature and pH in chemical compaction of sandstones: Journal of Sedimentary Research, v. 73, no. 1, p. 64-71.

Shibuya, T., Komiya, T., Nakamura, K., Takai, K. and Maruyama, S., 2010, Highly alkaline, high-temperature hydrothermal fluids in the early Archean ocean: Precambrian Research, v. 182, no. 3, p. 230-238.

Smit, D. E. and Swett, K., 1969, Devaluation of 'dedolomitization': Journal of Sedimentary Research, v. 39, no. 1, p. 379-380.

Smith, D. J., Jenkin, G. R. T., Naden, J., Boyce, A. J., Petterson, M. G., Toba, T., Darling, W. G., Taylor, H. and Millar, I. L., 2010, Anomalous alkaline sulphate fluids produced in a magmatic hydrothermal system — Savo, Solomon Islands: Chemical Geology, v. 275, no. 1–2, p. 35-49.

Soyk, D., 2010, Geologische Kartierung südöstlich von Cotillo, Fuerteventura, Spanien [Diploma mapping thesis]: Ruprecht-Karls-Universität Heidelberg, 135 pp.

Sposito, G., 2008, The Chemistry of Soils, 2nd ed, Oxford University Press., New York, 329 pp.

Spötl, C., 1990, Authigenic aluminium phosphate-sulphates in sandstones of the Mitterberg Formation, Northern Calcareous Alps, Austria: Sedimentology, v. 37, no. 5, p. 837.

Sprunt, E. S. and Nur, A., 1979, Microcracking and healing in granites: new evidence from cathodoluminescence: Science, v. 205, no. 4405, p. 495-497.

Środoń, J. and Eberl, D. D., 1984, Illite, *in* Bailey, S. W., ed., Micas: Reviews in Mineralogy 13, Mineralogical Society of America, Reno, NV, p. 495-544.

Środoń, J., Szulc, J., Anczkiewicz, A., Jewuła, K., Banaś, M. and Marynowski, L., 2014, Weathering, sedimentary and diagenetic controls of mineral and geochemical characteristics of the vertebrate-bearing Silesian Keuper: Clay Minerals, v. 49, no. 4, p. 569-594.

Staude, S., Bons, P. D. and Markl, G., 2009, Hydrothermal vein formation by extension-driven dewatering of the middle crust: An example from SW Germany: Earth and Planetary Science Letters, v. 286, no. 3-4, p. 387-395.

Steingötter, K., 2005, Geologie von Rheinland-Pfalz, Schweizerbart, Stuttgart, 400 pp.

Stern, L. A., Page Chamberlain, C., Reynolds, R. C. and Johnson, G. D., 1997, Oxygen isotope evidence of climate change from pedogenic clay minerals in the Himalayan molasse: Geochimica et Cosmochimica Acta, v. 61, no. 4, p. 731-744.

Stingl, V., 1984, Alpiner Buntsandstein und Werfener Schichten bei Leogang (Salzburg): Geologisch-Paläontologische Mitteilungen Innsbruck, v. 14, p. 1-19.

Stingl, V., 1987, Die fazielle Entwicklung des Alpinen Buntsandsteins (Skyth) im Westabschnitt der Nördlichen Kalkalpen (Tirol/Salzburg, Österreich): Geologische Rundschau, v. 76, no. 2, p. 647-664.

Stober, I. and Bucher, K., 2014, Hydraulic and hydrochemical properties of deep sedimentary reservoirs of the Upper Rhine Graben, Europe: Geofluids, p. n/a, DOI: 10.1111/gfl.12122 (Early View, Online Version).

Stober, I. and Jodocy, M., 2009, Eigenschaften geothermischer Nutzhorizonte im baden-württembergischen und französischen Teil des Oberrheingrabens: Grundwasser, v. 14, p. 127-137.

Stober, I. and Jodocy, M., 2011, Hydrochemie der Tiefenwässer im Oberrheingraben - Eine Basisinformation für geothermische Nutzungssysteme: Zeitschrift für Geologische Wissenschaften, v. 39, no. 1, p. 39-57.

Stoessell, R. K., Klimentidis, R. E. and Prezbindowski, D. R., 1987, Dedolomitization in Na-Ca-Cl brines from 100° to 200°C at 300 bars: Geochimica et Cosmochimica Acta, v. 51, no. 4, p. 847-855.

Straßer, R., 1907, Über Scheinkristalle aus dem Buntsandstein bei Heidelberg: Verhandlungen des Naturhistorisch-Medizinischen Vereins zu Heidelberg, v. 8, p. 371-396.

Sullivan, M. D., Macaulay, C. I., Fallick, A. E. and Haszeldine, R. S., 1997, Imported quartz cement in aeolian sandstone grew from water of uniform composition but has complex zonation: Terra Nova, v. 9, no. 5-6, p. 237-241.

Swartzlow, C., 1934, Two dimensional dendrites and their origin: American Mineralogist, v. 19, p. 403-411.

Switzer, G., 1949, Svanbergite from Nevada: American Mineralogist, v. 34, p. 104-108.

Szulc, J., 2000, Middle Triassic evolution of the northern Peri-Tethys area as influenced by early opening of the Tethyan Ocean: Annales Societatis Geologorum Poloniae, v. 70, p. 1-48.

Szurlies, M., 2007, Latest Permian to Middle Triassic cyclo-magnetostratigraphy from the Central European Basin, Germany: Implications for the geomagnetic polarity timescale: Earth and Planetary Science Letters, v. 261, no. 3–4, p. 602-619.

Szurlies, M., 2009, Buntsandstein unconformities and high-resolution base-level cycles: implications for the evolution of the Central European Basin using an integrated cyclomagnetostratigraphy. EGU General Assembly 2009, 19-24 April, 2009, Vienna, Austria. http://meetings.copernicus.org/egu2009, p.13017

Tatsumoto, M. and Patterson, C., 1980, Age studies of zircon and feldspar concentrates from the Franconia sandstone: Journal of Geology, v. 72, p. 232-242.

Thomson, A., 1959, Pressure solution and porosity, *in* Ireland, H. A., ed., Silica in Sediments: Special Publication 7, Society for Economic Paleontologists and Mineralogists, p. 92-110.

Timar-Geng, Z., Fügenschuh, B., Wetzel, A. and Dresmann, H., 2006, Low-temperature thermochronology of the flanks of the southern Upper Rhine Graben: International Journal of Earth Sciences, v. 95, no. 4, p. 685-702.

Timar-Geng, Z., Fügenschuh, B., Schaltegger, U. and Wetzel, A., 2004, The impact of the Jurassic hydrothermal activity on zircon fission track data from the southern Upper Rhine Graben area: Schweizerische Mineralogische und Petrographische Mitteilungen, v. 84, no. 3, p. 257-269.

Trusheim, F., 1961, Über Diskordanzen im Mittleren Buntsandstein Nordwestdeutschlands zwischen Ems und Weser: Erdöl-Zeitschrift, v. 77, p. 361-367.

Trusheim, F., 1963, Zur Gliederung des Buntsandsteins: Erdöl-Zeitschrift, v. 79, p. 277-292.

Turner, P., 1980, Continental Red Beds, Developments in Sedimentology, v. 29, Elsevier, Amsterdam, 562 p.

Valeton, I., 1953, Petrographie des süddeutschen Hauptbuntsandsteins: Heidelberger Beiträge zur Mineralogie und Petrographie, v. 3, p. 335-379.

Van Houten, F. B., 1968, Iron Oxides in Red Beds: Geological Society of America Bulletin, v. 79, no. 4, p. 399-416.

Van Lith, J. G. J., 1983, Gas fields of Bergen concession, The Netherlands, *in* Kaasschieter, J. P. H. and Reijers, T. J. A., eds., Petroleum Geology of the Southeastern North Sea and the Adjacent Onshore Areas, Springer Netherlands, The Hague, p. 63-74.

Velde, B., 1995, Compaction and Diagenesis, *in* Velde, B., ed., Origin and Mineralogy of Clays, Springer, Berlin, Heidelberg, New York, p. 220-246.

Wagner, G. A., 1975, Spaltspuren und ihre Bedeutung für die thermische Geschichte des Odenwaldes: Der Aufschluß, Sonderband 27, p. 79-85.

Walker, T. R., 1967, Formation of red beds in modern and ancient deserts: Geological Society of America Bulletin, v. 78, no. 3, p. 353.

Walker, T. R., 1976, Diagenetic origin of continental red beds, *in* Falke, H., ed., The Continental Permian in West, Central and South Europe: NATO Advanced Study Institute Series 22, D. Reidel Pub. Co, Dordrecht, Boston, p. 240-282.

Walker, T. R., Waugh, B. and Grone, A. J., 1978, Diagenesis in first-cycle desert alluvium of Cenozoic age, southwestern United States and northwestern Mexico: Geological Society of America Bulletin, v. 89, no. 1, p. 19-32.

Wasielka, N., 2012, The Buntsandstein east of the Upper Rhine Valley (Odenwald area): facies and diagenesis [M.Sc. Master Thesis]: Jagiellonian University of Krakow, 140 pp.

Waugh, B., 1978, Authigenic K-feldspar in British Permo-Triassic sandstones: Journal of the Geological Society, v. 135, p. 51-56.

Wentworth, C. K., 1922, A scale of grade and class terms for clastic sediments: Journal of Geology, v. 30, p. 377-392.

Werner, W. and Dennert, V., 2004, Lagerstätten und Bergbau im Schwarzwald: ein Führer unter besonderer Berücksichtigung der für die Öffentlichkeit zugänglichen Bergwerke, Landesamt für Geologie, Rohstoffe und Bergbau Baden-Württemberg, Freiburg im Breisgau, 334 pp.

White, A. F., Bullen, T. D., Schulz, M. S., Blum, A. E., Huntington, T. G. and Peters, N. E., 2001, Differential rates of feldspar weathering in granitic regoliths: Geochimica et Cosmochimica Acta, v. 65, no. 6, p. 847-869.

Wilson, M. D., 1992, Inherited grain-rimming clays in sandstones from eolian and shelf environments: Their origin and control on reservoir properties, *in* Houseknecht, D. W. and Pittman, E. D., eds., Origin, Diagenesis and Petrophysics of Clay Minerals in Sandstones, SEPM Society for Sedimentary Geology, Special Publication 47, p. 209-225.

Wilson, M. D. and Pittman, E. D., 1977, Authigenic clays in sandstones; recognition and influence on reservoir properties and paleoenvironmental analysis: Journal of Sedimentary Research, v. 47, no. 1, p. 3-31.

Wolburg, J., 1961, Sedimentationszyklen und Stratigraphie des Buntsandsteins in Nordwestdeutschland: Geotektonische Forschungen, v. 14, p. 7-74.

Wolburg, J., 1968, Vom zyklischen Aufbau des Buntsandsteins: Neues Jahrbuch für Geologie und Paläontologie, p. 535-559.

Wood, G. V. and Armstrong, A. K., 1975, Diagenesis and stratigraphy of the Lisbourne Group limestones of the Sadlerochit Mountains and adjacent areas, northeastern Alaska: United States Geological Survey Professional Paper, v. 857, p. 47.

Xie, Z. and Walther, J. V., 1993, Quartz solubilities in NaCl solutions with and without wollastonite at elevated temperatures and pressures: Geochimica et Cosmochimica Acta, v. 57, no. 9, p. 1947-1955.

Ziegler, P. A., 1990, Geological atlas of Western and Central Europe: Shell Internationale Petroleum Maatschappij, The Hague, 239 p.

Ziegler, P. A., 1992, European Cenozoic rift system: Tectonophysics, v. 208, no. 1–3, p. 91-111.

Zielinski, G. W., Poprawa, P., Szewczyk, J., Grotek, I., Kiersniwski, H. and Zielinski, R. L. B., 2012, Thermal effects of Zechstein salt and the Early to Middle Jurassic hydrothermal event in the central Polish Basin: American Association of Petroleum Geologists Bulletin, v. 96, no. 10, p. 1981-1996.

Zinkernagel, U., 1978, Cathodoluminescence of quartz and its application to sandstone petrology, Contributions to sedimentology 8, Schweizerbart, Stuttgart, 69 pp.

Zwingmann, H., Clauer, N. and Gaupp, R., 1998, Timing of fluid flow in a sandstone reservoir of the north German Rotliegend (Permian) by K-Ar dating of related hydrothermal illite, *in* Parnell, J., Dating and Duration of Fluid Flow and Fluid-Rock Interaction, Geological Society, London, Special Publications, 144, p. 91-106.

Appendix 1 Lithofacies Types after Miall (1977)

Facies Code	Lithofacies	Sedimentary structures	Interpretation
Gms	massive, matrix supported gravel	none	debris flow deposits
Gm	Massive or crudely bedded gravel	horizontal bedding, imbrication	longitudinal bars, lag deposits, sieve deposits
Gt	gravel, stratified	trough crossbeds	minor channel fills
Gp	gravel, stratified	planar crossbeds	linguid bars or deltaic growths from oder bar remnants
St	sand, medium to v. coarse, may be pebbly	solitary (theta) or grouped (pi) trough crossbeds	dunes (lower flow regime)
Sp	sand, medium to v. coarse, may be pebbly	solitary (alpha) or grouped (omikron) planar crossbeds	linguid, transverse bars, sand waves (lower flow regime)
Sr	sand, very fine to coarse	ripple marks of all types	ripples (lower flow regime)
Sh	sand, very fine to coarse	horizontal lamination, parting or streaming lamination	planar bed flow (l. and u. flow regime)
Sl	sand, fine	low angle (<10°) crossbeds	scour fills, crevasse splays, antidunes
Se	erosional scours with intraclasts	crude crossbedding	scour fills
Ss	sand, fine to coarse, may be pebbly	broad, shallow scours including eta cross-stratification	scour fills
Sse, She, Spe	sand	analogous to Ss, Sh, Sp	eolian deposits
Fl	sand, silt, mud	fine lamination, very fine ripples	overbank or waning flood deposits
Fsc	silt, mud	laminated to massive	backswamp deposits
Fcf	mud	massive, with freshwater molluscs	backswamp pond deposits
Fm	mud, silt	massive, desiccation cracks	overbank or drape deposits
Fr	silt, mud	rootlets	seatearth
C	coal, carbonaveous mud	plants, mud films	swamp deposits
P	carbonate	pedogenic features	soil

Appendix 2 Quartz Types after Bernet and Bassett (2005)

Quartz type	SEM-CL features	Optical features	Comments
Plutonic quartz	- light gray CL - microcracks and healed cracks (randomly oriented) - rare zoning	- monocrystalline or - <3 polycrystalline - non-undulose to weak undulose extinction	May contain fluid-inclusion trails and mineral inclusions (e.g. apatite or zircon)
Volcanic quartz	- light gray to black CL - either homogeneous or patchy CL - common zoning - large open cracks	- monocrystalline - non-undulose extinction - large open cracks	Inclusions and open cracks can be seen with both techniques. Cracks formed during rapid cooling.
Brittle deformed quartz (under very low-grade metamorphic conditions)	- microfractures or healed fractures with preferred orientation	- mono- or polycrystalline - weakly undulose extinction	Tectonically induced microfractures are possible in any quartz type that experiences brittle deformation. Several generations of oriented microfractures or healed fractures are possible in the same grain.
Ductile deformed quartz (under low-medium grade metamorphic conditions)	- deformation lamellae - complex shear	- weakly to strong undulose extinction - deformation lamellae	Tectonically induced deformation lamellae are possible in any quartz type that experiences ductile deformation. Complex shear patterns were not observed in this study see Seyedolali et al. (1997).
Low-grade to medium-grade metamorphic quartz	- light gray to black CL - patchy or mottled CL	- weakly to strong undulose extinction	Quartz grains of volcanic, plutonic, or other origin that experienced low- to medium-grade metamorphic overprint.
High-grade metamorphic quartz - recrystallized quartz	- black CL	- polycrystalline (quartz mosaics with non-undulose to weakly undulose extinction)	Also see Seyedolali et al. (1997) for more information on CL of high-grade metamorphic quartz. Recrystallized quartz is easy to identify with the optical microscope.
Vein quartz	- light gray to black CL - homogeneous CL - patchy CL - zoning - very rare microcracks	- polycrystalline - weakly to strongly undulose extinction	Vein quartz commonly very similar to metamorphic, recrystallized, or microcrystalline quartz.
Shocked quartz	- strong fracture pattern seen as black lines	- fractures and inclusions - strongly undulose extinction	Not observed in this study, information from Seyedolali et al. (1997) and Boggs et al. (2001).
Recycled detrital quartz with brittle deformation during burial and diagenesis	- grain shattering (against grain contact = diagenetic)	- mono- or polycrystalline depending on quartz type - weakly or strongly undulose extinction (depending on inherited extinction behaviour)	With the optical microscope, grains look as theugh if they experienced pressure solution. SEM-CL shows grain shattering (Dickinson and Miliken, 1995; Miliken and Laubach, 2000).
Microcrystalline quartz	- black CL	- microcrystalline	Better to identify with optical microscope.

Appendix 3 Point Counting Raw Data

Sample	Outcrop/Well	McBride Classification	Authigenic, Barite	Authigenic, Calcite	Authigenic, Dolomite	Authigenic, Fibrous Illite	Authigenic, Grain coating Hem	Authigenic, IC + Hem	Authigenic, IM + Hem	Authigenic, IR + Hem	Authigenic, Illite repl Kfs	Authigenic, Illite Coating	Authigenic, Kaolinite repl Kfs	Authigenic, Kaolinite	Authigenic, Meshwork Illite	Authigenic, Orthoclase	Authigenic, Pore filling Hem	Authigenic, Qtz attached to Mqtz	Authigenic, Qtz attached to Pqtz	Detrital, Alkali Feldspars	Detrital, Biotite	Detrital, Dolomite
C2 Ia	Cleebourg	SubArkose						5.67	1.00		1.33	0.33		0.33		1.00		8.00	0.33	16.00	0.33	
C2/2 IIa	Cleebourg	SubArkose				0.33		9.33	0.33		2.33	1.00	0.33	0.33		0.33	1.33	3.33		17.00		
C2/2 III	Cleebourg	SubArkose				1.00		5.00	3.33		4.67	1.67		0.67		0.33	0.33	1.33	0.33	16.67	1.00	
C2/2 IV d	Cleebourg	SubArkose						0.67			2.00	9.33		0.67	0.33		1.00	1.00		16.33	1.00	
C2/2 IVb 1a	Cleebourg	SubArkose						4.33	1.67		4.67	6.67			1.00			1.33		16.33		
C2/2 IVe	Cleebourg	SubArkose						4.00	0.33		1.67	5.67		2.00	0.33	0.33	0.33	1.67		14.33		
C2/2 VIb 1c	Cleebourg	SubArkose						2.33			4.00	8.00		0.33	0.67			1.33		17.33	0.33	
C2/2A III (2)	Cleebourg	SubArkose				2.00					3.33	7.00		0.33	3.00			1.33		14.00		
C2/A III 2	Cleebourg	SubArkose				0.67	0.33	2.33			0.33	5.67		0.33	0.33			1.33		15.33	0.33	
C5/1 VI	Cleebourg	SubArkose						11.33	0.33		2.67						1.33	1.00		17.33	1.67	
C5/1 Xa	Cleebourg	SubArkose				0.67		2.33	0.67		2.67			0.33				7.67		17.00		
Cl01	Cleebourg	Sublithic arenite						1.34	1.34			4.70		0.67	3.02		2.68	0.67		6.71	0.34	
Cl02	Cleebourg	Sublithic arenite										4.33			3.33		1.67	1.00		8.00	0.33	
Cl03	Cleebourg	SubArkose					1.00	5.67	9.33			1.33			3.00	0.33	4.33	0.67		11.33	0.67	
Cl04	Cleebourg	SubArkose				0.33	0.33	5.67	7.00		3.00	0.33				0.67	2.67	1.33		13.67	0.33	
Cl05	Cleebourg	SubArkose						7.00			0.67					0.33		5.33	0.33	10.00		
Cl06	Cleebourg	SubArkose						7.33	3.67		0.67	1.00			0.33	0.33		0.67		15.33	0.33	
Cl08	Cleebourg	SubArkose						6.00	4.33		3.33	3.33			3.00			0.33		14.33	2.33	
Cl09	Cleebourg	SubArkose						2.33	0.67		0.67	1.00				1.00		5.33	0.33	11.67	0.67	
Cl10	Cleebourg	SubArkose					1.33	3.67	3.67		1.67					0.33	7.00	1.67		10.67	0.33	
Cl14	Cleebourg	SubArkose					1.00	8.33	3.00		2.67	0.33					2.67	0.33		12.33	1.33	
Cl15	Cleebourg	SubArkose						4.00	0.67		2.67	5.67			1.67			0.33		13.33	0.33	
Cl16	Cleebourg	SubArkose				0.67		2.67	3.67		3.00	6.67			2.00			1.00		10.00		
Cl17	Cleebourg	SubArkose				1.33	0.33	4.67	1.67		1.67	0.67						8.33	0.67	6.00		
Cl18	Cleebourg	Sublithic arenite						3.33	3.33		3.00	4.67			2.33		1.33			7.67	1.67	
Cl19	Cleebourg	Arkosic Arenite					2.00	9.00	5.00		7.00						1.33	0.33		17.33	0.67	
Cl20	Cleebourg	SubArkose						2.00	1.00		7.33	3.67			4.33			0.33		16.67	0.33	

Sample	Outcrop/Well	Detrital, Extrabasinal - Non-sedimentary Lithoclast	Detrital, Extrabasinal - Sandstone Lithoclast	Detrital, Intrabasinal - Claystone Lithoclast	Detrital, Muscovite	Detrital, Opaque	Detrital, Quartz - Monocrystalline, strained (<5deg.)	Detrital, Quartz - Monocrystalline, unstrained	Detrital, Quartz - Polycrystalline, <4 crystallites	Detrital, Quartz - Polycrystalline, >4 crystallites	Detrital, Rutile	Detrital, Tourmaline	Detrital, Zircon	Matrix, Illitic	Matrix, Terrigenous	Porosity, Fracture	Porosity, Intergranular	Porosity, Secondary
C2 Ia	Cleebourg	5.33			0.67		15.00	20.67	1.00	7.33							13.67	2.00
C2/2 IIa	Cleebourg	7.33			0.67	1.67	10.00	24.67	2.33	7.00							7.67	2.67
C2/2 III	Cleebourg	7.67				0.33	23.67	13.00	2.00	8.00							5.67	3.33
C2/2 IV d	Cleebourg	9.67			1.00	0.67	22.67	20.33	2.33	3.00							7.00	1.00
C2/2 IVb 1a	Cleebourg	5.67			2.00	0.33	16.33	23.67	3.00	10.00		0.33	0.33				2.33	
C2/2 IVe	Cleebourg	9.33			1.33	0.33	18.33	21.67	1.00	5.67	0.33						4.00	7.33
C2/2 VIb 1c	Cleebourg	9.67			2.00	1.67	15.33	23.00	2.00	6.33			0.33				3.00	2.33
C2/2A III (2)	Cleebourg	3.67			0.67	0.67	19.33	22.67	2.00	10.33							8.33	1.33
C2/A III 2	Cleebourg	4.33			0.67	1.00	19.00	22.00	4.67	10.33	0.33		0.33				8.33	2.00
C5/1 VI	Cleebourg	10.33		1.33	1.00	0.33	22.33	16.33	2.00	7.67	0.33	0.33					2.33	
C5/1 Xa	Cleebourg	11.00					17.67	17.67	0.33	10.33							11.00	0.67
Cl01	Cleebourg	12.08			3.02		15.10	29.87	4.03	6.04	0.67				0.67		7.05	
Cl02	Cleebourg	14.67			2.00		19.00	19.67	4.33	10.00	0.33						11.33	
Cl03	Cleebourg	4.67			1.33		21.00	20.00	6.33	6.33	0.33		0.33				2.00	
Cl04	Cleebourg	2.67		1.67	0.33		15.00	21.00	5.00	11.67	0.33						7.00	
Cl05	Cleebourg	5.00					12.00	23.33	2.33	12.00							21.67	
Cl06	Cleebourg	6.00			0.67		12.67	29.00	3.33	11.67			0.33				5.67	1.00
Cl08	Cleebourg	7.67			5.33		22.67	23.33		2.00	0.33						1.67	
Cl09	Cleebourg	8.33			0.67		11.33	26.00	6.00	11.67							12.33	
Cl10	Cleebourg	4.33			0.33		15.33	37.00	1.00	9.00							2.00	0.67
Cl14	Cleebourg	10.00		1.00	0.67		15.67	25.33	3.00	9.00			0.33				2.67	0.33
Cl15	Cleebourg	6.33			1.00		14.67	27.67	4.00	8.67		0.33					7.33	1.33
Cl16	Cleebourg	4.67			1.00		22.67	28.00	2.00	5.67	0.33						5.67	0.33
Cl17	Cleebourg	3.00					14.67	24.67	0.67	11.33							19.33	1.00
Cl18	Cleebourg	10.33			3.33		21.67	25.67		6.33	1.00	0.33					4.00	
Cl19	Cleebourg	3.67			2.67		19.33	16.00	1.67	6.67	1.00						4.67	1.67
Cl20	Cleebourg	7.33			1.67		17.67	20.33	1.00	7.33	1.00						5.33	2.67

Sample	Outcrop/Well	McBride Classification	Authigenic, Barite	Authigenic, Calcite	Authigenic, Dolomite	Authigenic, Fibrous Illite	Authigenic, Grain coating Hem	Authigenic, IC + Hem	Authigenic, IM + Hem	Authigenic, IR + Hem	Authigenic, Illite repl Kfs	Authigenic, Illite Coating	Authigenic, Kaolinite repl Kfs	Authigenic, Kaolinite	Authigenic, Meshwork Illite	Authigenic, Orthoclase	Authigenic, Pore filling Hem	Authigenic, Qtz attached to Mqtz	Authigenic, Qtz attached to Pqtz	Detrital, Alkali Feldspars	Detrital, Biotite	Detrital, Dolomite
En 01	Well B 1	SubArkose						2.33	1.00			5.33			0.67	0.33	1.00	6.67	0.67	10.33		
EnII 01	Well B 2	Arkosic Arenite						5.00						0.67	0.33			6.33		20.67	0.33	
Et01	Ettlingen	SubArkose						7.33	1.33		0.33	0.67					1.00	5.33	1.33	8.67	0.33	
Et02	Ettlingen	SubArkose						3.33	0.67								1.67	17.67	5.33	7.67		
Et03	Ettlingen	SubArkose						7.67	1.67								3.33	2.67		11.00		
Et04	Ettlingen	SubArkose						5.33	1.67						0.33		3.33	6.33	0.67	13.33	0.33	
Et05	Ettlingen	SubArkose						8.67	0.67						0.33		2.67	6.33	1.00	7.00		
Et06	Ettlingen	SubArkose						9.33	2.33								0.67	2.67	0.33	5.67	0.33	
Et07	Ettlingen	SubArkose				0.33		9.33	1.00		0.33	1.33			1.33		1.67	2.33		14.33		
Et08	Ettlingen	SubArkose						4.67			0.33						0.67	16.00	1.33	5.67		
HB 1/2	Neustadt a.d.W./Hanbuch	SubArkose						1.00	0.67			5.33			2.33			2.00		18.00		
HB 1/3	Neustadt a.d.W./Hanbuch	Arkosic Arenite						2.00	1.33			11.00			5.00			2.00		28.89		
HB 1/4	Neustadt a.d.W./Hanbuch	SubArkose				0.32		4.17	0.64			4.49	0.64		3.21		0.32	1.60	0.32	15.28		
HB 1/5	Neustadt a.d.W./Hanbuch	SubArkose						3.02	1.34			3.02			1.68	0.34	1.01	3.69	0.67	16.00		
HB 1/6	Neustadt a.d.W./Hanbuch	Arkosic Arenite				0.33		2.00	2.33	0.67		4.67			1.00	0.33	1.00	4.00		22.22		
HB 1/7	Neustadt a.d.W./Hanbuch	Arkosic Arenite						0.67	2.33			3.67			1.00			2.67	0.33	22.67		
HB 1/8	Neustadt a.d.W./Hanbuch	SubArkose						1.00	1.33			6.33			2.00			3.67		14.00		
HB 15.11	Neustadt a.d.W./Hanbuch	Sublithic arenite						0.67				3.00			2.00			5.00		11.78		
HB 4/4	Neustadt a.d.W./Hanbuch	SubArkose						5.05	0.67			2.36			2.36	0.67		5.05	0.34	15.04	0.34	
HB 5/2	Neustadt a.d.W./Hanbuch	SubArkose						5.00	1.67			3.33			2.33		0.67	2.33		16.67		
HB 5/3	Neustadt a.d.W./Hanbuch	SubArkose						0.67	1.33			7.33			2.33			0.67		18.11	1.00	
HB 5/5	Neustadt a.d.W./Hanbuch	SubArkose				1.00		1.67	1.67			2.00			1.33	0.67	0.67	3.67		12.00		
HB 5/8	Neustadt a.d.W./Hanbuch	SubArkose						3.00	0.33			2.33			0.33			4.00		17.00		
HB 5/8.5	Neustadt a.d.W./Hanbuch	SubArkose						4.00	0.33			2.00			1.00	0.33		6.67		13.33		
HB 5/9	Neustadt a.d.W./Hanbuch	Arkosic Arenite						2.67	2.00	0.33		1.33			1.33		1.00	3.00		20.22		
HB 6/1	Neustadt a.d.W./Hanbuch	Arkosic Arenite						3.63	1.32			0.33			0.33		0.33	3.96		21.76		
HB 6/2	Neustadt a.d.W./Hanbuch	SubArkose				0.33		1.33	0.67			1.33			1.67			5.67		13.33		

Sample	Outcrop/Well	Detrital, Extrabasinal - Non-sedimentary Lithoclast	Detrital, Extrabasinal - Sandstone Lithoclast	Detrital, Intrabasinal - Claystone Lithoclast	Detrital, Muscovite	Detrital, Opaque	Detrital, Quartz - Monocrystalline, strained (<5deg.)	Detrital, Quartz - Monocrystalline, unstrained	Detrital, Quartz - Polycrystalline, <4 crystallites	Detrital, Quartz - Polycrystalline, >4 crystallites	Detrital, Rutile	Detrital, Tourmaline	Detrital, Zircon	Matrix, Illitic	Matrix, Terrigenous	Porosity, Fracture	Porosity, Intergranular	Porosity, Secondary
En 01	Well B 1	0.67			0.33		12.33	33.00	6.00	10.00					1.33		8.00	
EnII 01	Well B 2	9.33		1.67	0.33		16.00	20.67	0.67	8.33			0.67			2.00	7.00	
Et01	Ettlingen	1.67				0.67	13.33	34.33	7.00	13.00							3.67	
Et02	Ettlingen	2.33		1.67			10.00	30.67	6.67	10.33							2.00	
Et03	Ettlingen	2.33			0.33		18.33	29.33	6.00	11.33			0.33				5.33	0.33
Et04	Ettlingen	3.33			0.33		17.33	33.33	1.33	9.00			0.33				3.67	
Et05	Ettlingen	1.33				0.33	16.67	39.67	2.67	8.33						0.33	3.00	1.00
Et06	Ettlingen	2.00			0.67	0.67	17.33	36.67	4.33	14.67							2.33	
Et07	Ettlingen	4.67			0.33	0.33	13.33	31.67	3.00	7.67							5.00	2.00
Et08	Ettlingen	2.00					12.67	34.33	7.00	12.67			0.33				2.33	
HB 1/2	Neustadt a.d.W./Hanbuch	9.33		0.33	0.33		32.00	3.67	3.33	14.33	0.33						7.00	
HB 1/3	Neustadt a.d.W./Hanbuch	11.33					17.11	0.67	2.33	7.00	0.33						11.00	
HB 1/4	Neustadt a.d.W./Hanbuch	9.29		0.96	0.32		37.18	2.35	2.24	8.65	0.64						7.05	
HB 1/5	Neustadt a.d.W./Hanbuch	8.05			0.34		28.52	6.15	4.03	11.41							10.74	
HB 1/6	Neustadt a.d.W./Hanbuch	5.00			0.33		25.67	7.11	2.67	9.00					0.67		11.00	
HB 1/7	Neustadt a.d.W./Hanbuch	6.00					32.33	6.00	2.00	8.00	0.33						12.00	
HB 1/8	Neustadt a.d.W./Hanbuch	4.67					31.00	11.33	5.00	11.67							8.00	
HB 15.11	Neustadt a.d.W./Hanbuch	6.00		10.00			23.67	11.22	1.67	9.67							15.33	
HB 4/4	Neustadt a.d.W./Hanbuch	5.05		3.37			19.87	14.25	4.04	9.76					1.01		10.77	
HB 5/2	Neustadt a.d.W./Hanbuch	7.67					16.33	23.33	0.67	12.67							7.33	
HB 5/3	Neustadt a.d.W./Hanbuch	9.00					15.67	20.56	6.00	12.00					0.33		5.00	
HB 5/5	Neustadt a.d.W./Hanbuch	6.33		0.67			17.00	26.00	6.00	9.33			0.33				9.67	
HB 5/8	Neustadt a.d.W./Hanbuch	4.33					15.00	26.33	3.67	16.67							7.00	
HB 5/8.5	Neustadt a.d.W./Hanbuch	6.00		0.33			16.33	20.00	2.67	12.33							14.67	
HB 5/9	Neustadt a.d.W./Hanbuch	10.67					16.00	15.44	4.33	13.33			0.33				8.00	
HB 6/1	Neustadt a.d.W./Hanbuch	11.54		0.33			14.51	19.56	3.96	7.91							10.55	
HB 6/2	Neustadt a.d.W./Hanbuch	9.67					14.00	28.00	6.33	10.33							7.33	

Sample	Outcrop/Well	McBride Classification	Authigenic, Barite	Authigenic, Calcite	Authigenic, Dolomite	Authigenic, Fibrous Illite	Authigenic, Grain coating Hem	Authigenic, IC + Hem	Authigenic, IM + Hem	Authigenic, IR + Hem	Authigenic, Illite repl Kfs	Authigenic, Illite Coating	Authigenic, Kaolinite repl Kfs	Authigenic, Kaolinite	Authigenic, Meshwork Illite	Authigenic, Orthoclase	Authigenic, Pore filling Hem	Authigenic, Qtz attached to Mqtz	Authigenic, Qtz attached to Pqtz	Detrital, Alkali Feldspars	Detrital, Biotite	Detrital, Dolomite
HB 6/3	Neustadt a.d.W./Hanbuch	SubArkose						2.67	2.67			3.00			1.67	0.33		3.33		14.00		
HB 6/5	Neustadt a.d.W./Hanbuch	SubArkose				0.33		1.67	1.67			4.33	0.33		0.33			0.67		15.00		
HB 6/6	Neustadt a.d.W./Hanbuch	SubArkose						3.00	2.33			3.00						3.33		12.67		
HB 6/7	Neustadt a.d.W./Hanbuch	Lithic Arenite						3.01	1.00			2.01			2.01	0.67	0.33	3.34		11.04		
HB 6/8	Neustadt a.d.W./Hanbuch	SubArkose						2.33	1.00			3.67			1.33			2.00		14.33		
HB 6/9	Neustadt a.d.W./Hanbuch	Arkosic Arenite						1.97	2.96			2.30			2.63		0.66	1.97		24.64		
HB G 10	Neustadt a.d.W./Hanbuch	SubArkose						3.00	1.33			2.67				0.67	0.67	1.33		15.33		
HB G 13	Neustadt a.d.W./Hanbuch	SubArkose						2.34	2.01			5.35			2.01			0.33		15.38		
HB G 15.1	Neustadt a.d.W./Hanbuch	Arkosic Arenite						4.00	3.33			2.67			0.33	0.33		2.00		20.78		
HB G 2	Neustadt a.d.W./Hanbuch	SubArkose				0.67		2.33	2.67			4.00	0.67	0.67	1.67		1.33			18.56		
HB G 3.5	Neustadt a.d.W./Hanbuch	SubArkose						3.33	0.67			3.67		1.33	1.33			2.00		16.33		
HB G 5	Neustadt a.d.W./Hanbuch	SubArkose				0.33		5.00	1.33			1.67			0.67	0.33	0.33	2.00		16.11		
HB G 6	Neustadt a.d.W./Hanbuch	SubArkose				0.33		4.67	2.00			1.00		0.67	0.67	1.00	1.33	2.00		18.00	0.33	
HB03	Heidelberg Molkenkur	Lithic Arenite				0.33	0.99	1.99	0.66	0.33		0.33				0.33	2.32	11.92	2.98	9.60		
Hh01	Hirschhorn	SubArkose					4.33	2.00				0.33		0.33		1.00	2.33	9.33	1.00	11.33		
Hh02	Hirschhorn	SubArkose					7.00	2.67	1.00					1.00		0.33	4.67	5.67	0.67	10.00		
Hh03	Hirschhorn	Sublithic arenite					4.33	2.00								0.33	0.67	24.00	1.33	7.33		
Hh04	Hirschhorn	SubArkose					10.67	7.33	1.33								2.33			13.33		
Hh05	Hirschhorn	SubArkose					4.67	4.00	0.33					2.33			0.67	6.00		16.00		
HK 1	Heidelberg Kammerf. Br.	SubArkose						8.00	3.67							0.33	2.00	8.33	0.33	17.33		
HK 2	Heidelberg Kammerf. Br.	SubArkose						8.67	2.00					0.67		0.33		6.33	1.67	15.33		
L74 01	Well A 1	SubArkose					1.33	5.67	1.67			1.33		0.33	0.67			1.00		7.00		0.33
L76 01	Well A 2	Sublithic arenite	0.33	5.67	2.67			3.67										3.67		5.33		4.33
L76 02	Well A 2	SubArkose	1.00	0.33	0.33			10.00	2.00					1.00	0.33		0.33	1.67		12.33		
Lei 4/11	Leistadt	SubArkose				0.33		3.67				2.33			0.33		0.33	2.33	0.33	16.00		
Lei 4/12	Leistadt	SubArkose				0.33		4.67		0.33		1.33			0.67		0.33	3.00		15.00		
Lei 4/3	Leistadt	SubArkose						5.33				3.67			2.33	0.33	6.00	0.67		15.44		

Sample	Outcrop/Well	Detrital, Extrabasinal - Non-sedimentary Lithoclast	Detrital, Extrabasinal - Sandstone Lithoclast	Detrital, Intrabasinal - Claystone Lithoclast	Detrital, Muscovite	Detrital, Opaque	Detrital, Quartz - Monocrystalline, strained (<5deg.)	Detrital, Quartz - Monocrystalline, unstrained	Detrital, Quartz - Polycrystalline, <4 crystallites	Detrital, Quartz - Polycrystalline, >4 crystallites	Detrital, Rutile	Detrital, Tourmaline	Detrital, Zircon	Matrix, Illitic	Matrix, Terrigenous	Porosity, Fracture	Porosity, Intergranular	Porosity, Secondary
HB 6/3	Neustadt a.d.W./Hanbuch	8.67			0.67		14.67	25.00	3.67	11.00							8.67	
HB 6/5	Neustadt a.d.W./Hanbuch	8.67			0.33		15.00	22.67	4.00	8.00							17.00	
HB 6/6	Neustadt a.d.W./Hanbuch	7.33			0.67		11.67	32.00	1.67	11.00							11.33	
HB 6/7	Neustadt a.d.W./Hanbuch	7.02	20.40				9.36	23.08	3.34	7.69							5.69	
HB 6/8	Neustadt a.d.W./Hanbuch	7.33			0.33		15.67	30.67	1.67	11.00							8.67	
HB 6/9	Neustadt a.d.W./Hanbuch	7.89			0.33		12.81	22.45	3.61	7.56							8.21	
HB G 10	Neustadt a.d.W./Hanbuch	6.67		0.33			8.00	32.33	4.00	8.33	0.67		0.33				14.33	
HB G 13	Neustadt a.d.W./Hanbuch	7.69			0.33		10.03	32.44	2.68	9.70					0.33		9.36	
HB G 15.1	Neustadt a.d.W./Hanbuch	7.67		0.33			11.67	18.89	3.67	12.67					0.33		11.33	
HB G 2	Neustadt a.d.W./Hanbuch	9.67			0.67		8.33	25.44	3.67	9.00	0.33						10.33	
HB G 3.5	Neustadt a.d.W./Hanbuch	9.33		2.67	0.67		8.67	31.33	1.33	7.33	0.33						9.67	
HB G 5	Neustadt a.d.W./Hanbuch	8.00		0.33			8.33	31.56	2.67	12.00					0.33		8.67	0.33
HB G 6	Neustadt a.d.W./Hanbuch	10.00					9.67	24.00	3.00	11.67							9.67	
HB03	Heidelberg Molkenkur	1.66		17.55	0.33		4.64	23.18	2.65	10.60	0.66			1.66	1.99		2.98	
Hh01	Hirschhorn	4.00		2.00			10.00	26.67	1.67	12.00							8.00	3.67
Hh02	Hirschhorn	7.33		0.33			10.00	30.33	3.33	6.00					0.33		6.00	3.33
Hh03	Hirschhorn	6.33		3.00			7.00	23.67	3.00	8.00	0.67						3.33	5.00
Hh04	Hirschhorn	7.67		2.33	0.33		8.67	27.00	5.33	8.33	0.33						2.67	2.33
Hh05	Hirschhorn	2.67			0.33		11.33	26.33	4.33	9.00							7.67	4.33
HK 1	Heidelberg Kammerf. Br.	7.67				1.00	24.67	16.33	3.33	3.67							3.33	
HK 2	Heidelberg Kammerf. Br.	3.33			0.33	0.33	15.67	24.67	6.33	7.00		0.33					7.00	
L74 01	Well A 1	0.67			0.33	0.67	19.33	31.00	5.33	9.33			0.33			0.33	12.67	0.67
L76 01	Well A 2	2.67		6.33		0.33	17.00	22.00	5.67	6.00						1.67	12.00	0.67
L76 02	Well A 2	4.67			0.67	0.33	19.33	29.33	5.00	0.33							10.33	0.67
Lei 4/11	Leistadt	4.33		3.33			10.00	25.00	3.33	14.00	0.33				1.00		13.00	
Lei 4/12	Leistadt	8.67		3.67			11.00	19.33	7.00	13.00	0.33				1.33		9.67	
Lei 4/3	Leistadt	8.33			1.00		18.33	17.56	2.67	8.67	0.33			0.33	1.67		7.33	

Sample	Outcrop/Well	McBride Classification	Authigenic, Barite	Authigenic, Calcite	Authigenic, Dolomite	Authigenic, Fibrous Illite	Authigenic, Grain coating Hem	Authigenic, IC + Hem	Authigenic, IM + Hem	Authigenic, IR + Hem	Authigenic, Illite repl Kfs	Authigenic, Illite Coating	Authigenic, Kaolinite repl Kfs	Authigenic, Kaolinite	Authigenic, Meshwork Illite	Authigenic, Orthoclase	Authigenic, Pore filling Hem	Authigenic, Qtz attached to Mqtz	Authigenic, Qtz attached to Pqtz	Detrital, Alkali Feldspars	Detrital, Biotite	Detrital, Dolomite
Lei 4/4	Leistadt	Lithic Arenite						5.60				0.66			0.66		3.96	5.27		14.62	0.33	
Lei 4/7	Leistadt	Arkosic Arenite						5.00									6.00	3.33		21.78	0.33	
Lei 4/8	Leistadt	Sublithic arenite	0.31					4.69				0.63				0.31	3.75	5.63	0.94	15.10		
Lei 5/11	Leistadt	SubArkose						4.33	0.33			2.00			0.67		1.67	3.00		12.56	0.33	
Lei 5/5	Leistadt	Arkosic Arenite						1.33	3.00			4.33			0.67		10.33	1.67		22.44	1.00	
Lei 5/8	Leistadt	Arkosic Arenite						4.00	3.00			3.00	0.33		2.00		10.00			19.00	1.33	
Lei 5/9	Leistadt	Arkosic Arenite						6.33	4.33			2.00	0.33	0.67	0.67		5.67	1.00		19.11	1.00	
Ls01	Leistadt	SubArkose						1.60				0.96						2.56		12.18		
Ls02	Leistadt	SubArkose						5.67						0.33				2.00		13.00		
Ls03	Leistadt	SubArkose	0.33			0.33		3.67	0.33			1.33					0.33	5.33	1.33	10.33		
Ls04	Leistadt	SubArkose	0.67					5.00	2.33			1.33		1.33				2.00		8.67		
Ls05	Leistadt	SubArkose	0.33					5.33	0.67					0.33			13.33	3.33		9.00		
Ng01	Neckargemünd	Arkosic Arenite					8.67	1.00	0.33					0.33			7.67	1.33	0.33	20.00		
Ng02	Neckargemünd	SubArkose					5.33	6.67								0.33	6.67	0.33		16.67		
Ng03	Neckargemünd	SubArkose					3.67	1.33					0.67			1.00	1.00	17.33	0.33	15.33		
Ng04	Neckargemünd	Arkosic Arenite					7.67	1.33						0.33	0.33		5.00	6.33		18.67		
Ng05.1	Neckargemünd	SubArkose					7.00	1.67								0.33	5.00	10.67		14.00		
Ng05.2	Neckargemünd	SubArkose					4.00	3.00	4.33			0.67	0.67	0.67	1.00	0.33	1.00	5.00		15.00		
OM 3.1	Margaretenschlucht	SubArkose						11.67	2.67		0.33			0.33	0.33	0.33	0.67	4.33	1.33	9.33	0.33	
OM 4.3	Margaretenschlucht	Quartz		4.00	13.00			2.00										14.33	1.33	1.67		
OM 6.2	Margaretenschlucht	SubArkose						4.67	0.67					0.33	0.33	0.33	1.00	25.33	2.00	9.33		0.33
OM 7.2	Margaretenschlucht	Sublithic arenite		0.33	15.00			3.67	0.67		1.00			0.67		0.67	0.33	19.33	1.00	6.33		
OW 1.11	Wolfsschlucht	SubArkose				0.67		5.67	3.33					2.00	0.67	0.67	3.00	6.33	2.33	7.00		
OW 1.5	Wolfsschlucht	SubArkose				1.00		7.33	1.33		0.67			1.33	0.67	0.33	0.33	3.67	1.33	15.00		
OW 11.11	Wolfsschlucht	SubArkose		2.00				4.67	0.33					1.00	0.33	0.67		12.67	4.67	7.00		
OW 2.4 II	Wolfsschlucht	Sublithic arenite				0.67		5.00	1.67	0.67	0.67	0.33		2.33	1.00	0.67	0.67	5.67	1.67	10.00		
OW 6.4	Wolfsschlucht	SubArkose						2.67	2.00					0.67		0.67		17.67	5.00	10.33		

Sample	Outcrop/Well	Detrital, Extrabasinal - Non-sedimentary Lithoclast	Detrital, Extrabasinal - Sandstone Lithoclast	Detrital, Intrabasinal - Claystone Lithoclast	Detrital, Muscovite	Detrital, Opaque	Detrital, Quartz - Monocrystalline, strained (<5deg.)	Detrital, Quartz - Monocrystalline, unstrained	Detrital, Quartz - Polycrystalline, <4 crystallites	Detrital, Quartz - Polycrystalline, >4 crystallites	Detrital, Rutile	Detrital, Tourmaline	Detrital, Zircon	Matrix, Illitic	Matrix, Terrigenous	Porosity, Fracture	Porosity, Intergranular	Porosity, Secondary
Lei 4/4	Leistadt	4.29		14.84			12.20	8.57	4.62	11.87	0.33				1.65		10.55	
Lei 4/7	Leistadt	4.33		12.33			7.00	8.56	5.00	13.00	0.33			0.33	3.00		9.00	
Lei 4/8	Leistadt	7.81		9.38	0.31		10.31	16.46	2.81	9.69	0.31			1.88	1.25		8.44	
Lei 5/11	Leistadt	9.00		0.33	0.33		14.33	23.78	3.00	11.33	0.33			1.67	1.00		10.00	
Lei 5/5	Leistadt	9.33					13.67	11.89	2.67	9.67	0.33			2.00	1.00		4.67	
Lei 5/8	Leistadt	8.67			1.67		14.00	12.33	2.00	4.33	0.67			0.33	0.67		12.67	
Lei 5/9	Leistadt	10.67			2.00		18.00	11.89	2.67	6.67	1.67			0.33	0.33		4.67	
Ls01	Leistadt	8.65			0.32		15.71	17.95	7.05	14.74	0.32		0.32		0.64		16.99	
Ls02	Leistadt	6.33		2.67			11.67	23.67	4.00	7.00							22.00	1.67
Ls03	Leistadt	7.00		0.67			9.00	22.67	2.00	13.33	0.33				0.67		21.00	
Ls04	Leistadt	7.67					23.33	23.33	5.33	7.33			0.33				11.33	
Ls05	Leistadt	7.33					14.33	28.67	3.33	11.00							2.33	0.67
Ng01	Neckargemünd	1.67					12.00	30.00	3.00	5.67							6.33	1.67
Ng02	Neckargemünd	4.33					9.67	30.33	1.00	5.67	0.33		0.33				10.67	1.67
Ng03	Neckargemünd	5.33		5.67			9.00	25.67	3.00	6.00	0.33						3.67	0.67
Ng04	Neckargemünd	4.33					11.67	32.67	2.00	4.67	0.33		0.33				2.33	2.00
Ng05.1	Neckargemünd	7.33					10.33	27.67	1.67	7.33							6.00	1.00
Ng05.2	Neckargemünd	7.00					10.67	29.33	2.00	9.00			0.33				4.67	1.33
OM 3.1	Margaretenschlucht	3.33			0.33	1.00	24.00	21.00	5.00	12.00							1.33	0.33
OM 4.3	Margaretenschlucht	1.00					10.33	25.33	11.00	16.00								
OM 6.2	Margaretenschlucht	2.33		1.67			19.00	21.67	0.67	8.00							2.33	
OM 7.2	Margaretenschlucht	2.33		5.67	0.67		15.33	19.33	1.33	5.33							1.00	
OW 1.11	Wolfsschlucht	6.00		0.33	0.33		14.33	9.33	6.33	23.33							6.33	2.00
OW 1.5	Wolfsschlucht	1.33		6.33			9.00	20.00	8.33	16.33							4.67	1.00
OW 11.11	Wolfsschlucht	2.33		0.67			15.00	18.67	8.33	19.33			0.33				2.00	
OW 2.4 II	Wolfsschlucht	2.67		9.33			12.33	17.00	6.33	16.67							4.00	0.67
OW 6.4	Wolfsschlucht	1.33			0.33		14.00	19.00	8.33	13.67							4.00	0.33

Sample	Outcrop/Well	McBride Classification	Authigenic, Barite	Authigenic, Calcite	Authigenic, Dolomite	Authigenic, Fibrous Illite	Authigenic, Grain coating Hem	Authigenic, IC + Hem	Authigenic, IM + Hem	Authigenic, IR + Hem	Authigenic, Illite repl Kfs	Authigenic, Illite Coating	Authigenic, Kaolinite repl Kfs	Authigenic, Kaolinite	Authigenic, Meshwork Illite	Authigenic, Orthoclase	Authigenic, Pore filling Hem	Authigenic, Qtz attached to Mqtz	Authigenic, Qtz attached to Pqtz	Detrital, Alkali Feldspars	Detrital, Biotite	Detrital, Dolomite
P I B.1	Rodalben	SubArkose						5.67								0.33		5.33		10.33		
P I C.1	Rodalben	SubArkose						12.33								0.33	0.33	3.67		6.00		
P III A.1.3	Rodalben	SubArkose						1.67									23.67	0.33		5.33		
P III B.2.2	Rodalben	SubArkose						8.00	1.00					0.33		1.00	12.00	5.33		14.33		
P III B.3	Rodalben	SubArkose						11.67	0.67	0.33								2.67	0.33	12.00		
P V B.1.1	Rodalben	SubArkose						4.33	0.33								0.33	7.33	0.67	5.67		
P VI B.1.1	Rodalben	SubArkose						5.33								0.67		5.33	0.67	7.33		
P XII A.1	Rodalben	SubArkose						13.33	1.33								2.67	1.33		14.33		
P XII B.1	Rodalben	SubArkose						4.67										7.67	0.33	8.67		
P XV B	Rodalben	SubArkose						8.33						1.33				8.00		10.67		
R1 I b	Heidelberg Riesenstein	SubArkose						5.33	0.33			1.33			1.00	0.33	1.33	13.00	0.67	16.33		
R1 II b	Heidelberg Riesenstein	Arkosic Arenite						9.00	2.33			0.67		0.33	0.67		3.67	1.33	0.33	22.44		
R1 V b	Heidelberg Riesenstein	SubArkose						3.37						0.34	0.34	0.34	3.03	12.79	0.34	14.14		
R1 VI b	Heidelberg Riesenstein	SubArkose						3.68	1.34			0.33				0.67	2.01	5.35	0.33	17.61		
R2/1 II b	Heidelberg Riesenstein	SubArkose						3.33	1.00							0.33	7.33	4.67		11.67		
R2/1 IV b	Heidelberg Riesenstein	SubArkose						5.33	2.33			1.00					8.33	2.33	0.33	13.56	0.33	
R2/1 VII b	Heidelberg Riesenstein	SubArkose						2.33							0.33		4.67	14.00	0.67	12.00		
R2/1 X b	Heidelberg Riesenstein	Arkosic Arenite						5.41	0.34								2.03	7.77	0.34	20.83	0.34	
Rk01	Rockenau	SubArkose					5.33	3.67	1.00							0.33	1.00	11.67	0.67	13.33		
Rk02	Rockenau	Arkosic Arenite		0.33		0.33	4.33	6.00	7.00			0.67		0.33	0.33	0.67	2.67	4.33		19.33	0.33	
Rk03.1	Rockenau	SubArkose					1.00	4.33	2.00		1.00					2.00	1.67	10.67		14.33		
Rk04	Rockenau	Arkosic Arenite					8.67	6.00	1.67		1.00					1.33	1.00	2.33		19.33		
Rk05	Rockenau	Lithic Arenite					0.33	2.33	0.67							0.67	1.67	13.00	1.67	11.67		

Sample	Outcrop/Well	Detrital, Extrabasinal - Non-sedimentary Lithoclast	Detrital, Extrabasinal - Sandstone Lithoclast	Detrital, Intrabasinal - Claystone Lithoclast	Detrital, Muscovite	Detrital, Opaque	Detrital, Quartz - Monocrystalline, strained (<5deg.)	Detrital, Quartz - Monocrystalline, unstrained	Detrital, Quartz - Polycrystalline, <4 crystallites	Detrital, Quartz - Polycrystalline, >4 crystallites	Detrital, Rutile	Detrital, Tourmaline	Detrital, Zircon	Matrix, Illitic	Matrix, Terrigenous	Porosity, Fracture	Porosity, Intergranular	Porosity, Secondary
P I B.1	Rodalben	3.00					18.00	22.00	9.00	16.67							8.67	1.00
P I C.1	Rodalben	1.33					22.00	22.33	4.33	11.33							15.67	0.33
P III A.1.3	Rodalben	2.00					18.00	18.00	8.00	19.67							2.00	1.33
P III B.2.2	Rodalben	2.67			0.33		22.00	20.67	1.00	4.33							3.67	3.33
P III B.3	Rodalben	1.67					30.00	17.00	4.33	11.33							6.67	1.33
P V B.1.1	Rodalben	1.33					16.00	20.00	6.00	18.33							16.00	3.67
P VI B.1.1	Rodalben	4.67		1.00			17.67	17.00	7.33	17.33							14.67	1.00
P XII A.1	Rodalben	3.33				1.33	21.67	23.67	3.67	8.33							3.00	2.00
P XII B.1	Rodalben	3.67				0.33	21.33	21.00	4.33	13.67							13.33	1.00
P XV B	Rodalben	1.00					21.00	19.00	3.67	10.00							14.33	2.67
R1 I b	Heidelberg Riesenstein	3.00			0.33		7.33	30.00	3.33	11.00							5.33	
R1 II b	Heidelberg Riesenstein	5.33					12.67	15.89	4.00	15.00							6.33	
R1 V b	Heidelberg Riesenstein	4.04					10.10	29.63	6.40	8.08							7.07	
R1 VI b	Heidelberg Riesenstein	4.35			0.33		11.71	27.87	1.67	15.38							7.36	
R2/1 II b	Heidelberg Riesenstein	10.33		0.67	1.00		12.00	28.67	3.00	8.67					0.33		7.00	
R2/1 IV b	Heidelberg Riesenstein	6.33			1.00		20.67	22.78	2.00	10.67							3.00	
R2/1 VII b	Heidelberg Riesenstein	3.00			0.33		14.00	21.33	6.00	13.33							8.00	
R2/1 X b	Heidelberg Riesenstein	4.39		2.03			19.59	15.32	2.70	10.47	0.34				0.34		7.77	
Rk01	Rockenau	1.33		1.00			9.67	29.00	2.00	11.33							7.33	1.33
Rk02	Rockenau	7.00			0.33		9.67	25.33	1.33	4.67	0.33		0.33				3.67	0.67
Rk03.1	Rockenau	5.00			0.33		11.00	26.67	2.33	7.67							8.00	1.67
Rk04	Rockenau	4.67			0.33		12.33	26.33	0.33	7.67							6.67	0.33
Rk05	Rockenau	1.33		24.33			6.00	25.00	1.00	6.33		0.33					3.67	

Appendix 4 Thin Section Petrography

Sample	Outcrop/Well	Q	F	L	IGV	COPL	CEPL	ICOMPACT	Mean Grain Size (Phi)	Sorting (Folk)	WCP	Rock Colour
C2 Ia	Cleebourg	67.35	24.49	8.16	30.33	15.31	14.11	0.52	1.57	moderately well sorted		n/a
C2/2 IIa	Cleebourg	64.39	24.88	10.73	24.00	22.37	12.68	0.64	2.06	moderately well sorted		n/a
C2/2 III	Cleebourg	65.73	23.47	10.80	19.67	26.56	10.28	0.72	2.03	moderately well sorted		n/a
C2/2 IV d	Cleebourg	65.02	21.97	13.00	20.00	26.25	9.59	0.73	2.38	moderately well sorted		n/a
C2/2 IVb 1a	Cleebourg	70.67	21.78	7.56	17.33	28.63	10.71	0.73	2.38	moderately well sorted		n/a
C2/2 IVe	Cleebourg	66.35	20.38	13.27	18.67	27.46	10.64	0.72	2.29	moderately well sorted		n/a
C2/2 VIb 1c	Cleebourg	63.35	23.53	13.12	15.67	30.04	8.86	0.77	2.55	moderately well sorted		n/a
C2/2A III (2)	Cleebourg	75.46	19.44	5.09	22.00	24.36	10.34	0.70	2.36	moderately well sorted		n/a
C2/A III 2	Cleebourg	74.01	20.26	5.73	19.33	26.86	8.05	0.77	2.19	moderately well sorted		n/a
C5/1 VI	Cleebourg	62.50	22.41	15.09	16.33	29.48	9.87	0.75	2.75	moderately well sorted		n/a
C5/1 Xa	Cleebourg	62.16	22.97	14.86	22.67	23.71	8.90	0.73	1.80	moderately well sorted		n/a
Cl01	Cleebourg	74.55	9.09	16.36	21.48	24.86	10.84	0.70	2.80	moderately well sorted		bleached, red
Cl02	Cleebourg	70.04	10.57	19.38	21.67	24.68	7.78	0.76	2.55	well sorted	5.90	bleached
Cl03	Cleebourg	77.03	16.27	6.70	27.67	18.43	20.94	0.47	2.91	moderately sorted	4.15	beached, brown
Cl04	Cleebourg	74.53	19.34	6.13	25.33	20.98	14.49	0.59	2.06	moderately well sorted		brown, bleached
Cl05	Cleebourg	76.80	15.46	7.73	34.67	9.69	11.74	0.45	1.44	moderately well sorted		bleached, brown
Cl06	Cleebourg	72.65	19.66	7.69	19.00	27.16	9.71	0.74	2.43	moderately sorted	9.25	bleached, brown
Cl08	Cleebourg	68.57	20.48	10.95	18.67	27.46	12.33	0.69	3.30	well sorted		
Cl09	Cleebourg	73.33	15.56	11.11	23.00	23.38	8.17	0.74	2.29	moderately sorted	3.84	bleached, brown
Cl10	Cleebourg	80.60	13.79	5.60	19.67	26.56	12.98	0.67	2.01	moderately well sorted		brown, bleached
Cl14	Cleebourg	69.43	16.16	14.41	18.33	27.76	11.32	0.71	2.72	moderately well sorted	5.24	red, bleached
Cl15	Cleebourg	73.66	17.86	8.48	19.67	26.56	9.06	0.75	2.74	moderately well sorted	6.42	bleached
Cl16	Cleebourg	79.91	13.70	6.39	22.33	24.03	12.66	0.65	3.27	moderately well sorted	5.79	bleached, brown
Cl17	Cleebourg	85.08	9.94	4.97	37.00	6.35	16.55	0.28	1.26	moderately well sorted		bleached, brown
Cl18	Cleebourg	74.88	10.70	14.42	19.00	27.16	10.93	0.71	3.90	moderately well sorted	4.26	bleached, brown, red
Cl19	Cleebourg	67.53	26.80	5.67	22.33	24.03	13.42	0.64	2.92	well sorted		red
Cl20	Cleebourg	65.88	23.70	10.43	16.67	29.20	8.02	0.78	2.37	well sorted		bleached, red
En 01	Well B 1	84.79	14.29	0.92	26.00	20.27	14.35	0.59	2.23	well sorted		bleached

Sample	Outcrop/Well	Q	F	L	IGV	COPL	CEPL	ICOMPACT	Mean Grain Size (Phi)	Sorting (Folk)	WCP	Rock Colour
EnII 01	Well B 2	59.05	26.72	14.22	19.33	26.86	9.02	0.75	1.58	moderately well sorted		bleached
Et01	Ettlingen	86.75	11.11	2.14	20.67	25.63	12.64	0.67	1.72	moderately sorted	5.00	red
Et02	Ettlingen	83.17	11.06	5.77	30.67	14.90	24.39	0.38	1.64	moderately sorted	4.52	red
Et03	Ettlingen	82.98	14.04	2.98	20.67	25.63	11.40	0.69	1.88	moderately sorted	5.20	red
Et04	Ettlingen	78.54	17.17	4.29	21.33	25.00	13.25	0.65	2.03	moderately sorted	4.44	red
Et05	Ettlingen	88.99	9.25	1.76	22.67	23.71	15.00	0.61	2.25	moderately well sorted	6.29	red
Et06	Ettlingen	90.50	7.02	2.48	17.67	28.34	10.99	0.72	1.92	moderately well sorted	6.63	red
Et07	Ettlingen	74.55	19.20	6.25	22.33	24.03	13.17	0.65	2.34	moderately well sorted	8.79	red
Et08	Ettlingen	89.69	7.62	2.69	25.00	21.33	17.83	0.54	1.55	moderately well sorted	3.20	red
HB 1/2	Neustadt a.d.W./Hanbuch	65.84	22.22	11.93	18.33	27.76	8.19	0.77	1.90	moderately well sorted	5.92	bleached, brown
HB 1/3	Neustadt a.d.W./Hanbuch	40.26	42.90	16.83	32.33	12.81	18.60	0.41	2.50	moderately well sorted	8.92	bleached
HB 1/4	Neustadt a.d.W./Hanbuch	66.39	20.11	13.50	22.12	24.25	11.41	0.68	1.97	moderately well sorted	8.40	bleached
HB 1/5	Neustadt a.d.W./Hanbuch	67.57	21.57	10.86	25.50	20.80	11.69	0.64	1.88	moderately well sorted	8.18	bleached, brown
HB 1/6	Neustadt a.d.W./Hanbuch	62.02	31.01	6.98	27.33	18.81	13.26	0.59	2.00	well sorted	7.23	bleached, red
HB 1/7	Neustadt a.d.W./Hanbuch	62.77	29.44	7.79	22.67	23.71	8.14	0.74	1.87	well sorted	7.46	bleached
HB 1/8	Neustadt a.d.W./Hanbuch	75.97	18.03	6.01	22.33	24.03	10.89	0.69	1.92	moderately well sorted	6.68	bleached, red
HB 15.11	Neustadt a.d.W./Hanbuch	62.46	15.92	21.62	26.00	20.27	8.50	0.70	1.63	moderately well sorted	6.20	bleached, brown
HB 4/4	Neustadt a.d.W./Hanbuch	67.14	21.07	11.79	27.27	18.88	13.38	0.59	1.75	moderately well sorted	6.90	bleached, brown
HB 5/2	Neustadt a.d.W./Hanbuch	68.53	21.55	9.91	22.67	23.71	11.70	0.67	1.99	well sorted	6.16	bleached, red, brown
HB 5/3	Neustadt a.d.W./Hanbuch	66.67	22.27	11.07	17.33	28.63	8.80	0.76	1.97	moderately well sorted	6.12	bleached
HB 5/5	Neustadt a.d.W./Hanbuch	75.43	15.52	9.05	22.33	24.03	9.62	0.71	1.73	moderately well sorted		bleached, brown
HB 5/8	Neustadt a.d.W./Hanbuch	74.30	20.48	5.22	17.00	28.92	7.11	0.80	1.75	well sorted		bleached
HB 5/8.5	Neustadt a.d.W./Hanbuch	72.30	18.78	8.92	29.00	16.90	11.91	0.59	1.97	moderately well sorted		bleached, brown, red
HB 5/9	Neustadt a.d.W./Hanbuch	61.39	25.28	13.33	19.67	26.56	8.57	0.76	1.89	well sorted		bleached, brown
HB 6/1	Neustadt a.d.W./Hanbuch	57.73	27.35	14.92	20.44	25.84	7.33	0.78	1.86	well sorted		bleached
HB 6/2	Neustadt a.d.W./Hanbuch	71.84	16.33	11.84	18.33	27.76	7.95	0.78	1.86	well sorted	8.97	bleached
HB 6/3	Neustadt a.d.W./Hanbuch	70.56	18.18	11.26	22.33	24.03	10.38	0.70	2.08	moderately well sorted		bleached, brown, red
HB 6/5	Neustadt a.d.W./Hanbuch	67.73	20.45	11.82	26.00	20.27	7.18	0.74	1.98	moderately well sorted		bleached

Sample	Outcrop/Well	Q	F	L	IGV	COPL	CEPL	ICOMPACT	Mean Grain Size (Phi)	Sorting (Folk)	WCP	Rock Colour
HB 6/6	Neustadt a.d.W./Hanbuch	73.80	16.59	9.61	23.00	23.38	8.94	0.72	1.79	moderately well sorted		bleached
HB 6/7	Neustadt a.d.W./Hanbuch	53.06	13.47	33.47	18.06	28.00	8.91	0.76	1.94	moderately well sorted		bleached
HB 6/8	Neustadt a.d.W./Hanbuch	73.14	17.77	9.09	19.00	27.16	7.53	0.78	1.94	moderately well sorted		bleached
HB 6/9	Neustadt a.d.W./Hanbuch	58.81	31.21	9.99	20.70	25.60	9.29	0.73	2.16	moderately well sorted		bleached, brown
HB G 10	Neustadt a.d.W./Hanbuch	70.22	20.44	9.33	24.00	22.37	7.50	0.75	2.20	moderately well sorted		bleached, brown
HB G 13	Neustadt a.d.W./Hanbuch	70.39	19.74	9.87	21.40	24.93	9.04	0.73	2.10	moderately well sorted		bleached, brown
HB G 15.1	Neustadt a.d.W./Hanbuch	61.97	27.46	10.57	24.00	22.37	9.83	0.69	2.00	moderately sorted		bleached
HB G 2	Neustadt a.d.W./Hanbuch	62.20	24.85	12.95	23.67	22.71	10.31	0.69	1.98	moderately well sorted		bleached
HB G 3.5	Neustadt a.d.W./Hanbuch	63.20	21.21	15.58	22.00	24.36	9.33	0.72	2.19	moderately well sorted		bleached
HB G 5	Neustadt a.d.W./Hanbuch	69.06	20.39	10.55	20.33	25.94	8.64	0.75	1.96	moderately well sorted		bleached, brown
HB G 6	Neustadt a.d.W./Hanbuch	63.32	23.58	13.10	23.33	23.04	10.52	0.69	2.00	moderately well sorted		bleached, brown
HB03	Heidelberg Molkenkur/Bergbahn	58.77	13.74	27.49	25.17	21.16	17.49	0.55	2.15	moderately sorted	3.64	red
Hh01	Hirschhorn	74.38	16.75	8.87	28.67	17.29	17.09	0.50	1.92	moderately well sorted	4.42	red
Hh02	Hirschhorn	73.76	14.85	11.39	29.00	16.90	19.11	0.47	2.08	well sorted		red
Hh03	Hirschhorn	71.43	12.57	16.00	36.00	7.81	30.11	0.21	1.84	moderately well sorted		red
Hh04	Hirschhorn	67.89	18.35	13.76	24.33	22.03	16.89	0.57	2.23	moderately well sorted		red
Hh05	Hirschhorn	73.21	22.97	3.83	25.67	20.63	14.29	0.59	2.12	moderately well sorted		red
HK 1	Heidelberg KK-Verein	65.75	23.74	10.50	26.00	20.27	18.07	0.53	2.48	moderately well sorted	5.60	red
HK 2	Heidelberg KK-Verein	74.19	21.20	4.61	26.67	19.55	15.82	0.55	2.30	moderately sorted	4.96	red
L74 01	Well A 1	89.04	9.59	1.37	24.67	21.68	9.40	0.70	1.37	moderately sorted		bleached
L76 01	Well A 2	73.08	7.69	19.23	28.00	18.06	13.11	0.58	1.28	moderately sorted		bleached, red
L76 02	Well A 2	76.06	17.37	6.57	27.33	18.81	13.80	0.58	2.33	moderately well sorted		bleached, red
Lei 4/11	Leistadt	68.86	21.05	10.09	22.67	23.71	7.37	0.76	1.82	moderately well sorted	4.24	bleached, brown
Lei 4/12	Leistadt	64.81	19.31	15.88	20.33	25.94	7.90	0.77	1.72	well sorted	4.12	bleached, brown
Lei 4/3	Leistadt	66.51	21.75	11.74	25.67	20.63	14.55	0.59	2.01	well sorted	4.50	bleached, brown
Lei 4/4	Leistadt	52.48	20.59	26.94	26.70	19.51	13.00	0.60	1.56	moderately well sorted	3.24	bleached, brown
Lei 4/7	Leistadt	46.61	30.25	23.15	23.33	23.04	11.03	0.68	2.14	moderately well sorted	3.74	bleached, brown
Lei 4/8	Leistadt	54.88	21.11	24.02	24.69	21.66	12.73	0.63	1.96	moderately well sorted	4.16	bleached, brown

Sample	Outcrop/Well	Q	F	L	IGV	COPL	CEPL	ICOMPACT	Mean Grain Size (Phi)	Sorting (Folk)	WCP	Rock Colour
Lei 5/11	Leistadt	70.55	16.89	12.56	22.00	24.36	9.08	0.73	2.09	moderately sorted	3.84	bleached, brown
Lei 5/5	Leistadt	54.39	32.22	13.40	26.00	20.27	17.01	0.54	2.06	moderately well sorted	4.76	bleached, brown
Lei 5/8	Leistadt	54.14	31.49	14.36	34.67	9.69	19.87	0.33	2.70	well sorted	4.78	bleached, brown
Lei 5/9	Leistadt	56.84	27.70	15.46	25.33	20.98	16.33	0.56	2.74	moderately well sorted	5.20	bleached, brown
Ls01	Leistadt	72.69	15.97	11.34	22.12	24.25	3.88	0.86	2.55	moderately sorted	6.72	bleached, brown
Ls02	Leistadt	67.80	19.02	13.17	30.00	15.71	6.74	0.70	2.23	moderately well sorted	4.86	bleached, brown
Ls03	Leistadt	72.31	15.90	11.79	34.00	10.61	11.62	0.48	2.70	moderately sorted	4.48	bleached, brown
Ls04	Leistadt	78.41	11.45	10.13	24.00	22.37	9.83	0.69	1.62	moderately well sorted		bleached, brown
Ls05	Leistadt	77.83	12.22	9.95	25.67	20.63	18.52	0.53	1.57	moderately well sorted		bleached, brown
Ng01	Neckargemünd	70.05	27.65	2.30	26.00	20.27	15.68	0.56	3.00	moderately well sorted	4.72	red
Ng02	Neckargemünd	68.97	24.63	6.40	30.00	15.71	16.30	0.49	2.90	moderately well sorted	4.38	red
Ng03	Neckargemünd	62.38	21.90	15.71	28.33	17.67	20.31	0.47	2.18	moderately well sorted	3.96	red
Ng04	Neckargemünd	68.92	25.23	5.86	23.33	23.04	16.16	0.59	2.88	moderately well sorted	4.14	red
Ng05.1	Neckargemünd	68.78	20.49	10.73	30.67	14.90	20.99	0.42	2.45	moderately well sorted	4.32	red
Ng05.2	Neckargemünd	69.86	20.55	9.59	24.67	21.68	15.66	0.58	2.39	moderately well sorted		bleached, brown, red
OM 3.1	Margaretenschlucht	83.04	12.50	4.46	23.00	23.38	16.60	0.58	1.82	moderately sorted		n/a
OM 4.3	Margaretenschlucht	95.92	2.55	1.53	34.67	9.69	31.31	0.24	0.86	moderately well sorted		n/a
OM 6.2	Margaretenschlucht	78.31	14.81	6.88	37.00	6.35	32.47	0.16	2.13	moderately well sorted	3.34	n/a
OM 7.2	Margaretenschlucht	74.25	11.38	14.37	42.67	-2.91	42.88	-0.07	1.78	moderately well sorted		n/a
OW 1.11	Wolfsschlucht	80.00	10.50	9.50	31.00	14.49	21.09	0.41	1.33	moderately sorted	3.49	n/a
OW 1.5	Wolfsschlucht	70.31	19.65	10.04	22.00	24.36	13.11	0.65	1.98	moderately sorted	3.07	n/a
OW 11.11	Wolfsschlucht	85.98	9.81	4.21	28.33	17.67	21.68	0.45	1.03	moderately well sorted		n/a
OW 2.4 II	Wolfsschlucht	70.40	13.45	16.14	24.33	22.03	15.85	0.58	1.96	moderately sorted	7.10	n/a
OW 6.4	Wolfsschlucht	82.50	15.50	2.00	32.67	12.38	25.12	0.33	1.89	moderately sorted	3.60	n/a
P I B.1	Rodalben	83.12	13.08	3.80	20.00	26.25	8.36	0.76	2.24	moderately sorted	2.93	n/a
P I C.1	Rodalben	89.11	8.91	1.98	32.33	12.81	14.53	0.47	1.74	moderately well sorted	3.63	n/a
P III A.1.3	Rodalben	89.67	7.51	2.82	27.67	18.43	20.94	0.47	0.71	moderately sorted	2.00	n/a
P III B.2.2	Rodalben	73.85	22.05	4.10	31.33	14.08	23.77	0.37	2.28	moderately well sorted	3.71	n/a

Sample	Outcrop/Well	Q	F	L	IGV	COPL	CEPL	ICOMPACT	Mean Grain Size (Phi)	Sorting (Folk)	WCP	Rock Colour
P III B.3	Rodalben	82.10	15.72	2.18	22.33	24.03	11.90	0.67	2.12	moderately well sorted	5.93	n/a
P V B.1.1	Rodalben	89.60	8.42	1.98	29.00	16.90	10.80	0.61	1.70	moderately sorted	3.39	n/a
P VI B.1.1	Rodalben	82.03	10.14	7.83	26.67	19.55	9.65	0.67	2.27	moderately sorted	3.40	n/a
P XII A.1	Rodalben	76.44	19.11	4.44	21.67	24.68	14.06	0.64	3.11	moderately well sorted	3.58	n/a
P XII B.1	Rodalben	83.03	11.93	5.05	26.00	20.27	10.10	0.67	1.82	moderately sorted	3.37	n/a
P XV B	Rodalben	82.14	16.33	1.53	32.00	13.24	15.33	0.46	2.30	moderately well sorted	3.50	n/a
R1 I b	Heidelberg Riesenstein	72.77	23.00	4.23	28.67	17.29	19.30	0.47	1.98	moderately well sorted	4.61	red
R1 II b	Heidelberg Riesenstein	63.13	29.79	7.08	24.67	21.68	14.36	0.60	2.49	well sorted	5.28	red
R1 V b	Heidelberg Riesenstein	74.88	19.53	5.58	27.61	18.50	16.74	0.52	2.36	well sorted	4.10	red
R1 VI b	Heidelberg Riesenstein	72.06	22.41	5.53	21.07	25.25	10.25	0.71	2.40	well sorted	4.90	red
R2/1 II b	Heidelberg Riesenstein	69.78	15.56	14.67	23.67	22.71	12.88	0.64	2.59	moderately well sorted	5.46	red, brown
R2/1 IV b	Heidelberg Riesenstein	73.83	17.84	8.33	22.67	23.71	15.00	0.61	2.51	moderately well sorted	4.74	red
R2/1 VII b	Heidelberg Riesenstein	78.47	17.22	4.31	30.00	15.71	18.54	0.46	1.93	moderately well sorted	4.58	red, brown
R2/1 X b	Heidelberg Riesenstein	63.83	27.65	8.52	23.65	22.73	12.27	0.65	2.34	well sorted	4.34	red
Rk01	Rockenau	76.85	19.70	3.45	31.00	14.49	20.24	0.42	2.20	moderately well sorted	4.34	red, bleached, brown
Rk02	Rockenau	60.89	28.71	10.40	30.67	14.90	22.98	0.39	3.00	moderately well sorted	4.24	red, bleached
Rk03.1	Rockenau	71.14	21.39	7.46	29.67	16.11	18.18	0.47	2.55	moderately well sorted	3.84	bleached, red
Rk04	Rockenau	66.04	27.36	6.60	27.67	18.43	17.13	0.52	3.00	moderately sorted	4.24	red, bleached
Rk05	Rockenau	50.66	15.42	33.92	24.00	22.37	15.79	0.59	2.64	moderately sorted	4.02	red, brown

Appendix 5 Whole Rock Geochemistry Results

Analyte		Wgt	Mo	Cu	Pb	Zn	Ag	Ni	Co	Mn	Fe	As	U	Th	Sr	Cd	Sb	Bi	V	Ca	P	La	Cr	Mg	Ba	Ti	Al	Na	K	W	Zr	Sn	Y	Nb	Be	Sc	S
Unit		KG	PPM	PPM	PPM	PPM	PPM	PPM	PPM	PPM	%	PPM	PPM	PPM	PPM	PPM	PPM	PPM	PPM	%	%	PPM	PPM	%	PPM	%	%	%	%	PPM	PPM	PPM	PPM	PPM	PPM	PPM	%
MDL		0.01	2	2	5	2	0.5	2	2	5	0.01	5	20	2	2	0.4	5	5	2	0.01	0.002	2	2	0.01	1	0.01	0.01	0.01	0.01	4	2	2	2	2	1	1	0.1
Sample	**Outcrop/Well**																																				
C2/2AIII	Cleebourg	0.02	<2	3	6	10	<0.5	6	<2	39	0.66	22	<20	6	85	<0.4	<5	<5	18	0.02	0.017	16	78	0.11	421	0.17	2.70	0.08	2.57	<4	51	<2	6	4	<1	2	<0.1
C2/2IIa	Cleebourg	0.01	<2	8	8	9	<0.5	5	<2	74	1.17	25	<20	5	68	<0.4	<5	<5	12	0.02	0.013	8	18	0.07	392	0.06	2.27	0.08	2.28	<4	30	<2	4	3	<1	1	<0.1
C2/2III	Cleebourg	0.01	<2	3	10	7	<0.5	6	<2	42	0.63	14	<20	5	81	<0.4	<5	<5	15	0.02	0.016	14	91	0.10	452	0.12	2.58	0.07	2.45	<4	44	<2	6	4	<1	2	<0.1
C2/2IVb1a	Cleebourg	0.02	<2	4	10	13	<0.5	7	<2	60	1.16	27	<20	9	108	<0.4	<5	6	29	0.03	0.022	20	24	0.18	452	0.22	3.71	0.08	3.01	<4	87	3	11	6	2	3	<0.1
C2/2IVb1c	Cleebourg	0.02	<2	6	10	11	<0.5	6	<2	52	0.84	18	<20	3	98	<0.4	<5	<5	21	0.03	0.025	13	16	0.16	589	0.11	3.38	0.08	3.07	<4	45	<2	7	4	1	3	<0.1
C2/2IVd	Cleebourg	0.01	<2	4	8	39	<0.5	4	<2	50	0.62	<5	<20	4	93	<0.4	<5	<5	18	0.04	0.017	17	15	0.15	497	0.14	3.19	0.08	2.81	<4	54	3	9	4	1	2	<0.1
C2/2IVe	Cleebourg	0.02	<2	4	10	7	<0.5	4	<2	54	0.87	11	<20	6	87	<0.4	<5	<5	14	0.02	0.012	14	24	0.13	438	0.14	2.75	0.08	2.60	<4	55	3	9	6	<1	2	<0.1
C2Ia	Cleebourg	0.01	<2	4	6	3	<0.5	5	<2	40	0.55	14	<20	5	52	<0.4	<5	<5	5	0.01	0.008	4	73	0.03	321	0.03	1.64	0.06	1.71	<4	18	<2	3	<2	<1	<1	<0.1
C5/1VI	Cleebourg	0.01	<2	4	13	9	<0.5	9	<2	75	1.36	10	<20	8	100	<0.4	<5	<5	24	0.03	0.017	18	139	0.17	505	0.17	3.45	0.07	2.82	<4	66	<2	12	5	1	3	<0.1
C5/1Xa	Cleebourg	0.02	<2	6	9	4	<0.5	3	<2	34	0.53	32	<20	4	57	<0.4	<5	5	7	<0.01	0.010	6	7	0.05	337	0.04	1.81	0.07	1.87	<4	23	<2	8	2	<1	<1	<0.1
Cl20	Cleebourg	0.08	<2	3	8	7	<0.5	5	<2	41	0.79	7	<20	2	105	<0.4	<5	<5	19	0.03	0.019	14	17	0.16	524	0.14	3.63	0.08	2.94	<4	55	<2	9	4	1	3	<0.1
Cl1	Cleebourg	0.11	<2	3	8	12	<0.5	6	2	38	0.72	10	<20	7	127	<0.4	<5	<5	23	0.04	0.036	20	19	0.18	807	0.23	3.65	0.07	2.96	<4	64	<2	11	7	2	3	<0.1
Cl10	Cleebourg	0.02	<2	4	13	31	<0.5	9	3	81	2.91	173	<20	9	75	<0.4	<5	5	16	0.02	0.046	10	24	0.10	378	0.10	2.52	0.07	2.21	<4	53	<2	9	4	2	2	<0.1
Cl14	Cleebourg	0.16	<2	2	8	14	<0.5	6	<2	39	0.88	9	<20	9	150	<0.4	<5	<5	24	0.03	0.041	15	18	0.20	949	0.12	4.06	0.09	3.41	<4	50	<2	9	4	2	3	<0.1
Cl15	Cleebourg	0.07	<2	2	10	10	<0.5	5	<2	43	0.82	17	<20	8	116	<0.4	<5	8	22	0.03	0.016	18	19	0.19	486	0.17	3.90	0.08	3.16	<4	66	<2	9	6	1	3	<0.1
Cl16	Cleebourg	0.05	<2	2	14	5	<0.5	5	2	64	0.71	9	<20	<2	88	<0.4	<5	6	10	0.02	0.011	8	11	0.14	475	0.07	3.35	0.09	2.81	<4	36	<2	7	3	1	2	<0.1
Cl17	Cleebourg	0.05	<2	5	<5	6	<0.5	3	<2	46	0.94	62	<20	2	52	<0.4	<5	<5	6	<0.01	0.012	5	17	0.03	290	0.03	1.46	0.06	1.56	<4	21	<2	5	2	<1	<1	<0.1
Cl18	Cleebourg	0.08	<2	3	9	12	<0.5	6	<2	46	1.12	19	21	10	169	<0.4	<5	6	30	0.04	0.055	27	29	0.22	979	0.27	4.17	0.08	3.09	<4	108	3	16	8	3	4	<0.1
Cl19	Cleebourg	0.04	<2	3	7	10	<0.5	6	<2	65	1.55	11	<20	9	105	<0.4	<5	5	30	0.04	0.014	23	31	0.20	441	0.23	4.06	0.08	3.10	<4	104	<2	18	7	1	4	<0.1
Cl2	Cleebourg	0.10	<2	2	7	11	<0.5	6	<2	42	0.75	13	<20	8	123	<0.4	<5	10	22	0.04	0.039	17	18	0.17	840	0.17	3.58	0.07	2.94	<4	64	<2	14	6	2	3	<0.1
Cl3	Cleebourg	0.06	<2	4	7	47	<0.5	10	<2	48	2.86	98	<20	7	103	<0.4	<5	<5	34	0.03	0.094	13	20	0.16	735	0.11	3.61	0.08	2.89	<4	48	<2	11	4	7	3	<0.1
Cl4	Cleebourg	0.06	<2	2	15	10	<0.5	5	<2	44	1.15	47	<20	6	79	<0.4	<5	9	12	0.02	0.016	10	12	0.10	395	0.10	2.73	0.08	2.40	<4	43	<2	7	4	<1	2	<0.1
Cl5	Cleebourg	0.03	<2	4	<5	4	<0.5	2	<2	72	0.92	9	<20	6	44	<0.4	<5	<5	4	<0.01	0.006	5	18	0.03	302	0.03	1.24	0.06	1.64	<4	19	<2	4	3	<1	<1	<0.1
Cl6	Cleebourg	0.06	<2	3	6	7	<0.5	5	2	42	1.06	56	<20	3	77	<0.4	<5	7	12	<0.01	0.015	10	14	0.10	391	0.08	2.67	0.08	2.41	<4	39	<2	8	4	1	1	<0.1
Cl7	Cleebourg	0.05	<2	3	15	23	<0.5	12	5	66	1.56	42	<20	16	190	<0.4	<5	<5	53	0.02	0.040	28	52	0.33	686	0.45	5.61	0.08	3.55	<4	189	<2	17	13	4	7	<0.1

	Analyte	Wgt	Mo	Cu	Pb	Zn	Ag	Ni	Co	Mn	Fe	As	U	Th	Sr	Cd	Sb	Bi	V	Ca	P	La	Cr	Mg	Ba	Ti	Al	Na	K	W	Zr	Sn	Y	Nb	Be	Sc	S
	Unit	KG	PPM	PPM	PPM	PPM	PPM	PPM	PPM	PPM	%	PPM	PPM	PPM	PPM	PPM	PPM	PPM	PPM	%	%	PPM	PPM	%	PPM	%	%	%	%	PPM	PPM	PPM	PPM	PPM	PPM	PPM	%
	MDL	0.01	2	2	5	2	0.5	2	2	5	0.01	5	20	2	2	0.4	5	5	2	0.01	0.002	2	2	0.01	1	0.01	0.01	0.01	0.01	4	2	2	2	2	1	1	0.1
Sample	**Outcrop/Well**																																				
Cl9	Cleebourg	0.07	<2	2	10	8	<0.5	4	<2	43	0.64	16	<20	7	81	<0.4	<5	8	15	0.01	0.015	10	16	0.10	441	0.09	2.37	0.07	2.23	<4	36	<2	7	4	<1	2	<0.1
Et1	Ettlingen	0.07	<2	3	10	<2	<0.5	4	<2	51	0.96	<5	<20	<2	39	<0.4	<5	<5	6	<0.01	0.009	6	17	0.08	330	0.04	1.82	0.07	1.85	<4	26	<2	3	2	<1	<1	<0.1
Et10	Ettlingen	<0.01	4	49	10	75	<0.5	106	11	440	2.83	30	29	7	54	<0.4	<5	10	126	0.99	0.017	24	119	4.66	657	0.23	6.27	0.78	1.06	<4	136	<2	11	3	2	12	0.1
Et2	Ettlingen	0.06	<2	<2	8	<2	<0.5	3	<2	47	0.78	<5	<20	5	20	<0.4	<5	<5	2	<0.01	0.006	3	17	0.02	189	0.02	0.86	0.03	0.92	<4	13	<2	<2	<2	<1	<1	<0.1
Et3	Ettlingen	0.03	<2	2	11	<2	<0.5	4	<2	62	1.05	5	<20	4	41	<0.4	<5	10	5	0.01	0.018	7	17	0.07	539	0.05	1.65	0.07	1.75	<4	30	<2	4	<2	<1	<1	<0.1
Et4	Ettlingen	0.04	<2	2	8	<2	<0.5	3	<2	54	0.94	<5	<20	3	39	<0.4	<5	6	6	0.01	0.019	7	15	0.06	515	0.05	1.58	0.06	1.64	<4	27	<2	3	<2	<1	<1	<0.1
Et5	Ettlingen	0.06	<2	<2	7	<2	<0.5	3	<2	51	0.93	7	<20	5	37	<0.4	<5	<5	6	0.01	0.011	6	16	0.06	376	0.07	1.58	0.06	1.63	<4	34	<2	3	3	<1	<1	<0.1
Et6	Ettlingen	0.05	<2	<2	11	<2	<0.5	5	<2	85	0.94	<5	<20	3	28	<0.4	<5	<5	5	0.01	0.008	3	17	0.06	303	0.04	1.43	0.05	1.46	<4	21	<2	3	2	<1	<1	<0.1
Et7	Ettlingen	0.04	<2	<2	8	3	<0.5	6	<2	67	1.11	<5	<20	8	50	<0.4	<5	7	12	0.02	0.010	11	19	0.14	385	0.09	2.91	0.08	2.73	<4	40	<2	6	3	<1	1	<0.1
Et8	Ettlingen	0.07	<2	<2	<5	<2	<0.5	3	<2	34	0.57	<5	<20	<2	10	<0.4	<5	<5	<2	<0.01	0.003	2	16	0.01	77	0.01	0.44	0.02	0.47	<4	10	<2	<2	<2	<1	<1	<0.1
Et9	Ettlingen	0.07	<2	3	20	3	<0.5	4	<2	46	0.89	<5	<20	6	52	<0.4	<5	8	10	0.02	0.012	7	13	0.11	421	0.06	2.84	0.09	2.89	<4	26	2	6	4	<1	1	<0.1
HB1	Heidelberg Molkenkur	0.05	<2	6	19	9	<0.5	2	<2	59	0.84	12	<20	<2	69	<0.4	<5	<5	3	0.01	0.021	4	10	0.05	817	0.04	2.15	0.12	2.67	<4	21	<2	4	2	<1	<1	<0.1
HB1/2	Neustadt a.d.W.	<0.01	3	4	5	4	<0.5	11	<2	74	0.97	<5	<20	<2	55	<0.4	<5	<5	11	0.02	0.009	9	200	0.10	435	0.06	2.62	0.08	2.45	<4	36	<2	4	2	<1	1	<0.1
HB1/3	Neustadt a.d.W.	<0.01	4	13	14	5	<0.5	8	2	122	1.38	9	<20	5	76	<0.4	<5	6	12	0.03	0.011	12	26	0.17	570	0.10	3.75	0.10	3.44	<4	54	<2	6	4	<1	2	<0.1
HB1/4	Neustadt a.d.W.	<0.01	3	3	17	32	<0.5	2	<2	87	0.90	<5	<20	<2	51	<0.4	<5	<5	6	0.03	0.008	7	11	0.08	437	0.06	2.25	0.08	2.39	<4	33	<2	3	<2	<1	<1	<0.1
HB1/5	Neustadt a.d.W.	<0.01	4	5	14	76	<0.5	5	<2	149	1.63	<5	<20	3	52	<0.4	<5	<5	6	0.04	0.008	5	18	0.07	461	0.03	2.15	0.08	2.40	<4	24	<2	4	2	<1	<1	<0.1
HB1/6	Neustadt a.d.W.	<0.01	5	5	10	4	<0.5	13	2	118	1.34	<5	<20	<2	51	<0.4	<5	<5	7	0.02	0.008	5	252	0.05	456	0.03	2.10	0.08	2.40	<4	21	<2	3	<2	<1	<1	<0.1
HB1/7	Neustadt a.d.W.	<0.01	3	9	<5	2	<0.5	5	<2	78	0.89	5	<20	3	53	<0.4	<5	<5	6	0.02	0.007	7	19	0.07	427	0.05	2.21	0.08	2.34	<4	29	<2	3	3	<1	<1	<0.1
HB1/8	Neustadt a.d.W.	<0.01	4	5	14	40	<0.5	3	<2	148	1.45	<5	<20	3	44	<0.4	<5	<5	4	0.03	0.008	5	19	0.05	387	0.03	1.71	0.07	2.00	<4	19	<2	2	<2	<1	<1	<0.1
HB15.11	Neustadt a.d.W.	<0.01	4	8	6	7	<0.5	15	2	108	1.24	5	<20	<2	43	<0.4	<5	<5	8	0.01	0.005	4	244	0.03	395	0.03	1.62	0.07	1.96	<4	17	3	3	<2	<1	<1	<0.1
HB3	Neustadt a.d.W.	0.04	<2	9	23	11	<0.5	3	<2	67	0.96	14	<20	4	69	<0.4	<5	<5	3	0.02	0.026	6	13	0.05	816	0.03	2.12	0.11	2.50	<4	19	3	4	<2	<1	<1	<0.1
HB4/4	Neustadt a.d.W.	<0.01	9	18	19	6	<0.5	7	3	173	1.84	6	<20	<2	46	<0.4	<5	<5	6	0.01	0.005	6	20	0.05	400	0.03	1.87	0.07	2.13	<4	21	2	3	3	<1	<1	<0.1
HB5/2	Neustadt a.d.W.	<0.01	<2	4	<5	19	<0.5	3	<2	76	0.82	<5	<20	<2	46	<0.4	<5	<5	7	0.02	0.005	5	10	0.06	432	0.05	1.87	0.08	2.29	<4	27	<2	3	<2	<1	<1	<0.1
HB5/3	Neustadt a.d.W.	<0.01	3	4	<5	5	<0.5	10	<2	78	0.92	<5	<20	<2	52	<0.4	<5	<5	11	0.02	0.006	7	148	0.09	437	0.08	2.34	0.08	2.49	<4	38	<2	8	3	<1	<1	<0.1
HB5/5	Neustadt a.d.W.	<0.01	3	14	6	4	<0.5	6	2	107	1.24	<5	<20	<2	45	<0.4	<5	<5	6	0.01	0.005	5	12	0.05	391	0.03	1.80	0.07	2.02	<4	21	<2	3	2	<1	<1	<0.1

Analyte		Wgt	Mo	Cu	Pb	Zn	Ag	Ni	Co	Mn	Fe	As	U	Th	Sr	Cd	Sb	Bi	V	Ca	P	La	Cr	Mg	Ba	Ti	Al	Na	K	W	Zr	Sn	Y	Nb	Be	Sc	S
Unit		KG	PPM	PPM	PPM	PPM	PPM	PPM	PPM	PPM	%	PPM	PPM	PPM	PPM	PPM	PPM	PPM	PPM	%	%	PPM	PPM	%	PPM	%	%	%	%	PPM	PPM	PPM	PPM	PPM	PPM	PPM	%
MDL		0.01	2	2	5	2	0.5	2	2	5	0.01	5	20	2	2	0.4	5	5	2	0.01	0.002	2	2	0.01	1	0.01	0.01	0.01	0.01	4	2	2	2	2	1	1	0.1
Sample	**Outcrop/Well**																																				
HB5/8	Neustadt a.d.W.	<0.01	2	5	11	6	<0.5	11	<2	85	0.99	<5	<20	<2	52	<0.4	<5	<5	7	0.01	0.005	6	185	0.04	404	0.02	1.69	0.07	2.04	<4	18	<2	3	<2	<1	<1	<0.1
HB5/8.5	Neustadt a.d.W.	<0.01	4	6	<5	30	<0.5	4	<2	141	1.44	5	<20	<2	40	<0.4	<5	<5	6	0.02	0.005	4	11	0.04	360	0.02	1.46	0.06	1.83	<4	17	<2	3	<2	<1	<1	<0.1
HB5/9	Neustadt a.d.W.	<0.01	<2	8	8	3	<0.5	4	<2	65	0.82	<5	<20	<2	49	<0.4	<5	<5	7	0.01	0.005	5	9	0.05	432	0.03	1.92	0.08	2.36	<4	19	<2	3	<2	<1	<1	<0.1
HB6/1	Neustadt a.d.W.	<0.01	3	5	<5	5	<0.5	11	<2	92	1.00	<5	<20	<2	47	<0.4	<5	<5	7	0.01	0.005	5	163	0.05	422	0.04	1.91	0.07	2.23	<4	22	<2	3	<2	<1	<1	<0.1
HB6/10	Neustadt a.d.W.	<0.01	2	4	13	21	<0.5	4	<2	88	0.96	6	<20	<2	57	<0.4	<5	<5	10	0.03	0.008	10	11	0.09	457	0.09	2.40	0.08	2.52	<4	37	<2	4	3	<1	<1	<0.1
HB6/2	Neustadt a.d.W.	<0.01	3	14	<5	4	<0.5	6	<2	115	1.30	<5	<20	<2	46	<0.4	<5	<5	5	0.01	0.004	5	12	0.05	399	0.03	1.86	0.07	2.13	<4	20	<2	3	2	<1	<1	<0.1
HB6/3	Neustadt a.d.W.	<0.01	2	4	7	5	<0.5	11	<2	76	1.01	<5	<20	<2	47	<0.4	<5	<5	10	0.02	0.005	5	156	0.05	401	0.04	1.81	0.07	2.08	<4	23	<2	3	<2	<1	<1	<0.1
HB6/6	Neustadt a.d.W.	<0.01	4	6	<5	19	<0.5	4	<2	138	1.34	<5	<20	<2	49	<0.4	<5	<5	5	0.02	0.005	5	11	0.05	406	0.03	1.87	0.07	2.09	<4	23	<2	3	<2	<1	<1	<0.1
HB6/7	Neustadt a.d.W.	<0.01	<2	8	<5	3	<0.5	4	<2	69	0.77	<5	<20	<2	51	<0.4	<5	<5	6	0.02	0.005	6	8	0.05	436	0.04	1.95	0.08	2.23	<4	23	<2	3	<2	<1	<1	<0.1
HB6/8	Neustadt a.d.W.	<0.01	3	4	<5	4	<0.5	10	<2	86	0.97	<5	<20	<2	53	<0.4	<5	<5	8	0.02	0.006	6	157	0.06	425	0.04	1.97	0.07	2.15	<4	26	<2	20	2	<1	<1	<0.1
HB6/9	Neustadt a.d.W.	<0.01	<2	3	9	11	<0.5	4	4	93	0.79	<5	<20	<2	58	<0.4	<5	<5	8	0.02	0.007	9	9	0.08	467	0.06	2.34	0.08	2.49	<4	39	3	4	2	<1	<1	<0.1
HBG1.3	Neustadt a.d.W.	<0.01	3	12	<5	5	<0.5	6	2	103	1.20	<5	<20	<2	57	<0.4	<5	<5	8	0.01	0.008	8	13	0.07	467	0.07	2.40	0.08	2.49	<4	33	<2	4	3	<1	<1	<0.1
HBG1.5.1	Neustadt a.d.W.	<0.01	<2	4	<5	5	<0.5	9	<2	67	0.78	<5	<20	<2	63	<0.4	<5	<5	10	0.02	0.009	7	118	0.08	523	0.05	2.66	0.10	2.88	<4	25	<2	5	<2	<1	<1	<0.1
HBG2	Neustadt a.d.W.	<0.01	3	5	<5	17	<0.5	4	<2	117	1.16	5	<20	<2	57	<0.4	<5	<5	7	0.03	0.008	7	11	0.09	488	0.05	2.53	0.09	2.61	<4	26	<2	4	2	<1	<1	<0.1
HBG3.5	Neustadt a.d.W.	<0.01	<2	11	<5	6	<0.5	5	<2	81	0.96	6	<20	2	58	<0.4	<5	<5	10	0.02	0.009	13	15	0.08	485	0.17	2.42	0.09	2.55	<4	70	4	5	5	<1	<1	<0.1
HBG5	Neustadt a.d.W.	<0.01	4	4	<5	6	<0.5	11	<2	92	1.06	<5	<20	<2	57	<0.4	<5	<5	9	0.02	0.007	6	170	0.06	496	0.04	2.31	0.09	2.52	<4	23	<2	4	<2	<1	<1	<0.1
HBGb	Neustadt a.d.W.	<0.01	<2	3	<5	9	<0.5	3	<2	68	0.73	<5	<20	<2	57	<0.4	<5	<5	7	0.02	0.007	6	8	0.06	477	0.05	2.27	0.09	2.44	<4	26	<2	3	2	<1	<1	<0.1
Hh1	Hirschhorn	0.01	2	5	36	27	<0.5	12	3	95	1.22	7	21	<2	63	<0.4	<5	<5	5	0.02	0.018	4	145	0.04	424	0.03	2.02	0.08	1.93	<4	20	<2	5	3	<1	<1	<0.1
Hh2	Hirschhorn	0.04	<2	5	23	20	<0.5	5	<2	63	1.05	<5	<20	<2	60	<0.4	5	5	7	0.02	0.012	4	9	0.07	403	0.04	2.58	0.08	2.02	4	23	<2	5	2	<1	<1	<0.1
Hh3	Hirschhorn	0.04	<2	6	17	9	<0.5	3	<2	63	0.98	<5	<20	3	46	<0.4	<5	11	3	0.01	0.009	3	8	0.03	348	0.02	1.85	0.07	1.59	<4	15	<2	4	<2	<1	<1	<0.1
Hh4	Hirschhorn	0.03	<2	5	22	12	<0.5	7	<2	80	1.21	<5	<20	3	86	<0.4	<5	15	10	0.02	0.016	12	14	0.17	504	0.07	3.69	0.09	2.84	<4	34	<2	8	4	1	1	<0.1
Hh5	Hirschhorn	0.03	<2	5	17	7	<0.5	5	<2	75	1.22	<5	<20	2	65	<0.4	<5	10	9	0.02	0.014	8	13	0.08	432	0.09	2.58	0.08	2.04	<4	38	<2	7	4	<1	<1	<0.1
HK1	Heidelberg Kammerf. Br.	0.08	<2	5	15	5	<0.5	3	<2	64	0.84	18	<20	<2	55	<0.4	<5	<5	5	0.02	0.012	5	10	0.07	489	0.04	2.24	0.10	2.74	<4	23	3	3	2	<1	<1	<0.1
HK2	Heidelberg Kammerf. Br.	0.10	<2	13	18	11	<0.5	7	<2	109	0.93	15	<20	<2	60	<0.4	<5	<5	5	0.02	0.010	6	10	0.06	542	0.04	2.26	0.11	2.57	<4	24	<2	4	<2	<1	<1	<0.1
Lei4/11	Leistadt	<0.01	3	14	18	12	<0.5	5	2	117	1.31	6	<20	<2	43	<0.4	<5	<5	4	0.02	0.010	5	15	0.04	424	0.03	1.63	0.07	1.91	<4	21	<2	6	2	<1	<1	<0.1

Analyte		Wgt	Mo	Cu	Pb	Zn	Ag	Ni	Co	Mn	Fe	As	U	Th	Sr	Cd	Sb	Bi	V	Ca	P	La	Cr	Mg	Ba	Ti	Al	Na	K	W	Zr	Sn	Y	Nb	Be	Sc	S
Unit		KG	PPM	PPM	PPM	PPM	PPM	PPM	PPM	PPM	%	PPM	PPM	PPM	PPM	PPM	PPM	PPM	PPM	%	%	PPM	PPM	%	PPM	%	%	%	%	PPM	PPM	PPM	PPM	PPM	PPM	PPM	%
MDL		0.01	2	2	5	2	0.5	2	2	5	0.01	5	20	2	2	0.4	5	5	2	0.01	0.002	2	2	0.01	1	0.01	0.01	0.01	0.01	4	2	2	2	2	1	1	0.1
Sample	**Outcrop/Well**																																				
Lei4/12	Leistadt	<0.01	3	9	11	14	<0.5	9	<2	82	0.97	13	<20	<2	43	<0.4	<5	<5	5	0.02	0.009	4	144	0.04	423	0.03	1.58	0.07	1.86	<4	20	<2	5	<2	<1	<1	<0.1
Lei4/3	Leistadt	<0.01	3	13	9	11	<0.5	6	<2	122	1.31	6	<20	<2	57	<0.4	<5	<5	7	0.02	0.013	8	15	0.08	539	0.06	2.32	0.09	2.47	<4	28	<2	6	3	<1	<1	<0.1
Lei4/4	Leistadt	<0.01	3	5	13	17	<0.5	12	<2	131	1.17	15	<20	<2	102	<0.4	<5	<5	6	0.02	0.014	5	178	0.06	2705	0.03	1.97	0.08	2.17	<4	24	<2	8	<2	<1	<1	<0.1
Lei4/7	Leistadt	<0.01	3	12	12	10	<0.5	6	<2	103	1.25	9	<20	<2	50	<0.4	<5	<5	5	0.02	0.012	6	14	0.06	481	0.04	2.05	0.08	2.20	<4	24	<2	8	3	<1	<1	<0.1
Lei4/8	Leistadt	<0.01	5	7	13	18	<0.5	15	3	127	1.45	13	21	<2	77	<0.4	<5	<5	10	0.03	0.016	12	267	0.09	544	0.06	2.23	0.07	2.24	<4	30	<2	8	2	<1	1	<0.1
Lei5/11	Leistadt	<0.01	3	5	22	20	<0.5	9	<2	89	0.96	5	<20	<2	52	<0.4	<5	<5	6	0.02	0.010	8	157	0.06	498	0.05	2.04	0.08	2.24	<4	26	2	4	<2	<1	<1	<0.1
Lei5/5	Leistadt	<0.01	3	15	21	12	<0.5	7	<2	107	1.64	14	<20	<2	69	<0.4	<5	11	11	0.03	0.013	11	19	0.11	514	0.08	2.98	0.09	2.89	<4	40	<2	7	4	<1	2	<0.1
Lei5/8	Leistadt	<0.01	4	5	18	14	<0.5	13	<2	84	1.49	11	<20	3	87	<0.4	<5	<5	18	0.04	0.020	14	148	0.17	3424	0.11	3.55	0.09	3.09	<4	49	2	9	4	2	2	<0.1
Lei5/9	Leistadt	<0.01	3	11	17	13	<0.5	9	<2	101	1.74	10	<20	5	92	<0.4	<5	<5	22	0.04	0.021	19	24	0.20	1477	0.17	3.85	0.09	3.00	<4	69	3	11	6	2	3	<0.1
Ls1	Leistadt	0.04	<2	4	<5	5	<0.5	6	<2	60	1.29	13	<20	3	48	<0.4	<5	9	8	0.02	0.015	6	13	0.05	467	0.04	1.99	0.07	2.10	<4	26	<2	7	<2	<1	1	<0.1
Ls10	Leistadt	0.05	<2	5	21	4	<0.5	5	<2	90	1.25	7	<20	<2	99	<0.4	5	<5	7	0.02	0.012	7	12	0.07	2703	0.04	2.32	0.08	2.46	<4	26	<2	7	3	<1	<1	<0.1
Ls11	Leistadt	0.05	<2	5	13	4	<0.5	4	<2	70	1.07	6	<20	3	63	<0.4	<5	9	6	0.02	0.011	7	10	0.06	911	0.06	2.06	0.07	2.18	<4	29	<2	7	3	<1	<1	<0.1
Ls12	Leistadt	0.04	<2	5	16	19	<0.5	9	4	79	1.69	19	<20	3	100	<0.4	7	<5	23	0.04	0.018	18	28	0.23	812	0.18	4.49	0.10	3.07	4	70	<2	11	6	2	4	<0.1
Ls13	Leistadt	0.06	<2	5	13	8	<0.5	4	<2	55	1.01	10	<20	<2	63	<0.4	6	<5	9	0.02	0.013	8	14	0.07	646	0.06	2.35	0.08	2.21	<4	35	<2	7	2	<1	1	<0.1
Ls2	Leistadt	0.06	<2	5	11	4	<0.5	4	<2	52	0.79	7	<20	<2	58	<0.4	<5	<5	9	0.03	0.011	7	12	0.09	524	0.05	2.60	0.08	2.66	<4	31	<2	6	3	<1	1	<0.1
Ls3	Leistadt	0.07	<2	4	11	3	<0.5	2	<2	115	0.85	8	<20	3	60	<0.4	<5	6	9	0.02	0.011	7	10	0.07	542	0.06	2.38	0.08	2.61	<4	31	<2	6	<2	<1	1	<0.1
Ls4	Leistadt	0.07	6	3	13	8	<0.5	5	<2	88	5.81	250	<20	2	1825	<0.4	9	<5	17	0.03	0.043	2	14	0.05	809	0.03	1.69	0.06	1.44	<4	28	<2	9	<2	3	2	0.1
Ls5	Leistadt	0.05	<2	4	14	3	<0.5	4	<2	55	1.38	17	<20	<2	1312	<0.4	<5	5	3	<0.01	0.012	<2	10	0.03	2048	0.03	0.92	0.04	1.03	<4	15	<2	4	<2	<1	<1	<0.1
Ls7	Leistadt	0.08	<2	4	18	6	<0.5	8	<2	97	1.97	14	<20	<2	1659	<0.4	<5	<5	12	0.03	0.017	7	17	0.12	1140	0.08	2.63	0.08	2.30	<4	35	<2	7	3	1	2	<0.1
Ls9	Leistadt	0.02	16	<2	20	33	<0.5	12	5	470	26.45	268	<20	<2	2209	<0.4	7	8	27	0.04	0.091	2	25	0.04	443	0.01	0.77	0.02	0.45	<4	21	<2	15	<2	18	5	0.1
Ng1	Neckargemünd	0.07	<2	4	13	14	<0.5	4	<2	73	1.06	15	<20	<2	76	<0.4	<5	8	8	0.06	0.034	7	11	0.12	541	0.06	2.93	0.12	3.20	<4	28	<2	6	2	1	<1	<0.1
Ng2	Neckargemünd	0.03	<2	13	26	18	<0.5	6	<2	94	1.15	16	<20	3	76	<0.4	6	6	8	0.08	0.040	9	14	0.15	562	0.07	2.76	0.13	3.32	<4	31	<2	7	3	2	<1	<0.1
Ng3	Neckargemünd	0.05	<2	4	11	7	<0.5	3	<2	61	0.89	6	<20	<2	56	<0.4	5	6	4	0.05	0.025	3	9	0.03	443	0.03	1.98	0.10	2.23	<4	18	<2	5	2	<1	<1	<0.1
Ng4	Neckargemünd	0.05	<2	4	20	7	<0.5	3	<2	60	0.94	16	<20	<2	60	<0.4	<5	<5	8	0.06	0.031	6	12	0.08	463	0.05	2.63	0.10	2.87	<4	26	<2	5	<2	<1	<1	<0.1
Ng5	Neckargemünd	<0.01	3	4	21	51	<0.5	10	3	90	1.13	43	<20	3	74	<0.4	<5	7	14	0.03	0.014	9	118	0.17	579	0.08	3.64	0.12	3.36	<4	46	6	6	3	1	2	<0.1

Analyte		Wgt	Mo	Cu	Pb	Zn	Ag	Ni	Co	Mn	Fe	As	U	Th	Sr	Cd	Sb	Bi	V	Ca	P	La	Cr	Mg	Ba	Ti	Al	Na	K	W	Zr	Sn	Y	Nb	Be	Sc	S
Unit		KG	PPM	PPM	PPM	PPM	PPM	PPM	PPM	PPM	%	PPM	PPM	PPM	PPM	PPM	PPM	PPM	PPM	%	%	PPM	PPM	%	PPM	%	%	%	%	PPM	PPM	PPM	PPM	PPM	PPM	PPM	%
MDL		0.01	2	2	5	2	0.5	2	2	5	0.01	5	20	2	2	0.4	5	5	2	0.01	0.002	2	2	0.01	1	0.01	0.01	0.01	0.01	4	2	2	2	2	1	1	0.1
Sample	**Outcrop/Well**																																				
OM1.1	Margaretenschlucht	0.09	<2	4	19	3	<0.5	3	<2	58	1.09	8	<20	<2	71	<0.4	<5	<5	6	0.04	0.024	5	10	0.09	453	0.05	2.27	0.10	2.63	<4	25	3	4	3	<1	<1	<0.1
OM10.1	Margaretenschlucht	0.10	<2	4	12	12	<0.5	7	4	149	1.31	6	<20	11	102	<0.4	<5	<5	19	0.03	0.026	28	21	0.13	323	0.20	2.63	0.07	2.70	<4	80	2	9	5	<1	2	<0.1
OM10.2	Margaretenschlucht	0.08	<2	3	5	4	<0.5	2	<2	36	0.56	<5	<20	<2	150	<0.4	<5	<5	3	0.03	0.021	6	9	0.03	91	0.06	0.62	0.02	0.61	<4	27	<2	5	3	<1	<1	<0.1
OM2.2	Margaretenschlucht	0.14	<2	3	6	25	<0.5	12	6	223	1.76	17	<20	4	53	<0.4	<5	<5	9	0.24	0.030	7	15	0.18	394	0.11	2.27	0.08	2.33	<4	52	5	6	4	<1	1	<0.1
OM2.5	Margaretenschlucht	0.15	<2	4	8	12	<0.5	5	3	115	0.92	7	<20	<2	34	<0.4	<5	<5	4	0.03	0.013	3	11	0.05	280	0.04	1.34	0.06	1.51	<4	27	3	3	<2	<1	<1	<0.1
OM4.3	Margaretenschlucht	0.12	<2	3	<5	12	<0.5	7	3	393	1.11	19	<20	<2	40	<0.4	<5	<5	9	2.56	0.035	7	12	1.02	94	0.03	0.91	0.02	0.71	<4	15	<2	8	3	<1	2	<0.1
OM4.4	Margaretenschlucht	0.13	<2	4	13	3	<0.5	3	<2	55	0.75	10	<20	<2	42	<0.4	<5	<5	4	0.06	0.013	4	10	0.11	252	0.02	1.34	0.06	1.53	<4	14	4	2	<2	<1	<1	<0.1
OM4.4b	Margaretenschlucht	0.13	<2	4	12	8	<0.5	5	<2	72	1.19	17	<20	<2	79	<0.4	<5	<5	10	0.15	0.036	8	14	0.21	431	0.09	3.42	0.09	3.13	<4	42	5	6	4	<1	1	<0.1
OM5.2	Margaretenschlucht	0.10	<2	4	10	16	<0.5	10	3	109	2.37	57	<20	17	104	<0.4	<5	5	35	0.22	0.107	37	32	0.27	405	0.34	4.27	0.08	3.13	<4	136	6	15	10	1	5	<0.1
OM5.7	Margaretenschlucht	0.08	<2	4	7	6	<0.5	6	3	98	0.87	11	<20	2	40	<0.4	<5	<5	7	0.08	0.028	6	11	0.06	201	0.05	1.35	0.04	1.39	<4	21	<2	5	<2	<1	<1	<0.1
OM5.8	Margaretenschlucht	0.07	<2	5	9	14	<0.5	5	2	81	1.10	14	<20	<2	48	<0.4	<5	<5	14	0.08	0.027	6	13	0.11	259	0.06	1.76	0.07	1.77	<4	22	2	5	3	<1	1	<0.1
OM5.9	Margaretenschlucht	0.09	<2	3	13	8	<0.5	4	2	84	0.92	13	<20	3	56	<0.4	<5	5	8	0.06	0.028	7	13	0.07	260	0.06	1.66	0.06	1.75	<4	23	<2	4	<2	<1	<1	<0.1
OM6.1	Margaretenschlucht	0.09	<2	3	7	9	<0.5	7	3	113	1.23	19	<20	<2	74	<0.4	<5	<5	18	0.11	0.051	11	16	0.17	285	0.08	2.46	0.07	2.25	<4	28	4	7	3	<1	2	<0.1
OM6.8	Margaretenschlucht	0.05	<2	4	8	13	<0.5	7	3	111	1.33	13	<20	<2	56	<0.4	<5	<5	13	0.08	0.028	8	15	0.11	322	0.07	2.18	0.07	2.21	<4	27	3	5	4	<1	2	<0.1
OM7.2	Margaretenschlucht	0.10	<2	2	9	7	<0.5	3	3	331	0.76	13	<20	<2	57	<0.4	<5	<5	8	1.57	0.031	7	11	0.86	257	0.03	1.61	0.06	1.74	<4	15	3	7	<2	<1	1	<0.1
OM8.1	Margaretenschlucht	0.07	<2	6	15	55	<0.5	34	11	141	4.07	58	<20	7	138	<0.4	10	11	94	0.17	0.077	18	71	0.88	438	0.38	7.25	0.11	4.48	<4	103	4	13	13	6	12	<0.1
OM8.2	Margaretenschlucht	0.09	<2	5	9	12	<0.5	7	4	739	1.25	20	20	<2	100	<0.4	<5	<5	19	3.30	0.061	17	16	1.55	321	0.12	2.40	0.07	2.26	<4	38	4	11	4	<1	3	<0.1
OM8.3	Margaretenschlucht	0.07	<2	3	17	14	<0.5	7	2	259	1.35	8	20	4	63	<0.4	6	7	22	0.91	0.075	10	19	0.61	419	0.08	3.53	0.09	3.12	<4	37	5	9	2	<1	2	<0.1
OM8.4	Margaretenschlucht	0.15	<2	4	14	8	<0.5	5	<2	55	0.94	13	<20	2	59	<0.4	<5	<5	13	0.05	0.021	11	13	0.12	349	0.08	2.21	0.08	2.47	<4	28	2	6	3	<1	1	<0.1
OM9.5	Margaretenschlucht	0.07	<2	4	10	12	<0.5	8	3	89	1.64	21	<20	5	94	<0.4	<5	<5	29	0.15	0.038	18	22	0.36	380	0.19	3.25	0.10	3.04	<4	55	3	7	7	1	3	<0.1
OM9.6a	Margaretenschlucht	0.17	<2	2	10	6	<0.5	7	3	245	0.72	<5	<20	3	80	<0.4	<5	<5	13	0.65	0.027	6	10	0.45	352	0.04	2.55	0.08	2.76	<4	20	<2	5	<2	<1	1	<0.1
OM9.7e	Margaretenschlucht	0.11	<2	4	14	11	<0.5	6	<2	45	2.71	15	<20	4	71	<0.4	<5	<5	34	0.07	0.036	19	22	0.18	401	0.18	3.40	0.09	3.24	<4	57	5	9	7	<1	3	<0.1
OW1.2	Wolfsschlucht	0.07	<2	3	18	23	<0.5	15	4	86	1.66	32	<20	<2	66	<0.4	<5	7	12	0.03	0.027	3	12	0.14	647	0.05	3.02	0.11	3.07	<4	28	<2	4	<2	1	2	<0.1
OW1.4	Wolfsschlucht	0.09	<2	4	17	8	<0.5	7	<2	112	0.98	11	<20	<2	65	<0.4	6	<5	7	0.03	0.020	5	12	0.08	502	0.05	2.20	0.09	2.52	<4	23	<2	4	2	<1	2	<0.1
OW10	Wolfsschlucht	<0.01	4	53	15	82	<0.5	114	13	474	3.09	30	<20	8	60	0.6	<5	<5	134	1.09	0.018	33	126	5.20	807	0.25	7.19	0.87	1.32	<4	144	3	14	3	2	15	0.1

	Analyte	Wgt	Mo	Cu	Pb	Zn	Ag	Ni	Co	Mn	Fe	As	U	Th	Sr	Cd	Sb	Bi	V	Ca	P	La	Cr	Mg	Ba	Ti	Al	Na	K	W	Zr	Sn	Y	Nb	Be	Sc	S
	Unit	KG	PPM	PPM	PPM	PPM	PPM	PPM	PPM	PPM	%	PPM	PPM	PPM	PPM	PPM	PPM	PPM	PPM	%	%	PPM	PPM	%	PPM	%	%	%	%	PPM	PPM	PPM	PPM	PPM	PPM	PPM	%
	MDL	0.01	2	2	5	2	0.5	2	2	5	0.01	5	20	2	2	0.4	5	5	2	0.01	0.002	2	2	0.01	1	0.01	0.01	0.01	0.01	4	2	2	2	2	1	1	0.1
Sample	**Outcrop/Well**																																				
OW10.1	Wolfsschlucht	0.14	<2	3	13	5	<0.5	4	<2	71	0.79	6	<20	3	66	<0.4	<5	<5	8	0.04	0.035	7	13	0.09	421	0.08	2.18	0.08	2.40	<4	43	<2	5	2	<1	1	<0.1
OW11.12	Wolfsschlucht	0.04	<2	4	13	3	<0.5	3	<2	69	0.95	5	<20	3	46	<0.4	<5	<5	3	<0.01	0.008	3	9	0.03	366	0.03	1.49	0.08	1.80	<4	19	2	2	<2	<1	<1	<0.1
OW11.13a	Wolfsschlucht	0.08	<2	3	<5	<2	<0.5	<2	<2	41	0.66	<5	<20	<2	28	<0.4	<5	<5	<2	<0.01	0.005	<2	9	0.01	222	0.01	0.84	0.05	1.03	<4	11	<2	<2	<2	<1	<1	<0.1
OW11.14	Wolfsschlucht	0.04	<2	4	11	5	<0.5	4	<2	62	1.00	14	<20	<2	57	<0.4	<5	<5	5	0.01	0.011	7	11	0.05	360	0.05	1.64	0.07	1.88	<4	27	2	3	2	<1	<1	<0.1
OW11.15a	Wolfsschlucht	0.07	<2	4	10	3	<0.5	2	<2	76	1.04	<5	<20	<2	57	<0.4	<5	6	5	0.01	0.014	3	8	0.05	534	0.03	1.96	0.10	2.38	<4	21	<2	2	<2	<1	<1	<0.1
OW2.4	Wolfsschlucht	0.04	<2	4	16	10	<0.5	8	3	164	1.28	11	<20	<2	51	<0.4	<5	<5	11	0.03	0.021	5	10	0.17	445	0.06	2.57	0.08	2.34	<4	41	<2	5	3	<1	1	<0.1
OW3.2	Wolfsschlucht	0.15	<2	2	13	4	<0.5	4	<2	57	0.92	8	<20	3	65	<0.4	<5	<5	8	0.06	0.031	5	9	0.17	505	0.07	3.27	0.10	3.06	<4	31	<2	4	3	<1	1	<0.1
OW3.3	Wolfsschlucht	0.06	<2	4	10	8	<0.5	8	<2	55	1.01	23	<20	<2	65	<0.4	7	<5	7	0.04	0.022	4	12	0.08	506	0.05	2.29	0.10	2.71	<4	23	<2	4	<2	<1	1	<0.1
OW4.3	Wolfsschlucht	0.13	<2	3	15	3	<0.5	5	<2	85	0.94	6	<20	4	63	<0.4	<5	6	4	0.05	0.025	4	8	0.08	606	0.03	2.23	0.11	2.48	<4	19	<2	4	<2	<1	<1	<0.1
OW4.3a	Wolfsschlucht	0.17	<2	2	25	3	<0.5	4	<2	119	0.78	9	<20	<2	70	<0.4	<5	<5	5	0.06	0.026	3	9	0.11	665	0.03	2.73	0.14	3.01	<4	21	<2	4	<2	<1	1	<0.1
OW4.5	Wolfsschlucht	0.09	<2	4	14	5	<0.5	9	2	93	1.28	11	<20	<2	66	<0.4	<5	<5	12	0.10	0.040	7	14	0.18	506	0.08	3.13	0.10	2.88	<4	41	<2	6	4	<1	2	<0.1
OW4.7	Wolfsschlucht	0.06	<2	6	29	11	<0.5	12	3	697	1.28	17	<20	<2	54	0.4	<5	<5	5	0.05	0.025	3	11	0.08	625	0.02	2.13	0.11	2.39	<4	18	<2	5	<2	<1	3	<0.1
OW5.1	Wolfsschlucht	0.17	<2	3	15	5	<0.5	4	<2	79	1.07	6	<20	3	58	<0.4	6	<5	9	0.50	0.025	4	11	0.17	522	0.04	3.18	0.10	2.95	<4	24	3	4	2	<1	1	<0.1
OW5.1b	Wolfsschlucht	0.06	<2	3	8	6	<0.5	3	<2	57	0.91	10	<20	<2	52	<0.4	<5	<5	6	0.02	0.018	6	12	0.07	463	0.04	2.12	0.08	2.37	<4	24	3	4	3	<1	1	<0.1
OW6.2	Wolfsschlucht	0.49	<2	4	28	44	<0.5	68	11	199	4.72	212	<20	6	167	0.5	8	9	114	0.18	0.071	12	85	0.91	504	0.41	8.20	0.12	4.07	<4	93	5	10	13	8	15	<0.1
OW6.4	Wolfsschlucht	0.06	<2	4	12	<2	<0.5	3	<2	59	0.92	<5	<20	<2	39	<0.4	<5	<5	<2	0.02	0.014	3	9	0.03	348	0.03	1.40	0.07	1.58	<4	20	<2	3	2	<1	<1	<0.1
OW7.1	Wolfsschlucht	0.12	<2	3	17	4	<0.5	3	<2	56	0.80	<5	<20	<2	63	<0.4	<5	<5	5	0.01	0.010	4	9	0.11	488	0.03	2.43	0.10	2.64	<4	21	4	2	3	<1	<1	<0.1
OW7.4	Wolfsschlucht	0.14	<2	3	11	3	<0.5	2	<2	39	0.67	<5	<20	<2	52	<0.4	<5	<5	2	<0.01	0.009	2	8	0.06	1398	0.01	1.53	0.07	1.68	<4	14	<2	<2	<2	<1	<1	<0.1
OW8.1	Wolfsschlucht	0.10	<2	3	7	4	<0.5	2	<2	69	0.84	<5	<20	<2	50	<0.4	<5	<5	5	<0.01	0.009	4	10	0.07	378	0.04	1.75	0.08	1.82	<4	34	4	3	<2	<1	<1	<0.1
OW9.1	Wolfsschlucht	0.14	<2	3	7	4	<0.5	3	<2	72	0.90	6	<20	2	44	<0.4	5	<5	4	0.01	0.011	3	7	0.07	323	0.03	1.54	0.06	1.58	<4	20	3	3	<2	<1	<1	<0.1
P1A	Rodalben/Pirmasens	0.09	<2	4	22	79	<0.5	7	2	90	1.10	7	<20	3	75	<0.4	<5	<5	13	0.02	0.027	8	15	0.10	447	0.07	2.23	0.12	2.35	<4	50	<2	7	3	1	1	<0.1
P1B.2	Rodalben/Pirmasens	0.10	<2	5	14	16	<0.5	3	<2	68	0.58	<5	<20	<2	63	<0.4	<5	<5	3	0.01	0.011	5	9	0.02	397	0.04	1.47	0.08	1.80	<4	31	<2	3	2	<1	<1	<0.1
P1C.1	Rodalben/Pirmasens	0.08	<2	4	13	61	<0.5	6	<2	280	1.13	<5	<20	<2	34	<0.4	<5	<5	7	0.01	0.032	5	15	0.04	215	0.04	1.23	0.04	1.02	<4	24	2	3	2	<1	<1	<0.1
P1C.2	Rodalben/Pirmasens	0.09	<2	5	16	66	<0.5	5	<2	93	1.02	<5	<20	<2	57	<0.4	<5	<5	6	0.01	0.022	5	15	0.03	412	0.04	1.64	0.09	2.00	<4	25	2	3	2	<1	<1	<0.1
P1D.1	Rodalben/Pirmasens	0.09	<2	5	10	40	<0.5	6	3	269	1.26	<5	<20	2	52	<0.4	<5	<5	14	0.04	0.045	5	22	0.06	215	0.04	1.26	0.04	0.94	<4	29	<2	4	<2	<1	<1	<0.1

Analyte		Wgt	Mo	Cu	Pb	Zn	Ag	Ni	Co	Mn	Fe	As	U	Th	Sr	Cd	Sb	Bi	V	Ca	P	La	Cr	Mg	Ba	Ti	Al	Na	K	W	Zr	Sn	Y	Nb	Be	Sc	S
Unit		KG	PPM	PPM	PPM	PPM	PPM	PPM	PPM	PPM	%	PPM	PPM	PPM	PPM	PPM	PPM	PPM	PPM	%	%	PPM	PPM	%	PPM	%	%	%	%	PPM	PPM	PPM	PPM	PPM	PPM	PPM	%
MDL		0.01	2	2	5	2	0.5	2	2	5	0.01	5	20	2	2	0.4	5	5	2	0.01	0.002	2	2	0.01	1	0.01	0.01	0.01	0.01	4	2	2	2	2	1	1	0.1
Sample	**Outcrop/Well**																																				
P1E.1	Rodalben/Pirmasens	0.05	<2	4	58	20	<0.5	5	<2	236	1.22	<5	21	<2	83	<0.4	<5	<5	10	0.02	0.021	7	13	0.05	383	0.05	1.93	0.08	2.17	<4	26	<2	4	2	<1	<1	<0.1
P1E.2	Rodalben/Pirmasens	0.09	<2	4	14	23	<0.5	3	<2	157	0.89	<5	<20	<2	54	<0.4	<5	<5	7	0.02	0.041	5	10	0.03	315	0.02	1.38	0.06	1.52	<4	25	2	5	<2	<1	<1	<0.1
PIA.1.1	Rodalben/Pirmasens	0.09	<2	4	26	65	<0.5	8	<2	88	1.10	7	29	<2	79	<0.4	<5	<5	15	0.02	0.025	8	14	0.11	458	0.07	2.33	0.12	2.44	<4	44	3	7	<2	1	1	<0.1
PIB.1	Rodalben/Pirmasens	0.03	<2	4	12	10	<0.5	4	<2	79	0.93	<5	<20	<2	33	<0.4	<5	<5	<2	0.01	0.008	4	20	0.02	236	0.02	0.97	0.05	1.13	<4	22	4	3	2	<1	<1	<0.1
PIIIA.1	Rodalben/Pirmasens	0.04	<2	4	25	47	<0.5	6	<2	92	1.75	<5	<20	2	80	<0.4	<5	<5	18	0.01	0.017	8	12	0.07	503	0.07	2.38	0.11	2.46	<4	47	3	5	3	<1	<1	<0.1
PIIIA.1.3	Rodalben/Pirmasens	0.08	<2	<2	42	39	0.6	2	<2	69	5.19	7	22	4	59	1.5	<5	<5	71	1.61	0.748	9	16	0.03	309	0.02	1.39	0.07	1.33	6	26	<2	20	<2	1	2	<0.1
PIIIB.3	Rodalben/Pirmasens	0.09	<2	<2	31	21	<0.5	2	<2	64	0.74	12	<20	3	71	<0.4	<5	9	6	<0.01	0.010	6	12	0.03	401	0.04	1.59	0.09	1.88	<4	27	<2	3	<2	<1	<1	<0.1
PIVA.4Top	Rodalben/Pirmasens	0.06	<2	<2	25	33	<0.5	5	<2	141	1.08	10	<20	<2	73	<0.4	<5	7	13	0.05	0.040	9	24	0.06	327	0.07	1.89	0.06	1.69	<4	35	<2	5	3	<1	1	<0.1
PIVB.1	Rodalben/Pirmasens	0.15	<2	<2	12	33	<0.5	4	<2	98	0.88	<5	<20	<2	54	<0.4	<5	<5	11	0.03	0.029	7	18	0.05	278	0.06	1.43	0.05	1.23	<4	30	<2	4	2	<1	<1	<0.1
PIXA.2	Rodalben/Pirmasens	0.02	<2	3	24	24	<0.5	6	2	95	1.27	<5	<20	4	69	<0.4	<5	<5	12	0.02	0.026	7	23	0.06	436	0.06	2.26	0.10	2.49	<4	33	<2	4	3	<1	<1	<0.1
PIXA.3	Rodalben/Pirmasens	0.21	<2	<2	15	11	<0.5	3	<2	80	0.60	<5	<20	4	62	<0.4	<5	9	5	<0.01	0.020	5	14	0.03	344	0.03	1.43	0.08	1.82	<4	20	3	3	<2	<1	<1	<0.1
PVB.1.1	Rodalben/Pirmasens	0.05	<2	2	8	10	<0.5	3	<2	57	0.76	<5	<20	4	26	<0.4	<5	<5	3	0.01	0.018	3	16	0.02	160	0.02	0.75	0.04	0.76	<4	16	<2	3	<2	<1	<1	<0.1
PVB.4	Rodalben/Pirmasens	0.05	<2	4	8	17	<0.5	4	<2	87	1.14	<5	<20	3	29	<0.4	<5	<5	3	<0.01	0.033	4	19	0.02	188	0.02	0.85	0.04	0.77	<4	18	2	2	<2	<1	<1	<0.1
PVIIB.1	Rodalben/Pirmasens	0.09	<2	<2	12	46	<0.5	3	<2	100	0.81	<5	<20	2	32	<0.4	<5	<5	4	0.02	0.010	4	16	0.02	208	0.02	0.88	0.05	0.96	<4	22	<2	6	<2	1	<1	<0.1
PVIIIA.1	Rodalben/Pirmasens	0.05	<2	2	13	8	<0.5	4	<2	64	0.86	<5	<20	3	46	<0.4	<5	<5	4	<0.01	0.009	4	19	0.02	265	0.02	1.15	0.05	1.29	<4	19	<2	3	2	<1	<1	<0.1
PXIIB.1a	Rodalben/Pirmasens	0.09	<2	<2	23	10	<0.5	2	<2	48	0.73	<5	<20	7	37	<0.4	<5	<5	4	<0.01	0.010	5	15	0.02	241	0.04	1.04	0.04	1.03	<4	32	<2	5	<2	<1	<1	<0.1
PXIIIB.1	Rodalben/Pirmasens	0.13	<2	<2	15	13	<0.5	3	<2	44	0.62	10	<20	4	82	<0.4	<5	6	5	0.04	0.031	5	11	0.03	325	0.03	1.44	0.08	1.78	<4	23	2	3	<2	<1	<1	<0.1
PXIIIB.2	Rodalben/Pirmasens	0.03	<2	3	16	34	<0.5	5	<2	111	1.12	<5	<20	<2	59	<0.4	<5	<5	6	<0.01	0.014	5	20	0.04	295	0.04	1.48	0.07	1.60	<4	27	<2	4	2	<1	<1	<0.1
PXIX	Rodalben/Pirmasens	0.13	<2	<2	23	9	<0.5	3	<2	96	1.01	7	<20	5	61	<0.4	<5	<5	10	0.01	0.022	5	18	0.04	443	0.04	1.97	0.10	2.62	<4	25	<2	3	2	<1	<1	<0.1
PXVB	Rodalben/Pirmasens	0.05	<2	2	41	21	<0.5	5	<2	67	0.96	11	<20	5	69	<0.4	<5	<5	7	0.02	0.021	7	18	0.05	369	0.05	1.71	0.08	1.85	<4	36	<2	4	2	<1	<1	<0.1
PXVIA.2	Rodalben/Pirmasens	0.11	<2	56	12	25	<0.5	14	5	118	1.19	<5	<20	8	48	<0.4	<5	6	31	0.09	0.042	23	33	0.39	334	0.29	4.02	0.08	2.92	<4	105	3	11	9	1	4	<0.1
PXVIIB.1	Rodalben/Pirmasens	0.09	<2	5	17	18	<0.5	9	3	100	1.67	<5	<20	14	45	<0.4	<5	<5	25	0.08	0.044	35	31	0.23	341	0.31	3.28	0.07	3.46	<4	133	3	14	7	1	3	<0.1
PXVIIB.2.1	Rodalben/Pirmasens	0.04	<2	5	19	26	<0.5	13	4	128	2.15	<5	<20	11	54	<0.4	<5	6	35	0.08	0.035	27	38	0.34	394	0.30	4.48	0.09	3.18	<4	124	4	14	10	2	5	<0.1
PXVIIB.2.2	Rodalben/Pirmasens	0.14	<2	4	23	26	<0.5	14	3	124	1.97	<5	<20	11	53	<0.4	<5	<5	35	0.08	0.038	27	32	0.33	380	0.28	4.34	0.08	2.67	<4	118	4	13	9	2	4	<0.1
PXXATop	Rodalben/Pirmasens	0.06	<2	<2	7	7	<0.5	3	<2	52	0.77	<5	<20	4	60	<0.4	<5	<5	4	<0.01	0.011	6	18	0.03	370	0.05	1.49	0.08	1.72	<4	30	<2	5	<2	<1	<1	<0.1

Analyte		Wgt	Mo	Cu	Pb	Zn	Ag	Ni	Co	Mn	Fe	As	U	Th	Sr	Cd	Sb	Bi	V	Ca	P	La	Cr	Mg	Ba	Ti	Al	Na	K	W	Zr	Sn	Y	Nb	Be	Sc	S
Unit		KG	PPM	PPM	PPM	PPM	PPM	PPM	PPM	PPM	%	PPM	PPM	PPM	PPM	PPM	PPM	PPM	PPM	%	%	PPM	PPM	%	PPM	%	%	%	%	PPM	PPM	PPM	PPM	PPM	PPM	PPM	%
MDL		0.01	2	2	5	2	0.5	2	2	5	0.01	5	20	2	2	0.4	5	5	2	0.01	0.002	2	2	0.01	1	0.01	0.01	0.01	0.01	4	2	2	2	2	1	1	0.1
Sample	**Outcrop/Well**																																				
PXXB.1	Rodalben/Pirmasens	0.08	<2	<2	20	6	<0.5	4	<2	56	0.91	6	<20	3	65	<0.4	<5	10	8	<0.01	0.012	9	20	0.04	350	0.16	1.52	0.07	1.62	<4	137	2	9	4	<1	<1	<0.1
PXXID	Rodalben/Pirmasens	0.15	<2	<2	22	10	<0.5	3	<2	105	0.83	<5	<20	7	94	<0.4	<5	7	9	0.01	0.021	8	17	0.04	372	0.04	1.62	0.08	2.00	<4	25	<2	3	2	<1	<1	<0.1
PXXIII	Rodalben/Pirmasens	0.05	<2	3	12	13	<0.5	4	<2	76	1.19	7	<20	2	64	<0.4	<5	<5	7	0.01	0.044	5	18	0.03	354	0.03	1.56	0.07	1.80	<4	23	<2	3	3	<1	<1	<0.1
PXXIITop	Rodalben/Pirmasens	0.18	<2	3	17	16	<0.5	5	<2	183	1.03	5	<20	6	76	<0.4	<5	<5	11	0.02	0.025	8	21	0.06	535	0.08	2.68	0.12	3.24	<4	34	<2	3	4	<1	<1	<0.1
PXXIV	Rodalben/Pirmasens	0.08	<2	3	9	22	<0.5	6	<2	230	1.40	<5	<20	4	43	<0.4	<5	7	14	<0.01	0.054	6	28	0.04	198	0.04	1.12	0.04	0.90	<4	28	<2	3	3	<1	<1	<0.1
PXXVIA.1	Rodalben/Pirmasens	0.15	<2	<2	15	14	<0.5	3	<2	45	0.63	7	<20	<2	77	<0.4	<5	<5	6	0.01	0.015	6	10	0.05	521	0.05	2.11	0.11	2.50	<4	31	3	5	3	<1	<1	<0.1
PXXVIIA.1	Rodalben/Pirmasens	0.07	<2	3	13	30	<0.5	5	<2	144	0.91	6	<20	<2	56	<0.4	<5	<5	7	0.02	0.039	6	18	0.04	376	0.06	1.50	0.08	1.71	<4	48	<2	6	2	<1	<1	<0.1
R1Ib	Heidelberg Riesenstein	<0.01	<2	3	16	6	<0.5	5	<2	53	0.72	13	<20	<2	49	<0.4	<5	<5	3	0.03	0.014	5	96	0.04	468	0.03	1.74	0.09	2.19	<4	17	2	3	3	<1	<1	<0.1
R1IIb	Heidelberg Riesenstein	<0.01	2	3	19	9	<0.5	9	<2	67	0.90	21	<20	4	74	<0.4	<5	<5	8	0.05	0.025	8	130	0.13	610	0.05	2.73	0.11	3.07	<4	25	<2	5	2	<1	1	<0.1
R1Vb	Heidelberg Riesenstein	0.01	2	11	20	6	<0.5	4	<2	104	1.19	8	<20	<2	48	<0.4	<5	<5	2	0.02	0.013	4	15	0.03	475	0.03	1.66	0.08	2.03	<4	15	3	3	2	<1	<1	<0.1
R1VIb	Heidelberg Riesenstein	<0.01	3	4	8	10	<0.5	9	<2	83	1.03	19	<20	<2	57	<0.4	<5	<5	4	0.03	0.015	5	147	0.05	539	0.03	2.01	0.10	2.43	<4	19	3	3	2	<1	<1	<0.1
R2/1IIb	Heidelberg Riesenstein	0.01	3	9	70	146	<0.5	15	2	125	1.83	36	<20	<2	58	<0.4	<5	<5	9	0.02	0.029	8	18	0.08	550	0.10	2.26	0.08	2.33	<4	49	<2	6	4	2	1	<0.1
R2/1IVb	Heidelberg Riesenstein	0.01	2	4	30	73	<0.5	11	<2	86	1.34	26	24	<2	70	<0.4	<5	<5	10	0.03	0.015	10	111	0.11	500	0.08	2.63	0.09	2.74	<4	37	<2	5	3	<1	1	<0.1
R2/1VIIb	Heidelberg Riesenstein	<0.01	3	11	18	30	<0.5	11	4	480	1.86	16	<20	<2	42	<0.4	<5	<5	5	0.02	0.016	5	17	0.04	467	0.05	1.77	0.06	1.95	<4	21	3	5	3	<1	1	<0.1
R2/1Xb	Heidelberg Riesenstein	<0.01	<2	3	13	10	<0.5	7	<2	128	0.90	13	<20	<2	55	<0.4	<5	<5	6	0.02	0.012	6	116	0.05	501	0.04	2.00	0.09	2.35	<4	23	<2	3	<2	<1	<1	<0.1
RK1	Rockenau	0.11	<2	4	12	3	<0.5	8	<2	300	0.71	<5	<20	2	57	<0.4	<5	6	4	0.02	0.011	2	8	0.04	595	0.03	2.22	0.12	2.70	<4	17	<2	4	3	<1	<1	<0.1
RK2	Rockenau	0.04	<2	4	28	8	<0.5	5	<2	51	1.05	<5	<20	<2	87	<0.4	<5	8	14	0.03	0.026	12	13	0.21	848	0.08	4.49	0.13	4.14	<4	39	<2	6	3	1	2	<0.1
RK3	Rockenau	0.08	<2	5	18	9	<0.5	16	9	170	0.82	5	<20	<2	76	<0.4	<5	13	8	0.04	0.021	8	10	0.11	646	0.05	2.92	0.15	3.33	<4	26	<2	5	3	<1	1	<0.1
RK4	Rockenau	0.05	<2	5	18	4	<0.5	4	<2	69	0.98	<5	<20	5	76	<0.4	5	<5	9	0.06	0.028	6	9	0.13	681	0.05	3.39	0.15	3.74	<4	30	2	5	3	<1	1	<0.1
RK5	Rockenau	0.01	3	12	19	14	<0.5	8	3	165	1.90	8	<20	3	84	<0.4	<5	<5	20	0.04	0.037	15	22	0.19	838	0.08	3.34	0.11	2.81	<4	30	3	8	5	2	2	<0.1
RK6	Rockenau	0.02	<2	5	17	5	<0.5	7	<2	178	1.15	6	<20	<2	67	<0.4	5	16	5	0.04	0.019	5	11	0.06	630	0.03	2.41	0.14	2.99	<4	19	<2	5	2	<1	<1	<0.1

Appendix 6 Fluid Inclusion Thermometry Results

Sample	Outcrop	T_h °C	$T_{n\ gas}$ °C	$T_{n\ ice}$ °C	T_i °C	$T_{m\ ice}$ °C
Ls02	Leistadt	99.6	40.3			
Ls03	Leistadt	234.9	221.4	-40.4		-0.1
Ls03	Leistadt	59.2	53.2			
Ls03	Leistadt	53.8				
Ls03	Leistadt	148.4	89.9		-30.0	-27.0
Ls03	Leistadt	47.6	33.4			
Ls03	Leistadt	167.7	47.7			-30.0
HB01	HD Molkenkur	142.1			-15.0	-10.0
HB01	HD Molkenkur	219.9	115.0			
HB01	HD Molkenkur	367.4				-7.0
HB01	HD Molkenkur	121.9	61.8			
HB01	HD Molkenkur	139.5	79.7			
HB01	HD Molkenkur	250.0	211.1			
HK01	HD Im Kammerf.	76.6	20.8			
HK01	HD Im Kammerf.	134.8	82.3			
HK01	HD Im Kammerf.	292.9	237.8			
HK01	HD Im Kammerf.	156.5	140.3			
HK01	HD Im Kammerf.	348.4	318.0			-20.0
HK01	HD Im Kammerf.	60.0				-25.1
HK01	HD Im Kammerf.	110.5			-27.9	-20.0
HK01	HD Im Kammerf.	151.8	9.3			
Cl09	Cleebourg	276.6				
Cl09	Cleebourg	232.6				
Cl09	Cleebourg	124.1	36.4			
Cl09	Cleebourg	164.3	103.3		-8.1	-7.8
HB15.11	Hanbuch	151.9	52.7			
HB15.11	Hanbuch	173.0	113.6			
HB15.11	Hanbuch	162.8	92.1			
HB15.11	Hanbuch	202.7	148.4			
HB15.11	Hanbuch	209.0	157.4			
HB15.11	Hanbuch	201.7				
HB15.11	Hanbuch	111.4	75.6			

Appendix 7 X-Ray Fluorescence Results

Sample	SiO_2 (%)	TiO_2 (%)	Al_2O_3 (%)	Fe_2O_3 (%)	MnO (%)	MgO (%)	CaO (%)	Na_2O (%)	K_2O (%)	P_2O_5 (%)	Cr_2O_3 (%)	NiO (%)	SrO (%)	ZrO_2 (%)	BaO (%)	LOI	Total
Cl10a	84.63	0.21	5.229	4.691	0.012	0.175	0.038	0.085	2.604	0.101	0.003	0.002	0.01	0.022	0.045	1.10	98.95
Cl14a	83.828	0.263	8.493	1.431	0.007	0.363	0.064	0.129	4.007	0.091	0.008	0.002	0.021	0.017	0.107	1.08	99.91
C114b	83.465	0.269	8.449	1.445	0.006	0.357	0.064	0.119	4.025	0.094	0.005	0.002	0.02	0.021	0.109	1.08	99.53
Cl15a	84.557	0.347	7.857	1.252	0.007	0.331	0.061	0.104	3.595	0.034	0	0.001	0.016	0.029	0.054	1.00	99.25
Cl15b	84.596	0.345	7.903	1.252	0.006	0.308	0.057	0.101	3.581	0.041	0.001	0.001	0.016	0.029	0.053	1.00	99.29
Cl17a	92.066	0.065	3.172	1.557	0.007	0.076	0.028	0.064	1.802	0.027	0.004	0.002	0.008	0.008	0.03	0.27	99.19
Cl17b	91.17	0.067	3.102	1.551	0.007	0.06	0.031	0.075	1.776	0.032	0.002	0.002	0.008	0.009	0.035	0.27	98.20
Cl19a	81.682	0.48	8.405	2.496	0.009	0.374	0.075	0.113	3.619	0.034	0.003	0.001	0.014	0.06	0.054	2.59	100.01
Cl19b	82.019	0.48	8.384	2.502	0.009	0.371	0.074	0.09	3.633	0.035	0.005	0.002	0.015	0.052	0.048	2.59	100.31
Cl02a	86.584	0.372	7.8	1.216	0.006	0.34	0.075	0.109	3.512	0.094	0.002	0.001	0.018	0.033	0.097	0.88	101.14
Cl02b	84.643	0.368	7.598	1.224	0.007	0.315	0.068	0.107	3.501	0.09	0.005	0.002	0.018	0.031	0.094	0.88	98.95
Cl9a	90.841	0.201	5.466	1.134	0.007	0.197	0.041	0.1	2.621	0.041	0.005	0.002	0.012	0.017	0.049	0.63	101.36
Cl9b	89.193	0.197	5.355	1.142	0.007	0.189	0.03	0.099	2.616	0.039	0.006	0.002	0.012	0.017	0.05	0.63	99.58
C2/2IIa a	89.825	0.144	4.596	1.863	0.011	0.133	0.06	0.092	2.614	0.033	0.002	0.001	0.009	0.01	0.043	1.66	101.09
C2/2IIa b	89.469	0.149	4.584	1.865	0.011	0.142	0.039	0.095	2.613	0.03	0.004	0.001	0.009	0.015	0.045	1.66	100.73
C5/1VI a	84.381	0.39	7.576	2.223	0.012	0.309	0.06	0.087	3.359	0.037	0.032	0.002	0.015	0.035	0.058	0.35	98.93
C5/1VI b	84.528	0.396	7.539	2.223	0.01	0.31	0.063	0.104	3.346	0.047	0.034	0.002	0.015	0.037	0.06	0.35	99.06
Mean Values																	
Cl10	84.63	.21	5.23	4.69	.01	.18	.04	.09	2.60	.101	.003	.002	.010	.022	.045	1.10	98.96
Cl14	83.65	.27	8.47	1.44	.01	.36	.06	.12	4.02	.093	.007	.002	.021	.019	.108	1.08	99.73
Cl15	84.58	.35	7.88	1.25	.01	.32	.06	.10	3.59	.038	.001	.001	.016	.029	.054	1.00	99.28
Cl17	91.62	.07	3.14	1.55	.01	.07	.03	.07	1.79	.030	.003	.002	.008	.009	.033	.27	98.71
Cl19	81.85	.48	8.39	2.50	.01	.37	.07	.10	3.63	.035	.004	.002	.015	.056	.051	2.59	100.15
Cl02	85.61	.37	7.70	1.22	.01	.33	.07	.11	3.51	.092	.004	.002	.018	.032	.096	.88	100.05
Cl19	90.02	.20	5.41	1.14	.01	.19	.04	.10	2.62	.040	.006	.002	.012	.017	.050	.63	100.49
C2/2IIa	89.65	.15	4.59	1.86	.01	.14	.05	.09	2.61	.032	.003	.001	.009	.013	.044	1.66	100.91
C5/1VI	84.45	.39	7.56	2.22	.01	.31	.06	.10	3.35	.042	.033	.002	.015	.036	.059	.35	98.99

Appendix 8 X-Ray Diffractograms

Chart 1 XRD Clay Mineral Fraction - Cleebourg

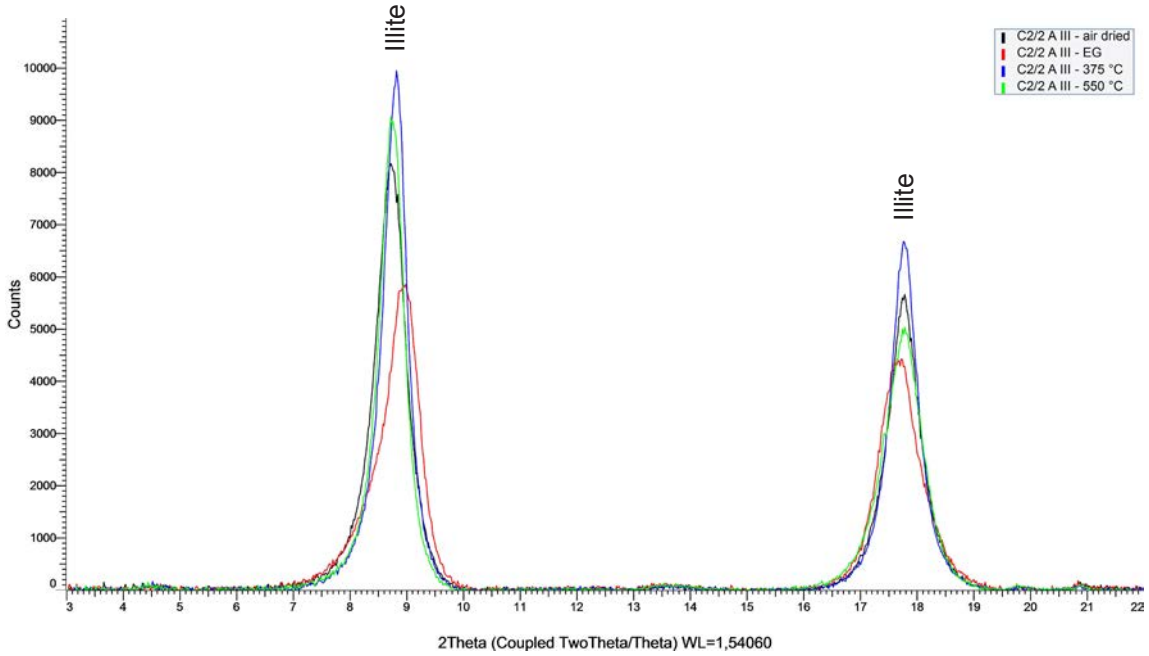

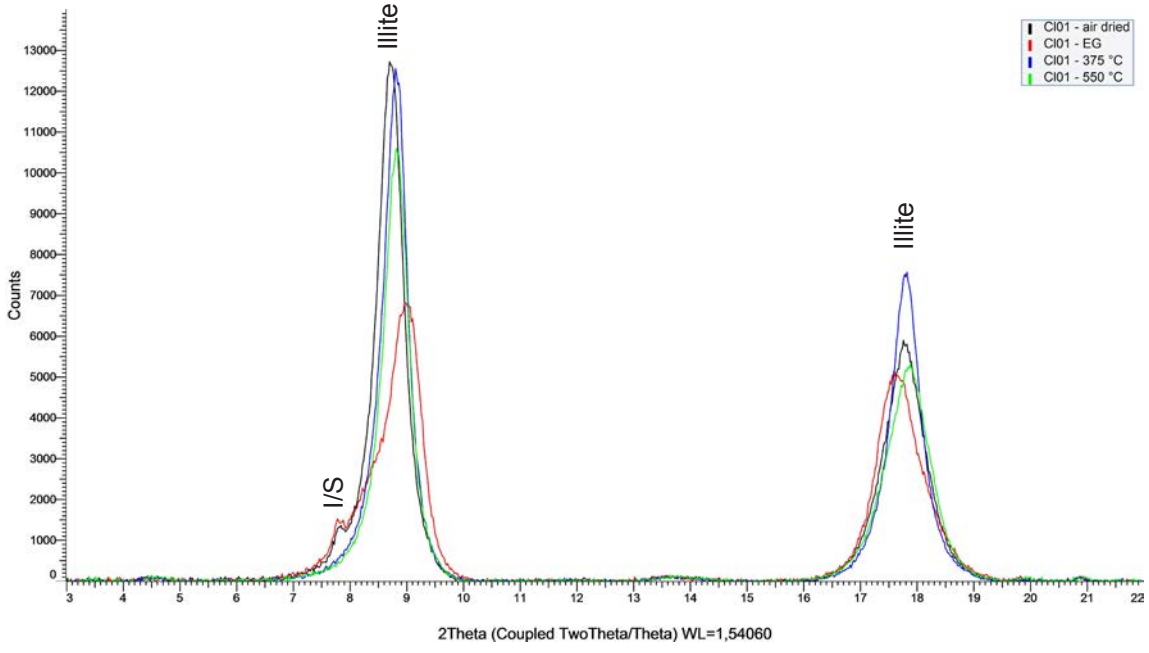

Chart 1 continued

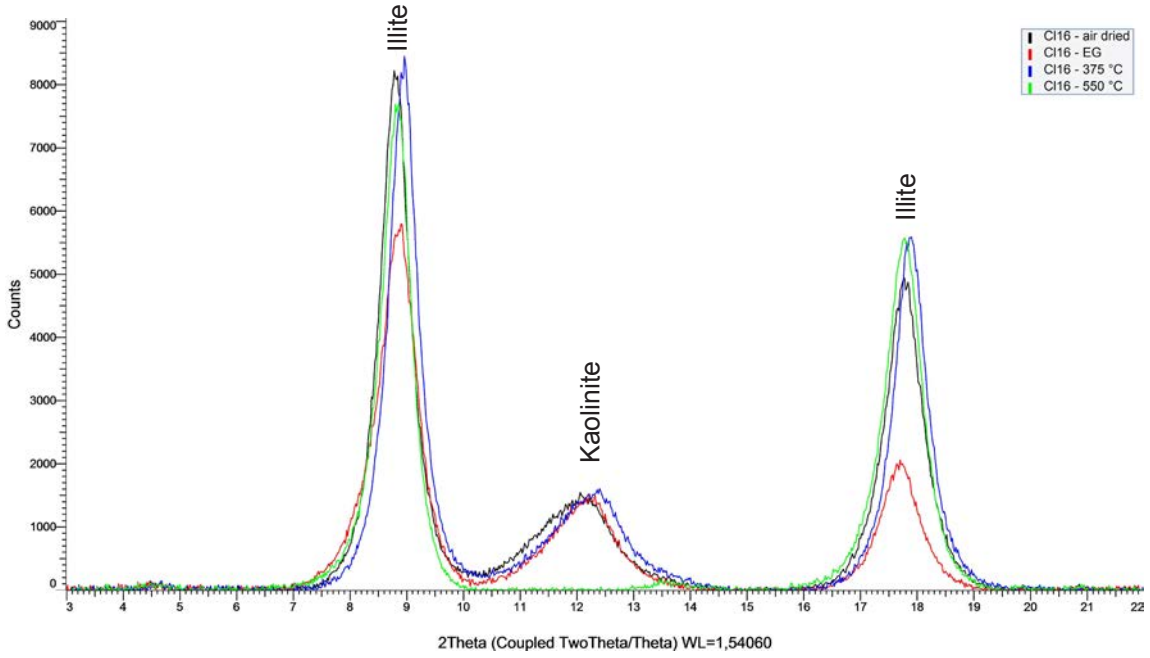

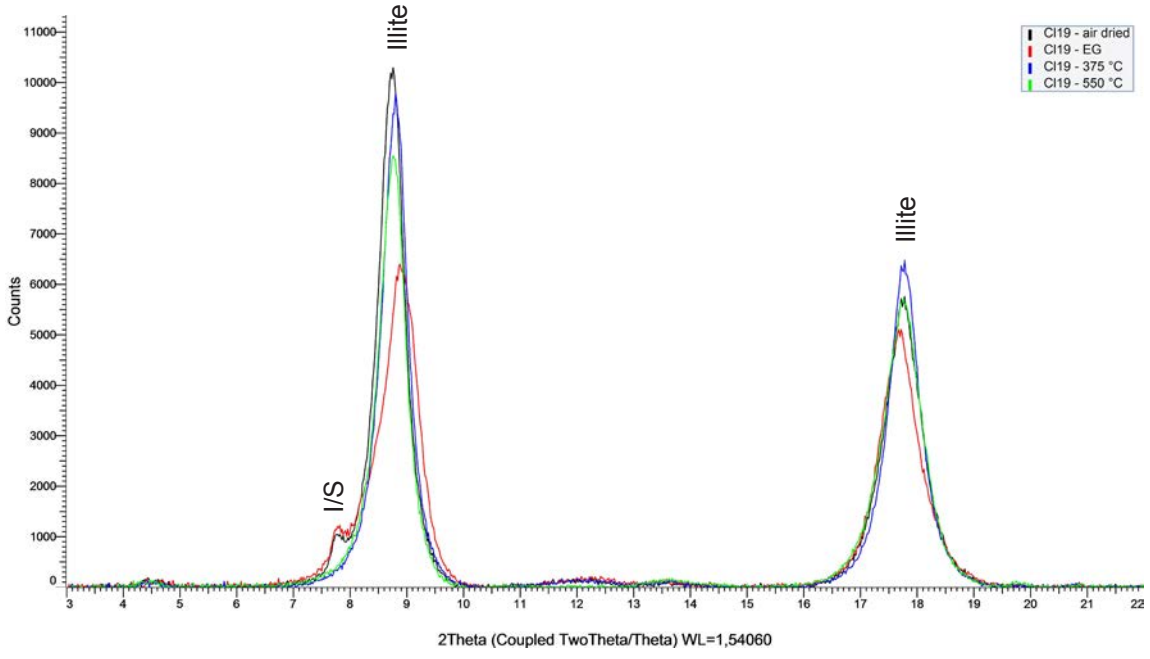

Chart 2 XRD Clay Mineral Fraction - Well B 1

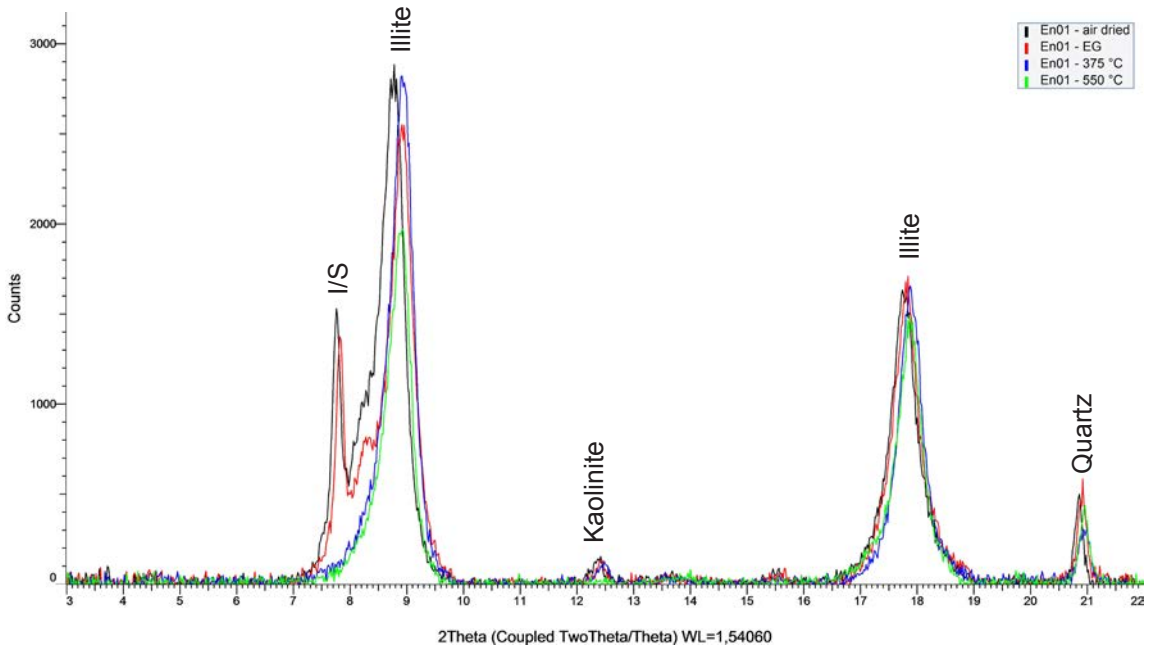

Chart 3 XRD Clay Mineral Fraction - Well B 2

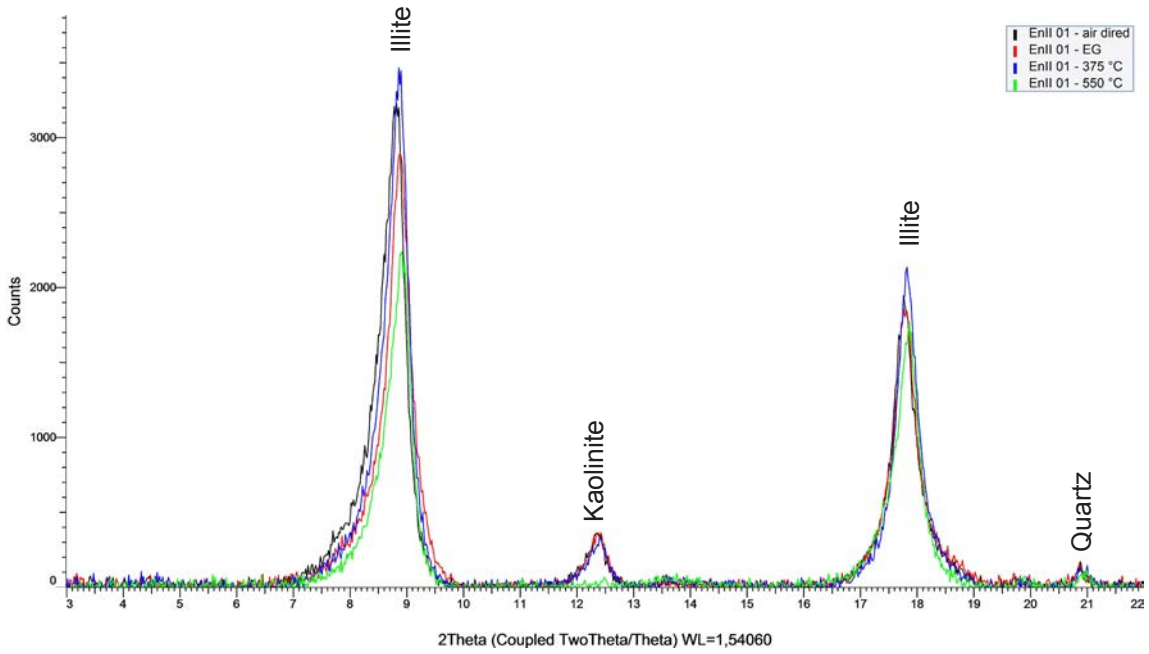

Chart 4 XRD Clay Mineral Fraction - Ettlingen

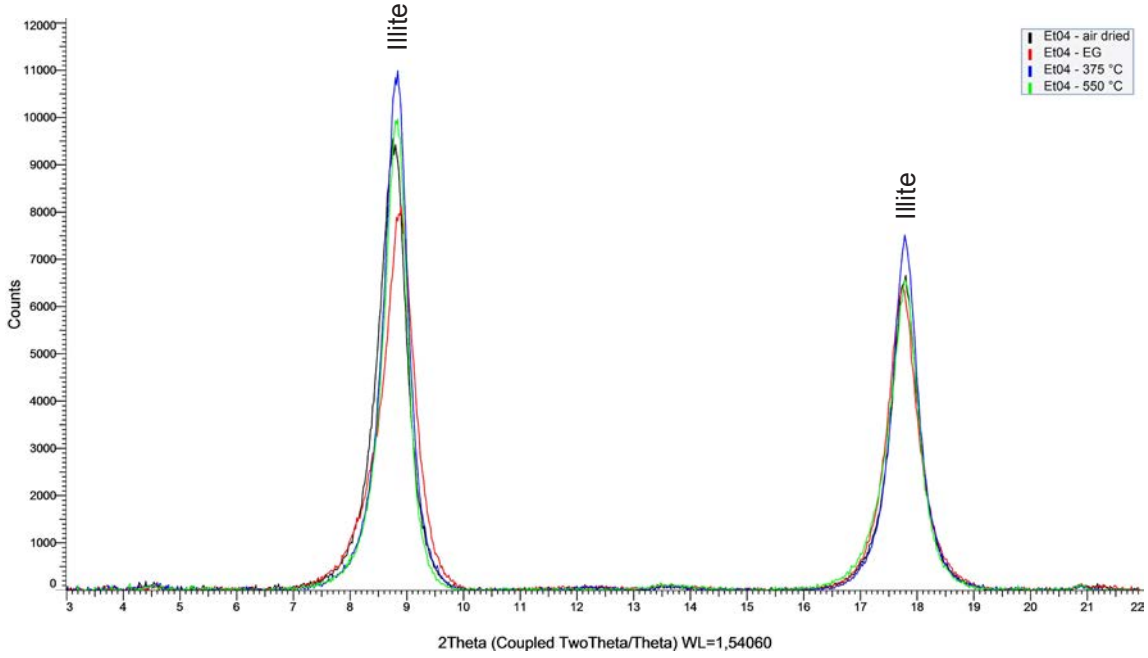

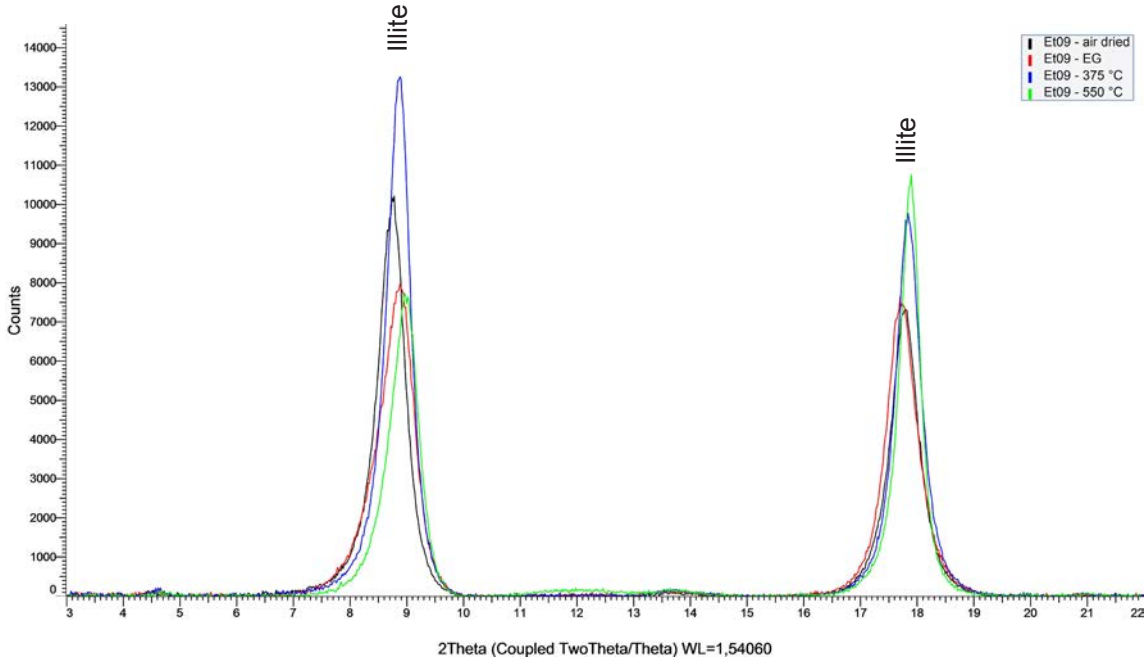

Chart 5 XRD Clay Mineral Fraction - Heidelberg, Molkenkur

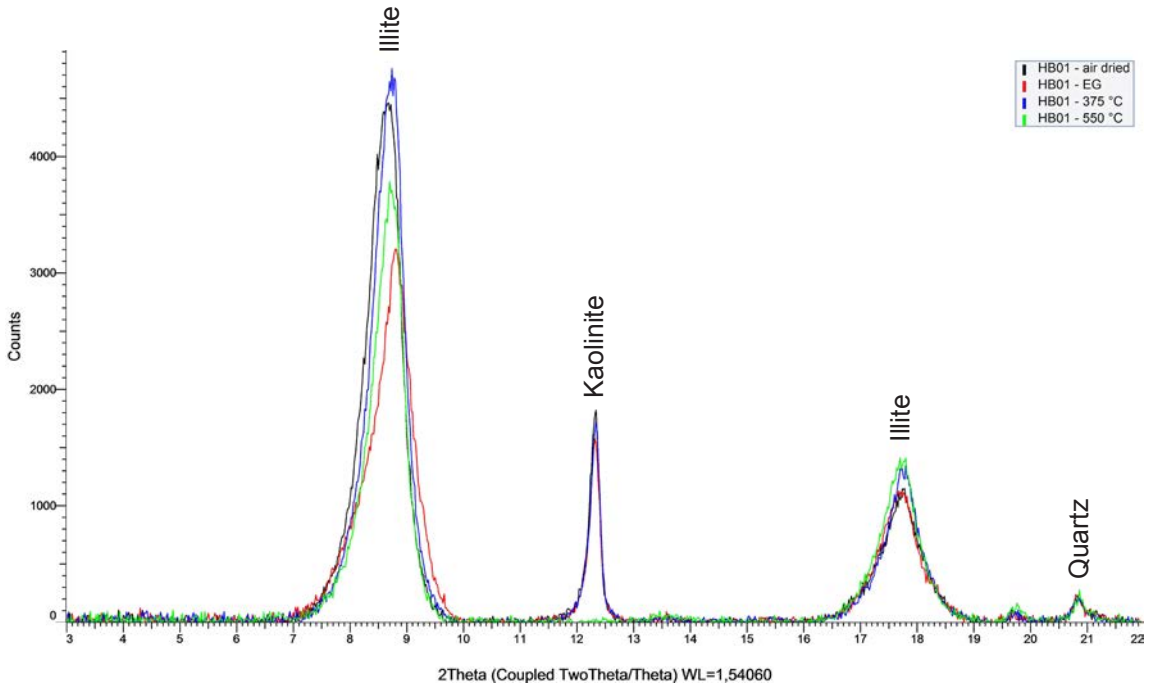

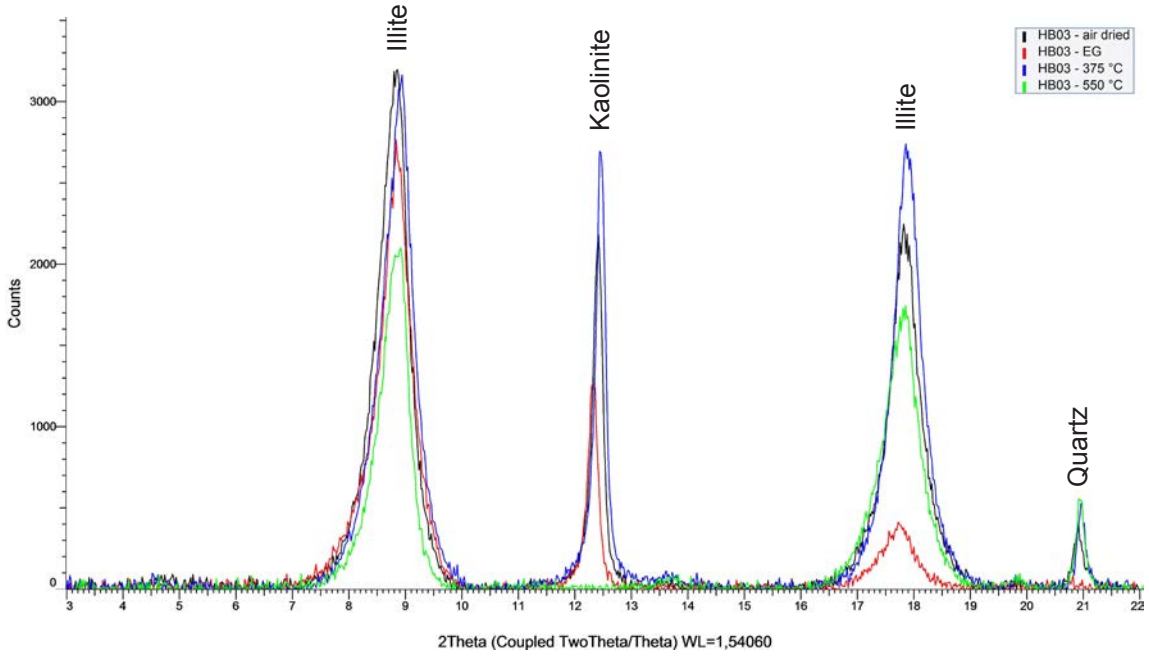

Chart 6 XRD Clay Mineral Fraction - Heidelberg, Im Kammerforst

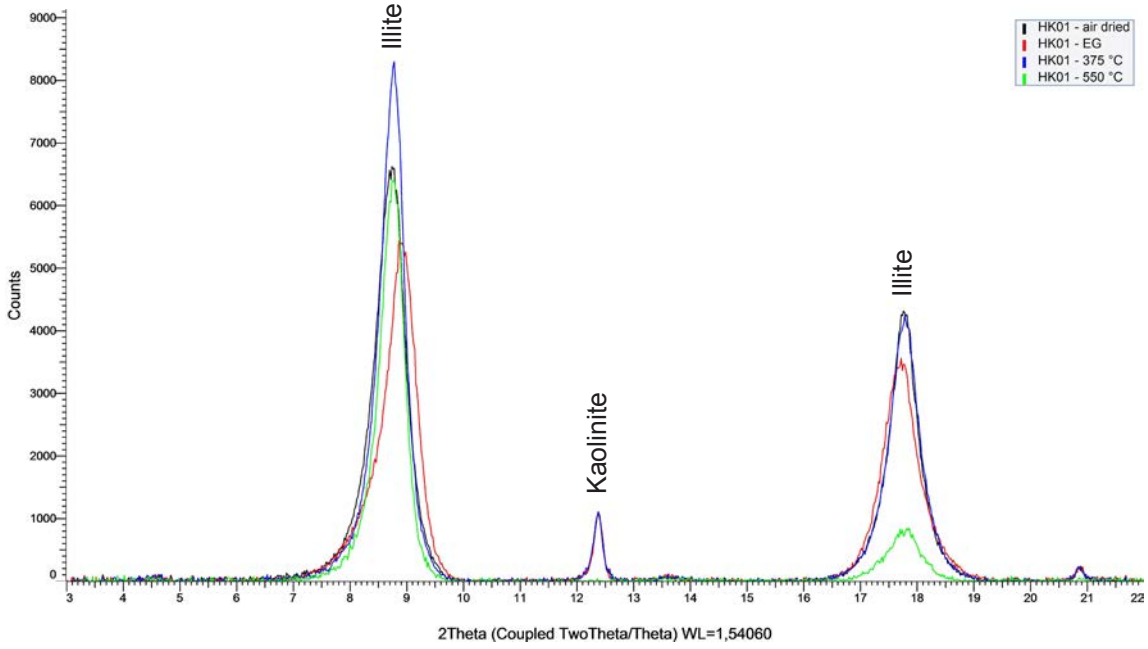

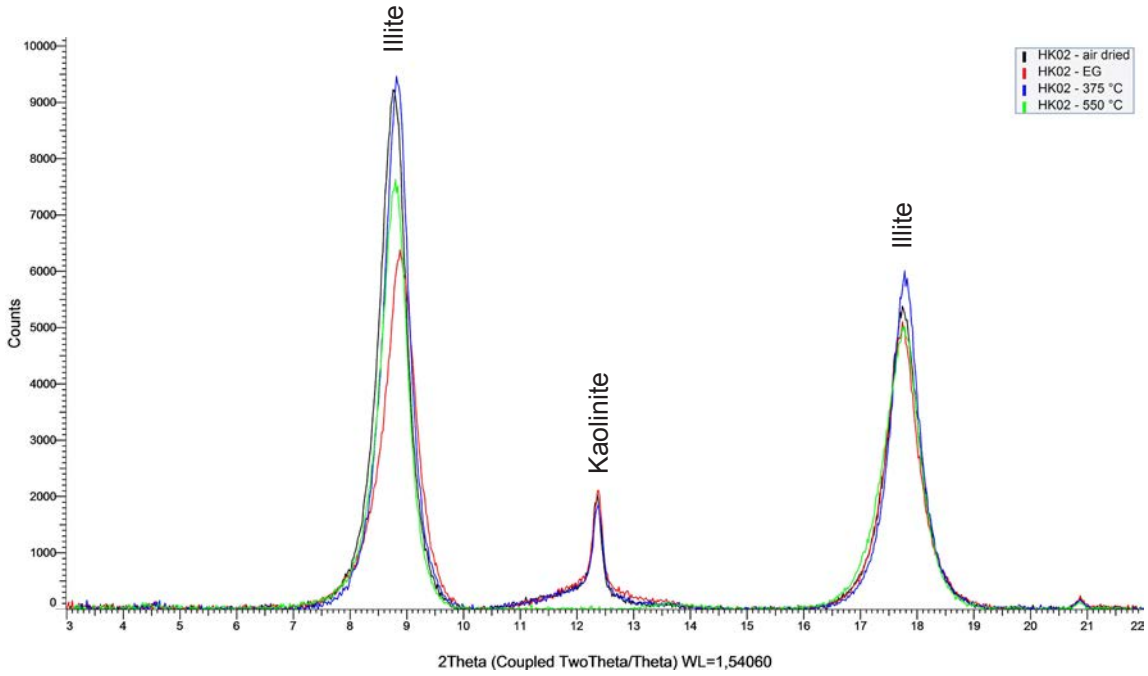

Chart 7 XRD Clay Mineral Fraction - Well A 2

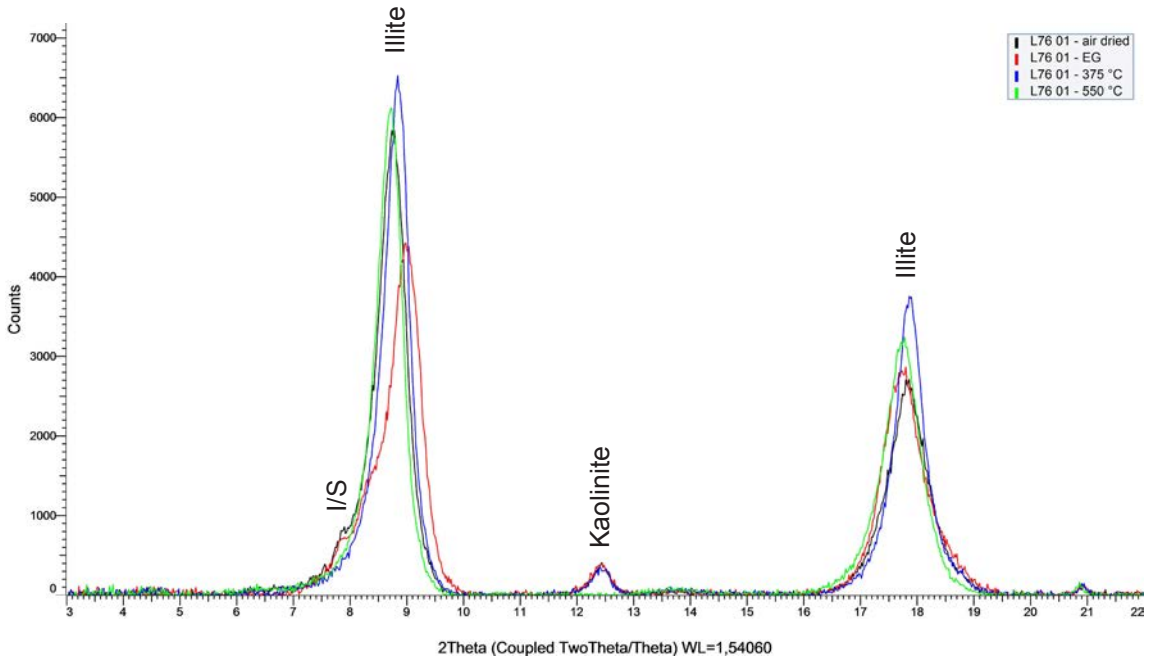

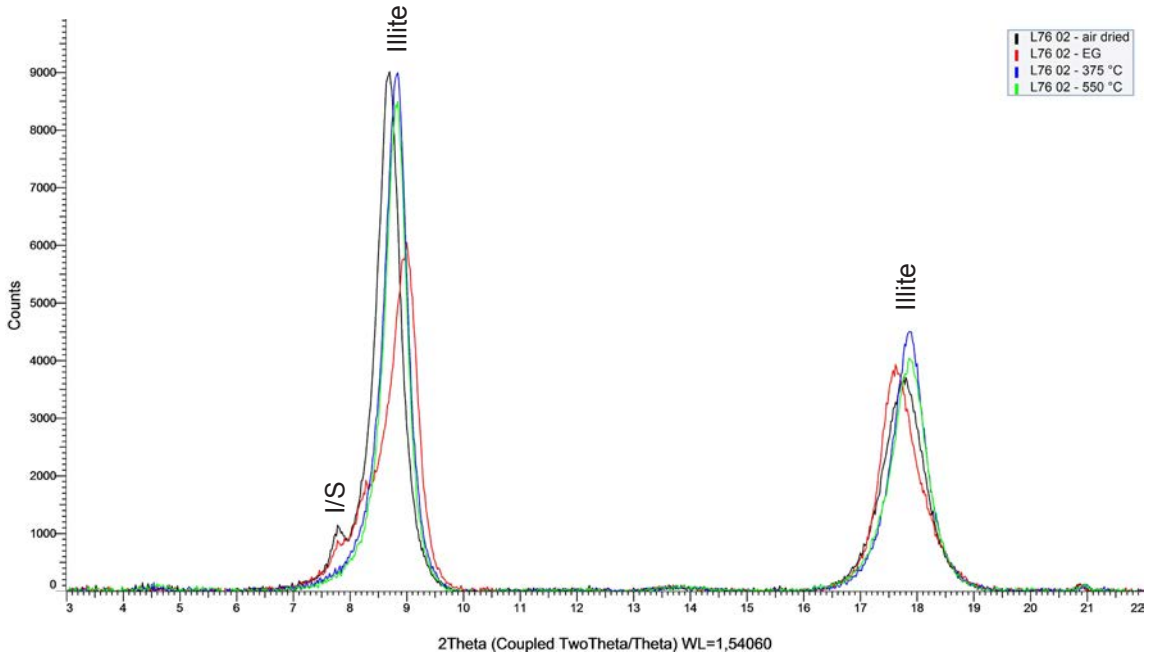

Chart 8 XRD Clay Mineral Fraction - Leistadt

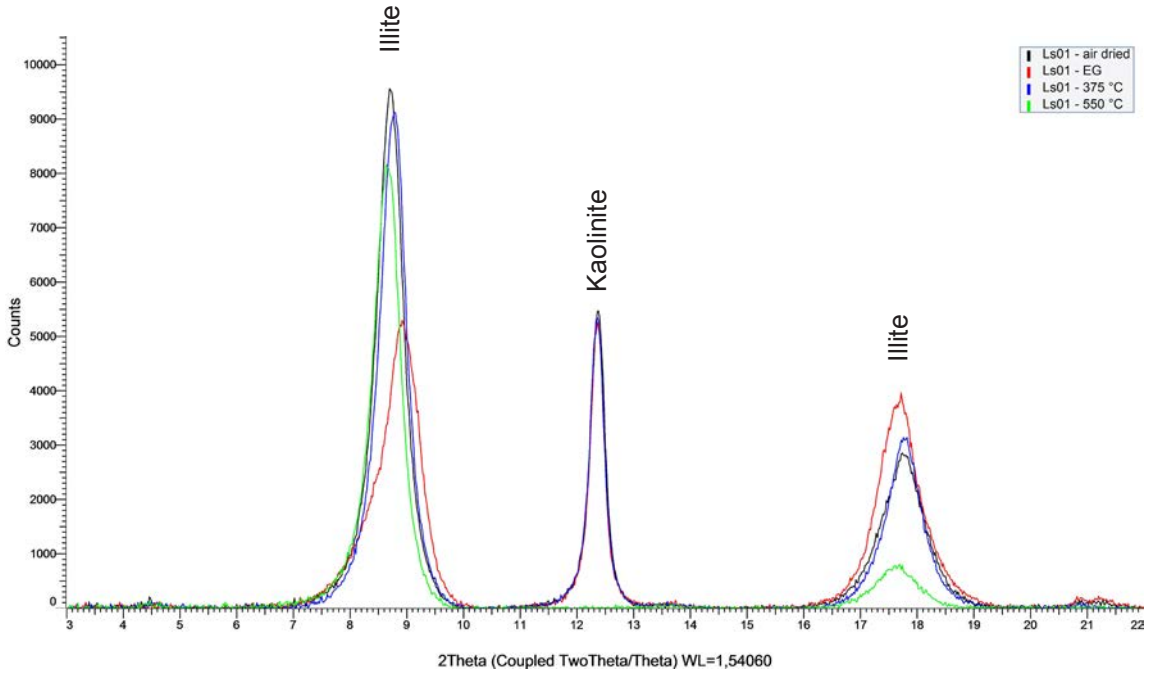

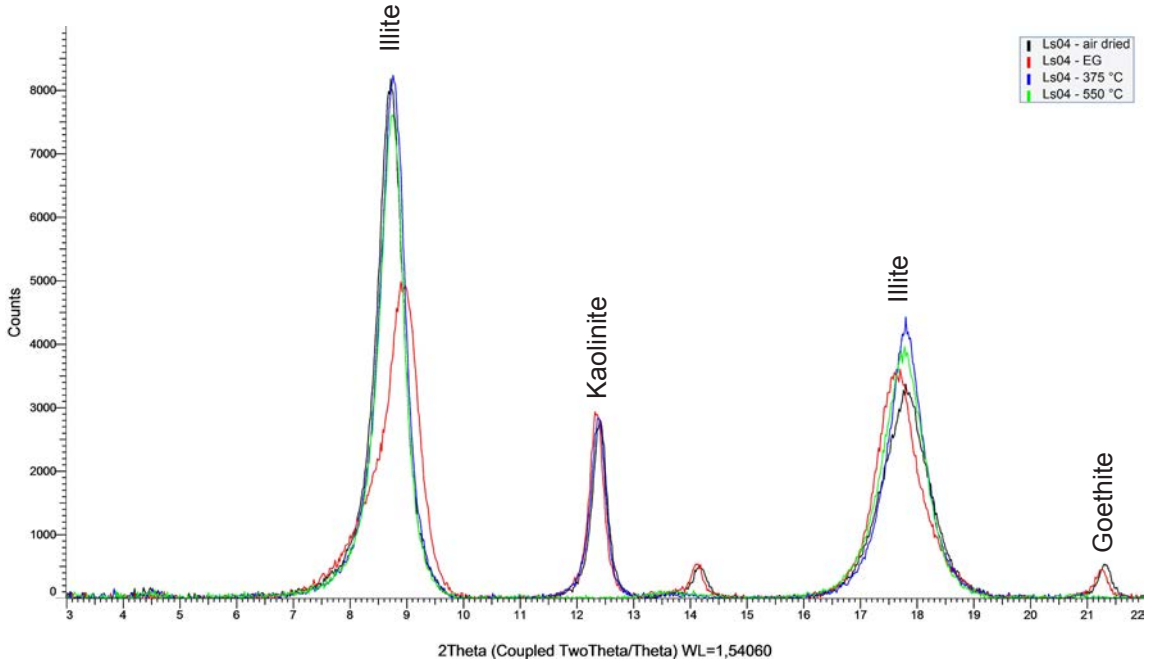

Chart 8 continued

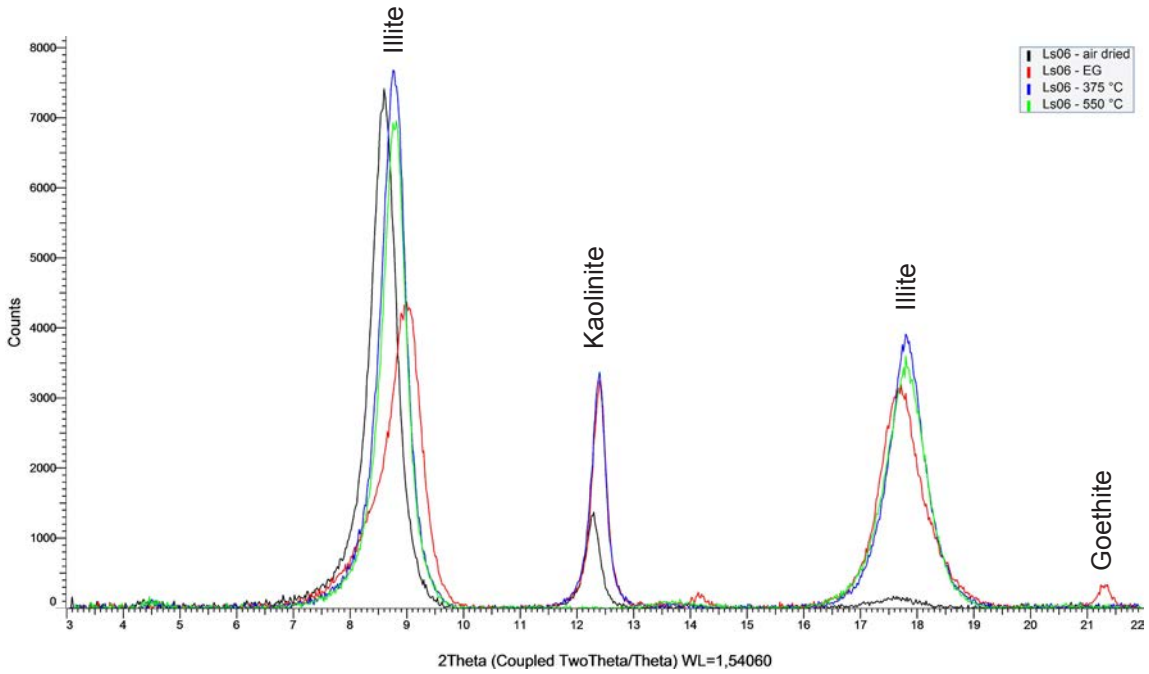

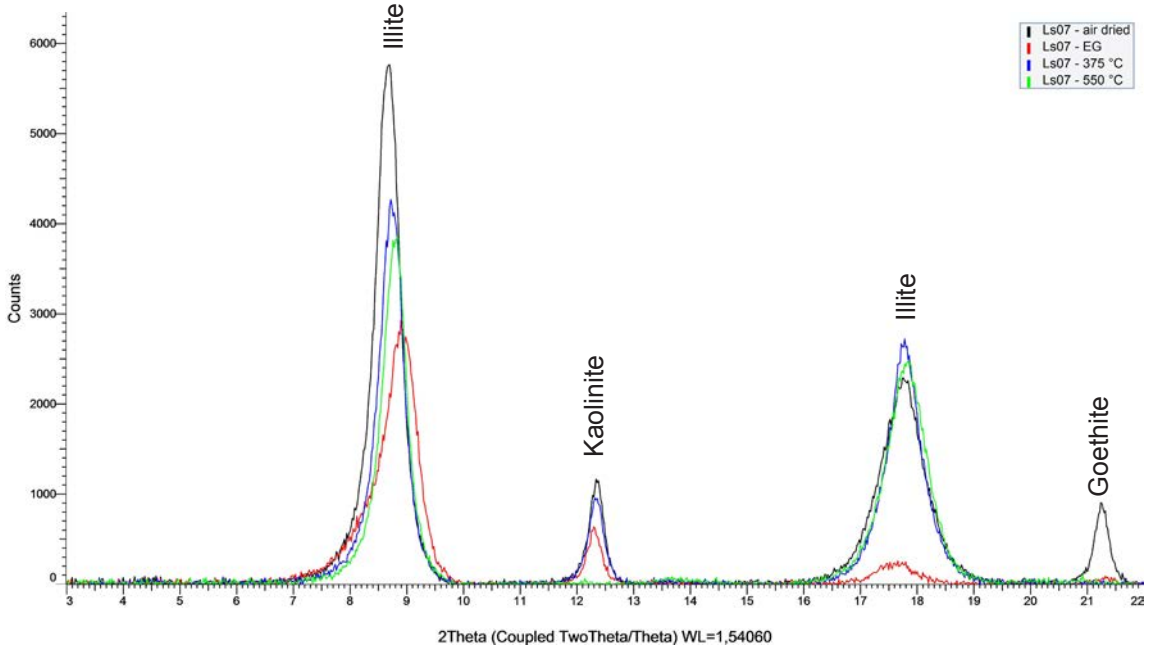

Chart 9 XRD Whole Rock - Mosbach

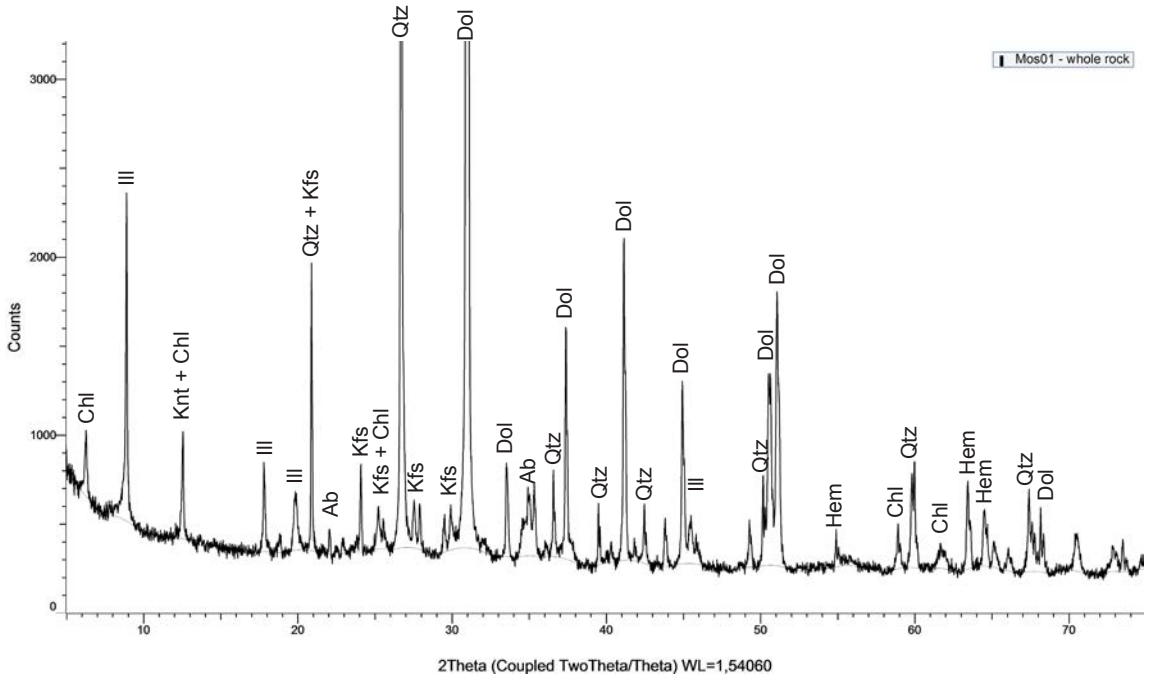

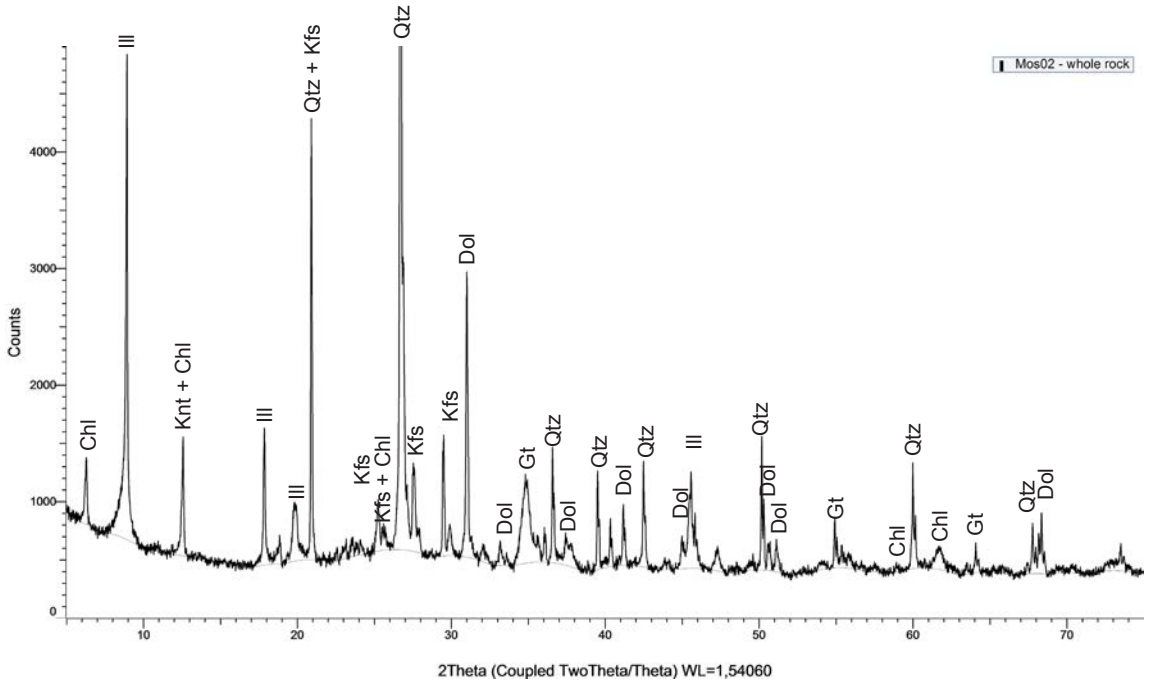

Chart 9 continued

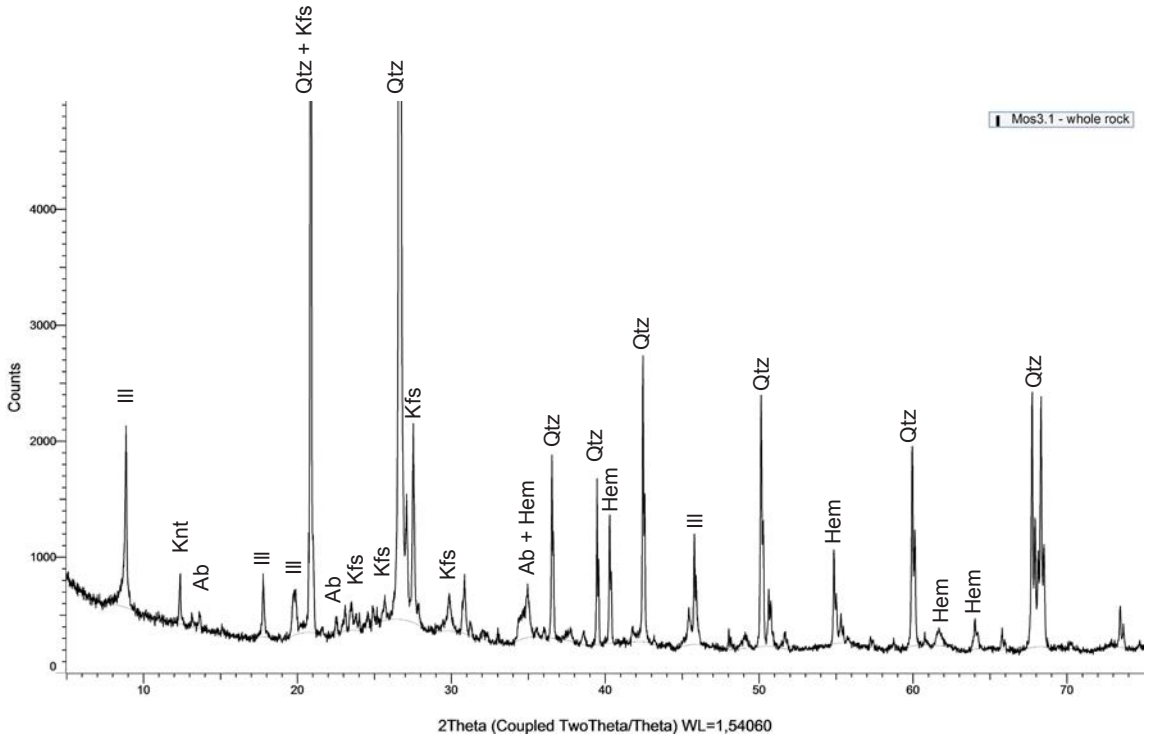

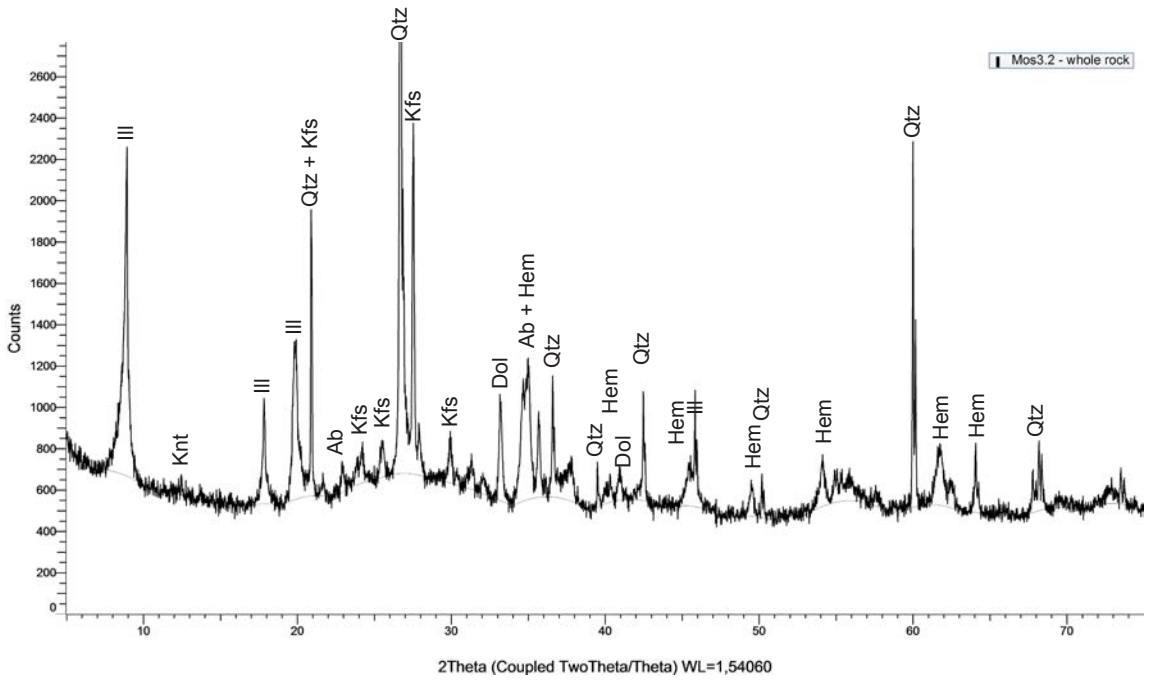

Chart 10 XRD Clay Mineral Fraction - Neckargemünd

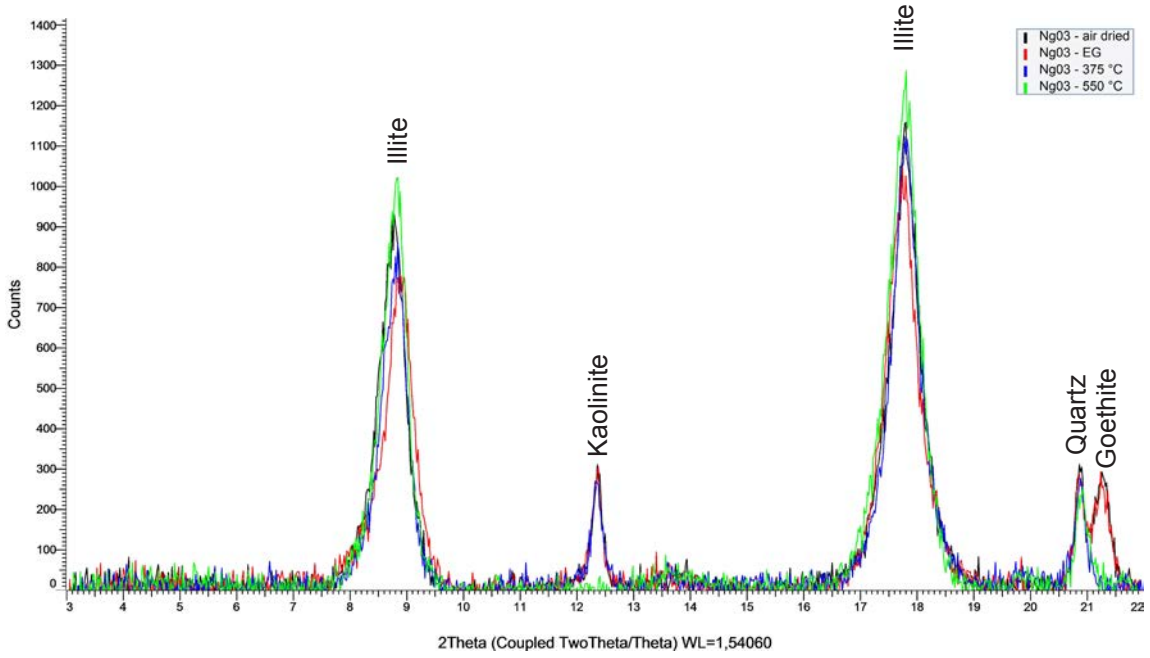

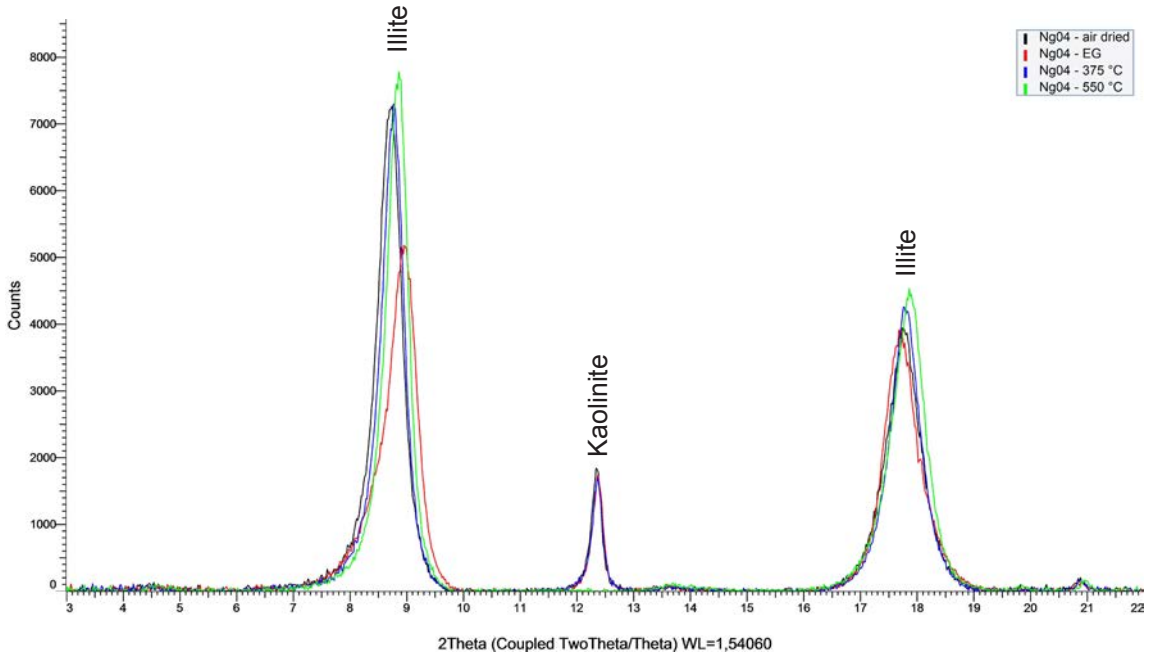

Chart 10 continued

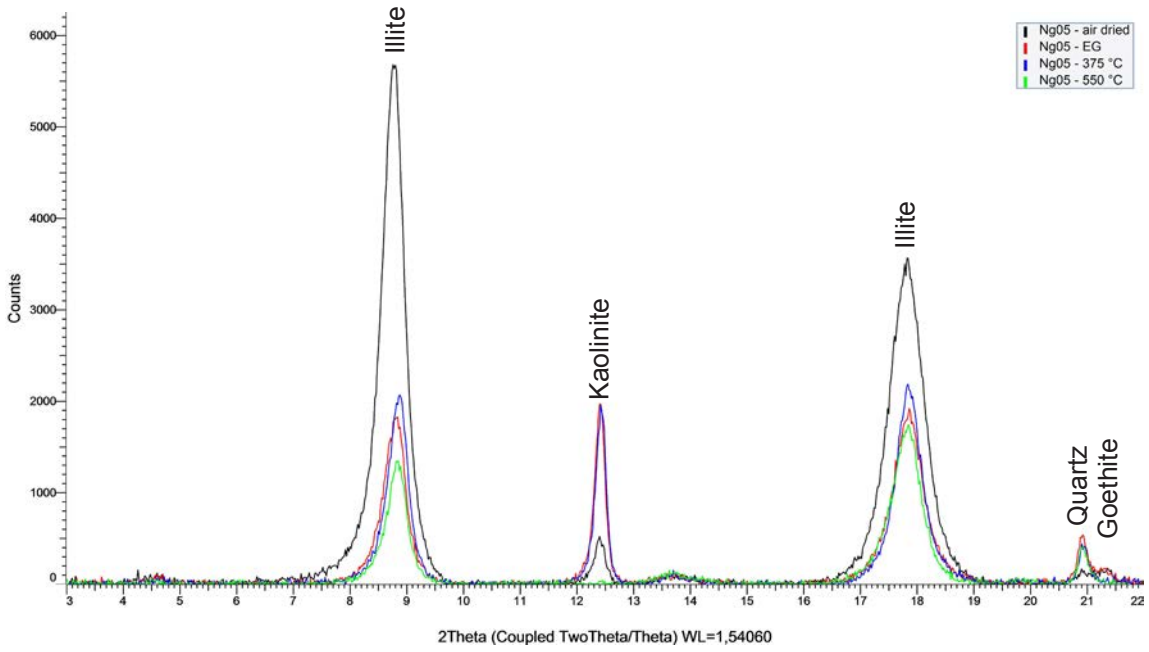

Chart 11 XRD Whole Rock - Pirmasens

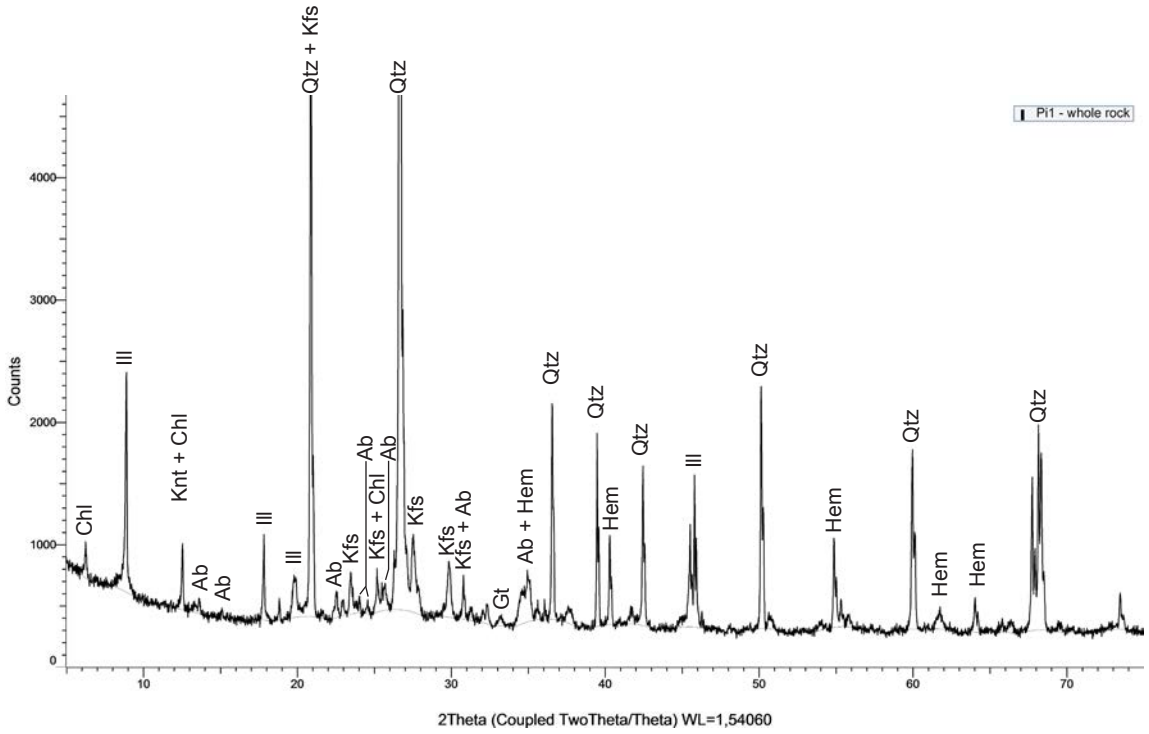

Chart 11 continued

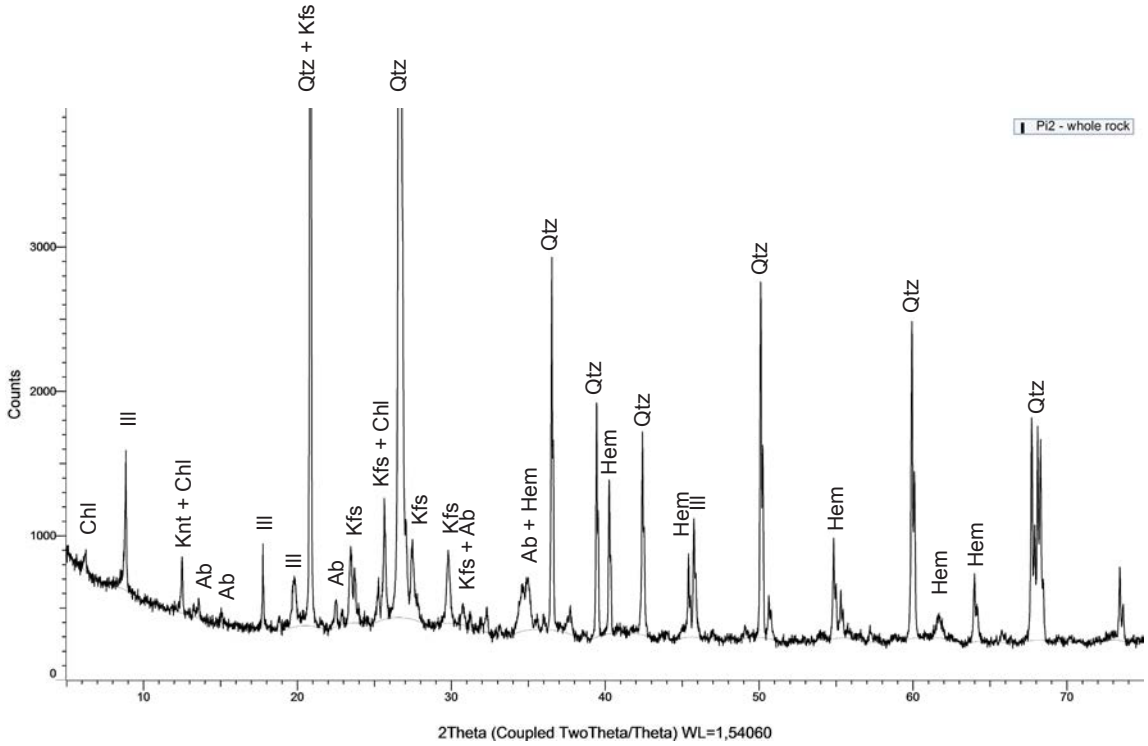

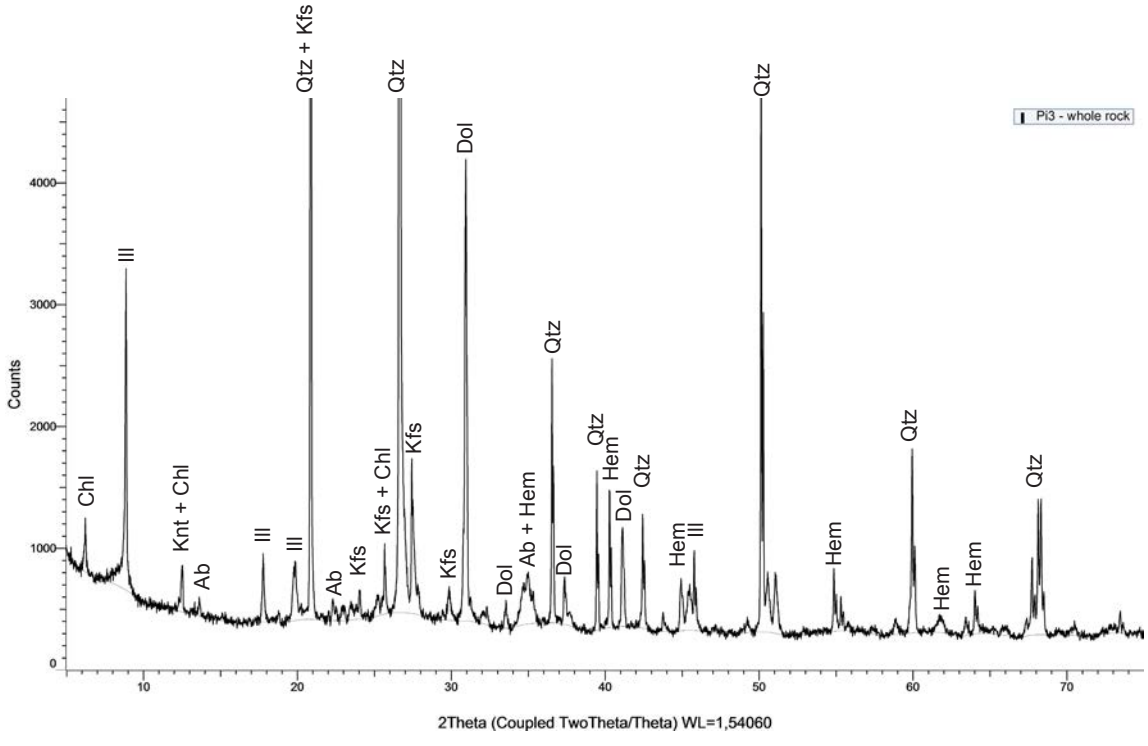

Chart 12 XRD Clay Mineral Fraction - Rockenau

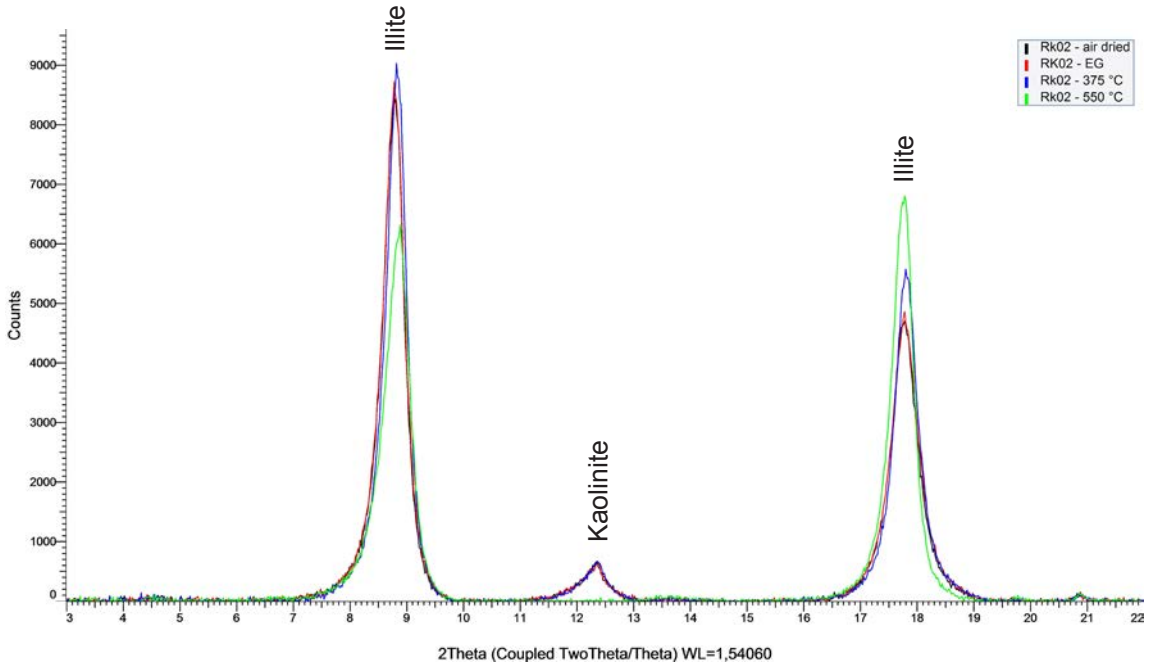

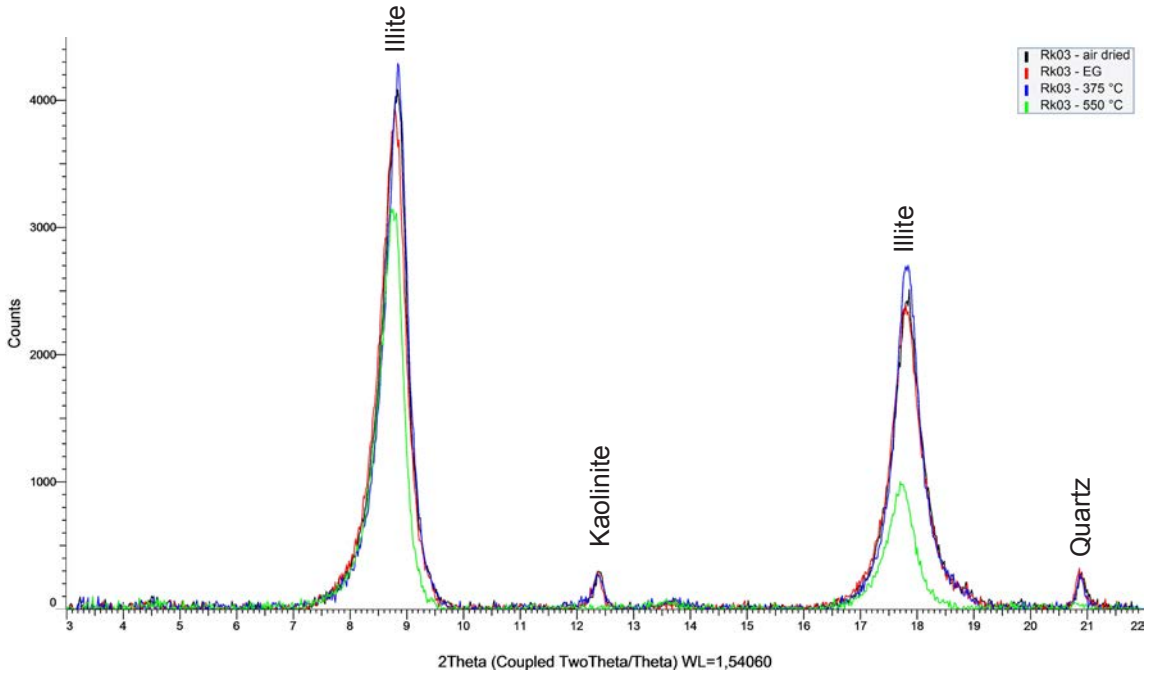

Appendix 9 Sample Locations and Sample Codes

Odenwald:	**Outcrop Name**	**Sample Code**	**Geographic Coordinates**	
	Molkenkur/Bergbahn	HB	49°26'23.33°N	8°42'53.40°E
Heidelberg	Im Kammerforst	HK	49°24'19.57°N	8°43'4.91°E
	Riesenstein	R	49°24'25.42°N	8°42'4.59°E
Neckargemünd	Dilsberger Str./Altes E-Werk	Ng	49°23'32.62°N	8°48'22.25°E
Hirschhorn	Kapelle Neckarschleife	Hh	49°27'17.18°N	8°54'31.59°E
Mosbach	Schreckberg	Mos	49°21'50.68°N	9°5'57.08°E
Rockenau	Steinbruch am Mühlberg	Rk	49°26'21.02°N	8°59'53.22°E
Neckargerach	Margaretenschlucht	OM	49°23'20.72°N	9°5'4.46°E
Zwingenberg	Wolfsschlucht	OW	49°25'18.89°N	9°1'56.38°E
Black Forest:				
Ettlingen	Schöllbronner Steig	Et	48°55'34.47°N	8°25'7.92°E
Alsace:				
Cleebourg	Am Schießstand	Cl; C	49°0'48.05°N	7°53'23.77°E
Haardt:				
Neustadt an der Weinstraße	Steinbruch Fa. Hanbuch	Hb	49°22'20.21°N	8°8'31.15°E
Leistadt	Steinbruch Fa. Göbel	Ls; Lei	49°28'36.50°N	8°9'21.16°E
Palatinate Forest:				
Pirmasens	B10/Rodalber Str.	Pir	49°12'41.48°N	7°36'38.90°E
Rodalben/Pirmasens	various outcrops	R + Roman numeral	Grabowska (2011)	

Danksagung

An erster Stelle geht mein Dank an meinen Doktorvater Thilo Bechstädt: Du hast mir sehr viele Freiheiten bei der Gestaltung dieses Forschungsprojekts gelassen und damit immenses Vertrauen entgegen gebracht. In den letzten Monaten haben Deine zahlreichen Anregungen, Vorschläge und unermüdlichen Korrekturen maßgeblich zur Qualität dieser Arbeit beigetragen!

Meine Kollegen am Institut für Geowissenschaften in Heidelberg: Christian, Georg, Lennart, Torben, Till, Dominik, Tom, Enric, Patrick, Seija und Hartmut. Ich werde die Zeit mit Euch vermissen!

Mein Heißkathoden-Paparazzo: Sven, danke für fast drei Jahre fleißiges und selbständiges Arbeiten. Du hast mir sehr geholfen!

Alexander Varychev hat mir am REM so manchen Trick und Kniff gezeigt, um das Beste aus der nicht ganz jungen Technik herauszuholen. Hans-Peter Meyer unterstützte nicht nur meine Arbeiten am REM, sondern half auch bei den XRD- und RFA-Messungen ohne große Umschweife weiter.

Das Präparatoren-Team mit Ilona Fin, Oliver Wienand und Joachim Fillauer hat immer für einen kontinuierlichen Nachschub an Dünnschliffen gesorgt.

Ilse Glass hat die vielen XRD-Messungen durchgeführt.

An das Labor für Molekulare Pflanzenbiologie am COS der Uni Heidelberg: Anna, Stefan, Eric, Monika und Gernot (Lyophilisierung rocks!). Ein riesen Dankeschön auch an Dr. Markus Wirtz und Prof. Rüdiger Hell, dass ihr mich vollkommen uneigennützig ein paar Tage in Eurem Labor arbeiten ließt. So mancher kann sich eine dicke Scheibe von Eurer Einstellung abschneiden!

Maria, Du hast alle paar Monate mit Deinen Erzen den manchmal grauen Alltag bunter gemacht.

Anna, Danke für Deine Unterstützung! Mit den Erfahrungen von Deinem Weg zur Promotion hast Du mir oft geholfen. Ohne Dich wär alles nur halb so schön.

Danke auch an die Kooperationspartner aus dem Projekt AuGE: Axel, René, Maria, Johanna, Silke, Harald Stollhofen, Sonja Philipp und Gerhard Kowalczyk.

Ohne die Finanzierung des Projekts AuGE durch das Bundesministerium für Umwelt und das Bundesministerium für Wirtschaft wäre diese Doktorarbeit nicht zustande gekommen.

Eidesstattliche Versicherung gemäß §8 der Promotionsordnung der Naturwissenschaftlich-Mathematischen Gesamtfakultät der Universität Heidelberg

1. Bei der eingereichten Dissertation zu dem Thema

   Diagenesis and reservoir quality of the Lower and Middle Buntsandstein (Lower Triassic), SW Germany

   handelt es sich um eine eigenständig erbrachte Leistung.

2. Ich habe nur die angegebenen Quellen und Hilfsmittel benutzt und mich keiner unzulässigen Hilfe Dritter bedient. Insbesondere habe ich wörtlich oder sinngemäß aus anderen Werken übernommene Inhalte als solche kenntlich gemacht.

3. Die Arbeit oder Teile davon habe ich bislang nicht an einer Hochschule des In- oder Auslands als Bestandteil einer Prüfungs- oder Qualifikationsleistung vorgelegt

4. Die Richtigkeit der vorstehenden Erklärungen bestätige ich.

5. Die Bedeutung der eidesstattlichen Versicherung und die strafrechtlichen Folgen einer unrichtigen oder unvollständigen eidesstattlichen Versicherung sind mir bekannt.

   Ich versichere an Eides statt, dass ich nach bestem Wissen die reine Wahrheit erklärt und nichts verschwiegen habe.

Heidelberg, _____ _____

Ort und Datum Unterschrift